UNIVERSIDAD NACIONAL AUTÓNOMA DE MEXICO

PROGRAMA DE MAESTRÍA Y DOCTORADO EN CIENCIAS QUÍMICAS

ÁCIDOS GLICOSÍDICOS CONSTITUTIVOS DE LAS RESINAS DE
Operculina macrocarpa: ELUCIDACIÓN ESTRUCTURAL Y EVALUACIÓN DE SU
POTENCIAL MODULADOR SOBRE LA RESISTENCIA A FÁRMACOS

TESIS

QUE PARA OPTAR POR EL GRADO DE

DOCTOR EN CIENCIAS

PRESENTA

M. en C. JOSÉ DE JESÚS LIRA RICÁRDEZ

Tutor: Dr. ROGELIO G. PEREDA MIRANDA
FACULTAD DE QUÍMICA

Ciudad Universitaria, Ciudad de México, Agosto de 2019

Jurado asignado:

Presidente:	Dr. Manuel Jiménez Estrada
Vocal:	Dra. Rachel Mata Essayag
Vocal:	Dr. Alexandre Toshirrico Cardoso Taketa
Vocal:	Dr. José Federico del Río Portilla
Secretario:	Dr. José Fausto Rivero Cruz

**Este trabajo se realizó en el laboratorio 123 del Departamento de Farmacia
del Conjunto E de la Facultad de Química, UNAM,
bajo la dirección del Dr. Rogelio G. Pereda Miranda**

_____

M. en C. José de Jesús Lira Ricárdez
Sustentante

_____

Dr. Rogelio G. Pereda Miranda
Asesor

AGRADECIMIENTOS

PUBLICACIONES Y ASISTENCIA A CONGRESOS:

- **Primera publicación:**   Publicado en linea: 12 de junio de 2019.
                               DOI: 10.1021/acs.jnatprod.9b00222

Resin Glycosides from the Roots of *Operculina macrocarpa* (Brazilian Jalap) with Purgative Activity

Jesús Lira-Ricárdez,[†] Rogelio Pereda-Miranda,*[,†][©] Jhon Castañeda-Gómez,[‡] Mabel Fragoso-Serrano,[†] Rosineide Costa Simas,[§] and Suzana Guimarães Leitão[§][©]

[†]Departamento de Farmacia, Facultad de Química and Programa de Maestría y Doctorado en Ciencias Químicas, Universidad Nacional Autónoma de México, Ciudad Universitaria, Mexico City 04510, Mexico

[‡]Grupo Químico de Investigación y Desarrollo Ambiental, Programa de Licenciatura en Ciencias Naturales y Educación Ambiental, Facultad de Educación, Universidad Surcolombiana, Neiva, Colombia

[§]Faculdade de Farmácia, Universidade Federal do Rio de Janeiro, CCS, Bloco A, Ilha do Fundão, 21941-902, Rio de Janeiro, Brazil

🅢 *Supporting Information*

- **Segunda publicación:**

Reversal of multidrug resistance by amphiphilic morning glory resin glycosides in bacterial pathogens and human cancer cells

Jesús Lira-Ricárdez & Rogelio Pereda-Miranda*

Sometido a la revista Phytochemistry Reviews: 08 de febrero de 2019;
Versión corregida enviada el día 03 de junio de 2019
(Clave: PHYT-D-19-00035), en proceso de aceptación.

- **Tercera publicación:**

Is the lipophilicity-hydrophilicity balance of macrocyclic resin glycosides important for their chemosensitizer activity in multidrug-resistant cells?

Jesús Lira-Ricárdez, Mabel Fragoso-Serrano, Susana Guimarães-Leitão, and Rogelio Pereda-Miranda*

Sometido a la revista Brazilian Journal of Pharmacognosy: 21 de junio de 2019

Los resultados de la presente disertación se presentaron en el congreso internacional:

Young Scientists' Meeting on Advances in Phytochemical Analysis
(Trends in Natural Products Research)
Organizada por la Sociedad Fitoquímica de Europa (PSE)
Sede: Universidad de Liverpool John Moores
Liverpool, Reino Unido
Del 02 de Julio al 05 de julio de 2019

ÍNDICE

ÍNDICE DE FIGURAS Y TABLAS

RESUMEN

La presente disertación doctoral presenta los resultados obtenidos del estudio químico y biológico realizado a la especie vegetal *Operculina macrocarpa* (Linn) Urb., conocida por la población brasileña como *jalapa* o *batata de purga* y, mundialmente, como raíz de jalapa brasileña. Esta especie proveniente de la región brasileña del noreste donde se emplea desde tiempos coloniales como laxante y "purificador" y, que en la actualidad, ha sido objeto de escasos estudios debido a la presencia de mezclas complejas de compuestos glicolipídicos de alta polaridad presentes en sus extractos que dificultan el aislamiento y la caracerización estructural de sus principios activos.

Derivado de este trabajo, se realizaron tres artículos de investigación original, que están organizados en los siguientes capítulos:

En el primer capítulo, se expone el proceso de separación, aislamiento, purificación y elucidación estructural de los compuestos glicolipídicos presentes en la fracción soluble en metanol del extracto de la raíz de jalapa brasileña de flores blancas. Mediante el uso de la cromatografía de líquidos de alta resolución (HPLC, por sus siglas en inglés), y aplicando las técnicas de reciclaje de pico, rasurado de pico y corte de núcleo, fue posible el aislamiento de tres compuestos lipohexasacáridos denominados ácidos macrocarposídicos A-C derivados del ácido operculínico H. Del mismo modo, se identifican los ácidos provenientes de los residuos acilantes de las cadenas oligosacáridas: 3-metilbutírico o isovalérico, tíglico y exogónico, el cual se presenta en mezcla epimérica. A través de los productos obtenidos por los procesos de saponificación y peracetilación de esta fracción cruda, se reconoció al ácido operculínico H como el ácido glicosídico mayoritario presente en esta fracción, junto con otros compuestos glicolipídicos minoritarios novedosos denominados como los ácidos operculínicos I-K y al ácido púrgico A, anteriormente descrito en la raíz de jalapa mexicana (*Ipomoea purga*).

En el segundo capítulo, se presenta una revisión bibliográfica crítica diseñada para proporcionar una visión profunda de los avances claves en la investigación que han permitido destacar las características fisicoquímicas y biológicas de las resinas glicosídicas aisladas en diversas especies de la familia de las convolvuláceas, centrándose en la actividad moduladora de estos productos naturales *in vitro* sobre las bombas de eflujo presentes en organismos procarióticos (bacterias Gram-positivo y Gram-negativo) y en células eucarióticas (células neoplásicas humanas) relacionadas con el fenotipo de la resistencia múltiple a fármacos (e.g., glicoproteína-P).

En el tercer capítulo, se presentan los resultados obtenidos de la evaluación *in vitro* de la actividad moduladora de las resinas glicosídicas descritas en la presente disertación sobre las bombas de eflujo relacionadas a la resistencia múltiple a fármacos (e.g., glicoproteína-P) en células tumorales derivadas de carcinoma mamario resistentes a vinblastina (MCF-7/Vin), así como su explicación en torno a la relación estructura química-actividad biológica de estos compuestos. Los resultados indicaron que la naturaleza anfifílica producto de un determinado grado de esterificación, complementada con la presencia de un sistema macrocíclico que restringe la libertad conformacional del núcleo oligosacárido, permite una mejor interacción con el sitio de acción de las bombas de eflujo y la generación de un efecto modulador significativo.

ABSTRACT

The following doctoral dissertation presents the results obtained from the chemical and biological studies carried out on the plant species *Operculina macrocarpa* (Linn) Urb., known as *jalapa* or *batata-da-purga* to the Brazilian population, and Brazilian Jalap root worldwide. This species from Northeastern Brazil has been used since colonial times as a laxative and "purifying agent". Today, it has been scarcely studied due to the presence of complex mixtures of high-polar glycolipids which difficult their isolation and structure elucidation.

Derived from this work, three full papers of original research were prepared, which are organized in the following chapters:

The first chapter describes the process of separation, isolation, purification and structural elucidation of the resin glycosides from the methanol-soluble fraction of the total extract from the Brazilian Jalap root. Through the use of high-performance liquid chromatography (HPLC), applying the techniques of peak-recycling, peak-shaving and heart-cutting, it was possible to isolate three lipohexasaccharide compounds called macrocarposidic acids A-C, which represent related natural products of operculinic acid H. Likewise, acylating residues of the oligosaccharide core were identified as exogonic (present as an epimeric mixture), 3-methylbutyric or isovaleric, and tiglic acids. Saponification and peracetylation of the crude drug allowed to recognize operculinic acid H as the major glycosidic acid in this fraction, together with other novel minor glycolipid compounds, called operculinic acids I-K, in addition to the known purgic acid A, previously described from the Mexican Jalap root (*Ipomoea purga*).

The second chapter presents a critical review designed to give an interesting insight into the physicochemical characteristics of the glycolipid compounds isolated

from several species of the Convolvulaceae family, and the justification for their biological activity, especially on the modulating activity of the efflux pumps in prokaryotic organisms (Gram-positive and Gram-negative bacteria) and eukaryotic cells (human neoplastic cells) and their *in vitro* pharmacological evaluation.

In the third chapter, the results obtained from the *in vitro* evaluation of the resin glycosides –described in the present dissertation– on their modulatory activity of vinblastine in multidrug resistant carcinoma cells (MCF-7/Vin) are presented, as well as the implications of the lipophilicity-hydrophilicity balance of macrocyclic resin glycosides as chemosensitizers. The potentiation of the modulatory activity of these glycolipids was found to be directly associated to the constrained macrolactone structure, as well as to their amphiphilicity, which seems to be important to facilitate the resin glycoside interaction with their efflux pump targets.

INTRODUCCIÓN

A través de miles de años, las sociedades humanas de diferentes épocas y culturas han recurrido a diversos tipos de recursos, algunos de ellos al alcance de la mano y otros, intangibles como sus dioses, para procurarse entre otros satisfactores, el alivio del dolor y de diversos padecimientos. De estos recursos, el mundo vegetal ocupa un lugar importante como recurso terapéutico, ya que su uso se mantiene en estrecha relación desde la antigüedad: al ingerir plantas, se encontraba la respuesta a su necesidad primaria de alimento y mediante el método de "prueba y error", aprendió que muchas de ellas, tenían otras propiedades como las de curar o paliar alguna enfermedad, e incluso ser la diferencia entre la curación o la muerte del que las consumía.[1]

Estos conocimientos han sido transmitidos a través de las generaciones, ya sea de manera oral en los principios de la civilización, seguidos del desarrollo pictórico en grabados y, con el desarrollo de la escritura, se llegaron a registrar los primeros compendios sobre los remedios herbolarios empleados en aquellos tiempos, tales como *Historias de las Plantas*, del médico y botánico griego Teofrasto, y *De Materia Médica,* manuscrito realizado por el médico griego Dioscórides, considerado como el predecesor de los libros sobre hierbas (libros florísticos) o "herbarios" de uso entre los siglos XVI y XIX, y que describe el uso terapéutico de 600 especies vegetales conocidas en la antigüedad clásica, tales como la escamonea, un extracto de naturaleza resinosa, obtenida de la raíz de la especie *Convolvulus scammonia*, una enredadera perteneciente a la familia Convolvulaceae, nativa de la región mediterránea y conocida por sus propiedades purgantes y colagogas (Fig. 1).[1, 2]

En México, como en Latinoamérica, los pueblos amerindios prehispánicos desarrollaron un amplio conocimiento en relación al uso de la herbolaria, tanto con fines rituales-ceremoniales por parte de la elite gobernante de los pueblos, como con fines terapéuticos para el tratamiento de diversos padecimientos de la población en

Figura 1. Imagen de la raíz de escamonea (*Convolvulus scammonia*). Imagen tomada del Códice *Juliana Anicia*; Dioscórides, *De Materia Médica*. Viena, Biblioteca Nacional de Austria, Cod. Med. Gr. I, fol. 331v.

general. Dentro de las prácticas herbolarias mesoamericanas, se destaca el uso de remedios laxantes y/o purgantes, conocidos entre los mexicas como "cacamotli tlanoquiloni", por la idea de que era posible alcanzar la "purificación del cuerpo" a través de diversos tipos de raíces tuberosas, que variaban en sus características morfológicas, hábitat y poder laxante.[3]

Con la llegada de los españoles, los conocimientos etnobotánicos de los mexicas, fueron registrados en distintos manuscritos de la época, como el *Libellus de Medicinalibus Indorum Herbis,* también conocido como el *Códice de la Cruz-Badiano*, en honor del médico indígena Martín de la Cruz quién dictó el contenido en náhuatl y, al traductor del texto al latín el también indígena Juan Badiano, profesor del Colegio de la Santa Cruz en el convento de Santiago de Tlatelolco. Este primer compendio de la tradición herbolaria prehispánica escrito en el siglo XVI, que comprende alrededor de 224 nombres de plantas nativas de mesoamérica, agrupadas y ordenadas de acuerdo

con la enfermedad y la hierba que la cura, junto con algunas ilustraciones de las especies vegetales, realizadas por los escribanos y artistas indígenas del colegio.[4,5]

Figura 2. Ilustraciones de especies del género Convolvulaceae en el Códice de la Cruz-Badiano. Imágenes tomadas de la Revista Arqueología Mexicana Edición Especial, vol. 50. 2013
A. Tlacacamohtli o camote (*Ipomoea batatas*) **B.** Huelicpahtli o raíz de jalapa (*Ipomoea purga*)

Algunos de los tratamientos englobados en este compendio, incluyen a especies de raíces tuberosas, tales como el *tlacacamohtli* o camote (*Ipomoea batatas*), empleado para "el calor del corazón", el *tlaquilin* o tumbavaqueros (*I. stans*), empleado para la sordera y la "pudrición" del oído, y especialmente, el *huelicpantli* o raíz de jalapa (*I. purga*), cuyo uso está registrado para "purificar el vientre" mediante un preparado de la raíz molida en agua caliente (Fig. 2).[4] Durante la época novohispana, este remedio se popularizó en la península Ibérica como "la raíz de Michoacán" (*Ipomoea jalapa*) o "la jalapa de Veracruz" y fue empleado como un sustituto menos drástico del tratamiento purgante y catártico de la raíz de escamonea, por lo que, éste fue distribuido y comercializado en Europa desde el siglo XVI, a tal grado que, en la

década de 1940, la región de Xico en Veracruz cultivaba y exportaba cerca de 40 toneladas de raíz seca de la jalapa (*I. purga*) a los Estados Unidos por año, manteniendo este nivel hasta la década de 1990, después de que su exportación se redujo a casi cero. No obstante, su comercialización continua en los mercados populares de los centros urbanos de nuestro país e inclusive se distribuyen extractos preparados por la compañía fitofarmacéutica Laboratorios Mixim S.A. de C.V.[5,6]

A la par de la conquista ibérica, los colonizadores portugueses introdujeron en sus posesiones en ultramar, la medicina galénica que se utilizaba en Europa en el siglo XVI, donde los remedios purgantes y laxantes gozaban de suma importancia terapéutica. Sirva como ejemplo, la escamonea (para expulsar bilis) y el preparado purgante denominado *hiera*, cuya composición incluye extractos de especies como la coloquíntida (*Citrullus colocynthis* L. Schrad.), agárico (hongos comestibles del género *Agaricus* L.), opopónax y sagapeno (mezcla de resinas solubles en agua y en alcohol, presuntivamente obtenidas de algunas especies de la familia Apiaceae), perejil (*Petroselinum crispum* (Mill.) Fuss), aristoloquia redonda (*Aristolochia rotunda* Moc. & Sessé ex Duch.), azahar (flores de *Citrus aurantium* L.), espiga de nardo (*Nardostachys jatamansi* (D. Don) DC.*)*, germandria o camedrio (*Teucrium chamaedrys* L.), mirra (resina obtenida de la corteza de la especie *Commiphora myrrha* (Nees) Engl.), canela, pimienta y suficiente miel como excipiente.[7]

Al igual que los compendios herbolarios realizados en México en el siglo XVI por los frailes catequizadores, como la *Historia General de Cosas de la Nueva España* de Fray Bernardino de Sahagún, se organizó el primer tratado europeo de la materia médica americana, denominado la *Historia Medicinal de las Cosas Que Se Traen de las Indias Occidentales* de Nicolás Monardes, un médico, comerciante y botánico establecido en Sevilla, que fue publicado en tres partes entre 1564 y 1574, y se difundió ampliamente en Europa durante el siglo XVI. En este trabajo, el médico sevillano se propuso estudiar y experimentar los remedios del Nuevo Mundo, para explotar sus

propiedades farmacológicas, describiendo por primera vez numerosas especies de diferentes latitudes americanas como la jalapa, el maíz, la patata dulce, la coca, el tabaco, entre otras. Su contribución a la farmacognosia fue muy relevante y facilitó la introducción en España y aceptación en Europa de las raíces de jalapa de México y, por lo tanto, también favoreció la adopción de los purgantes y congéneres de estas raíces mexicanas en las prácticas médicas del imperio colonial portugués.[8]

Mientras se popularizaron las raíces de jalapa mexicana, como sucedáneos de la raíz de escamonea en el territorio español, en Brasil, la raíz de Michoacán (el "*mechoacam*") se describió entre las primeras plantas medicinales brasileñas por el naturalista francés Pierre Domet en su obra *Histoire Générale de Drogues, Traitant de Plantes, des Animaux et Mineraux* (1694). En la primera descripción de las plantas de Ceará (*Coleção Descritiva das Plantas da Capitania do Ceará*) publicado por J. S. Feijó en 1799, el uso de la raíz de jalapa en esta provincia se indica por el nombre vernáculo de "*mechoacam*". Por lo tanto, esta referencia es una de las más antiguas sobre la utilización tradicional de la "batata de purga" en el noreste brasileño.[8]

Con el paso del tiempo, las poblaciones portuguesa y brasileña emplearon remedios herbolarios tradicionales de la familia Convolvulaceae, con actividades similares a la raíz de jalapa mexicana, tal es el caso del complejo medicinal de la raíz de jalapa brasileña, conformados por las especies *Operculina hamiltonii* y *Operculina macrocarpa*, los cuales son conocidos y comercializados por los herbolarios como "*batata de purga*" y son ampliamente comercializadas en el norte y nordeste brasileño por sus propiedades laxantes, purgantes y para el tratamiento de padecimientos cutáneos y ginecológicos (Fig. 3).[9]

Durante los siglos XIX y XX, los estudios realizados para el aislamiento y caracterización química de los componentes responsables de la actividad laxante de ciertas especies de la familia Convolvulaceae, empleando técnicas cromatográficas,

espectroscópicas y espectrométricas modernas, han permitido el aislamiento, la purificación y la elucidación estructural de diversas moléculas de naturaleza glicolipídica que conforman a las resinas glicosídicas de estos remedios tradicionales. En el caso de la jalapa brasileña, solamente se ha realizado el estudio a la fracción soluble en éter (jalapina) de la raíz de jalapa brasileña de flores blancas (*Operculina macrocarpa*), pero se sabe que la fracción responsable de la actividad fitoterapéutica de la raíz, se le confiere a la fracción insoluble en éter (ramnoconvolvulina), de la cual, solamente se han aislado sus productos de hidrólisis alcalina.[10]

Figura 3. Ilustraciones de especies del complejo medicinal de la raíz de jalapa brasileña: ***Izquierda:*** Jalapa brasileña de flores blancas (*O. macrocarpa*) ***Derecha***: Jalapa brasileña de flores amarillas (*O. hamiltonii*) Imágenes tomadas de Lorenzi, H, Abreu-Matos, F.J., *Plantas medicinais no Brasil. Nativas e exóticas.* Ed. Instituto Plantarum. Brasil, 2002. pp. 183-184

Por ello, en el siguiente trabajo, se describe por primera vez, el aislamiento, la purificación y la identificación estructural de los constituyentes individuales que componen a la fracción de convolvulina de la raíz de jalapa brasileña (*Operculina macrocarpa* Urb.), detallando el proceso de separación de los compuestos glicolipídicos de esta fracción, mediante el uso de técnicas cromatográficas y su elucidación estructural a través de técnicas espectroscópicas de resonancia magnética nuclear y espectrometría de masas.

ANTECEDENTES

1.   Jalapa Brasileña

La familia de las convolvuláceas es uno de los grupos más importantes de las dicotiledóneas, perteneciente al orden Solanales, en donde se incluyen entre 1,500 a 1,850 especies de tipo herbácea, trepadora, arbustivas e inclusive, arbóreas bajas con látex, presentando una distribución cosmopolita, principalmente en zonas de clima tropical y subtropical. Morfológicamente, estas plantas presentan hojas alternas, simples y enteras, que dependiendo de la especie pueden ser de tipo acorazonado, lanceolado (en forma de lanza) o palmiforme (similar a las hojas de la palmera); sus flores son grandes, vistosas, regulares, solitarias o en inflorescencias como cimas, racimos o panículas, con corola pentamérica simpétala (5 pétalos fusionados); y sus frutos son cápsulas con semillas pilosas.[11,12]

En esta familia, los géneros más grandes son *Convolvulus*, *Ipomoea*, *Merremia* y *Operculina*, este último perteneciente a la tentativa Tribu Merremieae, que comprende alrededor de 15 especies herbáceas y trepadoras con distribución pantropical. En Latinoamérica, se han reportado especies de este género, tales como la gallinita o pata de gallo (*O. pinnatifida*), distribuida ampliamente en la región Mesoamericana, y la campanilla chocolate (*O. pteripes*), que se distribuye desde México hasta la región Andina; la jalapa brasileña (*Operculina macrocarpa* (L.) Urb. syn. *Convolvulus macrocarpa* L.,), una especie trepadora bienal con tubérculos de epidermis de coloración pardo-grisáceo o pardo-negras, de forma fusiforme (forma de huso) o napiforme (forma de nabo), que al ser cortada en rodajas, su interior presenta anillos concéntricos de coloración blanco-grisáceo de 5 a 7 cm de diámetro, presenta hojas son de aspecto palmiforme y flores simpétalas de corola blanca; que al fecundarse, generan frutos capsulares de aspecto redondo, que contienen de una a cuatro semillas de aspecto duro y coloración oscura (Fig. 4).[9,11,12]

Figura 4. Morfología de la jalapa brasileña blanca (*Operculina macrocarpa*):
A. Corte transversal de la raíz tuberosa. B. Flor. C. Semillas.

Esta especie se conoce tradicionalmente como *batata-de-purga, jalapa-do-Brasil* o *jalapão*, siendo empleada principalmente en la región del nordeste de Brasil, por sus tubérculos que se han empleado con fines medicinales desde hace dos siglos, según las referencias etnobotánicas con la denominación de "*mechoacam*", nombre derivado de la similitud morfológica y etnobotánica de la raíz de jalapa mexicana (*I. purga*). Según las referencias etnobotánicas y farmacopeicas, los tubérculos, al ser rebanados, exudan una sustancia de aspecto amiláceo y lactescente denominada resina, que es el principio activo responsable de las actividades purgantes de esta raíz.[9]

Esta resina se obtiene y utiliza en tres modalidades tradicionales: la primera emplea la ralladura fresca de la raíz, y se disuelve en un vaso con agua, que debe ser tomado en ayuno para "depurar el organismo", "limpiar la sangre" o "dejar una piel fresca"; la segunda opción utiliza la resina extraída directamente de la raíz, que al secarse forma un polvo grisáceo o pardo conocido tradicionalmente como *goma-de-batata, tapioca-de-purga o batatão*, que se usa de la misma manera que la ralladura de la raíz, e inclusive se le puede adicionar directamente en golosinas para ser ingerido por los infantes, a modo de enmascarar su sabor y obtener sus propiedades laxantes; y la tercera es a partir de preparados fitoterapéuticos, que van desde píldoras hechas manualmente con la resina desecada, o extractos hidroalcohólicos de la raíz, los cuales pueden venir solos o en preparados llamados tinturas, que incluyen otros ingredientes naturales como los extractos de la cáscara de naranja (*Citrus aurantum*), nuez

moscada (*Myristica fragrans*), entre otros (Fig. 5) En la Farmacopea de los Estados Unidos de Brasil (1928), se describe que el contenido de resina no debe ser menor al 15% para considerarse que este producto proviene de esta especie vegetal.[9, 13]

Figura 5. Ejemplos de presentaciones fitofarmacéuticas de la raíz de jalapa brasileña.

2.   Resinas glicosídicas

La química de la familia Convolvulaceae es muy diversa, dado que se han aislado compuestos de diferente naturaleza biogenética (compuestos terpenoides, polifenólicos, flavonoides y antocianinas, entre otros), de los cuales destacan dos grupos importantes de metabolitos secundarios: los alcaloides de tipo ergolina, inicialmente aislados de la especie fúngica *Claviceps purpurea* (cornezuelo del centeno), y que han sido aislados en especies vegetales de esta familia conocidas ampliamente por sus propiedades alucinógenas desde tiempos antiguos, como en el caso de las semillas del "*ololiuqui*" (*Turbina corymbosa L.*) o del "badoh negro" (*Ipomoea tricolor*), de los cuales se han aislado los alcaloides ergina y ergonovina. Actualmente, se conoce que la biosíntesis de estos compuestos se asocia a la presencia

de hongos endófitos del género *Periglandula,* que cohabitan de modo simbiótico en los tejidos superficiales vegetales (epidermis de los haces foliares y tricomas).[14,15]

El segundo grupo de metabolitos secundarios son los glicolípidos o denominados colectivamente como resinas glicosídicas, compuestos de naturaleza lipoheterooligosacárida conformados por una aglicona de ácido graso saturado de 14 a 22 átomos de carbono, monohidroxilado, como los ácidos convolvulinólico (11*S*-hidroxitetradecanoico) y jalapinólico (11*S*-hidroxihexadecanoico); o dihidroxilado, como los ácidos ipoleárico (3*S*, 11*S*-dihidroxihexadecanoico), ipurólico (3*S*, 11*S*-dihidroxitetradecanoico) y operculinólico (3*S*, 12*S*-hidroxihexadecanoico), unido a un monosacárido o cadena oligosacárida lineal o ramificada, conformada por unidades de hexosas (D-glucosa) y epímeros de metilpentosas (D-fucosa, D-quinovosa, L-ramnosa y algunos casos, D-xilosa) que a su vez pueden estar parcialmente esterificadas con ácidos orgánicos como: acético, (*Z*)-2-metil-2-butenoico, butírico, *n*-decanoico, *n*-octanoico, *n*-hexanoico, cinámico, *n*-dodecanoico, *n*-tetradecanoico, isobutírico, isovalérico, 2-metil-butírico, 3-hidroxi-2-metilbutírico, propionico, tíglico, entre otros; confiriéndole una naturaleza anfipática a estos compuestos (Fig. 6).[16]
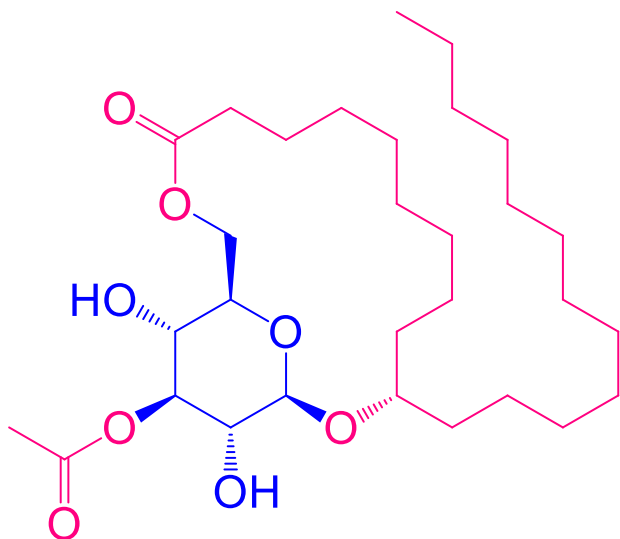
Figura 6. Estructura de una molécula glicolipídica (glomerásido B), la parte hidrofílica se representa en color azul y la porción lipofílica en color rojo purpureo.

Las resinas glicosídicas han sido aislados en especies vegetales de las familias Cariophyllaceae,[17,18] Scrophulariaceae[19] y Solanaceae,[20] aunque la principal fuente de compuestos glicolipídicos es la familia Convolvulaceae,[16] y pueden presentar estructuras lineales o ramificadas que presentan porciones esterificadas en su cadena oligosacárida o en la aglicona, así como estructuras macrocíclicas parcialmente aciladas, derivadas de la esterificación de la aglicona con un grupo hidroxilo de las unidades monosacáridas presentes en la molécula, o inclusive formando estructuras diméricas, entre dos unidades lipooligosacáridas parcialmente aciladas. Su alto peso molecular, complejidad estructural e importancia quimiotaxonómica y fitoterapéutica, las convierte en uno de los grupos de compuestos de mayor relevancia en los estudios fitoquímicos realizados a distintas especies de esta familia (Fig. 7).[16]
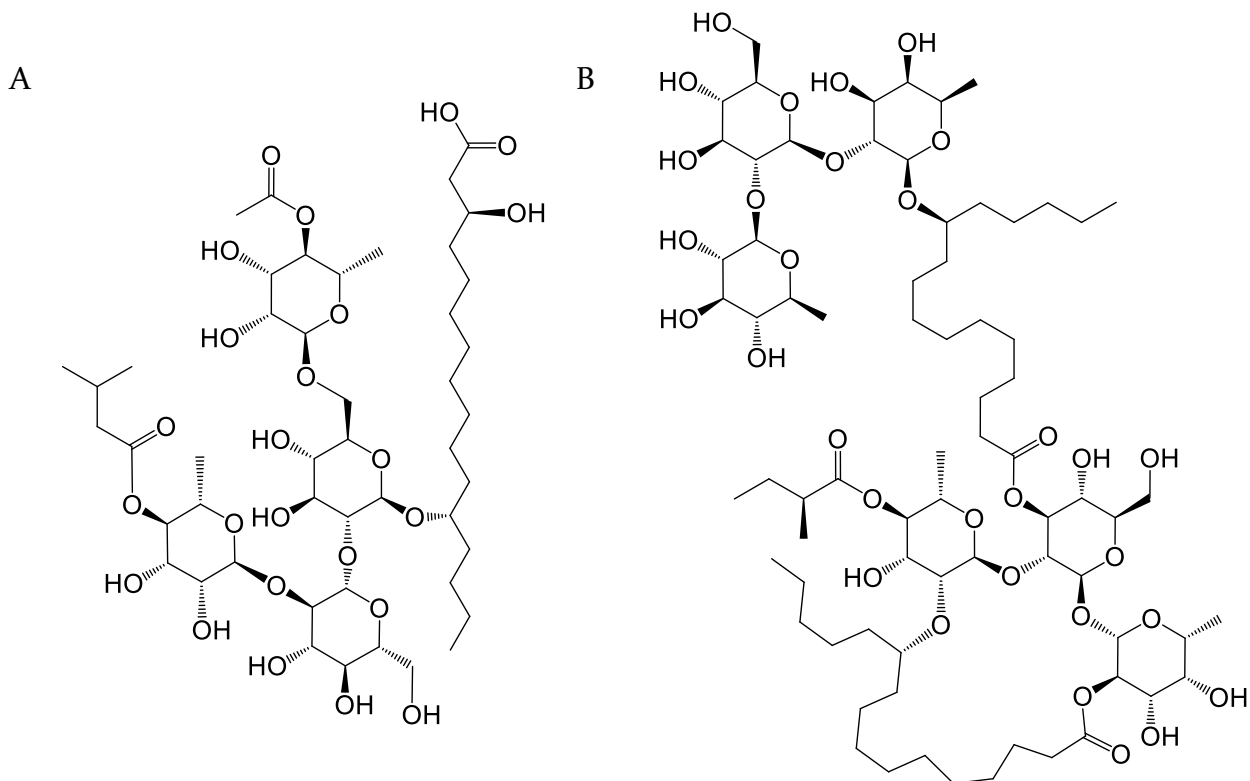
Figura 7. Estructuras de glicolípidos abiertos (**A.** Ácido criptofílico C) y homodimérico (**B.** Tricolorina H).

Los estudios fitoquímicos y farmacognósicos realizados a la raíz de jalapa brasileña, se han registrado desde principios del siglo XX, para poderlo diferenciar inicialmente de otros remedios fitoterapéuticos semejantes a ella, tales como la *Resina Drastica,* que se asocia con la raíz de escamonea europea (*Convolvulus scammonia* L.), por su potente propiedad catártica, la raíz de escamonea mexicana (*Ipomoea orizabensis* L.) y la raíz de jalapa de Veracruz (*Ipomoea purga* (Wender.) Hayne), a partir de estudios de solubilidad, cromatografía en capa fina, rotación óptica y determinación del material soluble en agua.[21,22]

Posteriormente, los estudios fitoquímicos realizados por Shellard (1961) a las muestras hidrolizadas de las resinas de los complejos medicinales de la jalapa mexicana y brasileña, permitieron corroborar las diferencias quimiotaxonómicas entre ellas, y así mismo, hacer la distinción entre los compuestos presentes en la mezcla resinosa mediante pruebas de solubilidad:

A. RESINAS DE LA JALAPA MEXICANA:

a) Jalapina. - En esta fracción se encuentran los compuestos solubles en éter y disolventes orgánicos no polares. A partir de su saponificación, se obtuvieron los ácidos acético, propiónico, tíglico, isobutírico, *n*-pentanoico (valérico), 2-metilbutírico y 3-metilbutírico (isovalérico) como ácidos volátiles, mientras que el ácido jalapinólico (ácido 11*S*-hidroxihexadecanoico) es el ácido graso constituyente de las compuestos glicolipídicos presentes, junto con la presencia de glucosa, fucosa y ramnosa como componentes de la cadena oligosacárida.[23] En años recientes, el estudio fitoquímico de esta fracción permitió el aislamiento de los purginósidos I-IV, como compuestos macrolactónicos derivados del lipopentasacárido ácido operculínico A, y de las purginas I-III, heterodímeros del ácido operculínico A (Fig. 8).[24, 25]
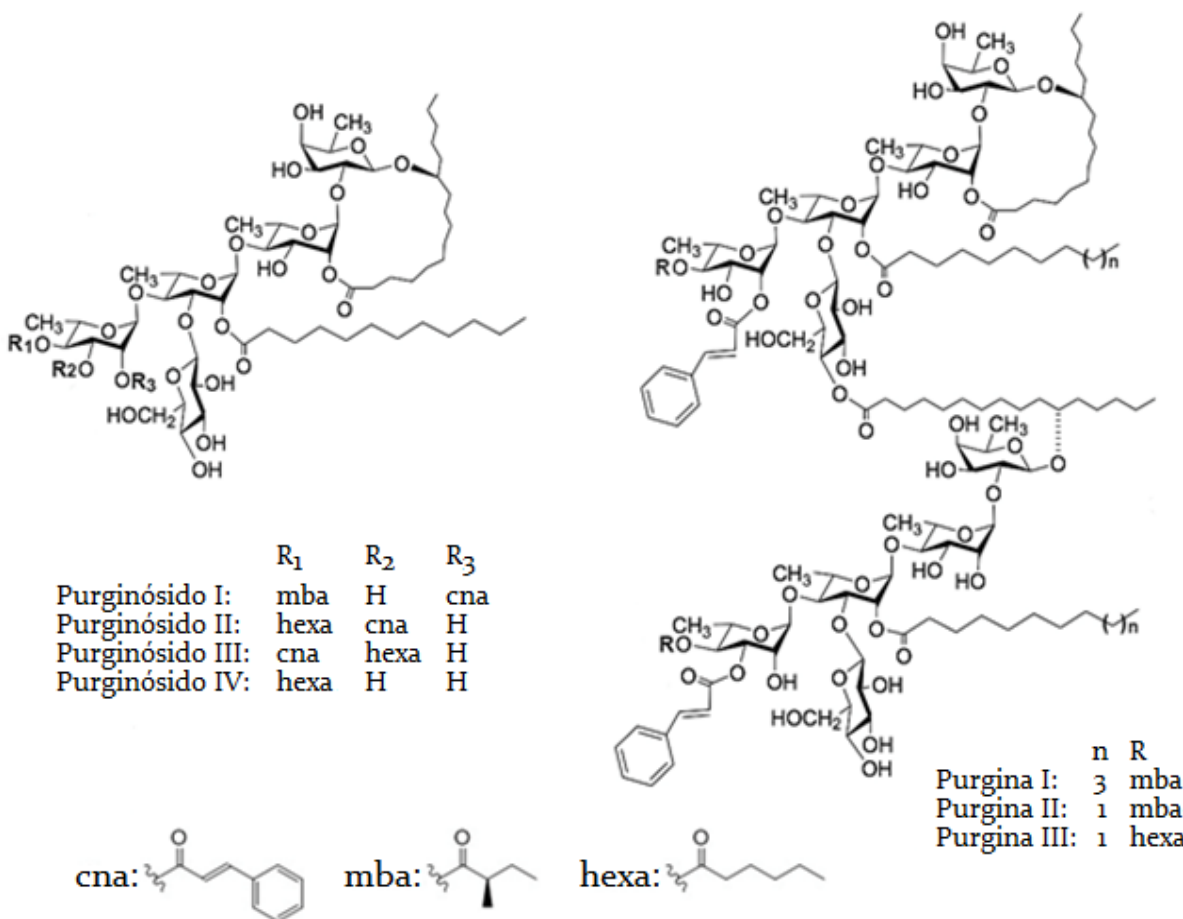
Figura 8. Estructuras químicas de los glicolípidos macrolactónicos y diméricos aislados de la fracción soluble en éter del extracto de la raíz de jalapa mexicana (*Ipomoea purga*).

b) Convolvulina. - En esta fracción se encuentran los compuestos solubles en metanol y disolventes orgánicos polares. A partir de su hidrólisis, se obtuvieron los ácidos volátiles anteriormente descritos, así como a los ácidos ipurólico (3S,11S-dihidroxitetradecanoico) y convolvulinólico (anteriormente descrito como un ácido hidroxipentadecanoico) como los ácidos grasos constituyentes de los compuestos glicolipídicos presentes, junto con la presencia de glucosa, fucosa y ramnosa como componentes de la cadena oligosacárida.[23] El estudio fitoquímico realizado a esta fracción permitió el aislamiento de los lipohexasacáridos ácidos púrgicos A-D, que difieren entre ellos por los ácidos grasos mono y/o dihidroxilados de distinta longitud

de cadena, junto con los bisdesmósidos jalapinósidos I, II y el macrociclo jalapinósido B como compuestos macrolactónicos derivados del ácido púrgico C y del ácido púrgico A, respectivamente (Fig. 9).[26-28]

	R_1	R_2	R_3	R_4	R_5	R_6	R_7
Jalapinósido I:	OQui	Ac	Mba	Mba	H	Dodeca	H
Jalapinósido II:	OQui	Ac	Mba	Nla	H	Dodeca	H
Jalapinósido B:	H	H	QB	H	Nla	H	Mba
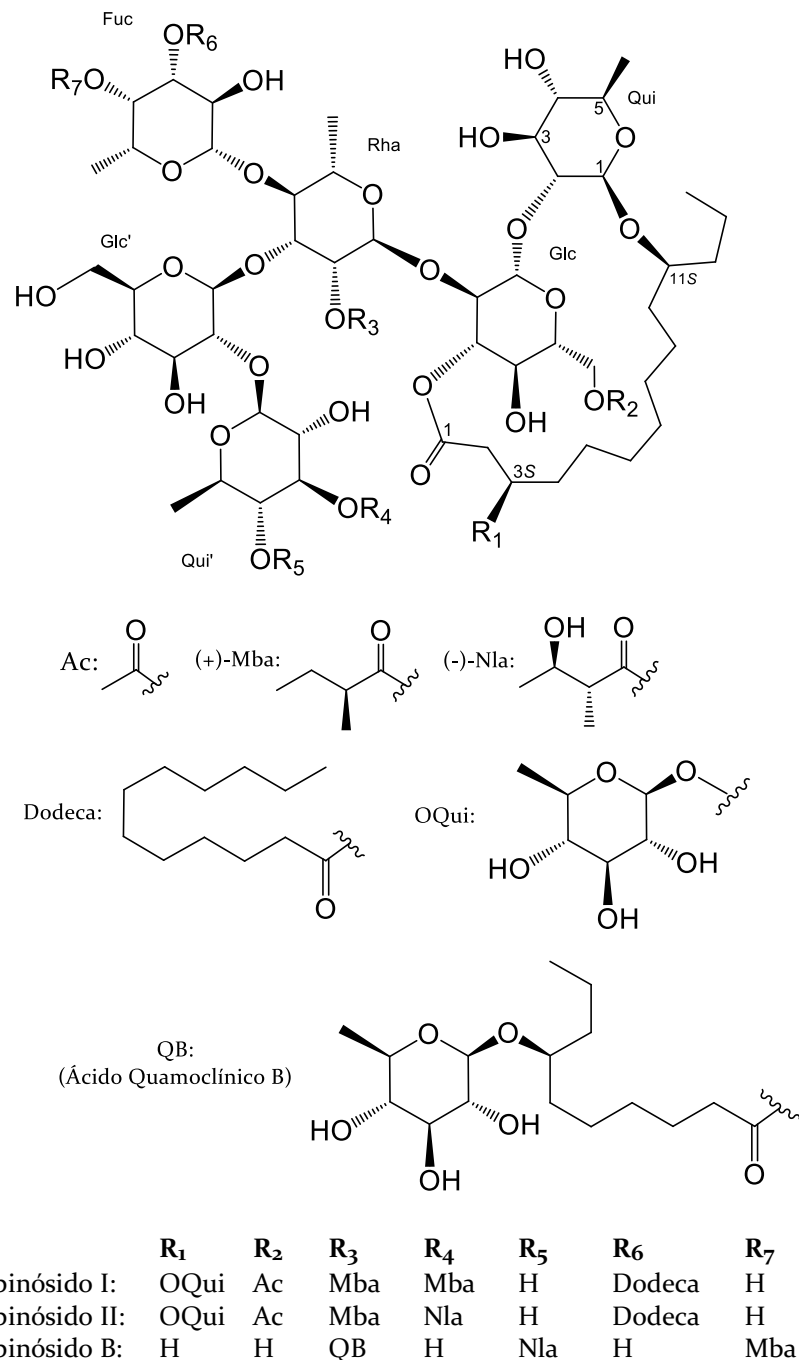
Figura 9. Estructuras químicas de los glicolípidos macrolactónicos aislados de la fracción soluble en metanol del extracto de la raíz de jalapa mexicana (*Ipomoea purga*).
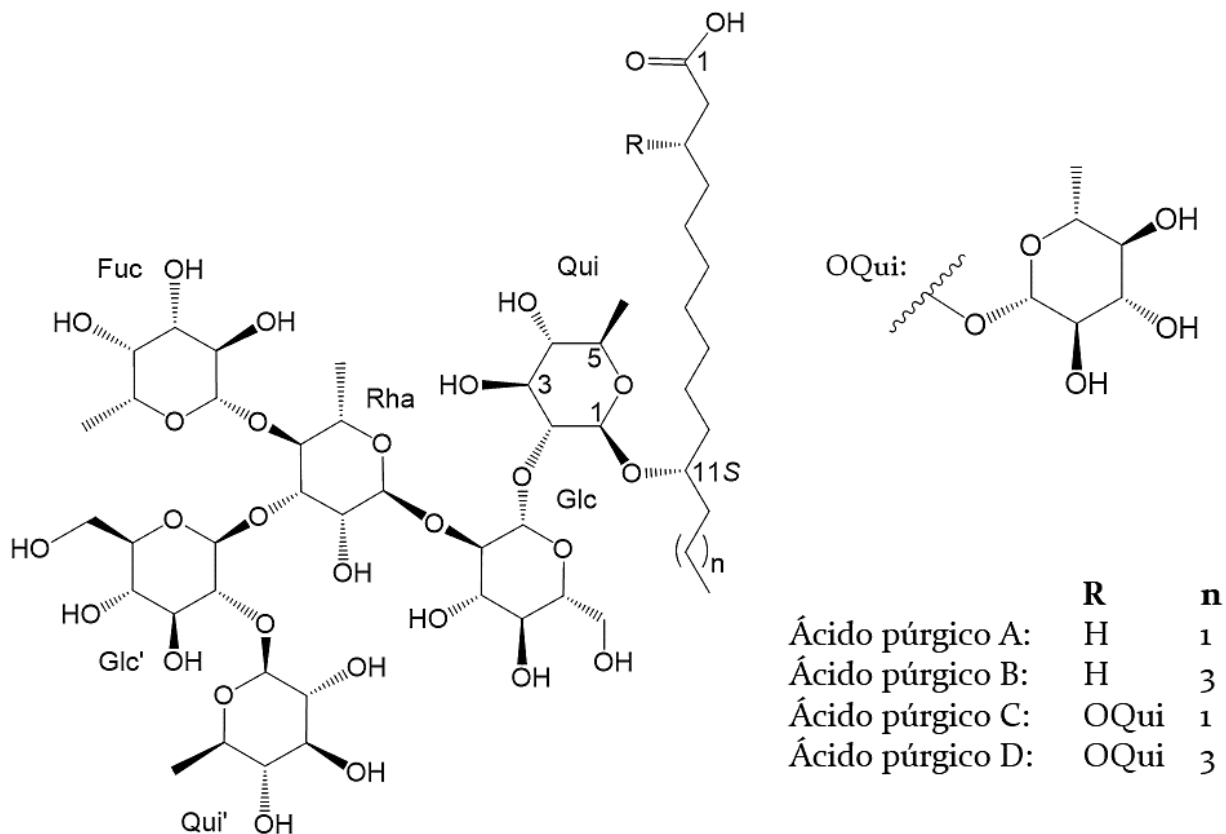
Figura 10. Ácidos glicosídicos aislados de la fracción soluble en metanol de la raíz de jalapa mexicana (*Ipomoea purga*).

En la medicina tradicional mexicana, la raíz de jalapa conforma un amplio complejo medicinal herbolario, que involucra especies tuberosas del género *Ipomoea*, tales como la raíz de escamonea mexicana (*Ipomoea orizabensis* (G. Pelletan) Ledeb. ex Steud, syn. *I. tyrianthina* Lindl.), el tumbavaqueros o quiebraplatos (*I. stans* Cav. e *I. tacambarensis* E. Carranza) y la raíz de Tampico (*I. simulans* D. Hanb.). En los análisis desarrollados para el control de calidad de los extractos de las raíces de la jalapa auténtica (*I. purga*) y dos sustitutos o falsas jalapas (*I. orizabensis* e *I. stans*) se pudo diferenciar el contenido de sus glicolípidos, distinguiendo a los ácidos púrgicos —hexasacáridos— como marcadores químicos de la verdadera raíz de jalapa, en contraste con los derivados del lipotetrasacárido —ácido escamónico A— y del lipopentasacárido —ácido operculínico B— que han sido aislados en los extractos de la escamonea mexicana y del tumbavaqueros, respectivamente (Fig. 10).[3]
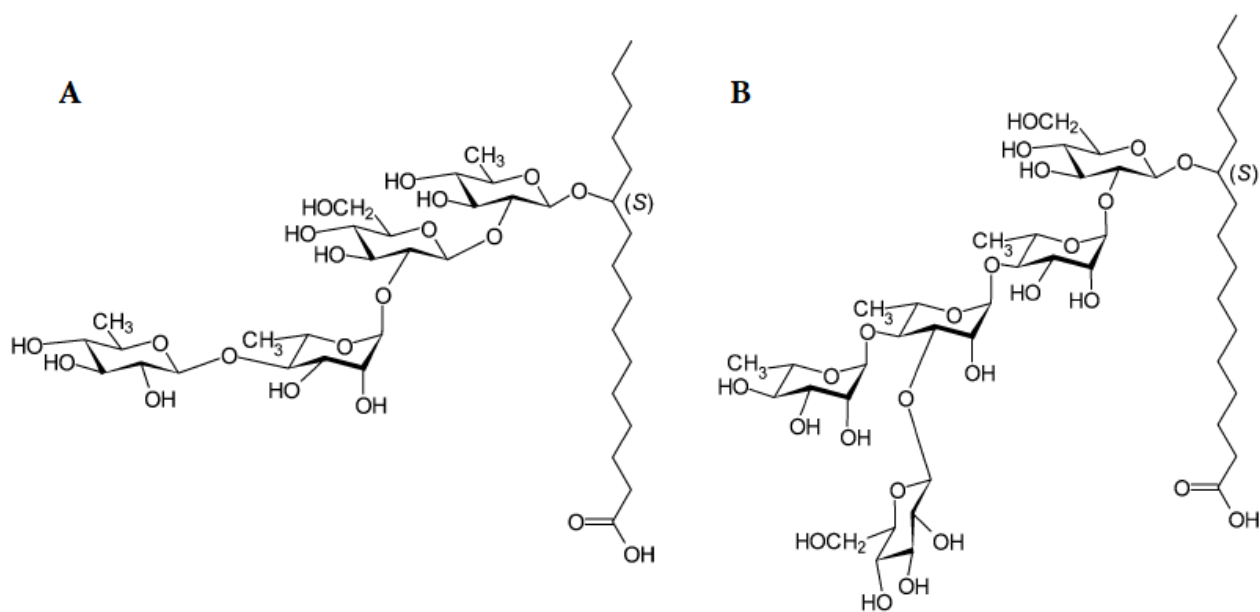
Figura 11. Estructuras químicas del ácido escamónico (**A**) y ácido operculínico B (**B**).

RESINAS DE LA JALAPA BRASILEÑA:

c) Jalapina. - En esta fracción se encuentran los compuestos solubles en éter y disolventes orgánicos no polares. A partir de su hidrólisis, se lograron aislar fucosa, glucosa y ramnosa como unidades monosacáridas y los ácidos *n*-decanoico y *n*-dodecanoico, mientras que el ácido jalapinólico (ácido 11*S*-hidroxihexadecanoico) es el ácido graso constituyente de los núcleos glicosídicos presentes.[29]

En la segunda mitad del siglo XX y principios del siglo XXI, los estudios fitoquímicos de la raíz de jalapa brasileña, se enfocaron en el aislamiento, la purificación y la caracterización de los componentes intactos presentes, tanto en la fracción de jalapina, como la de convolvulina. A partir de la primera, se lograron aislar 17 nuevas moléculas de naturaleza lipooligosacárida denominadas operculinas I-XVIII (Fig. 11), de los cuales, mediante hidrólisis alcalina, derivan los denominados ácidos operculínicos.[30-32]

	R_1	R_2	R_3	R_4	R_5	R_6
Operculina I:	H	OH	CH_3	Dodeca	Glc	Dodeca
Operculina II:	H	OH	CH_3	Deca	Glc	Deca
Operculina III:	OH	H	CH_2OH	Dodeca	Glc	Dodeca
Operculina IV:	OH	H	CH_2OH	Deca	Glc	Deca
Operculina VI:	H	OH	CH_3	Dodeca	H	Dodeca
Operculina VII:	H	OH	CH_3	Dodeca	Glc	Deca
Operculina VIII:	H	OH	CH_3	Deca	Glc	Dodeca
Operculina IX:	OH	H	CH_2OH	Dodeca	Glc	Deca
Operculina X:	OH	H	CH_2OH	Deca	Glc	Dodeca
Operculina XIII:	H	OH	CH_3	Dodeca	Glc	H
Operculina XIV:	H	OH	CH_3	Deca	Glc	H
Operculina XV:	H	OH	CH_3	H	Glc	Dodeca
Operculina XVI:	OH	H	CH_2OH	Dodeca	Glc	H
Operculina XVII:	OH	H	CH_2OH	Deca	Glc	H
Operculina XVIII:	OH	H	CH_2OH	H	Glc	Dodeca

	R_1	R_2
Operculina V:	Dodeca	Glc
Operculina XI:	Dodeca	H
Operculina XII:	H	Dodeca

Figura 12. Glicolípidos intactos aislados del extracto de jalapina la raíz de jalapa brasileña (*Operculina macrocarpa*).

23

Actualmente, se conocen siete ácidos operculínicos derivados de esta fracción (ácidos A-G), los tres primeros se aislaron como productos macrocíclicos de otras resinas presentes en especies de los géneros *Argyreia, Ipomoea* y *Merremia* (Fig. 12). De los ácidos operculínicos D-F, no han sido aislados productos macrocíclicos o lineales como en los casos anteriores; sin embargo, los ácidos operculínicos D y F son los primeros ejemplos de compuestos de naturaleza lipooligosacárida que presentan una unidad oligosacárida conteniendo xilosa enlazada a un ácido graso monohidroxilado.[33, 34]

	R₁	R₂	R₃	R₄
Ácido operculínico A:	H	OH	CH₃	Glc
Ácido operculínico B:	OH	H	CH₂OH	Glc
Ácido operculínico C:	H	OH	CH₃	H
Ácido operculínico D:	OH	H	H	Glc
Ácido operculínico E:	OH	H	CH₂OH	H
Ácido operculínico F:	OH	H	H	H
Ácido operculínico G:	H	OH	CH₃	GlcMe
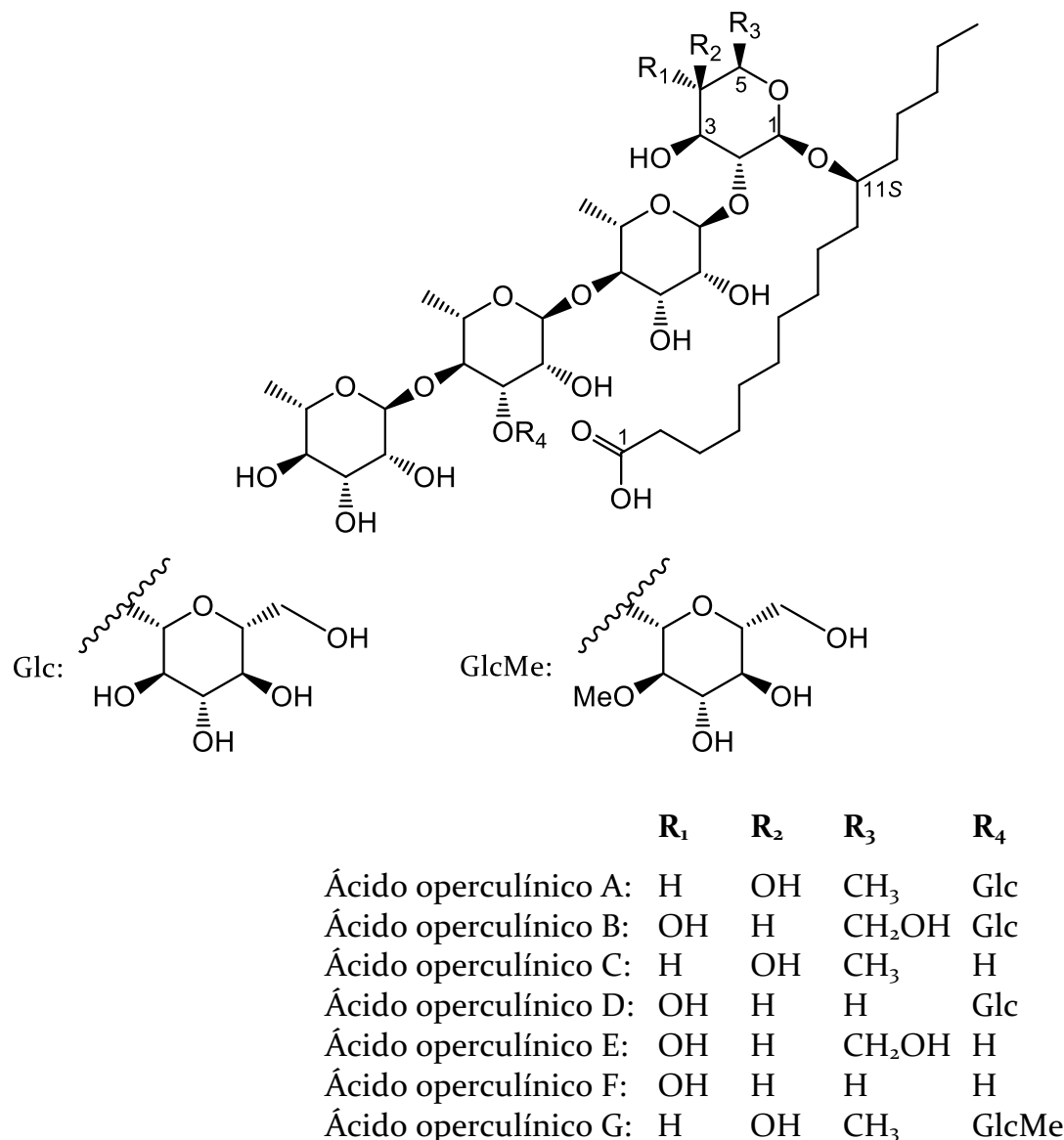
Figura 13. Ácidos glicosídicos aislados de la raíz de jalapa brasileña (*Operculina macrocarpa*).

d) Convolvulina. - En esta fracción se encuentran los compuestos solubles en etanol y disolventes orgánicos polares. A partir de su hidrólisis, se lograron aislar glucosa y ramnosa como unidades monosacáridas y los ácidos acético (etanoico), tíglico (ácido (*E*)-2-metil-buten-2-oico), *n*-valérico (ácido *n*-pentanoico), trimetilacético (ácido 2,2-dimetilpropiónico) y exogónico (ácido 3,6:6,9 diepoxidecanoico o 2-carboximetil-7-metil-1,6-dioxasipro-[4,4]-nonano), compuesto tipo espirocetálico conformado por dos anillos de oxolano y tres centros quirales, por lo que se conocen 4 diastereoisómeros epiméricos presentes en una mezcla que conforma alrededor de un 7% de los componentes ácidos de la resina. De esta mezcla, el 80% presenta la configuración absoluta *Z,Z* y *E,E* (Fig. 13). Este ácido se utiliza como el marcador químico para las resinas glicosídicas de la especie *Operculina macrocarpa.*[29,35,36]

E, E 3*S*, 6*S*, 9*R*

Z, Z 3*S*, 6*R*, 9*R*

E, Z 3*S*, 6*S*, 9*S*

Z, E 3*S*, 6*R*, 9*S*
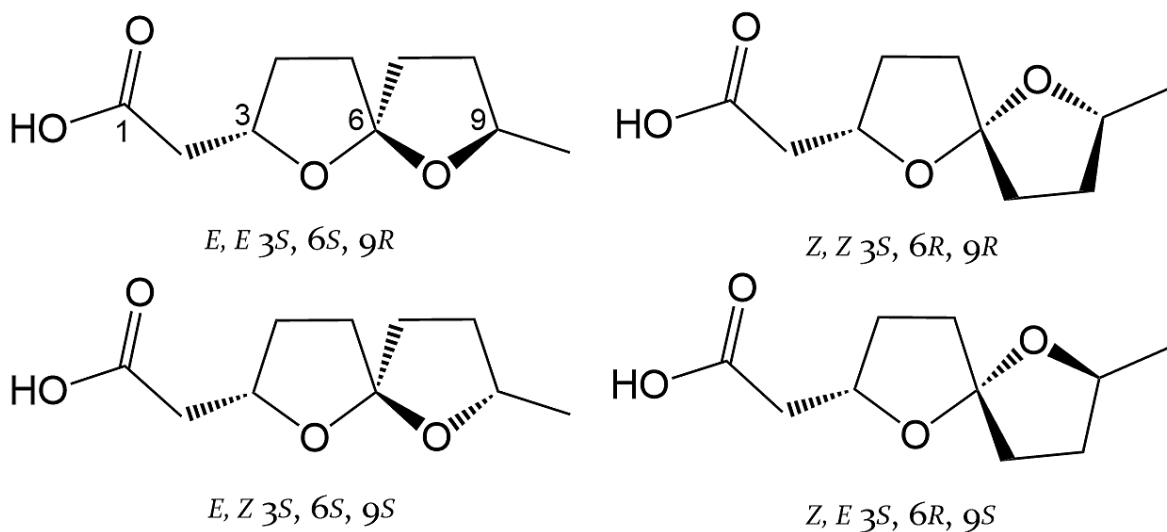
Figura 14. Estructuras químicas de los epímeros del ácido exogónico.

Los ácidos grasos hidroxilados presentes en esta fracción, son los ácidos operculinólico (ácido 3*S*, 12*S*-dihidroxihexadecanoico) y el ácido brasilioico (posiblemente un ácido trihidroxitetradecanoico).[29,35] En la última década, los estudios fitoquímicos del extracto de la raíz de jalapa brasileña, se han enfocado en los compuestos presentes en la fracción soluble en metanol (convolvulina). Hasta la fecha, ningún producto natural macrocíclico intacto ha sido aislado de esta fracción; sin embargo, se han obtenidos productos derivatizados mediante la esterificación de

la aglicona, empleando cloruro de indio (III) en metanol, lo que permitió el aislamiento, purificación e identificación de cuatro moléculas conformadas por el ácido operculínico H (Fig. 15), un núcleo lipohexasacárido compuesto por cuatro unidades de glucosa, dos unidades de ramnosa y una aglicona de ácido operculinólico.[34,36] Estos compuestos denominados IOM's (Fig. 14), presentan residuos acilantes de los ácidos tíglico, isovalérico y exogónico, el cual, se presenta con sus dos epímeros mayoritarios, debido a la interconversión estereoquímica del centro estereogénico C-6 en solución.[37]

	R₁	R₂	R₃	R₄
IOM-1:	Iva	Tga	H	H
IOM-2:	Iva	H	H	H
IOM-3:	Iva	Tga	Iva	H
IOM-4:	Iva	Tga	H	Iva
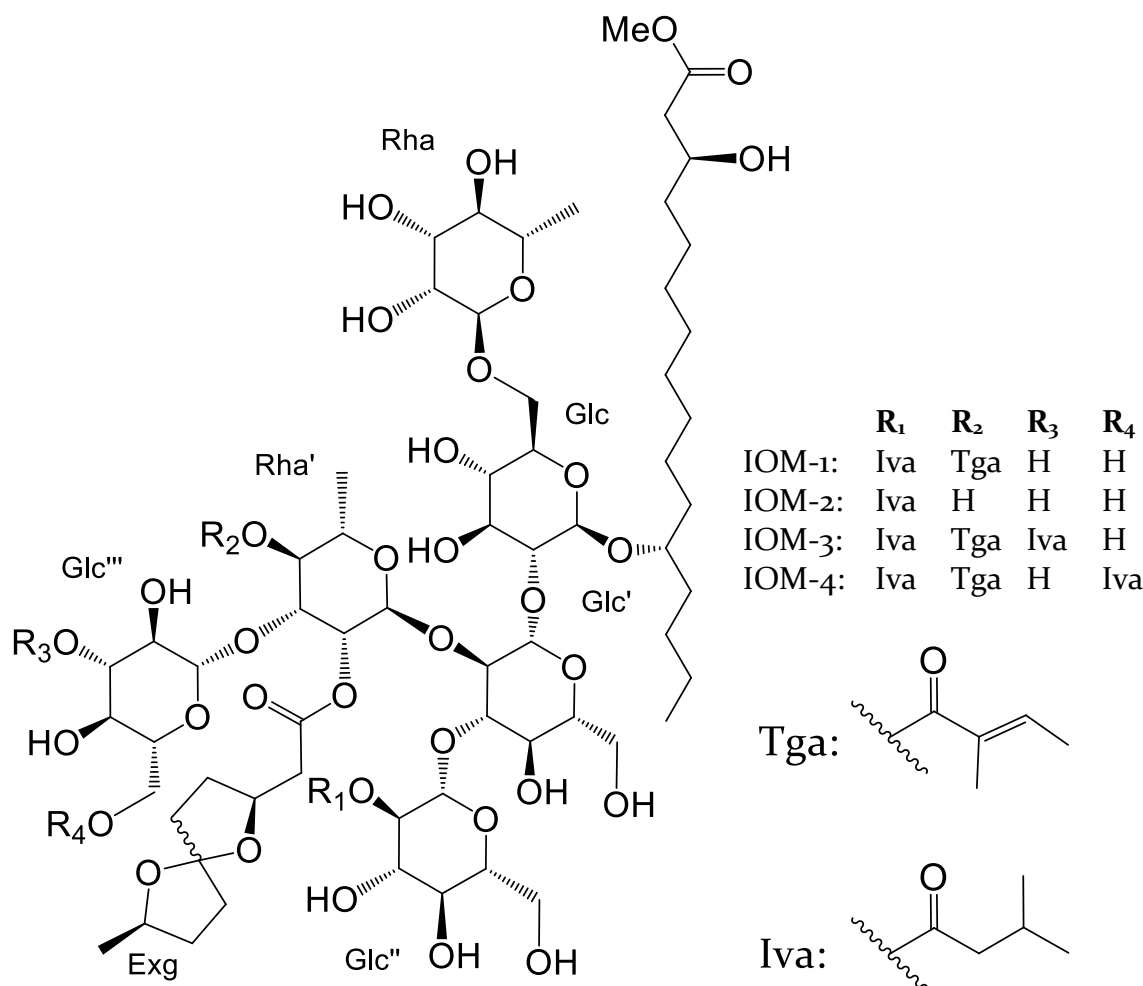
Figura 15. Glicolípidos esterificados provenientes del extracto de convolvulina de la raíz de jalapa brasileña (*Operculina macrocarpa*).
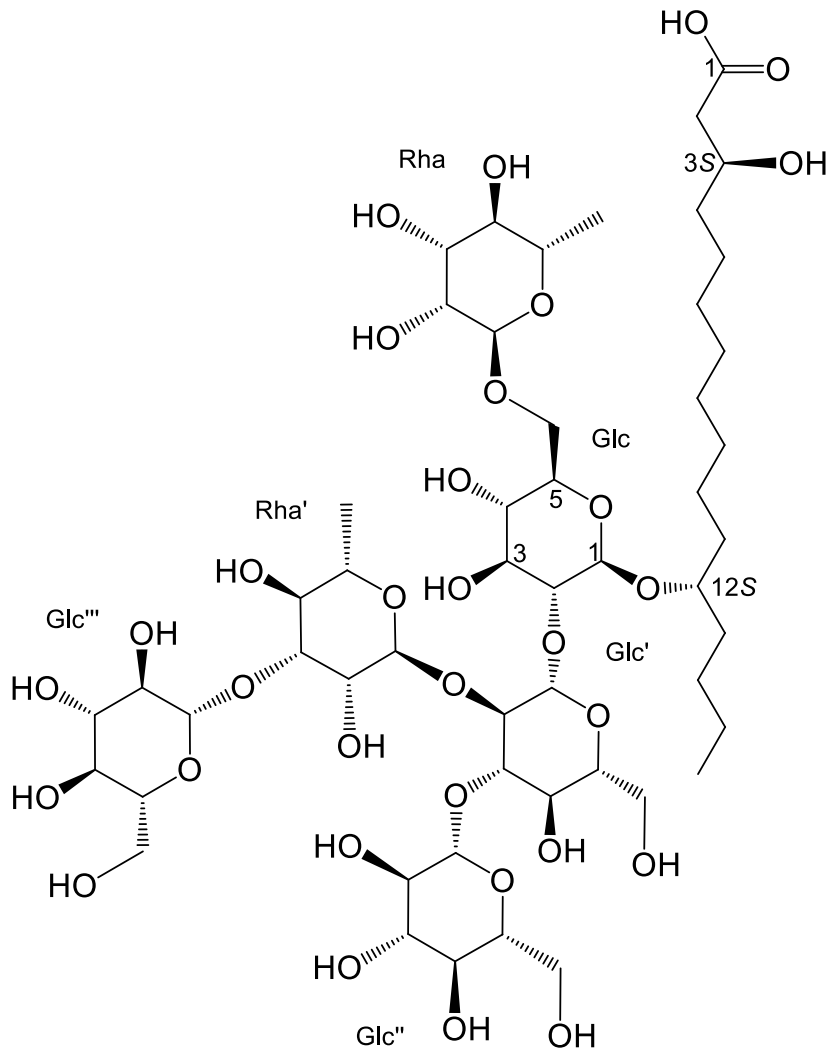
Figura 16. Estructura química del ácido operculínico H.

A partir de los estudios fitoquímicos realizados a la raíz de jalapa brasileña, se han estudiado distintas especies del género *Operculina*, empleadas en la herbolaria del Viejo Mundo. Tal es el caso de la raíz de jalapa de la India (*O. turpethum* Silva Manso), una especie ampliamente distribuida en el sudeste asiático, Australia e Islas del Pacífico, cuyas raíces y tallos se utilizan como laxantes y para el tratamiento de quemaduras, ictericia y dolores musculares o articulares. En los primeros estudios realizados al extracto hidrolizado de la fracción de la raíz, rica en resinas glicosídicas, permitieron el aislamiento de los ácidos turpetínicos A-E (Fig. 16), como primeros ejemplos de glicolípidos con ácidos grasos hidroxilados en la posición C-12.[38]

	R₁	R₂	n
Ácido turpetínico A:	OH	H	1
Ácido turpetínico B:	H	OH	2
Ácido turpetínico C:	H	OH	1
Ácido turpetínico D:	OH	H	2

Ácido turpetínico E
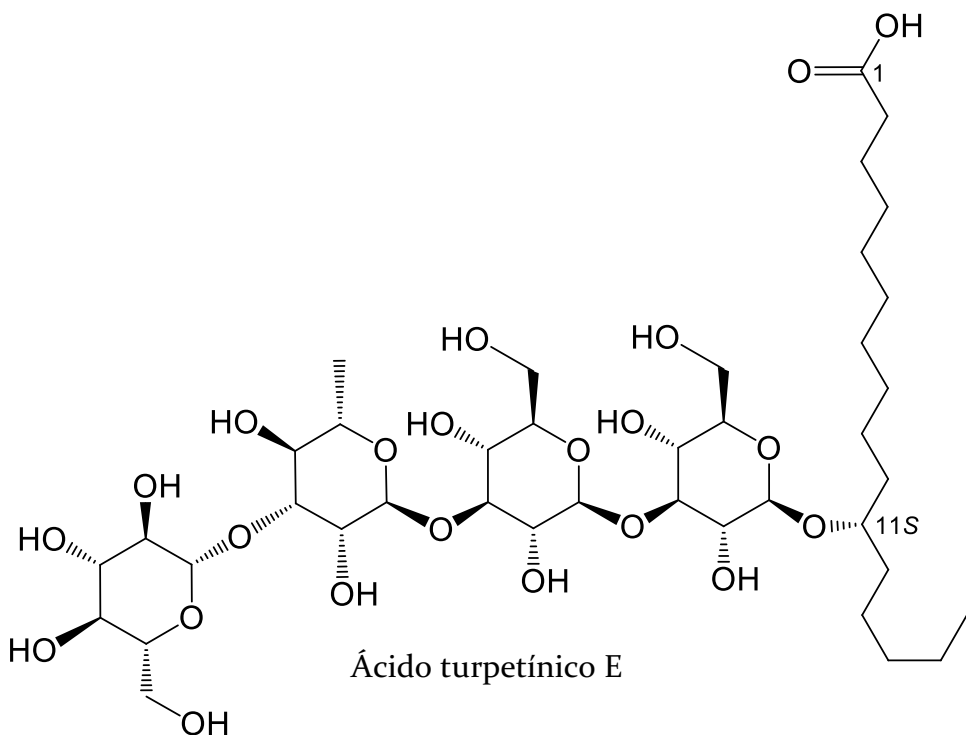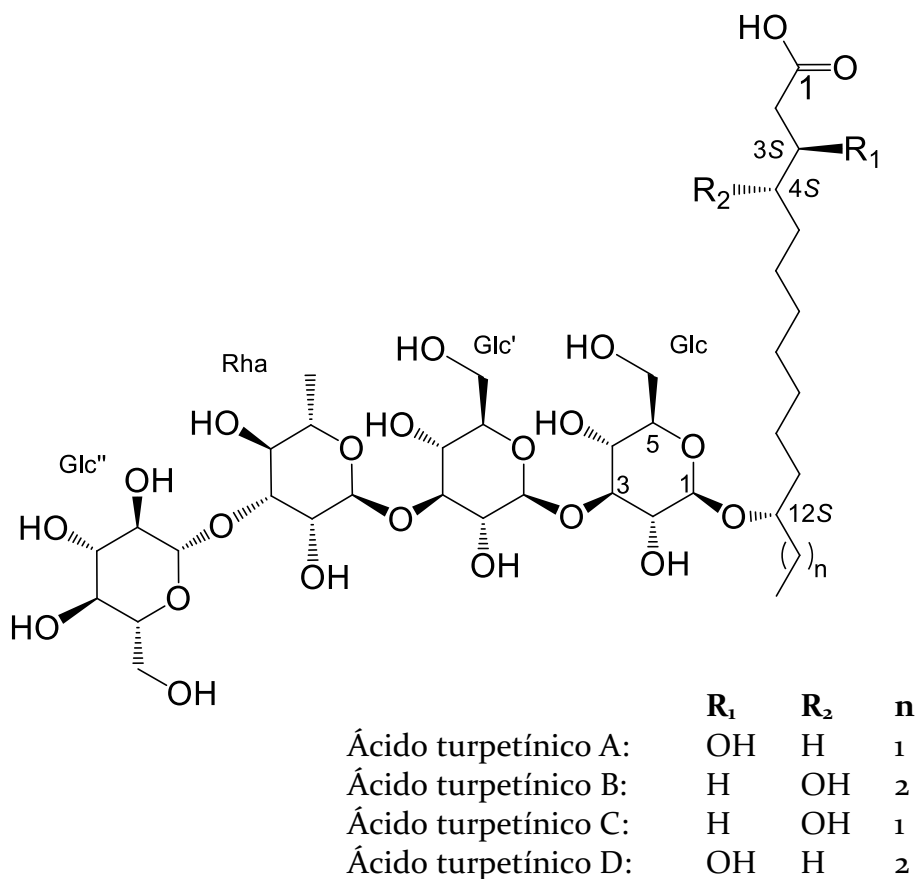
Figura 17. Ácidos glicosídicos aislados de la raíz de jalapa india (*Operculina turpethum*).

El estudio reciente al extracto de jalapina de las partes aéreas de la jalapa de la India, se aislaron tres nuevos núcleos lipopentasacáridos, denominados ácidos turpéticos A-C, los cuales, están compuestos por 3 unidades de ramnosa y 2 de glucosa, y residuos de ácido 12*S*-hidroxipentadecanoico, 12*S*-hidroxihexadecanoico y 12*S*-hidroxiheptadecanoico, respectivamente (Fig. 17). Asimismo, se han aislado los turpetósidos A y B, como sistemas macrocíclicos de los ácidos turpéticos A y B, respectivamente, compartiendo en sus estructuras dos residuos de 2-metil butanoilo y un residuo de tigloilo.[39]

	n
Ácido turpético A:	2
Ácido turpético B:	3
Ácido turpético C:	4

	n
Turpetósido A:	2
Turpetósido B:	3
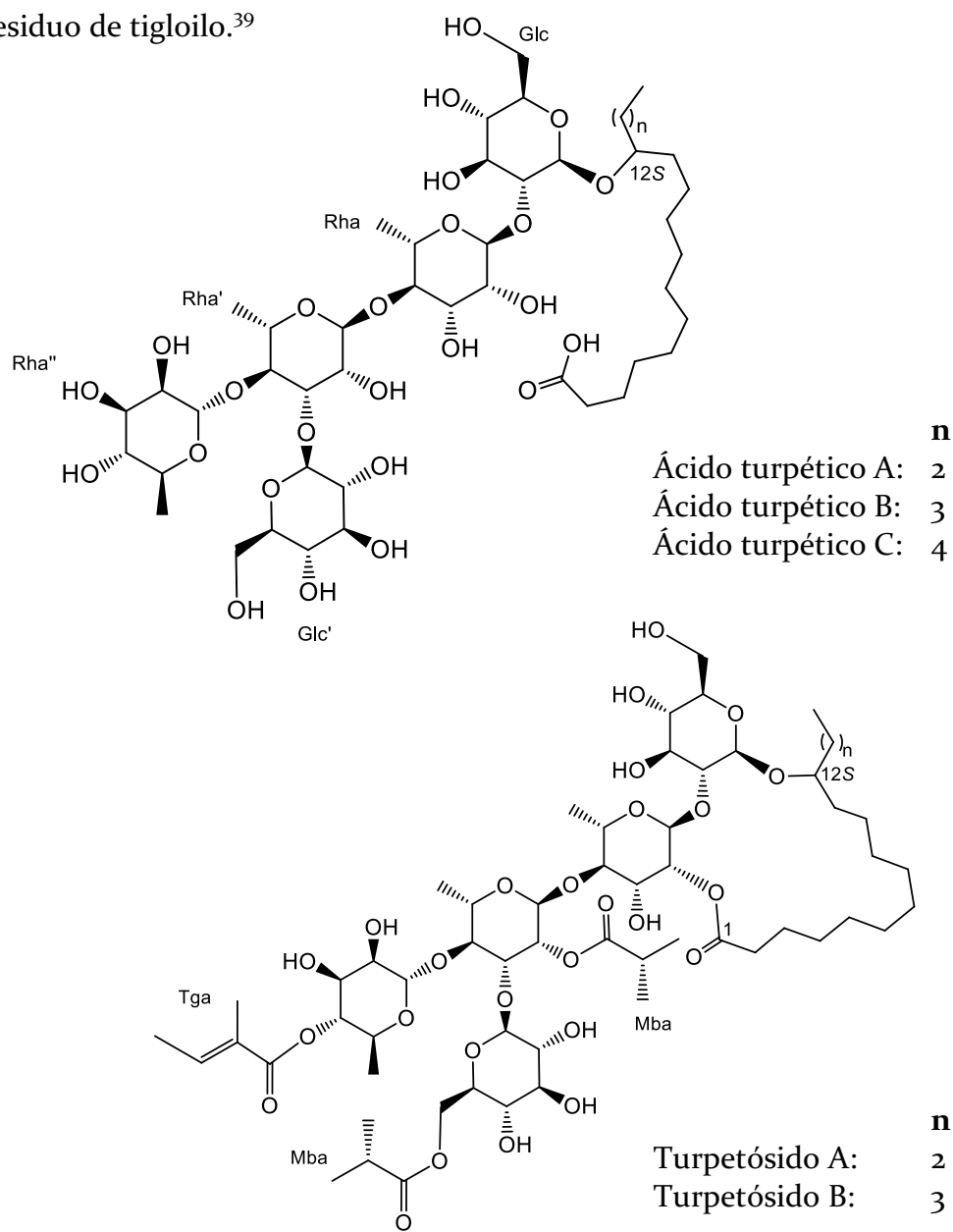
Figura 18. Glicolípidos intactos aislados de la raíz de jalapa de la India (*Operculina turpethum*).

En años recientes, se han aislado moléculas similares al ácido operculínico H en especies vegetales de la familia de las convolvuláceas, tales como la enredadera de campo (*Convolvulus arvensis* L.), una especie rastrera de origen europeo, utilizado en la medicina tradicional china como regulador de la menstruación y activador de la circulación sanguínea. A partir de la hidrólisis alcalina de la fracción rica en resinas glicosídicas del extracto total de la planta, se aislaron los ácidos arvénsicos A-D (Fig. 18), un núcleo lipoheptasacárido compuesto por cuatro unidades de glucosa, dos unidades de ramnosa y una unidad de fucosa, y un residuo de los ácidos mono o dihidroxipentadecanoicos y hexadecanoicos. Todavía, no se ha aislado algún compuesto macrocíclico de naturaleza glicolipídica que presente alguno de estos nuevos núcleos oligosacáridos.[40]

	R	n
Ácido arvénsico A:	H	1
Ácido arvénsico B:	H	2
Ácido arvénsico C:	OH	1
Ácido arvénsico D:	OH	2
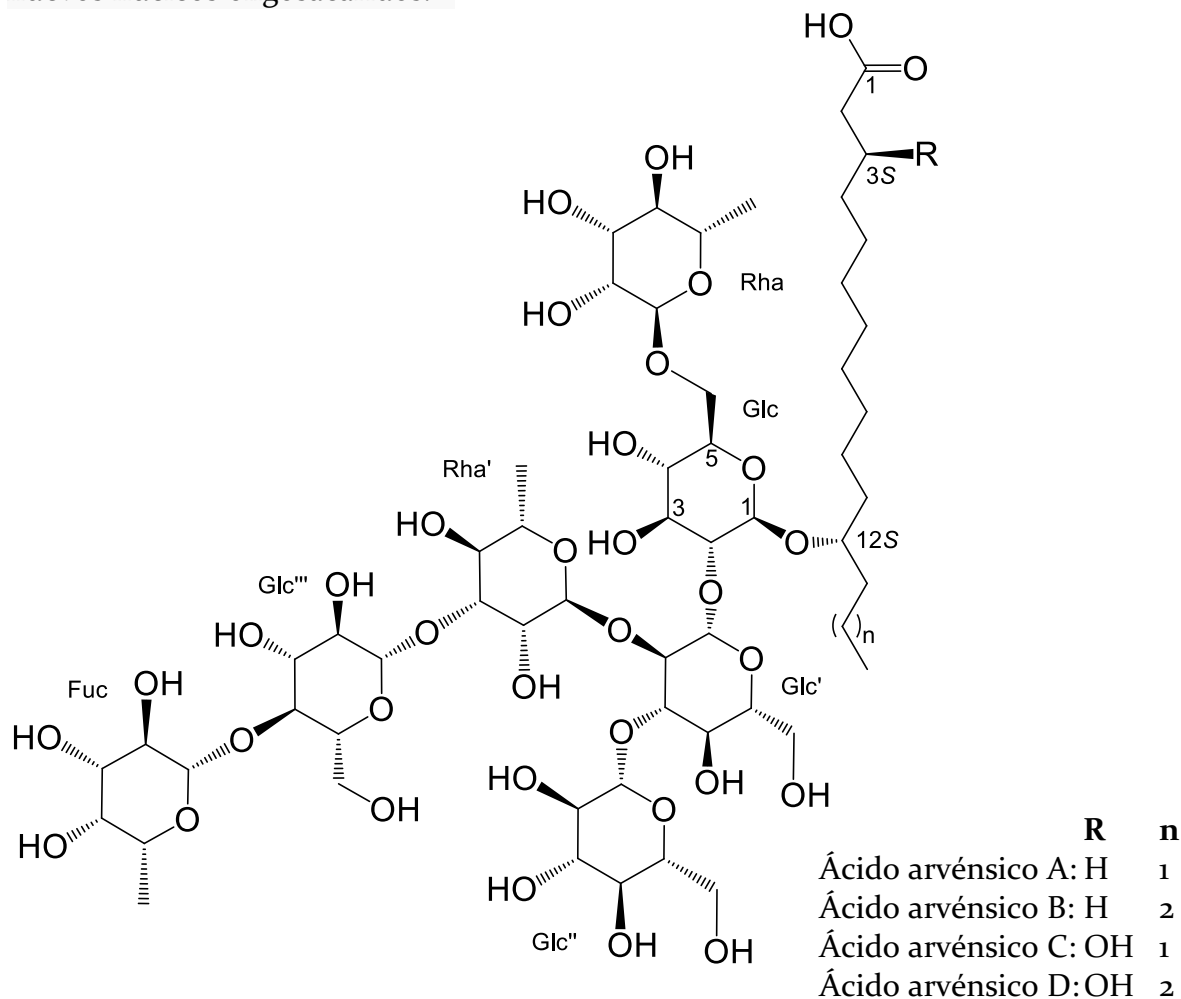
Figura 19. Ácidos glicosídicos aislados de la enredadera de campo (*Convolvulus arvensis*).

3.   Análisis químico-biológico de las resinas glicosídicas

La complejidad de las mezclas de glicolípidos presentes en los extractos vegetales confieren un cierto grado de dificultad para su análisis fisicoquímico, tanto por su comportamiento anfifílico en solución, como por la presencia de compuestos isoméricos de posición y/o estereoisoméricos (diastereoisómeros y epímeros); por lo cual, su separación, aislamiento y purificación requiere tanto del uso de técnicas analíticas instrumentales modernas, como de reacciones de degradación (hidrólisis ácida, saponificación) y/o derivatización (peracetilación, permetilación o esterificación) para realizar esta labor de manera óptima.[16]

En las últimas tres décadas, la cromatografía de líquidos de alta resolución (HPLC, por sus siglas en inglés) es una de las técnicas instrumentales más empleadas para el aislamiento y la purificación de los productos naturales, considerando su versatilidad para el desarrollo de condiciones instrumentales adecuadas de separación (como son las fases estacionaria y móvil, elución de modo isocrático o en gradiente y volumen de carga) al aprovechar las características fisicoquímicas de los compuestos de interés. Para los glicolípidos, estas condiciones se han adecuado principalmente al principio de la cromatografía de líquidos en fase reversa (RP-HPLC) para el fraccionamiento primario y el aislamiento de estos compuestos.[16, 40] Aunado a las condiciones de separación, la purificación de los glicolípidos mediante HPLC, se ha llevado a cabo exitosamente gracias a la técnica de reciclaje, que se realiza mediante la incorporación de una válvula de reciclaje adicional en un equipo cromatográfico a nivel preparativo o semipreparativo, que recircula a los picos de baja resolución hacia la columna de separación, para facilitar la separación de los compuestos con tiempos de retención y de factor de capacidad similares presentes en el eluato, hasta la observación de una resolución adecuada de los picos (Fig. 19). Adicional a esto, otra ventaja que supone el uso de esta técnica es que no requiere el uso de una mayor cantidad de fase móvil preparada en el momento.[41]

A
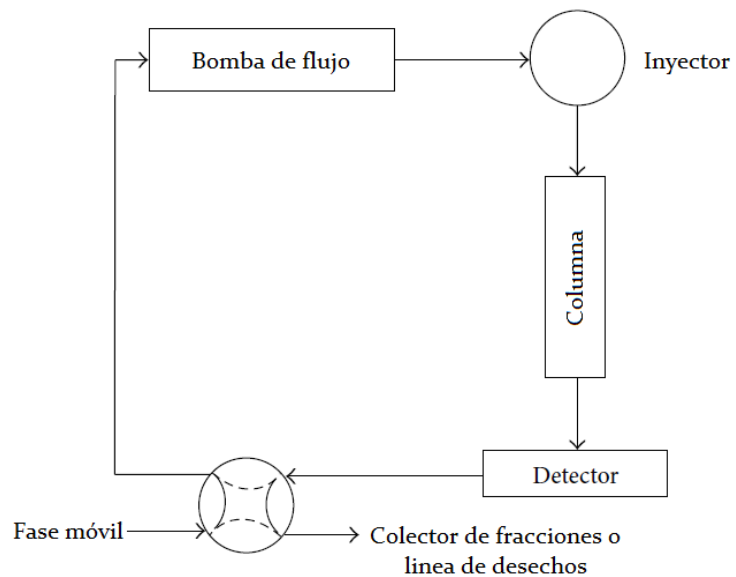
B
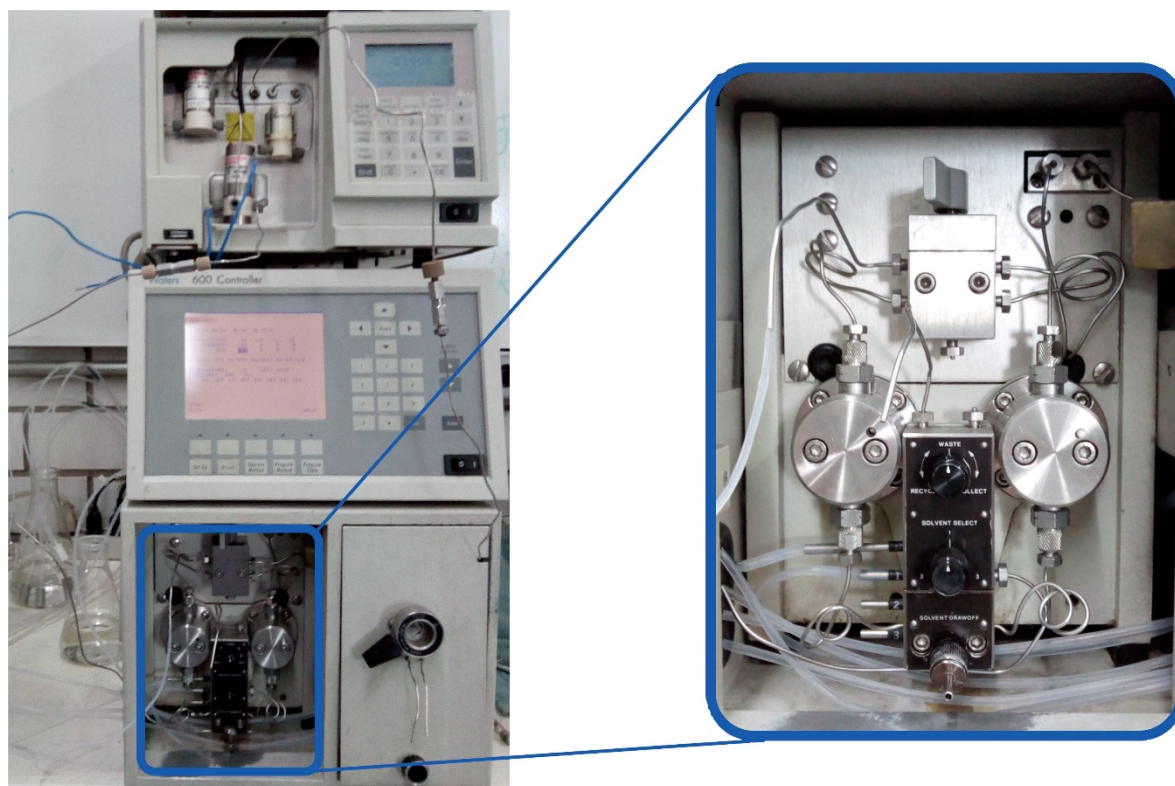
Figura 20. A. Diagrama del sistema de reciclaje para un equipo de cromatografía de líquidos de alta resolución (HPLC) B. Sistema de reciclaje de un equipo HPLC nivel semipreparativo.

Tras la obtención de los glicolípidos purificados, ya sea como productos intactos o químicamente modificados, se realiza su elucidación estructural mediante técnicas espectroscópicas como la resonancia magnética nuclear (NMR, por sus siglas en inglés), cuyos espectros monodimensionales permiten determinar la complejidad de la cadena oligosacárida, considerando las señales de los centros anoméricos de los monosacáridos que forman grupos de tipo acetálico (δ_H 4.5 - 7.0 ppm, δ_C 90 - 110 ppm) y determinan el número de unidades presentes en la cadena oligosacárida, mientras que los carbonos carbonílicos de los ácidos orgánicos que esterifican a la cadena oligosacárida, determinan el número y tipo de ácidos orgánicos presentes en el compuesto (δ_C 160 - 180 ppm); por último, los espectros bidimensionales de tipo homonuclear ^{1}H-^{1}H (COSY, TOCSY, NOESY) y heteronuclear ^{1}H-^{13}C (HSQC, HMBC) facilitan la observación de las secuencias de esterificación y glicosidación.[16]

Adicional al uso de la resonancia magnética nuclear, la técnica de la espectrometría de masas (MS, por sus siglas en inglés), es un auxiliar de la elucidación estructural de los glicolípidos intactos y/o saponificados, gracias al empleo de técnicas de ionización suave como la técnica de electrospray (ESI, por sus siglas en inglés), cuyos espectros permiten determinar el peso del compuesto a través de los iones protonados, desprotonados o cationizados, así como, inferir la presencia de los ácidos orgánicos y de los monosacáridos que forman parte del glicósido, por el cálculo de los pesos de los fragmentos generados por las rupturas de los enlaces tipo éster y glicosídico.[16]

Gracias a la descripción de las actividades purgantes y laxantes de las resinas glicosídicas presentes en los extractos de las especies vegetales anteriormente descritas, los estudios referentes a la actividad biológica de los glicolípidos sobre el sistema digestivo han permitido dilucidar el mecanismo de desequilibrio osmótico por inhibición de la expresión de la acuaporina 3 (AQP3), una proteína transmembranal que forma un poro celular para la difusión pasiva de agua y glicerol a través del epitelio

intestinal. Esta inhibición desencadena una respuesta de estrés celular mediado por inductores de la inflamación aguda, tales como las enzimas ciclooxigenasa-2 (COX-2) y el factor nuclear KB, y el eicosanoide prostaglandina E_2 (PGE_2) y, en conjunto, provocan la respuesta diarreica tras la administración oral de estos compuestos.[42]

En años recientes, se han evaluado otras actividades biológicas relacionadas con los glicolípidos, tales como las alelopáticas (inhibidores de la germinación de semillas)[16]; así como, sus propiedades terapéuticas como agentes antifúngicos[43], antimicrobianos[44, 45], antivirales[46], citotóxicos[47], ionoforéticos[48] e inhibidores de la actividad de la enzima α-glucosidasa[49] y, más recientemente, como moduladores de la actividad de la glicoproteína-P o factor de resistencia múltiple a fármacos (MDR1), una bomba de eflujo de naturaleza proteíca transmembranal dependiente del trifosfato de adenosina (ATP), que se encuentra expresada en las células endoteliales de los capilares del cerebro (barrera hematoencefálica) y del epitelio intestinal, así como, en las células cancerosas; y cuya función es la regulación de la excreción de fármacos, entre los que destacan agentes antituberculosos, antibióticos, antivirales, cardiotónicos, esteroidales, inmunosupresores, opioides, por citar algunos. En el caso de las neoplasias, se sabe que esta glicoproteína transmembranal es la determinante para el fenómeno de la resistencia cruzada a una gran variedad de quimioterápicos antineoplásicos (actinomicina D, doxorrubicina, etopósido, irinotecán, paclitaxel, alcaloides de la vinca, entre otros), por lo que, se han considerado como posibles candidatos para el diseño de novedosos medicamentos, que en terapias combinatorias, sean capaces de inhibir la actividad de la MDR1 para revertir el fenotipo de la resistencia a fármacos antitumorales y, en consecuencia, potenciar la actividad de los agentes antineoplásicos comerciales, ante neoplasias resistentes a la quimioterapia.[50]

BIBLIOGRAFÍA

1. Waizel-Bucay, J. Capítulo 11. *Las plantas en la Historia de la Medicina*. En: Waizel-Bucay, J. (ed.) *Las plantas medicinales y las ciencias Una visión mutildisciplinaria*. 1ª ed. Ed. Instituto Politécnico Nacional. México, 2008. pp. 181-182.

2. Langenheim, J.H. *Chapter 11: Miscelaneous Resins*. En: Langenheim, J.H. (ed.) Plant Resins: Chemistry, Evolution, Ecology and Ethnobotany. Ed. Timber Pass. Portland-Cambridge, 2003. pp. 418-421.

3. Pereda-Miranda, R., Fragoso-Serrano, M., Escalante-Sánchez, E., Hernández-Carlos, Linares, E., Bye, R. 2006. J Nat Prod 69: 1460-1466.

4. Bye, R., Linares, E. *Códice de la Cruz-Badiano*. Revista Arqueología Mexicana Edición Especial 50. México, 2013. pp. 8-14.

5. Yepez-Basurto, M. Capítulo 3. *Introducción a la Taxonomía Vegetal*. En: Waizel-Bucay, J. (ed.) *Las plantas medicinales y las ciencias Una visión mutildisciplinaria*. 1ª ed. Ed. Instituto Politécnico Nacional. México, 2008. pp. 69-79.

6. Linares, A., Rico-Gray, V., Carrión, G. 1994. Econ Bot 48: 84-89.

7. García Ballester, L. Enfermo y enfermedad en la obra de Galeno. *Medicina e Historia, 3ª época, 1, 10.* Publicación Médica Bihorm, Barcelona. 1985. 16 p.

8. López Piñero, J.M., López Terrada, M.L. *La Influencia Española en la Introducción en Europa de las Plantas Americanas (1493-1623)*. Cuadernos Valencianos de Historia de la Medicina y de la Ciencia. Universitat de Valencia, España, 1997. 214 pp.

9. Lorenzi, H, Abreu-Matos, F.J., *Plantas medicinais no Brasil. Nativas e exóticas*. Ed. Instituto Plantarum. Brasil, 2002. pp. 183-184.

10. Ono, M. 2017. J Nat Med *71*(4): 591-604.

11. German-Ramírez, M.T. Capitulo 15: Los principales grupos de vegetales. II. Las fanerógamas o espermatofitas. En: Waizel-Bucay, J (ed.) *Las plantas medicinales y las ciencias. Una visión multidisciplinaria.* Ed. Instituto Politécnico Nacional. México, 2008. pp. 301.

12. Felger, R.S., Austin, D.F., Van Devender, T.R., Sánchez-Escalante, J.J., Costea, M. 2012. Journal of the Botanical Research Institute of Texas 6(2): 459-527.

13.   Farmacopeia de los Estados Unidos do Brasil. 1928

14.   Eick, E. (ed). *Solanaceae and Convolvulaceae Secondary Metabolites. Biosynthesis, Chemotaxonomy, Biological and Economic Significance (A Handbook)*. Springer. Berlin, 2008. pp.215-219.

15.   Streiner, U, Leinster, E. 2018. Planta Medica. 9(2): 751-758.

16.   Pereda-Miranda, R., Rosas-Ramírez, D., Castañeda-Gómez, J. 2010. *Resin glycosides from the morning glory family*. En: Kinghorn, A.D. et. al. (eds.) *Progress in the Chemistry of Organic Natural Products* 92. Springer-Verlag/Wien. New York. pp. 82-83, 142-147.

17.   Asai, T., Fujimoto, Y. 2010. Phytochemistry. *71*(11-12): 1410-1417.

18.   Asai, T., Nakamura, Y., Hirayama, Y., Ohyama, K., Fujimoto, Y. 2012. Phytochemistry. 82: 149-157.

19.   Çalış, İ., Sezgin, Y., Dönmez, A. A., Rüedi, P., & Tasdemir, D. 2007. J. Nat. Prod. 70(1): 43-47.

20.   Yang, Y., Yawen, A. N., Wang, W., Ning, D. U., Zhang, J., Feng, Z., Jiang, J., Zhang, P. 2017. Acta Pharmaceutica Sinica B 7(4): 491-495.

21.   Atkins-Farwell, O. 1918. Journal of the American Pharmaceutical Association (1912). 7(10): 852-855.

22.   Ewing, C. O., Clevenger, J. F. 1918. Journal of the American Pharmaceutical Association (1912). 7(10): 855-858.

23.   Shellard, E. J. 1961. Planta Medica, 9(1): 102-116.

24.   Castañeda-Gómez, J., Pereda-Miranda, R. 2011. J. Nat. Prod. 74: 1148-1153.

25.   Castañeda-Gómez, J., Figueroa-González, G., Jacobo, N., Pereda-Miranda, R. 2013. J. Nat. Prod. 76: 64-71.

26.   Bautista, E., Fragoso-Serrano, M., Pereda-Miranda, R. 2015. J. Nat. Prod. 78: 168-172.

27.   Bautista, E., Fragoso-Serrano, M., Pereda-Miranda, R. 2016. Phytochemistry Letters 17: 85-93.

28. León-Rivera, I., del Río-Portilla, F., Enríquez, R. G., Rangel-López, E., Villeda, J., Rios, M. Y., Navarrete-Vázquez, G., Hurtado-Días, I., Gúzman-Valdivieso, U., Núñez-Urquiza, V., Escobedo-Martínez, C. 2017. Magn Reson Chem 55(3): 214-223.

29. Shellard. E. J. 1961. Planta Medica. 9(2): 141-145.

30. Ono, M., Nishi, M., Kawasaki, T., Miyahara, K. 1990. Chem Pharm Bull. 38(11): 2986-2991.

31. Ono, M., Kawasaki, T., Miyahara, K. 1991. Chem Pharm Bull 39(10): 2534-2539.

32. Ono, M., Fujimoto, K., Kawata, M., Fukunaga, T., Kawasaki, T., Miyahara, K. 1992. Chem Pharm Bull 40(6): 1400-1403.

33. Ono, M., Kawasaki, T., Miyahara, K. 1989. Chem Pharm Bull 37(12): 3209-3213.

34. Ono, M., Fukunaga, T., Kawasaki, T., Miyahara, K. 1990. Chem Pharm Bull 38(10): 2650-2655.

35. Ono, M., Nishioka, H., Fukushima, T., Kunimatsu, H., Mine, A., Kubo, H., & Miyahara, K. 2009. Chem Pharm Bull 57(3): 262-268.

36. Lawson, E. N., Jamie, J. F., Kitching, W. 1992. J Org Chem 57(1): 353-358.

37. Ono, M., Oda, S., Yasuda, S., Mineno, T., Okawa, M., Kinjo, J., Miyahara, H., Yoshimitsu, H, Nohara, T., Miyahara, K. 2017. Chem Pharm Bull 65(1): 107-111.

38. Wagner, H., Wenzel, G., Chari, V.M. 1978. Planta Medica 33(2), 144-151.

39. Ding, W., Jiang, Z., Wu, P., Xu, L., Wei, X. 2012. Phytochemistry 81: 165-174.

40. Fan, B.Y., Lu, Y., Yin, H., He, Y., Li, J.L., Chen, G.T. 2018. Fitoterapia 131: 209-214.

41. Sidana, J., Joshi, L. K. 2013. Chromatography Research International, 2013. DOI: 10.1155/2013/509812

42. Zhu, D., Chen, C., Bai, L., Kong, L., Luo, J. 2019. Evidence-Based Complementary and Alternative Medicine 2019. DOI: 10.1155/2019/9406342

43. Castelli, M.V., Cortés, J.C., Escalante, A.M., Bah, M., Pereda-Miranda, R., Ribas, J.C., Zacchino, S. A. 2002. Planta Medica 68(8): 739-742.

44. Pereda-Miranda, R., Kaatz, G.W., Gibbons, S. 2006. J Nat Prod 69(3): 406-409.

45. Corona-Castañeda, B., & Pereda-Miranda, R. 2012. Planta Medica 78(2): 128-131.

46. Ono, M., Takigawa, A., Kanemaru, Y., Kawakami, G., Kabata, K., Okawa, M., Kinjo, J., Yokomizo, K., Yoshimitsu, H., Nohara, T. 2014. Chem Pharm Bull 62(1): 97-105.

47. Fan, B.Y., Li, Z.R., Ma, T., Gu, Y.C., Zhao, H.J., Luo, J.G., Kong, L.Y. 2015. J Funct Foods 19: 141-154.

48. Pereda-Miranda, R., Villatoro-Vera, R., Bah, M., Lorence, A. 2009. Rev Latinoamer Quim 37: 144.

49. Rosas-Ramírez, D., Escandón-Rivera, S., Pereda-Miranda, R. 2018. Phytochemistry 148, 39-47.

50. Figueroa-González, G., Jacobo-Herrera, N., Zentella-Dehesa, A., Pereda-Miranda, R., 2012. J. Nat. Prod. 75: 93–97.

JUSTIFICACIÓN

Los estudios fitoquímicos realizados a varias especies de la familia de las convolvuláceas empleadas en la medicina tradicional latinoamericana han reconocido a los compuestos glicolipídicos –las resinas glicosídicas– como los responsables de las actividades terapéuticas relacionadas con su uso. Tal es el caso del complejo de la raíz de jalapa brasileña (*Operculina macrocarpa* y *O. hamiltonii*), cuyo uso tradicional como un remedio laxante y purgante se asocia con la presencia de dichos compuestos en sus extractos y, por lo tanto, se reconoció como un sucedáneo de la raíz de jalapa oficinal (*Ipomoea purga*) y de sus congéneres mexicanas (*I. orizabensis e I. stans*).

Estas complejas mezclas de compuestos de elevado peso molecular que constituyen las convolvulinas –resinas glicosídicas solubles en metanol– presentan severas dificultades para su purificación debido a su alta polaridad, quedando justificado en diversos estudios previos el empleo de reacciones químicas –principalmente degradativas– para facilitar el aislamiento y la elucidación estructural de los compuestos derivados. Asimismo, no hay registros en la literatura especializada sobre la evaluación del potencial modulador sobre la resistencia a fármacos en células de mamíferos para esta clase de compuestos anfipáticos y que podría proporcionar indicios sobre los requerimientos estructurales de las resinas glicosídicas y su correlación como agentes de reversión del fenotipo resistente en células tumorales humanas.

Por lo tanto, se plantea en la presente disertación el desarrollo de un estudio profuso para el análisis químico y biológico –evaluación citotóxica y moduladora de la resistencia múltiple a fármacos– de los componentes presentes en la fracción de naturaleza polar del extracto de *O. macrocarpa*.

OBJETIVO GENERAL

Analizar y determinar los compuestos glicolipídicos presentes en la fracción soluble en metanol del extracto de la raíz de la jalapa brasileña de flores blancas (*O. macrocarpa*) mediante la utilización de técnicas instrumentales cromatográficas, espectroscópicas y espectrométricas; y evaluar el potencial modulador de cada compuesto sobre el fenómeno de la resistencia múltiple a fármacos a traves de un método *in vitro*.

OBJETIVOS ESPECÍFICOS

1.-Identificar los componentes glicolipídicos mayoritarios y minoritarios de la fracción soluble en metanol, mediante reacciones de degradación y derivatización.

2.-Realizar la separación, el aislamiento y la purificación de los compuestos glicolípidicos de la fracción metanólica intacta, empleando técnicas instrumentales como la cromatografía de líquidos de alta resolución (HPLC) y aplicando las técnicas de reciclaje de pico, rasurado de pico y corte de núcleo.

3.-Establecer la estructura química de los compuestos aislados mediante el empleo de técnicas espectroscópicas (resonancia magnética nuclear mono y bidimensional) y espectrométricas de alta resolución (HRESIMS).

4.-Evaluar el potencial modulador de cada compuesto aislado y sus derivados, mediante un modelo *in vitro* en células de carcinoma mamario resistentes a vinblastina (MCF-7/Vin).

CAPÍTULO I

Resinas glicosídicas de la raíz de
Operculina macrocarpa (jalapa brasileña)
con actividad purgante

Journal of Natural Products

Factor de Impacto: 4.257

Resin Glycosides from the Roots of *Operculina macrocarpa* (Brazilian Jalap) with Purgative Activity

Jesús Lira-Ricárdez,[†] Rogelio Pereda-Miranda,*[,†] Jhon Castañeda-Gómez,[‡] Mabel Fragoso-Serrano,[†] Rosineide Costa Simas,[§] and Suzana Guimarães Leitão[§]

[†]Departamento de Farmacia, Facultad de Química and Programa de Maestría y Doctorado en Ciencias Químicas, Universidad Nacional Autónoma de México, Ciudad Universitaria, Mexico City 04510, Mexico

[‡] Grupo Químico de Investigación y Desarrollo Ambiental. Programa de Licenciatura en Ciencias Naturales y Educación Ambiental, Facultad de Educación. Universidad Surcolombiana, Neiva, Colombia

[§]Faculdade de Farmacia, Universidade Federal do Rio de Janeiro, CCS, Bloco A, Ilha do Fundão, 21941-902, Rio de Janeiro, Brazil

ABSTRACT: Analysis of the methanol-soluble resin glycosides from the roots of *Operculina macrocarpa* was assessed by generating NMR profiles of five glycosidic acids obtained through saponification, acetylation, and recycling HPLC purification. Operculinic acid H (**1**), two novel hexasaccharides, operculinic acids I (**2**) and J (**3**), the known purgic acid A (**4**), as well as a quinovopyranoside of (-)-(7*R*)-hydroxydecanoic acid, operculinic acid K (**5**), were isolated. Three intact resin glycosides related to **1**, the novel macrocarposidic acids A (**6**) and B (**7**), in addition to the previously known macrocarposidic acid C (**8**), were also purified with isovaleroyl, tigloyl, and exogonoyl [(3*S*,9*R*)-3,6:6,9-diepoxydecanoyl] groups as esterifying residues. A selective intramolecular lactonization was produced to generate a macrocyclic artefact (**17**) during acetylation of **1**, resembling the distinctive structure of the Convolvulaceous resin glycosides.

Plant members of the purgative Brazilian jalap complex (popularly known as "jalapa-do-Brasil", "batata-de-purga", "jalapão", and "batatão" in Portuguese) have been recognized as species belonging to the genus *Operculina* (Figure 21, and S1 Supporting Information). Currently, the precise identification of the officinal Brazilian laxative roots corresponds to *O. macrocarpa* (L.) Urb. (syns. *Convolvulus macrocarpus* L. and *Ipomoea operculata* Mart.).[1] In recognition of their therapeutic benefits, similar to those of the Mexican jalaps, namely, *I. purga* (the officinal jalap) and its congeners or false jalaps (*I. orizabensis* and *I. stans*),[2] the settlers of South America conferred the

Figure 21. Brazilian jalap root: crude drug, powders, and phytopharmaceuticals. Brazilian jalap continues to be extensively traded for medicinal purposes in the Brazilian Northern regions as crude drug, in addition to many products made with the roots and the resin glycoside contents: A) Roots; B) Dried-roots cut into slices; C) Commercialized powders, pulverized "batatão" and "jalapa" for sale in a public market; D) Syrup of batatão (Hypolito), hydro-alcoholic extracts (Sobral Pharmaceutical Industry) and pills. All products were purchased at the Mercado 2000, Santarém, Pará, Brazil in september 2015.

common name of "jalapa" to this bindweed with white flowers and resin-producing acrid-tasting tuber-shaped roots restricted to the Northeastern and Southeastern states of Brazil.[1c]

The first references to the use of these roots in Brazil can be traced back more than three centuries with the name of mechoacam[1c] (Figure 22 and S2, Supporting Information), after one of the Mexican jalap roots which was well known in Europe since its introduction in the 16th century as "Indian rhubarb" or "Michoacan root" (*Convolvulus mechoacan* or *I. jalapa*). Its effects are similar, although considered moderate in potency, to those of skammonia or scammony (*Convolvulus scammonea*), a native species from the Eastern Mediterranean and the Near East, which was important to medieval medicine and has been used since pre-Christian times throughout the Roman Empire. These New World morning glories were also accepted as a succedaneum of the scammony root.[3] The Portuguese and Spanish colonizers introduced to their possessions in the Americas European galenic medicine, with laxatives possessing a great therapeutic importance. Thus, Brazilian jalap species, as occurred with Mexican jalaps[2c] in the Spanish empire, were accepted and widely in Brazil, because they have moderate effects as depuratives and laxatives, and then continued to be traded extensively in the Northern and Northeastern Brazilian regions.

Ethnobotanical and phytopharmaceutical publications[4] quote the uses of Operculina species as purgative, anthelmintic, blood purifier, skin cleanning, anti-stroke remedies, and as a treatment for uterine infection in the form of dried root

slices (crude drug). Moreover, many products have been made with their roots and/or resin glycoside contents, which include powders, pills, syrups, hydro-alcoholic extracts, and tinctures with some other herbal ingredients for oral administration (Figure S1, Supporting Information).[1] Resin glycosides have shown the ability to increase membrane permeability and transport on both cations (Na^+, K^+, and Ca^{2+} ions) and anions (Cl^-), which could trigger an imbalance in cellular homeostasis through pore-forming activity.[5] This could be the mechanism of action for the cathartic activity of resin glycosides, acting as osmotic laxatives,[5a] which cause an increase in water elimination and in peristalsis of the intestine via a decreased expression of aquaporin 3 in colon cells and activation of the pro-inflammatory nuclear factor κB–NF and cyclooxygenase (COX-2) pathways.[5b]

Phytochemical studies of *Operculina* species have shown that resin glycosides are the principal chemical entities found in the root extracts of these medicinal plants, which represent a mixture of some different glycolipids formed by monohydroxy and dihydroxy long-chain fatty acids (C_{15}-C_{17}) bonded to linear or branched heteropolysaccharides.[6-11] Three glycosidic acids, turpethic acids A-C, and two macrocyclic resin glycosides, turpethosides A and B, all having a common pentasaccharide moiety composed by two units of D-glucose and three moieties of L-rhamnose with 12-hydroxy fatty acid aglycones of different chain lengths, were obtained from the aerial parts of the Indian jalap, *O. turpethum*.[11] The ether-soluble resin glycosides (the jalapin fraction) of *O. macrocarpa* were first analyzed through saponification, where *n*-decanoic and *n*-dodecanoic acids were identified as the
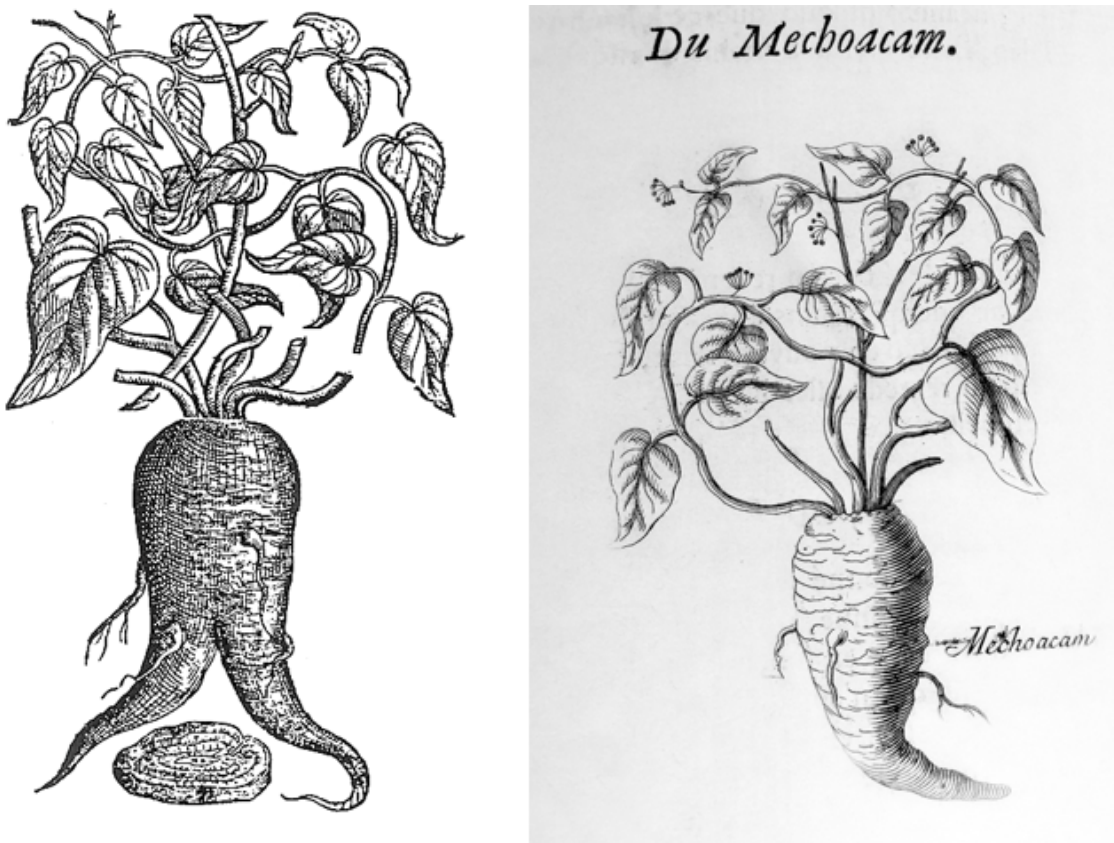
Figure 22. Illustrations of the root of Michoacan in European herbals. Left: XVI century European woodcut print of the root of Michoacan (*Ipomoea jalapa*) which because of the mildness of its effects became popular in herbal medicine as a New World substitute for the drastic purgative scammony (From Gerald's *Herbal*. London. J. Norton, 1597). Right: The root of Michoacan (Mechoacam) is described among the Brazilian medicinal plants by the French naturalist Pierre Pomet in his work *Histoire Générale des Drogues, Traitant de Plantes, des Animaux, & des Mineraux* (1694). In the Descriptive Collection of Plants from Ceará (*Coleção Descritiva das Plantas da Capitania do Ceará*) published by J. S. Feijó in 1799, the use of jalap root is indicated by the vernacular name of michoacam; thus, this reference is one of the oldest on the traditional utilization of "batata de purga" in Northeastern Brazil.

esterifying residues, and operculinic acids A-G as the glycosidic acid cores, with all of them constituted by the same aglycone, jalapinolic acid ($11S$-hydroxyhexadecanoic acid), and different tetra- and pentasaccharides conformed by D-glucose, L-rhamnose, D-fucose, and D-xylose moieties.[7] Operculins I-XVIII were isolated as macrolactone-type resin glycosides from this lipophilic fraction.[8] From the convolvulin fraction (ether-insoluble resin glycosides), recently analyzed by saponification, acetic, *n*-pentanoic, 2-methylbutanoic, 3-methylbutanoic, (*2E*)-methylbut-2-enoic (tiglic), and

48

3,6:6,9 diepoxydecanoic (exogonic) acids were characterized as the esterifying residues of operculinic acid H (**1**), the major glycosidic acid core, this is composed of operculinolic acid (3S,12S-dihydroxyhexadecanoic acid), as the aglycone, and a hexasaccharide core formed by four units of D-glucose and two L-rhamnose moeties.[9] Recently, a mild methanolysis-processed convolvulin fraction was analyzed by HPLC techniques and four epimeric mixtures of resin glycoside methyl esters (**8-11**) were isolated with well-preserved isovaleroyl, tigloyl, and exogonoyl esterifying residues of compound **1**, as the oligosaccharide core.[10]

As part of a continuing effort to elucidate the structural diversity of the Convolvulaceous resin glycosides as potential modulators of efflux pumps in multidrug resistant (MDR) Gram-positive[12] and -negative bacteria,[13] as well as in mammalian cancer cells,[14] the present study was conducted to contribute to the chemical analysis of the glycosidic acid content of the officinal Brazilian jalap. Operculinic acid H (**1**), two novel hexasaccharides, operculinic acids I (**2**) and J (**3**), in addition to purgic acid A (**4**) and a monosaccharide, operculinic acid K (**5**), were isolated, as their peracetylated derivatives, by recycling HPLC and characterized from the alkaline hydrolyzed-convolvulin fraction of an authentic root sample of *O. macrocarpa*. Three acylated derivated of operculinic acid H, macrocarpic acids A-C (**6-8**), were also isolated from the intact precipitated resin glycosides. Extensive work was performed exploring 1D and 2D NMR spectra (such as ^{13}C-filtered heteronuclear HSQC and HMBC methods) for assessing the ^{1}H and ^{13}C NMR chemical shifts in order to complete the structure elucidation of the isolated glycosidic acids.

RESULTS AND DISCUSSION

The convolvulin fraction of *O. macrocarpa* was obtained by precipitation with MeOH and saponified to give an organic solvent-soluble acidic fraction and a water-soluble product mixture. GC-MS analysis of the lipophilic acid fraction permitted the identification of 2-methyl-butyric, tiglic, isovaleric, and exogonic acids. The aqueous layer was partitioned with *n*-butanol for obtaining a glycosidic acid-rich organic layer, which was further acetylated to give a residue that was analyzed by TLC (Figure S3, Supporting Information), and resolved by preparative recycling HPLC (Figure S4, Supporting Information).[15] This separation was performed by application of hydrophobic chromatography in reversed-phase medium in order to achieve the purification of the peracetylated oligosaccharides. After saponification of each pure derivative, four minor glycosidic acids (**2-5**), in addition to operculinic acid H (**1**), the principal known glycosidic acid from the Brazilian jalap, were obtained.[9b] Each individual saponified derivative (**1-5**) was hydrolyzed in acid and the monosaccharide reaction mixtures underwent derivatization with L-cysteine to form thiazolidines, which were identified by GC-MS as their TMS ethers. This analysis confirmed the L-series for rhamnose and the D-series for glucose by coelution with derivatized common naturally occurring sugars.

The positive HRESIMS of peracetylated operculinic acid H (**12**, t_R 10.15 min; Figure S4, Supporting Information) showed a sodium adduct ion at *m/z* 2007.73859 [M + Na]$^+$ (mass accuracy +1.0 ppm) with a molecular formula of $C_{88}H_{128}O_{50}Na$, which exhibited a difference of $C_2H_2O_2$ from the sodium adduct ion for the peracetylated operculinic

acid I (**13**; t_R 12.03 min; Figure S4, Supporting Information) at m/z 1949.72595 [M + Na]$^+$ (calcd error: d = -2.6 ppm) with a molecular formula of $C_{86}H_{126}O_{48}Na$ (Figure S23, Supporting Information), indicating the absence of one acetyloxy group as a substituent in **13** (Figure S5, Supporting Information). The positive ESIMS spectrum of peracetylated operculinic acid J (**14**, m/z 1949.72618 [M + Na]$^+$, $C_{86}H_{126}O_{48}Na$ calcd error: δ = -2.5 ppm; Figure S31, Supporting Information) showed the same molecular weight calculated for peracetylated operculinic acid I (**13**). Saponification of both peracetylated derivatives **12** and **13** afforded operculinic acids H (**1**; m/z 1251.54862 [M + Na]$^+$, $C_{52}H_{92}O_{32}Na$ calcd error: δ = +1.8 ppm)[9b] and I (**2**; 1235.55259 [M + Na]$^+$, $C_{52}H_{92}O_{31}Na$ calcd error: δ = +0.9 ppm), respectively. Basic hydrolysis of derivative **14** afforded operculinic acid J (**3**) with a sodium adduct ion at m/z 1235.55359 [M + Na]$^+$ ($C_{52}H_{92}O_{31}Na$ calcd error: δ = +1.7 ppm). Consequently, this analysis indicated the existence of a pair of diastereoisomers for derivatives **13** and **14**.

The structure elucidation of these compounds started with a derivatization process for dereplication of their aglycones since the sugar analysis indicated the presence of the same oligosaccharide in these compounds and, therefore, their aglycones were responsible for the observed differences in mass. The acid hydrolysis of **1-3** also liberated their aglycones, which were isolated and submitted to treatment with diazomethane and trichloromethylsilane to obtain the silylated derivatives of their corresponding fatty acid methyl esters, which were analyzed by GC-MS (Figures S6-S8, Supporting Information).[2c] The mass spectrum for the monohydroxyhexadecanoic acid from **2** showed that the hydroxy group was substituted at the C-12 position (Figure

S7, Supporting Information) since the a-cleavage on either side of the trimethylsiloxyl group gave diagnostic ions at m/z 301 ($[C_{13}H_{24}O_3TMS]^+$) and 159 ($[C_5H_{10}OTMS]^+$), while substitution in **3** was inferred at C-11 (Figure S8, Supporting Information) from the ions at m/z 287 ($[C_{12}H_{22}O_3TMS]^+$) and 173 ($[C_6H_{12}OTMS]^+$).[2c,16] In contrast, the a-cleavages at C-3 and C-12 in 3*S*,12*S*-dihydroxyhexadecanoic (operculinolic) acid from **1** (Figure S6, Supporting Information) afforded fragments at m/z 389 ($[C_{13}H_{23}O_4(TMS)_2]^+$), 175 ($[C_4H_6O_3TMS]^+$), and 159 ($[C_5H_{10}OTMS]^+$). The dextrorotatory optical activities registered for the aglycones of **2** ($[\alpha]^{22}_D$ + 1.0; *c* 0.1, CHCl$_3$) and **3** ($[\alpha]^{22}_D$ + 7.0; *c* 0.1, CHCl$_3$) were in line with the previous observations that monohydroxylated fatty acids with a dextrorotation possess an *S* absolute configuration.[16] Therefore, the aglycone for compound **2** was identified as the previously described 12*S*-hydroxyhexadecanoic acid.[11] For compound **3**, its aglycone was characterized as (11*S*)-hydroxyhexadecanoic acid,[2c] which is the most frequently found aglycone in the morning glory resin glycosides.[4]

The ^{1}H and ^{13}C NMR spectra showed that **1** and **2** (Table 1), as well as their peracetylated derivatives **12-14** (Tables 2 and 3; Figures S9 and S12, Supporting Information), are constituted by the same hexasaccharide moiety formed by four units of D-glucose and two units of L-rhamnose. The chemical shifts for **2** were identical with those previously described for the methyl ester derivative of operculinic acid H (**1**).[9b] The coupling constants for the methine protons, including the anomeric signal, in the oligosaccharide core indicated that all sugar units were in their pyranose forms with a β-configuration for D-glucose in a $^4C_1$ conformation and the α-configuration for

L-rhamnose in a $^1C_4$ conformation.[4] In their ^1H NMR spectra, six anomeric signals in the low-field region were identified. For example, in the ^1H-detected heteronuclear ($^1J_{CH}$) HSQC correlation for **2** (Figure S40, Supporting Information) the following anomeric signals were assigned: Glc-1 (δ_H 4.95, δ_C 102.9), Glc'-1 (δ_H 5.84, δ_C 102.3), Glc''-1 (δ_H 4.94, δ_C 104.9), Glc'''-1 (δ_H 5.45, δ_C 106.4), Rha-1 (δ_H 5.47, δ_C 102.8), and Rha'-1 (δ_H 6.37, δ_C 102.0), which were identical to those determined for **1**.[9b] Glycosylation sites were identified by comparison of the ^1H NMR spectra of **1** and **2** and their peracetylated oligosaccharides (**12** and **13**), since acylation of the free OH groups causes a typical downfield shift (0.5–1.5 ppm) of the hydroxy-substituted geminal protons, while protons directly involved in the glycosidic linkage remain almost unaffected with a very small deshielding effect (0.1-0.4 ppm).[4] Therefore, comparison of the ^1H- and ^{13}C-NMR chemical shifts for **1** and **2** (Table 1) with those registered for their peracetylated derivatives (**12** and **13**; Tables 2 and 3) indicated that signals for Glc-2, Glc-6, Glc'-2, Glc'-3, and Rha'-3 did not exhibit any acylation shift, demonstrating that the sugar linkages were established at these positions. Subsequently, the following key connectivities for the inter-glycosidic linkages were observed in the HMBC experiment of **13** (Figure S30, Supporting Information), which confirmed the proposed sequence of glycosylation: (a) between Agl H-12 (δ_H 3.87) and Glc C-1 (δ_C 101.4); (b) Glc H-1 (δ_H 4.88) and Agl C-12 (δ_C 81.1); (c) Glc' H-1 (δ_H 5.07) and Glc C-2 (δ_C 72.4); (d) Glc' C-1 (δ_C 101.1) and Glc H-2 (δ_H 4.29); (e) Rha' C-1 (δ_C 98.4) and Glc' H-2 (δ_H 4.12); (f) Rha' H-1 (δ_H 5.77) and Glc' C-2 (δ_C 76.5); (g) Rha' H-3 (δ_H 4.83) and Glc''' C-1 (δ_C 101.7); (h) Glc C-6 (δ_C 67.9) and Rha H-1 (δ_H 5.24); (i) Rha C-1 (δ_C 99.1) and Glc H_2-6 (δ_H 3.92 and

4.09); finally, (j) Glc″ C-1 (δ_C 100.1) and Glc′ H-3 (δ_H 4.58). The same connectives were also observed for the oligosaccharide cores of compounds **12** and **14** (Tables 2 and 3; Figures S22 and S35, Supporting Information).
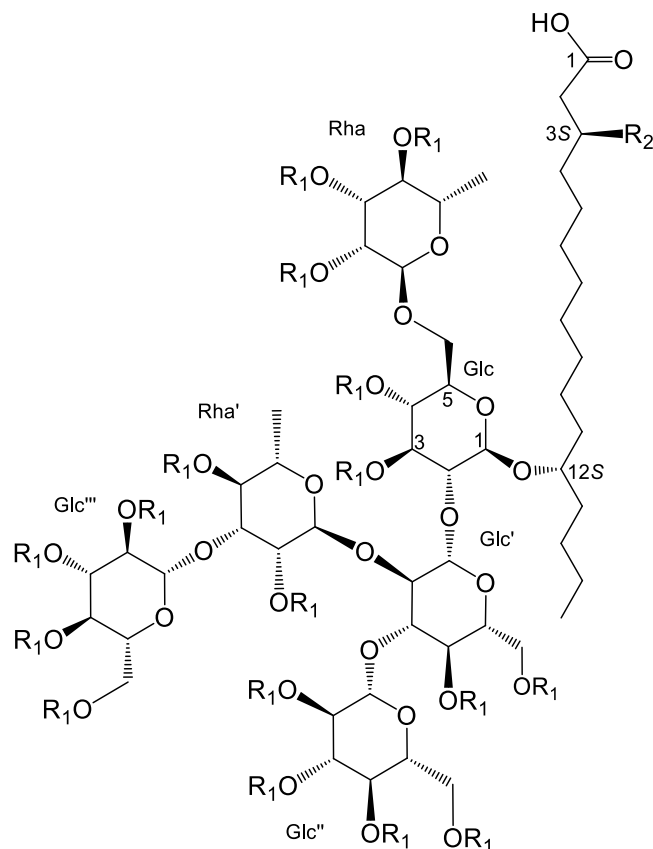
1:	R_1 = H, R_2 = OH	
2:	R_1 = H, R_2 = H	
12:	R_1 = COCH$_3$, R_2 = OCOCH$_3$	
13:	R_1 = COCH$_3$, R_2 = H	

Figure 23. Chemical structures of the operculinic acid H (1), I (2) and their peracetyl derivatives (12 and 13, respectively).

Table 1. ^{1}H and ^{13}C NMR Data of **1** and **2** in C_5D_5N
(800 and 200 MHz, δ in ppm, and J in Hz)

position	1 δ_H	δ_C	2 δ_H	δ_C
Glc-1	4.96 d (7.5)	102.6	4.95 d (7.4)	102.9
2	4.36-4.38	78.9	4.36 dd (7.4, 9.0)	78.9
3	4.57-4.59	79.5	4.59 m	79.7
4	3.91 dd (9.0, 9.0)	72.1	3.88 dd (9.1, 9.1)	72.0
5	4.07-4.02	75.8	4.04 m	76.3
6a	4.06 m	68.3	4.03 m	68.6
6b	4.60 m		4.56	
Glc′-1	5.84 d (7.5)	101.6	5.84 d (7.6)	102.3
2	4.24 dd (9.0, 7.5)	77.5	4.25 dd (7.6, 9.0)	77.6
3	3.94 dd (9.0, 9.0)	89.9	3.95 dd (9.0, 9.0)	90.1
4	3.98 dd (9.0, 9.0)	70.3	3.99 m	72.1
5	3.77-3.80	77.5	3.77 m	77.8
6a	4.17 m	62.7	4.19 m	63.1
6b	4.37 m		4.37 m	
Glc″-1	4.96 d (7.5)	104.5	4.94 d (7.6)	104.9
2	3.95 dd (9.0, 7.5)	75.3	4.03 m	75.2
3	4.23 m	78.7	4.23 m	78.6
4	4.09 m	71.7	4.07 m	72.4
5	4.04 m	78.5	4.02 m	78.9
6a	4.19 m	62.4	4.21 m	62.7
6b	4.57 m		4.56 m	
Glc‴-1	5.44 d (7.6)	106.1	5.45 d (7.3)	106.4
2	4.11 dd (9.0, 7.6)	75.9	4.10 m	76.7
3	4.18 dd (9.0, 9.0)	78.3	4.15 m	78.4
4	4.10-4.08	71.6	4.06 m	70.6
5	3.98 m	78.2	3.99 m	78.8
6a	4.17 m	62.8	4.17 m	63.0
6b	4.46 dd (11.3, 2.4)		4.45 dd (11.7, 2.5)	
Rha-1	5.45 brs	102.4	5.47 brs	102.8
2	4.52 m	72.0	4.59 m	72.6
3	4.52 m	73.2	4.53 dd (8.8, 3.2)	73.5
4	4.27 dd (9.5, 9.5)	74.1	4.27 dd (9.0, 8.8)	74.4
5	5.11 dq (9.5, 6.1)	69.2	4.31 dq (9.0, 6.1)	70.0
6	1.65 d (6.1)	18.8	1.62 d (6.1)	19.0
Rha′-1	6.33 brs	101.9	6.37 brs	102.0
2	5.12 m	71.6	5.11 m	71.8
3	4.85 dd (9.0, 3.1)	83.1	4.86 m	83.4
4	4.51 dd (9.0, 9.0)	72.7	4.53 dd (9.4, 9.4)	73.1
5	5.10 dq (9.9, 6.1)	69.2	5.10 dq (9.4, 6.2)	69.5
6	1.78 d (6.1)	19.0	1.79 d (6.2)	19.3
Ag-1	-	176.3		175.6
2a	2.68 dd (4.2, 14.3)		2.48 t (7.6)	
2b	2.73 dd (7.7, 14.3)			
3	4.41 m		1.86 qui (7.6)	
12	3.78 m		3.92 m	
15	1.43 m		1.34 m	
16	0.88 t (7.3)		0.92 t (7.4)	

Table 2. ^{1}H NMR Data of **12-14** in C_5D_5N *(δ in ppm, J in Hz)*

position	12[a]	13[b]	14[b]
Glc-1	4.88 d (7.9)	4.88 d (7.9)	4.88 d (7.9)
2	4.29 dd (9.2, 7.9)	4.29 dd (9.2, 7.9)	4.29 dd (9.2, 7.9)
3	5.78-5.76 m	5.77 m	5.77 m
4	5.38 dd (9.7, 9.7)	5.38 dd (9.7, 9.7)	5.38 dd (9.7, 9.7)
5	4.09 m	4.10 m	4.10 m
6a	3.92 dd (12.6, 5.6)	3.92 dd (12.6, 5.6)	3.92 dd (12.6, 5.6)
6b	4.09 m	4.09 m	4.09 m
Glc′-1	5.07 d (7.6)	5.07 d (7.6)	5.07 d (7.6)
2	4.22-4.12 m	4.22-4.12 m	4.22-4.12 m
3	4.58, dd (9.7, 9.7)	4.58 dd (9.7, 9.7)	4.58 dd (9.7, 9.7)
4	5.34 dd (9.7, 9.7)	5.34 dd (9.7, 9.7)	5.34 dd (9.7, 9.7)
5	4.22-4.17 m	4.22-4.12 m	4.22-4.12 m
6a	4.40, dd (12.0, 1.6)	4.40 dd (12.0, 1.6)	4.40 dd (12.0, 1.6)
6b	4.65 dd (12.0, 4.0)	4.65 dd (12.0, 4.0)	4.65 dd (12.0, 4.0)
Glc″-1	5.28 d (7.6)	5.28 d (7.6)	5.28 d (7.6)
2	5.30-5.26 m	5.30-5.26 m	5.30-5.26 m
3	5.85 dd (9.0, 9.0)	5.85 dd (9.0, 9.0)	5.85 dd (9.0, 9.0)
4	5.45 dd (9.7, 9.7)	5.45 dd (9.7, 9.7)	5.45 dd (9.7, 9.7)
5	4.22-4.17 m	4.22-4.17 m	4.22-4.17 m
6a	4.23-4.15 m	4.23-4.15 m	4.23-4.15 m
6b	4.72 dd (12.0, 1.6)	4.72 dd (12.0, 1.6)	4.72 dd (12.0, 1.6)
Glc‴-1	5.50 d (7.8)	5.49 d (7.8)	5.49 d (7.8)
2	5.49 m	5.49 m	5.49 m
3	5.78-5.76 m	5.78-5.76 m	5.78-5.76 m
4	5.58 dd (9.0, 9.0)	5.58 dd (9.0, 9.0)	5.58 dd (9.0, 9.0)
5	4.30 dd (9.0, 8.1, 4.0)	4.30 dd (9.0, 8.1, 4.0)	4.30 dd (9.0, 8.1, 4.0)
6a	4.49 dd (12.0, 8.1)	4.49 dd (12.0, 8.1)	4.49 dd (12.0, 8.1)
6b	4.66 dd (12.0, 4.0)	4.66 dd (12.0, 4.0)	4.66 dd (12.0, 4.0)
Rha-1	5.24 br s	5.24, br s	5.24, br s
2	5.79 m	5.79 m	5.79 m
3	5.72 dd (10.2, 3.5)	5.72 dd (10.3, 3.5)	5.72 dd (10.6, 3.6)
4	5.58 m	5.58 m	5.58 m
5	4.18-4.12 m	4.18-4.12 m	4.18-4.12 m
6	1.37 d (6.2)	1.37 d (6.2)	1.37 d (6.2)
Rha′-1	5.76 brs	5.77 brs	5.77 brs
2	5.94 brd (4.3, 1.0)	5.94 brd (4.2)	5.94 brd (4.2)
3	4.83 dd (10.4, 4.3)	4.83 dd (10.4, 4.3)	4.83 dd (10.4, 4.3)
4	5.60 m	5.60 m	5.60 m
5	4.72 m	4.72 m	4.72 m
6	1.60 d (6.2)	1.61 d (6.2)	1.61 d (6.2)
5b			
Ag-2a	2.93 dd (15.7, 5.3)	2.56 t (7.6)	2.50 t (7.5)
2b	3.00 dd (15.7, 7.6)		
3	5.79 m	1.87 m	1.82 m
4	1.91 m	1.50 m	1.47 m
10	1.54 m, 1.49 m	1.54 m,	1.73 m, 1.66 m
11	1.81 m, 1.71 m	1.80 m, 1.70 m	3.89 m
12	3.87 qui (4.6)	3.87 qui (5.3)	1.69 m
13	1.64 m	1.65	1.26 m
14	1.54 m	1.55 m	1.44 m
15	1.46	1.45 m	1.32 m
16	0.99 t (7.2)	1.00 t (7.5)	1.01 t (7.2)

[a]Data measured at 700 MHz. [b]Data measured at 600 MHz.

Table 3. ^{13}C NMR Data of **12-14** in C_5D_5N (δ in ppm)

position	12[a]	13[b]	14[b]
Glc-1	101.4	101.4	101.4
2	72.4	72.4	72.4
3	76.7	76.7	76.7
4	70.8	70.8	70.8
5	73.4	73.4	73.4
6	67.9	67.9	67.9
Glc′-1	101.1	101.1	101.1
2	76.5	76.5	76.5
3	82.2	82.1	82.1
4	69.4	69.4	69.4
5	72.3	72.2	72.2
6	63.1	63.1	63.1
Glc″-1	100.1	100.1	100.1
2	73.2	73.2	73.2
3	73.7	73.7	73.7
4	69.1	69.1	69.1
5	72.3	72.3	72.3
6	62.3	62.3	62.3
Glc‴-1	101.8	101.7	101.7
2	72.2	72.2	72.2
3	73.9	73.9	73.9
4	69.3	69.3	69.3
5	76.7	76.7	76.7
6	62.1	62.1	62.1
Rha-1	99.1	99.1	99.1
2	70.3	70.2	70.2
3	70.3	70.4	70.4
4	71.6	71.6	71.6
5	67.5	67.4	67.4
6	18.2	18.1	18.2
Rha′-1	98.4	98.4	98.4
2	72.2	72.1	72.1
3	75.4	75.2	75.2
4	73.4	73.3	73.3
5	67.6	67.6	67.6
6	18.2	18.1	18.2

[a]Data measured at 175 MHz. [b]Data measured at 150 MHz.

Comparison of the ^{1}H NMR spectra (Figure S10 and S11, Supporting Information) for both peracetylated derivatives (**12** and **13**) clearly identified the following

spectroscopic differences on the upfield region for their aglycone signals: (a) the presence of the two double of doublet signals of an ABX system centered at δ_H 2.93 and 3.00 (1H each) for **12**, which was assigned to the methylene C-2 (δ_C 42.1) vicinal to the carboxylic acid (C-1, δ_C 176.2) and to the acetyloxy group at C-3 (δ_H 5.79); (b) the corresponding signal in compound **13** was upfield-shifted as a triplet-like signal at d_H 2.56 (δ_C 36.4, Agl-2), which confirmed a monohydroxylated hexadecanoic acid. In the ^{13}C NMR spectra (Figure S12, Supporting Information), both derivatives displayed exactly the same oligosaccharide core with the only difference being an additional signal for the substituted C-3 position (δ_C 73.1) in derivative **12**. Major spectroscopic differences were observed for the aglycone chemical shifts of compounds **12** and **13** (Table 4; Figure S13, Supporting Information) with three chemical shifts corresponding to the methylenes C-4 (δ_C 35.2), C-11 (δ_C 35.0), and C-13 (δ_C 34.7), adjacent to the hydroxylated methine carbons C-3 and C-12 in derivative **12**, and only two downfield-shifted methylenes at C-11 (δ_C 35.0) and C-13 (δ_C 34.7) in peracetylated compound **13**, which confirmed that 12*S*-hydroxyhexadecanoic acid is its aglycone.[11]

The ^{1}H NMR spectrum for both diastereoisomers, compounds **13** and **14**, were almost superimposable with the only difference being the chemical shift for the triplet signal assigned to the methylene C-2 in **14**. This signal was upfield-shifted at δ_{H-2} 2.50 (Figure S10, Supporting Information) in accordance with the presence of (11*S*)-hydroxyhexadecanoic acid (jalapinolic acid) as the aglycone for **14**, instead of the (12*S*)-hydroxyhexadecanoic acid found in **13** (δ_{H-2} 2.56). The ^{13}C NMR chemical shift differences observed for the aglycones of **13** and **14** (Table 4) resulted from the well-

known α– and β–inductive paramagnetic effects and the diamagnetic γ-effects determined by the electronegativity of the oxygenated functional group that alters the resonance position of the neighboring carbons along the fatty acid chain (Figure S13, Supporting Information).[17a] It was possible to make full assignment of most of the carbon signals for both 12-hydroxylated fatty acids based on their HSQC and HMBC data as well as by comparison with the observed carbon shifts with previously established data for model saturated fatty acids.[17b] These assignments were also assisted by prediction of the ^{13}C NMR chemical shifts using Mnova NMRPredict software.[18] Accordingly, the structure of operculinic acid I (**2**) was characterized as (12*S*)-hydroxyhexadecanoic acid 12-*O*-β-D-glucopyranosyl-(1→3)-*O*-α-L-rhamno-pyranosyl-(1→2)-[*O*-β-D-glucopyranosyl-(1→3)]-*O*-β-D-glucopyranosyl-(1→2)-[*O*-α-

Table 4. ^{13}C NMR Data for aglycones of **12-14** in C$_5$D$_5$N

position	12[a]	13[b]	14[b]
1	176.2	176.1	176.3
2	42.1	36.4	34.5
3	73.1	26.5	26.1
4	35.2	30.1*	30.2*
5	26.2	30.2*	30.3*
6	30.8*	30.8*	30.3*
7	30.5*	30.5*	30.4*
8	30.4*	30.4*	30.4*
9	30.3*	30.3*	26.3
10	25.3	25.4	35.7
11	35.0	35.0	80.1
12	81.2	81.1	35.8
13	34.7	34.7	25.5
14	28.2	28.1	32.6
15	23.6	23.5	23.3
16	14.7	14.7	14.6

[a]Data measured at 175 MHz. [b]Data measured at 150 MHz. *Interchangeable signals.

L-rhamnopyranosyl-(1→6)]-*O*-*β*-D-glucopyranoside. Consequently, the structure of operculinic acid J (**3**) was characterized as the diastereisomer of **2** with (11*S*)-hydroxyhexadecanoic acid as the aglycone and the same hexasaccharide core: (11*S*)-hydroxyhexadecanoic acid 11-*O*-*β*-D-glucopyranosyl-(1 →3)-*O*-*α*-L-rhamnopyranosyl-(1→2)-[*O*-*β*-D-glucopyranosyl-(1→3)]-*O*-*β*-D-glucopyranosyl-(1→2)-[*O*-*α*-L-rhamno-pyranosyl-(1→6)]-*O*-*β*-D-glucopyranoside.

3: R = H
14: R = COCH3
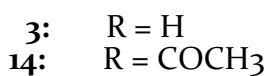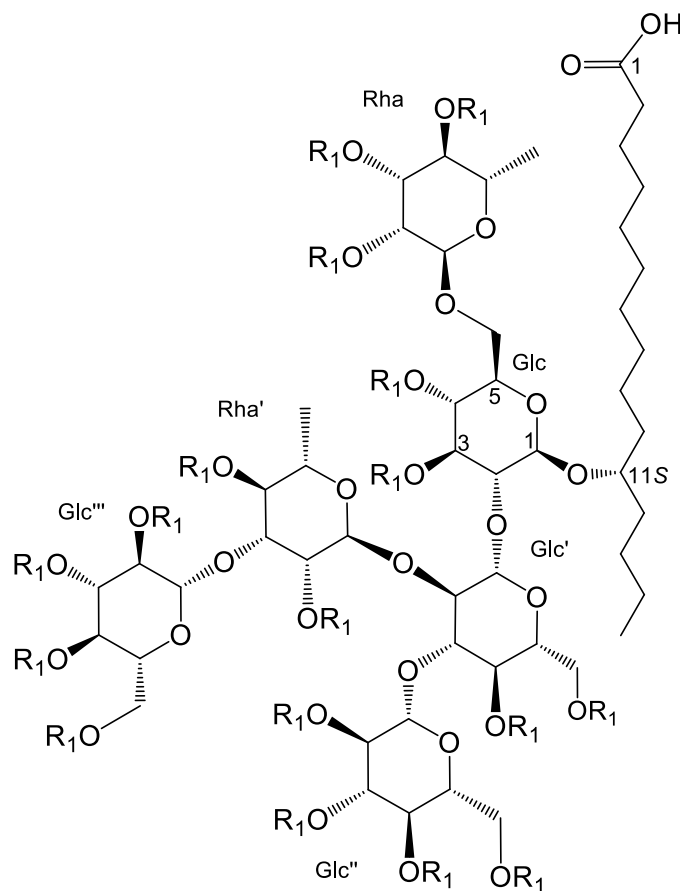
Figure 24. Chemical structures of the operculinic acid J (**3**) and his peracetyl derivative (**14**).

High-resolution positive ESIMS of the peak with t_R 20.9 min (**15**; Figure S4, Supporting Information) showed a sodium adduct ion at m/z 1805.69141 [M + Na]$^+$ (mass accuracy +1.4 ppm; Figure S42, Supporting Information) with a molecular formula of $C_{80}H_{118}O_{44}Na$ (exact mass requires 1805.68882), which accounted for the presence of a monohydroxylated tetradecanoic acid moiety glycosidically linked to a hexasaccharide. Saponification of **15** afforded glycosidic acid **4** (m/z 1175.53162 [M + Na]$^+$; $C_{50}H_{88}O_{29}Na$ requires 1175.53034, δ = +1.1 ppm). The ^{1}H and ^{13}C NMR data (Table 5) of **4** and **15** showed features identical to those previously reported for the peracetylated methyl ester derivative of purgic acid A,[2c] a hexasaccharide from the Mexican jalap root (*I. purga*), consisting of four deoxyhexoses and two hexoses (glucose). COSY, TOCSY and HSQC spectra were useful to identify six separate spin systems for sugar skeletons and permitted the identification of the same glycosylation sequence previously described for purgic acid A methyl ester[2c] (Figures S45-50, Supporting Information).

Glycosidic acid **4** was subjected to acid hydrolysis to liberate the aglycone which was further methylated, silylated, and analyzed by GC-EIMS (Figure S43, Supporting Information) to identify the hydroxyl group substitution at C-11 of tetradecanoic acid since α-cleavage to the trimethylsiloxy group gave diagnostic ions at m/z 287 ([$C_{12}H_{22}O_3TMS$]$^+$) and 145 ([C_4H_8OTMS]$^+$). Therefore, compound **4** was identified as the known (11*S*)-hydroxytetradecanoic acid 11-*O*-β-quinovopyranosyl-(1→2)-*O*-β-D-

glucopyranosyl-(1→3)-O-[β-D-fucopyranosyl-(1→4)]-O-α-L-rhamnopyranosyl-(1→2)-

O-β-D-glucopyranosyl-(1→2)-O-β-D-quinovopyranoside.[3]

4:   R = H
15:   R = COCH3
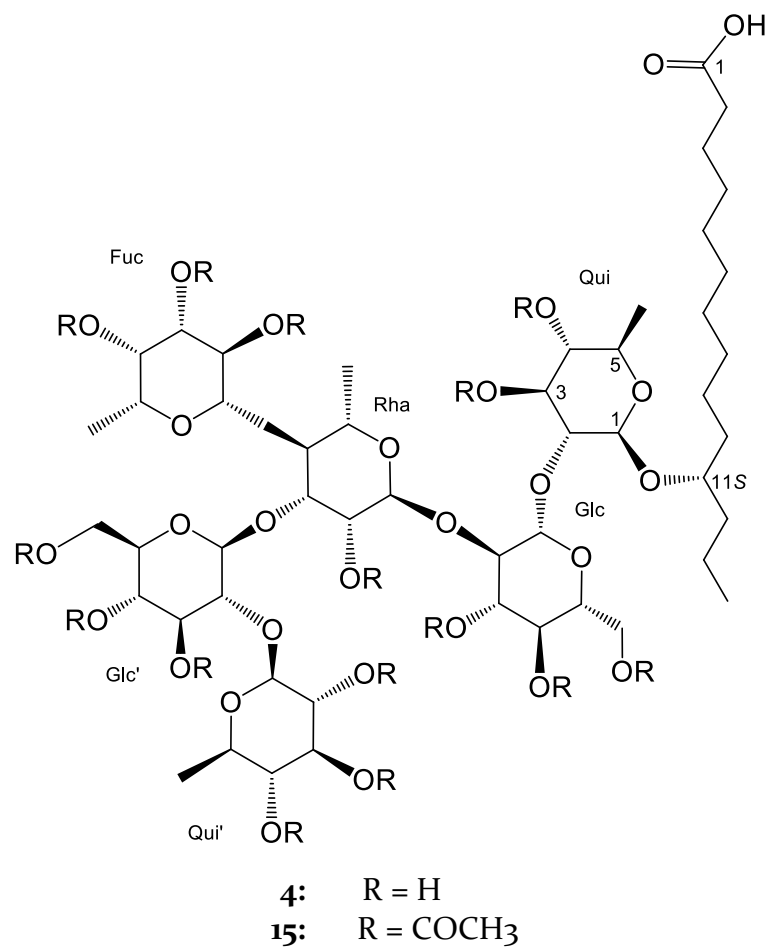
Figure 25. Chemical structures of the purgic acid A (**4**) and his peracetyl derivative (**15**)

Table 5. ¹H and ¹³C NMR Data of **4** and **15** in C_5D_5N (δ in ppm)

position	**4**[a] δ_H	δ_C	**15**[b] δ_H	δ_C
Qui-1	4.76, d (7.5)	102.3	4.72 d (7.6)	101.2
2	4.14-4.18 m	80.7	4.23 dd	77.3
3	4.59 dd (9.0, 9.0)	78.5	5.62 m	72.9*
4	3.53 dd (9.0, 9.0)	77.2	5.10 t (9.6)	74.7
5	3.71 dq (9.0, 6.1)	72.3	4.37-4.31, m	69.6
6	1.46 d (6.1)	18.6	1.33 d (6.4)	16.5
Glc-1	5.72 d (7.7)	102.4	5.16 d (7.8)	101.6
2	4.34 dd (8.7, 7.7)	73.5	4.24 dd (8.7, 7.8)	72.9*
3	4.29-4.23 m	77.5	5.71 m	74.2
4	3.80-3.74m	73.7	5.38 dd (9.8, 9.8)	70.2
5	3.76 m	77.8	4.12 ddd (9.8, 4.6, 2.6)	72.6
6a	4.44 m	63.2	4.37-4.27 m	63.0
6b	4.23 m		4.66-4.61 m	
Rha-1	6.41 br s	100.2	5.50 br s	97.7
2	4.87 br s	71.6	5.70 m	76.5
3	5.27 dd (9.3, 3.0)	78.5	4.68-4.61 m	78.7
4	4.80 dd (9.3, 9.3)	78.9	4.37-4.29 m	77.4
5	5.16 dq (9.3, 6.1)	67.9	4.55-4.51 m	68.0
6	1.93 d (6.1)	19.6	1.87 d (6.2)	19.5
Glc′-1	6.18 d (8.0)	100.7	5.48 d (7.8)	102.8
2	4.06-4.00	84.4	4.28 dd (7.8, 6.1)	78.4
3	4.52 dd (9.0, 9.0)	76.8	5.60 m	75.4
4	4.05-3.97	72.2	5.33 dd (9.6, 9.6)	70.3
5	4.15-4.12	79.4	4.37-4.31 m	69.8*
6a	4.54-4.52	62.7	4.42 dd (12.0, 2.6)	63.7
6b	4.18-4.12		4.55-4.51 m	
Qui′-1	5.11	104.7	5.28 d (8.3)	102.0
2	4.09 dd (9.8, 8.3)	76.2	5.51 dd (9.8, 8.3)	72.5
3	4.04-3.97	77.5	5.68 m	74.1
4	3.65 dd (9.0, 9.0)	76.7	5.52 dd (9.8, 9.8)	74.5
5	3.76, dq (9.0, 6.0)	73.7	4.00 dq (9.8, 6.2)	71.4
6	1.67 d (6.0)	19.0	1.48 d (6.2)	18.5
Fuc-1	5.75 d (7.7)	102.9	5.62 d (7.9)	101.4
2	4.35-4.23	74.7	5.82 dd (10.0, 7.9)	69.8*
3	4.35-4.23	77.5	5.64 m	76.1
4	4.04-3.97	72.3	5.91 dd (7.9, 3.5)	71.5
5	4.18-4.12	71.2	4.37-4.29 m	71.9
6	1.53 (6.5)	17.3	1.36 d (6.7)	18.2
Ag-1		176.6		176.7
2	2.56 t (7.5)	36.9	2.57 t (7.5)	35.6
3	1.84 m	26.5	1.88	26.3
10	1.70 m	34.8	1.68 m	34.9
11	3.79 m	80.2	3.77 m	81.0
12	1.76 m, 1.56 m	37.5	1.76 m, 1.59 m	37.5
13	1.56 m	19.3	1.57 m	19.1
14	0.96 t (7.2)	14.8	0.99 t (7.1)	14.9

[a]Data measured at 700 MHz (¹H, J in Hz) and 175 MHz (¹³C).
[b]Data measured at 400 MHz (¹H, J in Hz) and 100 MHz (¹³C).*Interchangeable signal.

This oligosaccharide core has been found in macrocyclic resin glycosides as jalapinosides I-II[14c,15b] and B,[19] and also with glycosylated to either (3S,11S)-dihydroxytetradecanoic or (3S,11S)-dihydroxyhexadecanoic acids, in the resin glycosides isolated from the cypress-vine morning glories, *I. quamoclit* (*Quamoclit pinnata*)[20] and *I. × multifida* (a hybrid between *I. quamoclit* and *I. hederifolia*),[21] purgative species commonly cultivated in gardens.

Peracetyl operculinic acid K (**16**, t_R 8.3 min; Figure S4, Supporting Information) was found as a monosaccharide of decanoic acid with a cationized molecule at *m/z* 483.22120 [M + Na]$^+$ (mass accuracy δ = +2.3 ppm; Figure S51, Supporting Information), which indicated a molecular formula of $C_{22}H_{36}O_{10}Na$. Saponification of **16** afforded operculinic acid K (**5**; positive ESIMS *m/z* 357.18801 [M + Na]$^+$, mass accuracy δ = -1.0 ppm). NMR spectra of **5** and its peracetylated derivative (**16**) (Figures S52 and S53, Supporting Information) showed signals assigned to a monosaccharide of hydroxydecanoic acid. The HSQC spectrum for **5** (Figure S54, Supporting Information) identified one anomeric carbon signal, in addition to five oxygenated carbon signals (a quinovose unit), one methine for the oxygenated aglycone carbon, eight methylenes, and two methyls (one for the methylpentose), which were closely related to those previously described for quamoclinic acid B.[20] The observed $^3J_{CH}$ correlation in compound **1** between the methyl group at δ_H 0.90 (Agl-10) and the methylene carbon at δ_C 37.6 (C-8), which is vicinal to the substituted C-7 (δ_C 80.5), supported the presence of 7-hydroxydecanoic acid, as the aglycone (Figure S58, Supporting Information). The optical rotation of **5** ([α]$^{22}_D$ -20.0) differed from the

value described for quamoclinic acid B[20] ($[\alpha]^{22}_D$ -39.4). Thus, this confirmed the presence of a diastereoisomer in the aglycone with major differences observed in the chemical shifts for the methylene signals. Acidic hydrolysis of **5** yielded a levorotatory aglycone ($[\alpha]^{22}_D$ -3.3; *c* 0.1, CHCl$_3$), supporting the C-7 (*R*)-absolute configuration,[16] in addition to D-quinovose. Consequently, operculinic acid K (**5**) was characterized as 7*R*-hydroxydecanoic acid 7-*O*-β-D-quinovopyranoside. Levorotatory (*R*)-hydroxylated fatty acids have been rarely found as aglycones or acylating residues in Convolvulaceous resin glycosides, only two example are described: (-)-11(*R*)-hydroxyhexadecanoic acid (*ent*-jalapinolic acid) in ipomeic acid from *I. pes-caprae*[22] and (-)-8(*R*)-hydroxydodecanoic in murucoidin X, isolated from *I. murucoides.*[16]

Positive-ion ESIMS of peracetylated derivative **17** (t_R = 25.4 min; Figure S4, Supporting Information) afforded a sodium adduct ion at *m/z* 1947.71159 [M + Na]$^+$ (mass accuracy δ = -1.9 ppm; Figure S59, Supporting Information) with a molecular formula of C$_{86}$H$_{124}$O$_{48}$Na (exact mass requires 1947.71542). Saponification of this derivative liberated an H$_2$O-soluble derivative identical to operculinic acid H (**1**). The

4:   R = H
15: R = COCH3
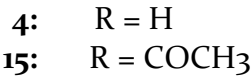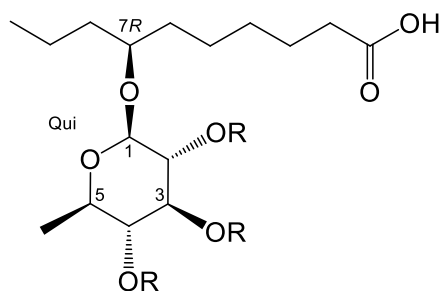
Figure 26. Chemical structures of the operculinic acid K (**5**) and his peracetyl derivative (**16**)

^{1}H NMR spectrum of **17** (Table 6; Figure S61, Supporting Information), in combination with COSY and TOCSY contourplots (Figures S64 and S67, Supporting Information), indicated the presence of a hexasaccharide core, while the multiplicities and coupling constants for two α-L-rhamnose and four β-D-glucose units were clearly recognized. Comparison of the ^{1}H and ^{13}C NMR spectra for **12** (Tables 2 and 3) and **17** (Table 6; Figures S62 and S63, Supporting Information) showed that both derivatives presented a similar hexasaccharide core with major differences being the chemical shifts for the terminal Glc″ moiety, the rest of the spectra were superimposable, including the aglycone signals (Table 4).

The interglycosidic connectivities were confirmed by HMBC long-range heteronuclear coupling correlations ($^3J_{CH}$) and used to confirm the same glycosilation sequence for **12** and **17** (Figure S70, Supporting Information). Seventeen methyl signals (δ_H 1.95-2.35) for the acetyl groups were clearly observed for compound **17**, in comparison with eighteen signals in the spectrum of **12**. ESIMS analysis indicated a difference of 60 Da ($C_2H_2CO + H_2O$) between the observed sodium adduct cation [M + Na]$^+$ of both peracetylated glycoside acids, namely *m/z* 2007.73859 for compound **12** and *m/z* 1947.71159 for compound **17**. This situation suggested an intramolecular macrolactonization of operculinic acid H (**1**) mediated by the standard acetylation conditions (Ac$_2$O in pyridine).[23] Spectroscopic evidences for the macrolactone were obtained from the IR spectrum where the lack of the diagnostic absorptions for the carbocyclic acid moiety in **1** was observed: the wide O-H stretch in the region of 3300-

$2500 \ cm^{-1}$ and the intense C=O stretch in $1720 \ cm^{-1}$. Instead a strong C=O stretch at $1743 \ cm^{-1}$ was recorded for derivative **17** (Figure S60, Supporting Information).
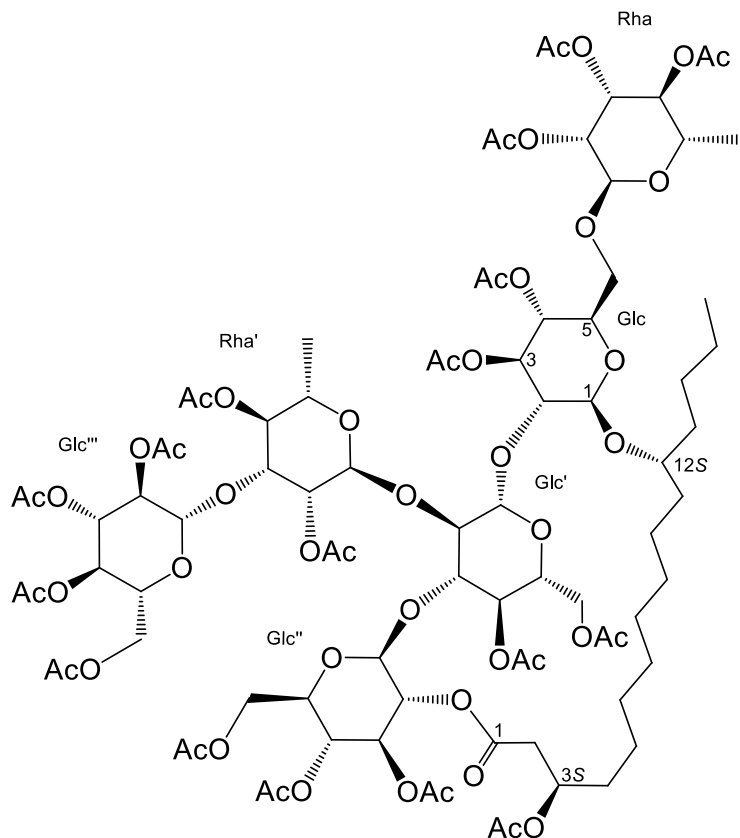
Figure 27. Chemical structures of the peracetylated operculinic acid H macrolactone (**17**).

Although in the ^{13}C NMR, the carbonyl signal for the lactone was assigned through the observed $^{2}J_{CH}$ between the aglycone C-1 at δ_C 170.1 and the C-2 methylene protons at δ_H 2.99 and 3.00, overlapping of the pyranose H-2 and H-4 signals for the terminal Glc″ with other hexasaccharide signals in pyridine-d_5 did not allow to assign the correct position for the macrolactonization (Figure S69, Supporting Information). Therefore, NMR data for this derivative **17** were recorded in MeOH-d_4 in order to

modify the ^{1}H NMR spectrum dispersion (Figure S77, Supporting Information). HMBC was used to identifying the position of lactonization; first, the lactone carbonyl group was assigned through the cross-peak (${}^2J_{CH}$) observed for aglycone C-1 (δ_C 170.1) and the methylene of C-2 (2.56 and 2.57); then, the observed ${}^3J_{CH}$ connectivity between the aglycone C-1 and H-2 (δ_H 4.73) of Glc″. The structure of this artifact, resembling the distinctive macrolactones of the resin glycosides,[4] denoted a remarkably selectivity for the intramolecular lactonization at C-2 of the terminal Glc″, since this artifact was the only macrolactone produced during the peracetylation of **1**.

During the recycling HPLC purification process of compound **13** (t_R 12.0 min; Figure S4, Supporting Information), a minor constituent was also obtained (**18**), which corresponded to the peracetylated derivative of dehydrated operculinic acid H (ESIMS positive mode: m/z 1947.71870 [M + Na]⁺, $C_{86}H_{124}O_{48}Na$ calcd error: δ = +1.7 ppm). Comparison of the ^{1}H NMR spectra for compounds **12-14** and **18** showed noticeable differences associated with the chemical shifts for the methylene group C-2 in **12-14** and its nonexistence in **18** (Figure S80, Supporting Information), in addition to the presence of two vinylic protons with a ${}^3J_{H-H}$ *trans* (15.4 Hz) and conjugated to the carboxylic moiety, which were centered at δ_H 6.28 (δ_{C-2} 124.2) and 7.34 (δ_{C-3} 149.2) in compound **18** (Figures S81 and S82, Supporting Information). This derivative displayed the same oligosaccharide core signals observed in compounds **12-14**. The ^{13}C NMR spectra of **18** showed eleven methylenes, two of which were downfield-shifted for C-11 (δ_C 35.2) and C-13 (δ_C 34.8), in addition to C-4 (δ_C 32.9) at the γ position to the carboxylic acid, which identified the presence of a 12-hydroxy-2-hexadecenoyl moiety

as the aglycone (Figure S79, Supporting Information). This derivative could represent an artifact that was produced by either a dehydration reaction during acetylation of **1** or a dehydroacetylation of **12** during the work-up of the reaction. Hydrogenation of derivative **18** afforded peracetylated operculinic acid I (**13**).

Table 6. ^{1}H and ^{13}C NMR Data of **17** in C$_5$D$_5$N and CD$_3$OD (δ in ppm, J in Hz)

position	C$_5$D$_5$N^a		CD$_3$OD^b	
	δ_H	δ_C	δ_H	δ_C
Glc-1	4.81 d (7.7)	101.7	4.46 d (7.6)	102.6
2	4.25 dd (9.4, 7.7)	77.2	3.87 m	78.0
3	5.77 dd (9.4, 9.4)	76.9	5.32 dd (9.3, 9.3)	78.0
4	5.34 dd (9.4, 9.4)	70.4	4.96 dd (9.3, 9.3)	71.2
5	4.06 m	73.5	3.88 m	73.2
6a	3.92 dd (11.5, 6.1)	67.9	3.60 m	67.8
6b	4.09 dd (11.5, 2.6)		3.82 dd (11.3, 2.5)	
Glc'-1	5.09 d (7.9)	101.4	4.71 d (7.6)	101.9
2	4.12 dd (9.2, 7.9)	76.4	3.68 m	76.3
3	4.64 dd (9.2, 9.2)	81.7	4.12 dd (7.6, 9.0)	81.9
4	5.32 dd (9.2, 9.2)	69.2	4.83 dd (9.0, 9,0)	69.6
5	4.17-4.14 m	72.4	3.84 m	72.8
6a	4.38 dd (12.2, 2.4)	63.0	4.12 m	63.4
6b	4.67 dd (12.2, 4.7)		4.34 dd (12.2, 4.8)	
Glc''-1	5.32 d (7.8)	99.8	4.88 m	100.1
2	5.48-5.50 m	69.1	4.73 dd (7.6, 9.4)	73.7
3	5.89 dd (9.0, 9.0)	73.6	5.41 dd (9.4, 9,4)	74.0
4	5.30 m	69.3	5.02 dd (9.3, 9.3)	69.6
5	4.32-4.30 m	72.6	4.15 ddd (10.3, 4.0, 2.3)	73.0
6a	4.17-4.19 m	62.2	4.10 m	62.8
6b	4.72 dd (12.6, 3.8)		4.48 dd (12.6, 4.0)	
Glc'''-1	5.51 d (7.6)	101.5	4.96 d (7.6)	101.8
2	5.48-4.50 m	72.2	4.87 m	72.5
3	5.80 dd (9.4, 9.4)	73.8	5.20 dd (9.4, 9.4)	74.5
4	5.62 m	69.5	5.13 dd (9.4, 9.4)	69.5
5	4.32-4.30 m	72.3.7	3.87 m	72.4
6a	4.40 dd (12.3, 3.4)	61.7	4.02 dd (12.6, 2.4)	61.9
6b	4.80 dd (12.3, 2.4)		4.60 dd (12.6, 2.9)	
Rha-1	5.24 brs	99.1	4.80 br s	99.5
2	5.80 dd (3.6, 1.7)	70.2	5.24 m	70.6
3	5.72 dd (10.2, 3.6)	70.2	5.24 m	70.8
4	5.59 dd (10.2, 10.2)	71.5	5.00 dd (9.9, 9,9)	71.8
5	4.18 m	67.5	3.95 dq (9.8, 6.2)	67.6
6	1.37 d (6.2)	18.2	1.18 d (6.2)	17.8

Rha'-1	5.74 brs	98.6	5.24 br s	98.8
2	5.96 dd (4.3, 1.0)	71.7	5.40 dd (1.6, 3.0)	72.5
3	4.84 dd (10.0, 4.3)	75.0	4.33 m	75.6
4	5.56 dd (10.0, 10.0)	73.7	4.93 dd (9.7, 9.7)	73.3
5	4.72 m	67.8	4.33 m	67.6
6	1.56 d (6.3)	18.3	1.22 d (6.2)	17.9
Agl-1		170.1	-	170.1
2a	2.98 dd (16.2, 5.5)	38.6	2.56 brs	38.8
2b	3.01 dd (16.2, 6.2)		2.57 brs	
3	5.62 m	71.2	5.13 m	71.8
4	1.96m, 1.75 m	34.1	1.73, 1.51 m	34.4
11	1.83 m, 1.70 m	35.4	1.65, 1.51 m	36.0
12	3.85 m	81.0	3.60 m	82.7
13	1.65 m	34.6	1.51 m	35.3
14	1.54 m	28.2	1.38 m	28.4
15	1.44 m	23.5	1.32 m	24.0
16	1.00 t (7.5)	14.7	0.92 t (7.5)	14.6

[a]Data measured at 800 MHz (^{1}H, J in Hz) and 200 MHz (^{13}C). [b]Data measured at 700 MHz (^{1}H, J in Hz) and 175 MHz (^{13}C).
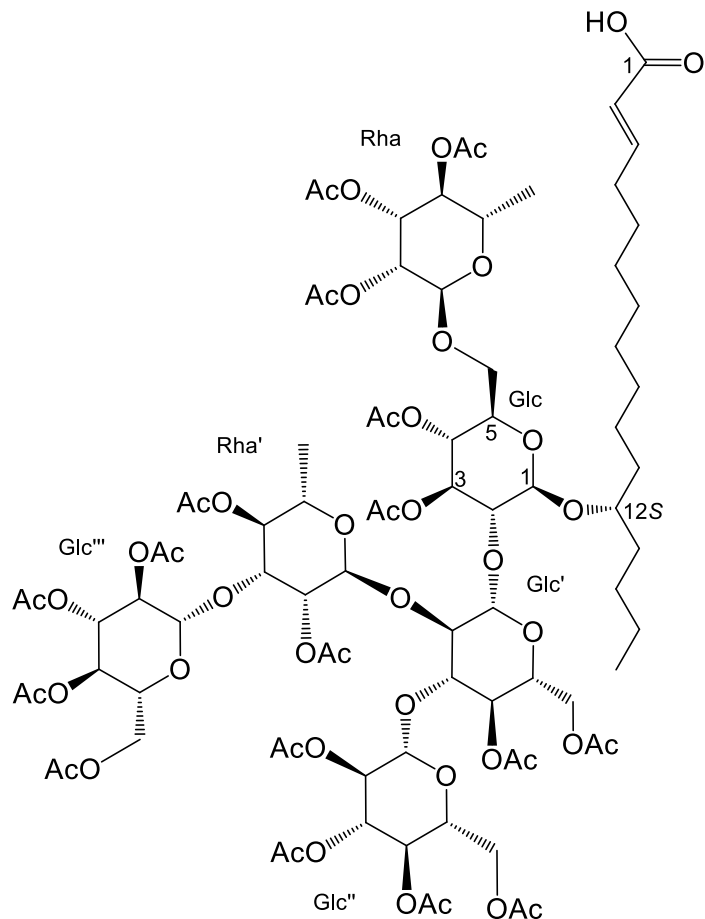
Figure 28. Chemical structures of the peracetylated dehydrated operculinic acid H (**18**).

The precipitated intact convolvulin fraction was separated by recycling reversed-phase HPLC affording three major acylated glycosidic acids which were named as macrocarpic acids A-C (**6-8**). Minor constituents were present in extremely low quantities making their resolution a difficult task. Common features in both ^{1}H and ^{13}C NMR spectra of the three compounds **6-8** are noted in Tables 7 and 8, respectively. All spectra showed the presence of the same oligosaccharide core of **1** formed by 4 units of glucose and 2 units of rhamnose, bonded to operculinolic acid as the aglycone, and acylated by four short chain fatty acids. In ^{1}H NMR spectra, downfield shifted signals were observed for protons at C-2 and C-4 of the second rhamnose unit (Rha′), C-2 of the third glucose (Glc″), and C-2 or C-3 of the fourth glucose (Glc‴); thus, indicating acylation at these positions on the three oligosaccharide cores when compared with **1**. The ^{13}C chemical shift for the carbonyl group of the acyclic aglycone ($\delta_{C\text{-}1}$175-177) suggested the absence of a macrolactone group (e.g. δ_C 170.1 for **18**), which designated the same acyclic structure related to **1** for these isolated glycosidic acids (**6-8**).

Positive ESIMS of macrocarposidic acid A (**6**) afforded a sodium adduct ion at m/z 1681.7805 [M + Na]$^+$, with a molecular formula of $C_{77}H_{126}O_{38}Na$ (exact mass requires 1681.78193; mass accuracy -0.8 ppm; Figure S83, Supporting Information). In the NMR spectra analysis (Figure S84, Supporting Information), the presence of the acylating residues were easily identified from their diagnostic ^{1}H NMR signal (Table 7): one isovaleroyl group ($\delta_{H\text{-}2}$ 2.23 d, J = 6.7 Hz), two tigloyl groups ($\delta_{H\text{-}3}$ 6.89 dq, J = 7.0, 1.2 Hz and $\delta_{H\text{-}3'}$ 6.98 dq, J = 7.2, 1.6 Hz), and one exogonoyl group, which exists in their

two major configurational epimers ($\delta_{H\text{-}2b}$ 2.76 dd, J = 15.7, 7.1 Hz, $\delta_{H\text{-}2b}$ 2.56 dd, J =15.6, 6.3 Hz and $\delta_{H\text{-}2a'}$ 2.90 dd, J = 15.9, 7.4 Hz, $\delta_{H\text{-}2a'}$ 2.64 dd, J =15.9, 5.8 Hz). These mixture of two unresolvable diastereoisomers which only differ in the configuration at the spiro center C-6 of this acylating residue is present in a ratio of approximately 1:0.9 (from integration of NMR signal) for *E,E* 3*S*,6*S*,9*R* and *Z,Z* 3*S*,6*R*,9*R*.[24] The epimerization of this chiral center easily occurs in solution making impossible the separation of the resulting mixture.[10,24] The exact position for each acyl group on the oligosaccharide core was then determined by the observed key connectivities ($^3J_{CH}$) in the HMBC spectra (Figure S89, Supporting Information). For example, the following correlations were observed: (a) Rha' H-2 (δ_H 5.54; 5.52) and exogonyl C-1 (δ_C 172.7; 172.3, respectively); (b) Rha' H-4 (δ_H 5.13) and tigloyl (Tga$_1$) C-1 (δ_C 169.4); (c) Glc'' H-2 (δ_H 4.78) and isovaleroyl C-1 (δ_C 173.3); finally, (d) Glc''' H-3 (δ_H 4.93 and 4.94) and tigloyl (Tga$_2$) C-1 (δ_C 168.9). Therefore, compound **6** was identified as the novel (3*S*,12*S*)-hydroxyhexadecanoic acid 12-*O*-(3-*O*-tigloyl)-*β*-D-glucopyranosyl-(1→3)-*O*-(2-*O*-(3*S*,9*R*)-exogonoyl, 4-*O*-tigloyl)-*α*-L-rhamnopyranosyl-(1→2)-[*O*-(2-*O*-isovaleroyl)-*β*-D-glucopyranosyl-(1→3)]-*O*-*β*-D-glucopyranosyl-(1→2)-[*O*-*α*-L-rhamnopyranosyl-(1→6)]-*O*-*β*-D-glucopyranoside.

Positive ESIMS of macrocarposidic acid B (**7**) afforded a sodium adduct ion at *m/z* 1683.7988 [M + Na]$^+$, with a molecular formula of $C_{77}H_{128}O_{38}Na$ (exact mass requires 1683.79758; mass accuracy +0.7 ppm; Figure S90, Supporting Information). Positive ESIMS spectrum of compound **8** showed the same molecular weight calculated for compound **7**: *m/z* 1683.7984 [M + Na]$^+$, $C_{77}H_{128}O_{38}Na$ (exact mass requires 1683.79758;

	R₁	R₂	R₃	R₄	R₅	R₆
6:	Iva	Tga	H	Tga	H	H
7:	Iva	Tga	Iva	H	H	H
8:	Iva	Tga	H	Iva	H	H
9:	Iva	Tga	H	H	H	CH₃
10:	Iva	H	H	H	H	CH₃
11:	Iva	Tga	H	H	Iva	CH₃

Iva:

Tga:
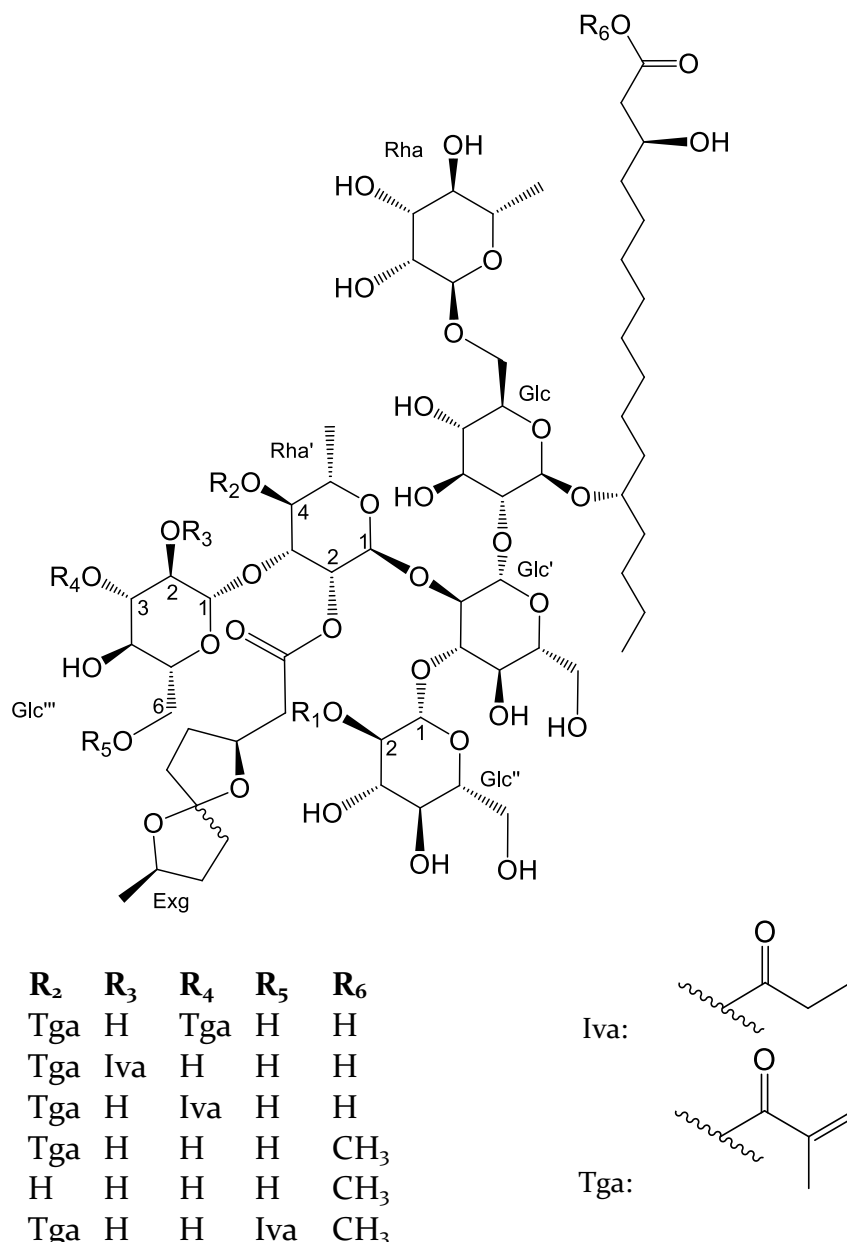
Figure 29. Chemical structures of the macrocarposidic acids A-C (**6-8**) and IOM's compounds (**9-11**).

mass accuracy +0.5 ppm; Figure S97, Supporting Information). The difference of two atomic mass units in relation with the molecular weight of macrocarposidic acid A (**6**) indicated the replacement of one tigloyl moiety in **6** by an isovaleroyl group in compounds **7** and **8**. Key $^3J_{CH}$ connectivities assigned by HMBC confirmed that both

compounds were constitutional isomers with different connectivities for the esterifying residues. The following interactions were registered for compound **7** (Figure S96, Supporting Information): correlations for the carbonyl carbon of Tga ($\delta_{C\text{-}1}$ 168.9) with H-4 of Rha' (δ_H 5.13), H-2 of Glc'' (δ_H 4.77) with C-1 of Iva$_1$ (δ_C 173.3), H-2 of Glc''' (δ_H 4.64) with C-1 of Iva$_2$ (δ_C 173.4), and Rha' H-2 (δ_H 5.38) and exogonoyl C-1 (δ_C 171.9; 172.0). The substitution pattern for compound **8** (Figure S103, Supporting Information) was deduced through the cross-peak observed for Tga ($\delta_{C\text{-}1}$ 168.9) with Rha' H-4 (δ_H 5.13) and H-3 of Glc''' (δ_H 4.93) with C-1 of Iva$_2$ ($\delta_{C\text{-}1}$ 174.4). The rest of this oligosaccharide core was substituted by the same acylating residues as described above for compound **6**. Compound **8** was previously isolated as a methyl ester derivative (originally named as IOM-3) from the convolvulin fraction of the Brazilian jalap after mild methanolysis with indium (III) chloride and purification by HPLC.[10]

Therefore, compound **7** was characterized as (3*S*,12*S*)-hydroxyhexadecanoic acid 12-*O*-(2-*O*-isovaleroyl)-*β*-D-glucopyranosyl-(1→3)-*O*-(2-*O*-(3*S*,9*R*)-exogonoyl,4-*O*-tiglo-yl)-*α*-L-rhamnopyranosyl-(1→2)-[*O*-(2-*O*-isovaleroyl)-*β*-D-glucopyranosyl-(1→3)]-*O*-*β*-D-glucopyranosyl-(1→2)-[*O*-α-L-rhamnopyranosyl-(1→6)]-*O*-*β*-D-glucopyranoside, while **8** was identified as (3*S*,12*S*)-hydroxyhexadecanoic acid 12-*O*-(3-*O*-isovaleroyl)-*β*-D-glucopyranosyl-(1→3)-*O*-(2-*O*-(3*S*,9*R*)-exogonoyl,4-*O*-tigloyl)-*α*-L-rhamnopyrano-syl-(1→2)-[*O*-(2-*O*-isovaleroyl)-*β*-D-glucopyranosyl-(1→3)]-*O*-*β*-D-glucopyranosyl-(1→2)-[*O*-α-L-rhamnopyranosyl-(1→6)]-*O*-*β*-D-glucopyranoside.

Up to now, the chemical diversity of the morning glory resin glycosides isolated from the ether-insoluble fraction (convolvulin) has showed the presence of high

molecular weight oligomers, primarily acyclic hexasaccharides, as well as variations in the levels of some individual macrolactone-type acylsugars, diverging in the lengths of their fatty acid aglycones, in line with the chemical diversity previously described for the Indian jalap (*O. turpethum*); for example, the Mexican jalap (*I. purga*) incorporates either (11*S*)-hydroxytetradecanoic (convolvulinolic) or (11*S*)-hydroxyhexadecanoic (jalapinolic) acids, while the Brazilian jalap (*O. macrocarpa*) includes hydroxylated fatty acid aglycones of different chain lengths, mainly 3*S*,12*S*-dihydroxyhexadecanoic (operculinolic) acid.

Table 7. ^{1}H Data of **6-8** in CD$_3$OD (δ in ppm, and J in Hz)

position	6^a	7^b	8^a
Glc-1	4.24 d (7.8)	4.24 d (7.8)	4.24 d (7.8)
2	3.61-3.64	3.61-3.64	3.61-3.64
3	3.61-3.64	3.61-3.64	3.61-3.64
4	3.68 dd (9.0, 9.0)	3.68 dd (9.0, 9.0)	3.68 dd (9.0, 9.0)
5	3.91 m	3.91 m	3.91 m
6a	3.95-4.01	3.95-4.01	3.95-4.01
6b	3.55-3.58	3.55-3.58	3.55-3.58
Glc′-1	5.04 d (7.8), 5.06 d (7.8)	5.06 d (7.8)	5.04 d (7.8), 5.06 d (7.8)
2	3.53 m	3.52 m	3.53 m
3	3.88 m	3.88 m	3.88 m
4	3.14 dd (9.4, 9.4)	3.14 dd (9.4, 9.4)	3.14 dd (9.4, 9.4)
5	3.29-3.31	3.29-3.31	3.29-3.31
6a	3.56 m	3.56 m	3.56 m
6b	3.88-3.90	3.88-3.90	3.88-3.90
Glc″-1	4.68 d (7.8), 4.69 d (7.8)	4.66 d (7.8), 4.68 d (7.8)	4.68 d (7.8), 4.69 d (7.8)
2	4.78 dd (7.8, 9.6)	4.77 dd (7.8, 9.6)	4.78 dd (7.8, 9.6)
3	3.71 dd (9.6, 9.6)	3.71 dd (9.6, 9.6)	3.71 dd (9.6, 9.6)
4	3.37 dd (9.6, 9.6)	3.37 dd (9.6, 9.6)	3.37 dd (9.6, 9.6)
5	3.62 m	3.62 m	3.62 m
6a	3.68 m	3.68 m	3.68 m
6b	3.92 dd (12.0, 22)	3.90 dd (12.0, 22)	3.90 dd (12.0, 22)
Glc‴-1	4.57 d (7.8)	4.69 d (7.6), 4.70 d (7.6)	4.58 d (7.8)
2	3.26 dd (7.8, 9.5)	4.64 dd (7.6, 9.5)	3.26 dd (7.8, 9.5)
3	4.93 dd (9.5, 9.5), 4.94 dd (9.5, 9.5)	3.30 dd (7.6, 9.5)	4.93 dd (9.5, 9.5), 4.94 dd (9.0, 9.0)
4	3.42 dd (9.5, 9.5), 3.45 dd (9.5, 9.5)	3.62 m	3.42 dd (9.5, 9.5), 3.45 dd (9.5, 9.5)
5	3.46 m	3.46 m	3.46 m
6a	3.90 dd (12.0, 22)	3.90 dd (12.0, 22)	3.90 dd (12.0, 22)
6b	3.67 m	3.67 m	3.67 m
Rha-1	4.73 br s	4.73 br s	4.73 br s
2	3.83 dd (1.7, 3.4)	3.83 dd (1.7, 3.4)	3.83 dd (1.7, 3.4)
3	3.63 m	3.63 m	3.63 m
4	3.37 dd (9.5, 9.5)	3.37 dd (9.5, 9.5)	3.37 dd (9.5, 9.5)
5	3.62 m	3.62 m	3.62 m
6	1.23 d (6.4)	1.23 d (6.4)	1.23 d (6.4)
Rha′-1	5.34 br d	5.34 br d	5.34 br d
2	5.52 dd (1.5, 3.8), 5.54 dd (1.5, 3.8)	5.38 m	5.52 dd (1.5, 3.8), 5.54 dd (1.5, 3.8)
3	4.34 dd (3.8, 9.8), 4.33 dd (3.8, 9.8)	4.43 m	4.34 dd (3.8, 9.8), 4.33 dd (3.8, 9.8)
4	5.13 dd (9.8, 9.8)	5.13 dd (9.8, 9.8)	5.13 dd (9.8, 9.8)
5	4.63-4.59	4.55 m	4.63-4.59
6	1.16 d (6.2)	1.14 d (6.2)	1.16 d (6.2)
Ag-2a	2.34 dd (4.4, 15.4)	2.32 dd (4.4, 15.4)	2.34 dd (4.4, 15.4)
2b	2.45 dd (8.5, 15.4)	2.44 dd (8.5, 15.4)	2.45 dd (8.5, 15.4)
3	3.97 m	3.97 m	3.97 m
12	3.55 m	3.55 m	3.55 m
16	0.92 t (7.0)	0.92 t (7.0)	0.92 t (7.0)

Exg-2a	2.64 dd (5.8, 15.7), 2.90 dd (7.4, 15.9)	2.60 dd (5.8, 15.7), 2.93 dd (7.4, 15.9)	2.64 dd (5.8, 15.7), 2.90 dd (7.4, 15.9)
2b	2.56 dd (6.3, 15.7), 2.76 dd (7.1, 15.6)	2.54 dd (6.3, 15.7), 2.78 dd (7.1, 15.6)	2.56 dd (6.3, 15.7), 2.76 dd (7.1, 15.6)
3	4.12 m, 4.50 m	4.12 m, 4.50 m	4.12 m, 4.50 m
9	4.12 dq (5.9, 8.9), 4.50 m	4.12 dq (5.9, 8.9), 4.50 m	4.12 dq (5.9, 8.9), 4.50 m
10	1.19 d (6.1), 1.32 d (6.1)	1.20 d (6.1), 1.32 d (6.1)	1.19 d (6.1), 1.31 d (6.1)
Tga-3	6.98 dq (1.6, 7.2)	7.05 dq (1.6, 7.2)	6.98 dq (1.6, 7.2)
4	1.83 d (7.2)	1.83 d (7.2)	1.83 d (7.2)
5	1.85 br s	1.93 br s	1.85 br s
Tga'-3	6.89 dq (1.2, 7.0)		
4	1.81 d (7.0)		
5	1.85 br s		
Iva-2	2.23 d (6.7)	2.23 d (6.7)	2.23 d (6.7)
3	2.08 m	2.08 m	2.08 m
4	0.99-1.01 m	0.99-1.01 m	0.99-1.01 m
5	0.99-1.01 m	0.99-1.01 m	0.99-1.01 m
Iva'-2		2.25 d (6.7)	2.25 d (6.7)
3		2.08 m	2.08 m
4		0.99-1.01 m	0.99-1.01 m
5		0.99-1.01 m	0.99-1.01 m

[a]Data measured at 400 MHz. [b]Data measured at 500 MHz.

Table 8. ^{13}C NMR Data of **6-8** in CD$_3$OD (δ in ppm)

position	6[a]	7[b]	8[a]
Glc-1	103.5	103.5	103.5
2	78.8	78.8	78.8
3	79.9	79.9	79.9
4	71.9	71.9	71.9
5	77.2	77.2	77.2
6	68.6	68.6	68.6
Glc′-1	101.7	101.7	101.7
2	76.3, 76.2	76.3, 76.2	76.3, 76.2
3	84.9	84.9	84.9
4	70.7	70.7	70.7
5	77.8*	77.8*	77.8*
6	63.6	63.6	63.6
Glc″-1	100.7	100.7	100.7
2	75.2, 75.1	75.2, 75.1	75.2, 75.1
3	75.5	75.5	75.5
4	72.2*	72.2*	72.2*
5	72.6	72.6	72.6
6	62.5	62.5	62.5
Glc‴-1	105.5	102.8, 102,9	105.5
2	73.3	74.2, 74.3	73.3
3	78.8, 79.1	72.1	78.8, 79.1
4	69.6, 69.8	69.6, 69.8	69.6, 69.8
5	77.6, 77.8*	77.6, 77.8*	77.6, 77.8*
6	62.7	62.7	62.7
Rha-1	102.4	102.4	102.4
2	72.2*	72.2*	72.2*
3	73.2	73.2	73.2
4	73.9	73.9	73.9
5	69.8	69.8	69.8
6	18.1	18.1	18.1
Rha′-1	97.3	97.3	97.3
2	72.9, 73.3	72.9, 73.3	72.9, 73.3
3	77.8, 79.2	77.8, 79.2	77.8, 79.2
4	73.9	73.9	73.9
5	67.7	67.7	67.7
6	18.4	18.4	18.4
Agl-1	176.6	176.6	176.6
2	43.7	43.7	43.7
3	69.6	69.6	69.6
12	84.3	84.3	84.3
16	14.5	14.5	14.5
Exg-1	172.3, 172.7	171.9, 172.0	172.3, 172.7
2	41.7, 43.7	41.7, 43.8	41.8, 43.8
3	75.5, 76.9	75.5, 76.9	75.5, 76.9
6	116.5, 116.8	116.4, 116.7	116.5, 116.8
9	33.1, 33.6	33.1, 33.6	33.1, 33.6
10	21.3, 22.9	21.3, 22.8	21.3, 22.9

Tga-1	169.4		
2	129.8		
3	138.5		
4	14.5		
5	12.2		
Tga'-1	168.9	168.9	168.9
2	129.3	129.3	129.4
3	139.9	139.9	139.9
4	14.8	14.8	14.8
5	12.7	12.7	12.7
Iva-1	173.3	173.3	173.3
2	43.9	43.9	43.9
3	26.7	26.4	26.7
4	22.9	22.9	22.9*
5	22.8	22.8	22.8*
Iva'-1		173.4	174.4
2		44.0	44.5
3		26.7	26.8
4		22.9	22.9*
5		22.8	22.8*

[a]Data measured at 100 MHz. [b]Data measured at 125 MHz. *Interchangeable signals.

EXPERIMENTAL SECTION

General Experimental Procedures. Melting points were determined on a Fisher-Johns apparatus and are uncorrected. Low-resolution ESIMS data were measured using a Waters SQD2 system (Waters) equipped with an electrospray ionization source (ESI) by direct infusion of the purified compounds. The exact mass of the molecules was obtained by direct infusion on an LTQ-Orbitrap XL Hybrid FT Mass Spectrometer (Thermo Fisher Scientific, San Jose, CA, USA) equipped with an Electrospray Finnigan Ion Max source. Each sample (1 mg) was dissolved in 1 mL of MeOH and 250 μL were diluted with 100 μL of MeOH-H_2O (9:1, v/v) containing 0.1% formic acid to enhance the ionization process and directly infused into the ESI source for positive ion mode at a flow rate of 5 μL/min. Each sample was analyzed in full-scan mode using a *m/z* 100–3000 mass range, under the following instrumental conditions: AGC target 5×104, 500 ms maximum inject time, 1 microscan, scan time 1.9 s, resolving power 100.000, capillary temperature 270 °C; spray voltage applied to the needle 3.5 kV, capillary voltage 37 V, nebulizer gas (nitrogen) flow rate set at 5 arbitrary units, acquisition time 1 min. Direct infusion ESI-MS spectra were deconvoluted by Xcalibur for Qual Browser v. 2.2. SP1 2.2 (Thermo Fischer Scientitific). HRMS of intact isolated compounds were carried out using a quadrupole time-of-flight mass spectrometer (MS Q-TOF G6530, Agilent Technologies) equipped with an electrospray ionization ion source. The finalized operating ESI source conditions were as follows, using a *m/z* 50–3200 mass range: capillary voltage set at 3500 V; skimmer voltage, 65 V; fragmentor voltage, 175 V; desolvation gas (325 °C; 8 L/min) and nebulizing gas (nitrogen, 50 psi).

The collision energies were set at 20–40 eV with 30 milli-seconds excitation time for collision-induced dissociation (CID) experiments. HPLC analyses were carried out on a Waters instrument (Millipore Corp., Waters Chromatography Division, Milford MA) with a 600E multisolvent delivery system and a 996 photodiode array detector. NMR spectra were recorded in C_5D_5N solution, using micro NMR sample tubes (2.5 mm O.D. stem; sample volume 115 μL at 30 mm height), on Varian VNMRS instruments at 400 and 500 MHz, a Jeol ECZR at 600 MHz, or on Bruker Avance III HD spectrometers at 700 and 800 MHz, using tetramethylsilane as an internal standard. GC-MS was performed on a Hewlett-Packard 5890-II instrument coupled to a JEOL SX-102A spectrometer. GC conditions: HPMS-5 (5%-phenyl)-methylpolysiloxane column (30 m × 0.25 mm, film thickness 0.25 μm); He, linear velocity 30 cm/s; 50 °C isothermal for 3 min, linear temperature gradient to 300 at 20 °C/min; final temperature hold, 10 min. MS conditions: ionization energy, 70 eV; ion source temperature, 280 °C; interface temperature, 300 °C; scan speed, 2 scans s^{-1}; mass range, 33-1000 Da.

Plant Material. Roots of Brazilian jalap (*Operculina macrocarpa*) were obtained from an original sample on deposit at the Pharmacognosy Drug Collection of the Departamento de Produtos Naturais e Alimentos Dispensary, Faculdade de Farmacia, Universidade Federal do Rio de Janeiro. Its authenticity has been determined by Prof. Renato Jose de Siqueira Jaccoud according to pharmacopeic methodologies.[1a,4b]

Extraction and Isolation. The whole dried root (600 g) was powdered and extracted by subsequent percolations with a mixture of hexanes (1 × 4 L), dichloromethane (4 × 4 L), and methanol (4 × 4 L). Every extract was evaporated to

dryness under reduced pressure to obtain, after removal of the solvents, a waxy residue-soluble in hexane (0.28 g), and two dark brown syrups (7.64 g and 78.62 g from CH_2Cl_2 and MeOH, respectively). The MeOH-soluble extract was suspended in deionized water (3×100 mL) and submitted to sonication for 30 min to yield a water-insoluble fraction (41 g), which was dissolved in MeOH and kept for twelve hours at 0 °C to facilitate the precipitation of the convolvulin fraction (32 g). The supernatant was partitioned with n-BuOH (3×250 mL) and evaporated to dryness to obtain an additional amount of resin glycosides (4.7 g).

Alkaline Hydrolysis of the Convolvulin Fraction. A solution of the methanol-soluble extract resin glycoside fraction (5 g) in 5% KOH–H_2O (128.5 mL) was refluxed at 95 °C for 4 h. Reaction mixture was acidified to pH 4.0 and extracted with CH_2Cl_2 (2×50 mL). The organic layer was washed with H_2O, dried over anhydrous Na_2SO_4, and evaporated under reduced pressure (326.4 mg). The residue from the organic phase was directly analyzed by GC-MS afforded four peaks: 3-methylbutyric acid (t_R 6.49 min): m/z $[M]^+$ 102 (3), 87 (15), 69 (5), 60 (100); 2-methylbutyric (t_R 6.55 min): m/z $[M]^+$ 102 (3), 87 (33), 74 (100), 69 (10), 57 (45); tiglic acid (t_R 7.13 min): m/z $[M]^+$ 100 (70), 85 (35), 55 (100); and exogonic acid (t_R 8.92 min): m/z $[M]^+$ 200 (2), 167 (5), 156 (10), 145 (30), 127 (35), 112 (17), 101 (68), 96 (30), 85 (90), 83 (38), 70 (25), 56 (100), 55 (100). The aqueous layer was extracted with n-BuOH (3×50 mL) and concentrated to give a pale-yellowish solid (2.68 g), which was further acetylated (Ac_2O–C_5H_5N, 2:1) to give a residue (2.54 g).

HPLC Separation of Peracetylated Glycosidic Acids (12-16). The peracetylated glycosidic acid mixture (500 mg) was subjected to preparative HPLC on a Waters Symmetry Prep C_{18} column (19 × 300 mm; 7 μm). The elution was isocratic with $CH_3CN–H_2O$ (9:1), using a flow rate of 8 mL/min and a sample injection of 500 μL (20–100 mg/mL). Each eluate across six observed resolved peaks were collected by the technique of heart cutting and independently reinjected to the HPLC system and further recycled to achieve chromatographic homogeneity after ten to twenty cycles[15a] to afford: **12** (65.2 mg, t_R = 10.2 min), **14** (12.1 mg, t_R = 13.3 min), **15** (8.8 mg, t_R = 20.9 min), and **17** (28.5 mg, t_R = 25.4 min). Peak with t_R = 12.0 min afforded after eight cycles two constituents (Figure S4, Supporting Information): **13** (18.4 mg) and **18** (10.5 mg). Peak with t_R = 8.3 min afforded after 8.5 mg of peracetylated monosaccharide **16**.

Peracetylated operculinic acid H (12): white solid, mp 96-98 °C; ORD (*c* 0.4, MeOH) $[\alpha]^{22}_{589}$ −20.0, $[\alpha]_{578}$ −21.0, $[\alpha]_{546}$ −24.1, $[\alpha]_{436}$ −39.5; ¹H NMR (700 MHz, C_5D_5N) and ¹³C NMR (175 MHz, C_5D_5N) data, see Tables 2 and 3. HRESIMS *m/z* 2007.73859 [M + Na]⁺ (calcd for $C_{88}H_{128}O_{50}Na$ requires 2007.73655, δ = +1.0 ppm).

Peracetylated operculinic acid I (13): white solid, mp 84-88 °C; ORD (*c* 0.17, MeOH) $[\alpha]^{22}_{589}$ −18.2, $[\alpha]_{578}$ −20.0, $[\alpha]_{546}$ −21.8, $[\alpha]_{436}$ −34.7; ¹H NMR (600 MHz, C_5D_5N) and ¹³C NMR (150 MHz, C_5D_5N) data, see Tables 2 and 3. HRESIMS *m/z* 1949.72595 [M + Na]⁺ (calcd for $C_{86}H_{126}O_{48}Na$ requires 1949.73107, δ = −2.6 ppm).

Peracetylated operculinic acid J (14): white solid, mp 85-87 °C; ORD (*c* 0.05, MeOH) $[\alpha]^{22}_{589}$ −6.0, $[\alpha]_{578}$ −6.0, $[\alpha]_{546}$ −8.0, $[\alpha]_{436}$ −10.0; ¹H NMR (400 MHz, C_5D_5N) and ¹³C

NMR (100 MHz, C$_5$D$_5$N) data, see Tables 2 and 3. HRESIMS m/z 1949.72618 [M + Na]$^+$ (calcd for C$_{86}$H$_{126}$O$_{48}$Na requires 1949.73107, δ = −2.5 ppm).

Peracetylated purgic acid A (15): white solid, mp 101-103 $^\circ$C; ORD (c 0.09, MeOH) $[\alpha]^{22}_{589}$ −11.1, $[\alpha]_{578}$ −11.1, $[\alpha]_{546}$ −14.2, $[\alpha]_{436}$ −17.8; ^{1}H NMR (400 MHz, C$_5$D$_5$N) and ^{13}C NMR (100 MHz, C$_5$D$_5$N) data, see Table 5. HRESIMS m/z 1805.69141 [M + Na]$^+$ (calcd for C$_{80}$H$_{118}$O$_{44}$Na requires 1805.68882, δ = +1.4 ppm).

Peracetylated operculinic acid K (16): syrup; ORD (c 0.09, MeOH) $[\alpha]^{22}_{589}$ −16.4, $[\alpha]_{578}$ −17.9, $[\alpha]_{546}$ −20.0, $[\alpha]_{436}$ −31.4; ^{1}H NMR (400 MHz, C$_5$D$_5$N): δ 5.68 (1H, dd, J = 9.6, 9.6 Hz, Qui-3), 5.42 (1H, dd, J = 9.7, 8.0 Hz, Qui-2), 5.17 (1H, dd, J = 9.6, 9.6 Hz, Qui-4), 4.87 (1H, d, J = 8.0 Hz, Qui-1), 3.82 (1H, dq, J = 9.6, 6.2 Hz, Qui-5), 3.72 (1H, m, Agl-7), 2.57 (2H, t, J = 7.2 Hz, H$_2$-2 Agl), 2.16 (3H, s, CH_3CO-), 2.05 (3H, s, CH_3CO-), 2.01 (3H, s, CH_3CO-), 1.84 (2H, m, Agl-3), 1.29 (3H, d, J = 6.2 Hz, Qui-6), 0.89 (3H, t, J = 7.0 Hz, Agl-10); ^{13}C-NMR (100 MHz, C$_5$D$_5$N): δ 176.7 (Agl-1), 170.7 (CH$_3$$CO$-), 170.3 (CH$_3$$CO$-), 170.0 (CH$_3$$CO$-), 100.6 (Qui-1), 80.4 (Agl-7), 74.4 (Qui-4), 74.0 (Qui-3), 73.1 (Qui-2), 70.3 (Qui-5), 37.6 (Agl-8), 35.4 (Agl-2), 34.8 (Agl-6), 30.2 (Agl-4), 26.1 (Agl-3), 25.4 (Agl-5), 21.1 (CH_3CO-), 20.9 (CH_3CO-), 20.8 (CH_3CO), 19.0 (Agl-9), 18.0 (Qui-6), 14.6 (Agl-10); HRESIMS m/z 483.22120 [M + Na]$^+$ (calcd for C$_{22}$H$_{36}$O$_{10}$Na requires 483.22006, δ = +2.3 ppm).

Peracetylated operculinic acid H macrolactone (17): white solid, mp 97-99 $^\circ$C; ORD (c 0.17, MeOH) $[\alpha]^{22}_{589}$ −18.2, $[\alpha]_{578}$ −18.8, $[\alpha]_{546}$ −21.2, $[\alpha]_{436}$ −34.7; ^{1}H NMR (800 MHz, C$_5$D$_5$N) and ^{13}C NMR (200 MHz, C$_5$D$_5$N) data, see Table 6. HRESIMS m/z 1949.71159 [M + Na]$^+$ (calcd for C$_{86}$H$_{124}$O$_{48}$Na requires 1947.71542, δ = −1.9 ppm).

Peracetylated dehydrated operculinic acid H (**18**): white powder, mp 87-89 °C; $[\alpha]^{22}_{589}$ −21.1, $[\alpha]_{578}$ −21.1, $[\alpha]_{546}$ −24.2, $[\alpha]_{436}$ −40.0; negative ESIMS *m/z* 1925 [M − H]⁻;

¹H NMR (C₅D₅N, 400 MHz) δ 4.87 (1H, d, *J* = 7.4 Hz, Glc-1), 4.29 (1H, dd, *J* = 9.0, 7.9 Hz, Glc-2), 5.77 (1H, m, Glc-3), 5.38 (1H, dd, *J* = 9.7, 9.7 Hz, Glc-4), 4.10 (1H, m, Glc-5), 3.93 (1H, dd, *J* = 12.6, 5.6 Hz, Glc-6a), 4.08 (1H, br s, Glc-6b), 5.07 (1H, d, *J* = 7.6 Hz, Glc′-1), 4.16 (1H, d, *J* = 7.6 Hz, Glc′-2), 4.58 (1H, dd, *J* = 9.7, 9.7 Hz, Glc′-3), 5.36 (1H, dd, *J* = 9.7, 9.7 Hz, Glc′-4), 4.13 (1H, m, Glc′-5); 4.40 (1H, dd, *J* = 11.9, 2.9 Hz, Glc′-6a), 4.65 (1H, br d, *J* = 11.9 Hz, Glc′-6b), 5.28 (1H, m, Glc″-1), 5.28 (1H, m, Glc″-2), 5.84 (1H, dd, *J* = 9.7, 9.7 Hz, Glc″-3), 5.44 (1H, dd, *J* = 9.7, 9.7 Hz, Glc″-4), 4.21 (1H, d, *J* = 10.5 Hz, Glc″-5), 4.14 (1H, d, *J* = 12.5 Hz, Glc″-6a), 4.73 (1H, m, Glc″-6b), 5.50 (1H, br s, Glc‴-1), 5.46 (1H, m, Glc‴-2), 5.77 (1H, dd, *J* = 9.7, 9.7 Hz, Glc‴-3), 5.60 (1H, dd, Glc‴-4), 4.30 (1H, m, Glc‴-5), 4.49 (1H, d, *J* = 12.5 Hz, Glc‴-6a), 4.65 (1H, d, *J* = 12.5 Hz, Glc‴-6a), 5.24 (1H, br s, Rha-1), 5.78 (1H, m, Rha-2), 5.72 (1H, d, *J* = 10.2, 3.5 Hz, Rha-3), 5.58 (1H, m, Rha-4), 4.12 (1H, dq, Rha-5), 1.37 (3H, d, *J* = 6.3 Hz, Rha-6), 5.76 (1H, br s, Rha′-1), 5.94 (1H, br d, *J* = 4.2 Hz, Rha′-2), 4.82 (1H, dd, *J* = 10.0, 4.2 Hz, Rha′-3), 5.57 (1H, m, Rha′-4), 4.72 (1H, m, Rha′-5), 1.60 (3H, d, *J* = 6.2 Hz, Rha′-6), 7.34 (1H, t, *J* = 15.5, 7.0 Hz, Agl-3), 6.28 (1H, d, *J* = 15.5 Hz, Agl-2), 2.30 (2H, Agl-4), 3.88 (1H, m, Agl-12), 1.01 (3H, t, *J* = 7.2 Hz, Agl-16); ¹³C NMR (100 MHz, C₅D₅N) δ 101.4 (CH, Glc-1), 72.6 (CH, Glc-2), 76.7 (CH, Glc-3), 70.9 (CH, Glc-4), 73.5 (CH, Glc-5), 68.0 (CH₂, Glc-6), 101.1 (CH, Glc′-1), 76.4 (CH, Glc′-2), 82.0 (CH, Glc′-3), 69.6 (CH, Glc′-4), 72.4 (CH, Glc′-5), 63.0 (CH₂, Glc′-6), 100.0 (CH, Glc″-1), 73.3 (CH, Glc″-2), 73.6 (CH, Glc″-3), 69.2 (CH, Glc″-4), 72.3 (CH, Glc″-5), 62.2 (CH₂, Glc″-6), 101.7 (CH, Glc‴-1), 72.3 (CH, Glc‴-2), 73.9 (CH, Glc‴-

3), 69.2 (CH, Glc'''-4), 76.5 (CH, Glc'''-5), 62.0 (CH$_2$, Glc'''-6), 99.2 (CH, Rha-1), 70.5 (CH, Rha-2), 70.2 (CH, Rha-3), 71.7 (CH, Rha-4), 67.5 (CH, Rha-5), 18.2 (CH$_3$, Rha-6), 98.3 (CH, Rha'-1), 72.2 (CH, Rha'-2), 75.4 (CH, Rha'-3), 73.4 (CH, Rha'-4), 67.6 (CH, Rha'-5), 18.2 (CH$_3$, Rha'-6), 175.8 (CO, Agl-1), 149.2 (CH, Agl-3), 124.2 (CH, Agl-2), 81.3 (CH, Agl-12), 35.17 (Agl-11) , 34.82 (Agl-13), 32.9 (CH$_2$, Agl-4), 30.93, 30.54, 30.30, 29.95, 29.09, 28.28, 25.39, 23.64 (Ag-15), 14.8 (CH$_3$, Agl-16); HRESIMS m/z 1947.71870 [M + Na]$^+$ (calcd for C$_{86}$H$_{124}$O$_{48}$Na requires 1947.71542, δ = +1.7 ppm).

Acid Hydrolysis and Sugar Analysis. A sample of each individual operculinic acid (4 mg) in 4 N HCl (10 mL) was heated at 90 °C for 2 h. The reaction mixture was diluted with H$_2$O (5 mL) and extracted with CH$_2$Cl$_2$ (2 × 30 mL). The aqueous phase was neutralized with 1 N KOH and extracted with n-BuOH (2.5 mL), then washed with H$_2$O (2 × 2.5 mL) and concentrated. The sugar residues (0.5 mg each) were reacted with L-cysteine hydrochloride (0.5 mg) in pyridine (150 μL) at 60 °C for 1 h.[23] Then, the thiazolidine products were converted into volatile derivatives by treatment with chlorotrimethylsilane (0.1 mL, Sigma Sil-A). The reaction mixtures were independently dried, dissolved in CHCl$_3$ (100 μL), filtered, and then analyzed (inyection volume: 1 μL) by CG: HPMS-5 (20 m × 0.18 mm, film thickeness 0.18 µm); injector temperature: 300 °C; oven temperature: 100 °C isothermal for 3 min, linear gradient to 300°C at 20°C/min; carrier gas, He (1.0 mL/min). Retention times for TMS derivatives of common sugars were used for identification by coelution experiments: D-xylose, t_R 10.74 min; L-rhamnose (Rha), t_R 11.10 min; D-quinovose (Qui), t_R 11.45 min;

D-fucose t_R 11.60 min; D-glucose (Glc), t_R 11.73 min; L-glucose, t_R 14.85 min. This analysis led to the identification of Glc and Rha from **1**, **2** and **3**. Qui was found in **5**.

Hydrogenation of Derivative 18. A solution of peracetylated dehydroxylated operculinic acid H (**18**; 5 mg) in MeOH (2 mL) with 10 % Pd/C (10 wt %; Aldrich, 205699) in H_2 atmosphere was stirred for two days at ordinary pressure and temperature. After filtration, the solution was concentrated by removing MeOH using a rotary evaporator to give a white solid, which was identical with peracetylated operculinic acid I (**13**).

Alkaline Hydrolysis of Compounds 12-16. Individual solutions of peracetylated **12-16** (5-10 mg for each one), in 5% KOH–H_2O (1 mL) were refluxed at 95 ℃ for 3 h. Then, the reaction mixtures were acidified to pH 5.0 and extracted with n-BuOH (2 × 10 mL) and concentrated to give colorless solids. Saponification of compound **12** yielded a mixture (7.2 mg) of operculinic acid H (**1**; m/z 1251 $[M + Na]^+$) and its dehydrated derivative, which were resolved by recycling HPLC on a Waters μBondapak amino (NH_2) column (19 × 300 mm; 10 μm) with CH_3CN–H_2O (4:1) to afford 6.5 mg of **1** and 0.7 mg of its dehydrated derivative derivative (m/z 1233 $[M + Na]^+$). Saponification of compound **13** produced operculinic acid I (**2**, 4.2 mg); compound **14** afforded operculinic acid J (**3**; 2.9 mg); derivative **15** produced purgic acid A (**4**; 4.8 mg); and, finally, derivative **16** yielded operculinic acid K (**5**; 4.0 mg).

Operculinic acid H (1): white solid, mp 153-156 ℃ ORD (c 0.02, MeOH) $[\alpha]^{22}_{589}$ −35.0, $[\alpha]_{578}$ −50.0, $[\alpha]_{546}$ −50.2 $[\alpha]_{436}$ −60.0; ^1H NMR (800 MHz, C_5D_5N) and ^{13}C NMR (200

MHz, C$_5$D$_5$N) data, see Tables 1 and 2. HRESIMS m/z 1227.55112 [M – H]$^-$ (calcd for C$_{52}$H$_{91}$O$_{32}$ requires 1227.54989, δ = +1.0 ppm).

Operculinic acid I (2): white solid, mp 153-156 °C; ORD (c 0.34, MeOH) $[\alpha]^{22}_{589}$ –12.0, $[\alpha]_{578}$ –15.1, $[\alpha]_{546}$ –18.2, $[\alpha]_{436}$ –19.5; ^{1}H NMR (800 MHz, C$_5$D$_5$N) and ^{13}C NMR (200 MHz, C$_5$D$_5$N) data, see Tables 1 and 2. HRESIMS m/z 1235.55259 [M + Na]$^+$ (calcd for C$_{52}$H$_{92}$O$_{31}$Na requires 1235.55147, δ = +0.9 ppm).

Operculinic acid J (3): white solid, mp 159-161 °C; ORD (c 0.34, MeOH) $[\alpha]^{22}_{589}$ –10.0, $[\alpha]_{578}$ –10.6, $[\alpha]_{546}$ –12.1, $[\alpha]_{436}$ –19.7; HRESIMS m/z 1235.55359 [M + Na]$^+$ (calcd for C$_{52}$H$_{92}$O$_{31}$Na requires 1235.55147, δ = +1.7 ppm).

Purgic acid A (4): white solid, mp 101-103 °C; ORD (c 0.07, MeOH) $[\alpha]^{22}_{589}$ –14.3, $[\alpha]_{578}$ –17.1, $[\alpha]_{546}$ –20.2, $[\alpha]_{436}$ –22.9; ^{1}H NMR (700 MHz, C$_5$D$_5$N) and ^{13}C NMR (175 MHz, C$_5$D$_5$N) data, see Table 6. HRESIMS m/z 1175.53162 [M + Na]$^+$ (calcd for C$_{50}$H$_{88}$O$_{29}$Na requires 1175.53034, δ = +1.1 ppm).

Operculinic acid K (5): syrup; ORD (c 0.07, MeOH) $[\alpha]^{22}_{589}$ –20.0, $[\alpha]_{578}$ –21.4, $[\alpha]_{546}$ –24.3, $[\alpha]_{436}$ –37.1; ^{1}H NMR (700 MHz, C$_5$D$_5$N): δ 4.79 (1H, d, J = 7.4 Hz, Qui-1), 4.19 (1H, dd, J = 8.7, 8.7 Hz, Qui-3), 3.96 (1H, dd, J = 8.7, 7.4 Hz, Qui-2), 3.87 (1H, 1H, m, Agl-7), 3.77 (1H, dq, J = 8.7, 6.3 Hz, Qui-5), 3.71 (1H, dd, J = 8.7, 8.7 Hz, Qui-4), 2.54 (2H, m, CH$_2$ Agl-2), 1.62 (3H, d, J = 6.3 Hz), 0.93 (3H, t, J = 7.1 Hz, Agl-10); ^{13}C-NMR (175 MHz, C$_5$D$_5$N): δ 175.7 (Agl-1), 103.8 (Qui-1), 79.1 (Agl-7), 78.2 (Qui-3), 77.2 (Qui-4), 75.8 (Qui-2), 73.1 (Qui-5), 38.1 (Agl-8), 37.3 (Agl-2), 35.0 (Agl-6), 30.4 (Agl-4), 26.7 (Agl-3), 25.2 (Agl-5), 19.2 (Agl-9), 19.0 (Qui-6), 14.7 (Agl-10); HRESIMS m/z 357.18801 [M + Na]$^+$ (calcd for C$_{16}$H$_{30}$O$_7$Na requires 357.18837, δ = –1.0 ppm).

Identification of Aglycones. The organic layer residues obtained from the acid-catalyzed hydrolysis of each operculinic acid were evaporated to dryness, dissolved in $CHCl_3$ (5 mL), and treated with CH_2N_2 to give a residue which was derivatized with Sigma Sil-A for 5 min at 70 °C and analyzed by GC-MS to identify the silylated derivatives[18] of: 3S,12S-dihydroxyhexadecanoic (operculinolic) acid methyl ester (t_R 16.1 min) for **1**: m/z 389 (15, $[C_{13}H_{24}O_4(TMS)_2]^+$), 341 (65), 243 (30), 175 (45, $[C_4H_6O_3TMS]^+$), 159 (70, $[C_5H_{10}OTMS]^+$); 12-hydroxyhexadecanoic acid methyl ester (t_R 14.5 min) for **2**: m/z 301 (45, $[C_{13}H_{24}O_3TMS]^+$), 159 (100, $[C_5H_{10}OTMS]^+$); 11-hydroxyhexadecanoic acid methyl ester (t_R 14.7 min) for **3**: m/z 287 (45, $[C_{12}H_{22}O_3TMS]^+$) and 173 (95, $[C_6H_{12}OTMS]^+$); and 11-hydroxytetradecanoic acid methyl ester (t_R 14.1 min) for **4**: 287 (75, $[C_{12}H_{22}O_3TMS]^+$) and 145 (100, $[C_4H_8OTMS]^+$).

HPLC Separation of Macrocarpic Acids (6-8). The precipitated mixture of intact glycosidic acids (500 mg) was subjected to preparative HPLC on a Waters Symmetry Prep C_{18} column (19 × 300 mm; 7 μm). The elution was isocratic with $CH_3CN–H_2O$ (9:1), using a flow rate of 8 mL/min and a sample injection of 500 μL (20–100 mg/mL). Each eluate across three observed resolved peaks were collected by the technique of heart cutting and independently reinjected to the HPLC system and further recycled to achieve chromatographic homogeneity after ten to twenty cycles[15a] to afford: **6** (14.0 mg mg, t_R = 9.98 min), **7** (8.8 mg, t_R = 11.40 min), and **8** (11.2 mg, t_R = 10.55 min).

Macrocarposidic acid A (6): white solid, mp 117-119 °C; ORD (c 0.29, MeOH) $[\alpha]^{22}_{589}$ −18.6, $[\alpha]_{578}$ −19.3, $[\alpha]_{546}$ −22.1, $[\alpha]_{436}$ −35.2, $[\alpha]_{365}$ −49.3; ^{1}H NMR (400 MHz, C_5D_5N) and

^{13}C NMR (100 MHz, C$_5$D$_5$N) data, see Tables 7 and 8. HRESIMS *m/z* 1681.7805 [M + Na]$^+$ (calcd for C$_{77}$H$_{126}$O$_{38}$Na requires 1681.78193, δ = -0.8 ppm).

Macrocarposidic acid B (7): white solid, mp 158-160 °C; ORD (*c* 0.26, MeOH) $[\alpha]^{22}_{589}$ −20.0, $[\alpha]_{578}$ −20.4, $[\alpha]_{546}$ −23.1, $[\alpha]_{436}$ −37.7, $[\alpha]_{365}$ −53.1; ^{1}H NMR (500 MHz, C$_5$D$_5$N) and ^{13}C NMR (125 MHz, C$_5$D$_5$N) data, see Tables 7 and 8. HRESIMS *m/z* 1683.7988 [M + Na]$^+$ (calcd for C$_{77}$H$_{128}$O$_{38}$Na requires 1683.79758, δ = +0.7 ppm).

Macrocarposidic acid C (8): white solid, mp 160-162 °C; ORD (*c* 0.17, MeOH) $[\alpha]^{22}_{589}$ −14.7, $[\alpha]_{578}$ −15.9, $[\alpha]_{546}$ −17.6, $[\alpha]_{436}$ −27.6, $[\alpha]_{365}$ −38.2; ^{1}H NMR (400 MHz, C$_5$D$_5$N) and ^{13}C NMR (100 MHz, C$_5$D$_5$N) data, see Tables 7 and 8. HRESIMS *m/z* 1683.7984 [M + Na]$^+$ (calcd for C$_{77}$H$_{128}$O$_{38}$Na requires 1683.79758, δ = +0.5 ppm).

ASSOCIATED CONTENT

Supporting Information

Photographies for plant material and phytopharmaceuticals. TLC and HPLC analyses of the peracetylated saponified extract. ^{1}H and ^{13}C NMR spectra, including 2D experiments, for glycosidic acids and their peracetylated derivatives, as well as for macrocarpic acids. EIMS spectra for silylated methyl ester aglycones. This material is available free of charge via the Internet at http://pubs.acs.org.

AUTHOR INFORMATION

Corresponding Author

*Tel: +52 55 5622-5288. Fax: +52 55 5622 5329. E-mail: pereda@unam.mx.

Author Contributions

Based on the Ph.D. thesis of J. Lira-Ricárdez (Posgrado en Ciencias Químicas, UNAM).

ORCID

Suzana Guimarães Leitão: 0000-0001-7445-074X

Rogelio Pereda-Miranda: 0000-0002-0542-0085

Notes

The authors declare no competing financial interest.

REFERENCES

(1) (a) Dias da Silva, R. A. *Código Pharmacêutico Brasileiro. Pharmacopeia dos Estados Unidos do Brasil*; Companhia Editora Nacional: São Paulo, 1929; pp. 535-536. (b) Barbosa, W.L.R. Etnofarmácia, Fitoterapia Popular e Ciência Farmacêutica; Editora CRV, Curitiba, 2011: p 83. (c) Lorenzi, H.; Abreu-Matos, F. J. *Plantas Medicinais no Brasil. Nativas e Exóticas*; Instituto Plantarum: Nova Odessa, São Paulo, 2002; pp 183-184.

(2) (a) Enriquez, R. G., Leon, I., Perez, F., Carpenter, K. A., Puzzuoli, F. V., Reynolds, W. F. *Can. J. Chem.* **1992**, *70*, 1000-1008. (b) Hernández-Carlos B.; Bye, R.; Pereda-Miranda, R. *J. Nat. Prod.* **1999**, *62*, 1096-1100. (c) Pereda-Miranda, R.; Fragoso-Serrano, M.; Escalante-Sánchez, E.; Hernández-Carlos, B.; Linares, E.; Bye, R. *J. Nat. Prod.* **2006**, *69*, 1460-1466. (d) Castañeda-Gómez, J.; Pereda-Miranda, R. *J. Nat. Prod*. **2011**, *74*, 1148-1153.

(3) Pereda-Miranda, R.; Rosas-Ramírez, D.; Castañeda-Gómez, J. In *Progress in the Chemistry of Organic Natural Products*; Kinghorn, A. D., Falk, H., Kobayashi, J., Eds.; Springer-Verlag: New York, 2010; Vol. 92, Chapter 2, pp 77-152.

(4) (a) Brandão, M. G.; Cosenza, G. P.; Grael, C. F.; Netto Junior, N. L; Monte-Mór, R. L. *Rev. Bras. de Farmacog.* **2009**, *19*, 478-487. (b) Michelin, D. C.; Finati, S. C. G.; Sacramento, L. V. S.; Vilegas, W.; Salgado, H. R. N. *Rev. Bras. de Farmacog.* **2010**, *20*, 18-22. (c) Galvão, M. A.; Ferreira, M. R.; Nunes, B. M.; Santana, A. S.; Randau, K. P.; Soares, L. A. *Rev. Bras. de Farmacog.* **2014**, *24*, 683-690.

(5) (a) Pereda-Miranda, R.; Villatoro-Vera, R.; Bah, M.; Lorence, A. *Rev. Latinoamer. Quim.* **2009**, *37*:144-154. (b) Zhu, D.; Chen, C.; Bai, L.; Kong, L.; Luo, J. *Evid.-Based Compl. Alt.* **2019**, DOI: 10.1155/2019/9406342.

(6) Ono, M. *J. Nat. Med.* **2017**, *71*, 591-604.

(7) (a) Ono, M.; Kawasaki, T.; Miyahara, K. *Chem. Pharm. Bull.* **1989**, *37*, 3209-3212. (b) Ono, M.; Fukunaga, T.; Kawasaki, T.; Miyahara, K. *Chem. Pharm. Bull.* **1990**, *38*, 2650-2656.

(8) (a) Ono, M.; Nishi, M.; Kawasaki, T.; Miyahara, K. *Chem. Pharm. Bull.* **1990**, *38*, 2986-2991. (b) Ono, M.; Kawasaki, T.; Miyahara, K. *Chem. Pharm. Bull.* **1991**, *39*, 2534-2539. (c) Ono, M.; Fujimoto, K.; Kawata, M.; Fukunaga, T.; Kawasaki, T.; Miyahara, K. *Chem. Pharm. Bull.* **1992**, *40*, 1400-1403.

(9) (a) Wagner, H., Kazmaier, P. *Phytochemistry* **1977**, *16*, 711-714. (b) Ono, M.; Nishioka, H.; Fukushima, T.; Kunimatsu, H.; Mine, A.; Kubo, H.; Miyahara, K. *Chem. Pharm. Bull.* **2009**, *57*, 262-268.

(10) Ono, M.; Oda, S.; Yasuda, S.; Mineno, T.; Okawa, M.; Kinjo, J.; Miyashita, H.; Yoshimitsu, H.; Nohara, T.; Miyahara, K. *Chem. Pharm. Bull.* **2017**, *65*, 107-111.

(11) Ding, W.; Jiang, Z. H.; Wu, P.; Xu, L.; Wei, X. *Phytochemistry* **2012**, *81*, 165-174.

(12) (a) Pereda-Miranda, R.; Kaatz, G. W.; Gibbons, S. *J. Nat. Prod.* **2006**, 69, 406-409. (b) Chérigo, L.; Pereda-Miranda, R.; Fragoso-Serrano, M.; Jacobo-Herrera, N.; Kaatz, G. W.; Gibbons, S. *J. Nat. Prod.* **2008**, *71*, 1037-1045. (c) Chérigo, L.; Pereda-Miranda, R.; Gibbons, S. *Phytochemistry* **2009**, *70*, 222-227. (d) Escobedo-Martínez, C.; Cruz-

Morales, S.; Fragoso-Serrano, M.; Rahman, M. M.; Gibbons, S.; Pereda-Miranda, R. *Phytochemistry* **2010**, *71*, 1796-1801.

(13) (a) Corona-Castañeda, B.; Pereda-Miranda, R. *Planta Med.* **2012**, *78*, 128-131. (b) Corona-Castañeda, B.; Chérigo, L.; Fragoso-Serrano, M.; Gibbons, S.; Pereda-Miranda, R. *Phytochemistry* **2013**, *95,* 277-283. (c) Corona-Castañeda, B.; Rosas-Ramírez, D.; Castañeda-Gómez, J.; Aparicio-Cuevas, M. A.; Fragoso-Serrano, M.; Figueroa-González, G.; Pereda-Miranda, R. *Phytochemistry* **2016**, *123*, 48-57.

(14) (a) Figueroa-González, G.; Jacobo-Herrera, N.; Zentella-Dehesa, A.; Pereda-Miranda, R. *J. Nat. Prod.* **2012**, *75*, 93-97 (b) Castañeda-Gómez, J.; Figueroa-González, G.; Jacobo-Herrera, N.; Pereda-Miranda, R. *J. Nat. Prod.* **2013**, 76, 64-71. (c) Bautista, E.; Fragoso-Serrano, M.; Pereda-Miranda, R. *J. Nat. Prod*. **2015**, *78*, 168-172. (d) Cruz-Morales, S.; Castañeda-Gómez, J.; Rosas-Ramírez, D.; Fragoso-Serrano, M.; Figueroa-González, G.; Lorence, A.; Pereda-Miranda, R. *J. Nat. Prod.* **2016**, *79*, 3093-3104.

(15) (a) Pereda-Miranda, R.; Hernández-Carlos, B. *Tetrahedron* **2002**, *58*, 3145-3154. (b) Bautista, E.; Fragoso- Serrano, M.; Pereda-Miranda, R. *Phytochem. Lett*. **2016**, *17*, 85-93.

(16) Chérigo, L.; Pereda-Miranda, R.; Fragoso-Serrano, M.; Jacobo-Herrera, N.; Kaatz, G.W.; Gibbons, S. *J. Nat. Prod.* **2008**, *71*, 1037-1045.

(17) (a) Wehrli, F.W.; Wehrli, T. *Interpretation of Carbon-13 NMR Spectra*, John Wiley & Sons Ltd., Chichester, UK, 1976, p. 37. (b) Lie Ken Jie, M. S.; Mustafa, J. *Lipids* **1997**, *32*, 1019-1034.

(18) Gómez, J. C. C.; Bernstein, M.; Sýkora, S. In *Structure Elucidation in Organic Chemistry: The Search for the Right Tools*, Cid, M.M., Bravo. J. Eds., Wiley-VCH Verlag GmbH & Co. KGaA, Weinheim, Germany, 2015; pp. 445-492.

(19) León-Rivera, I., Río-Portilla, F., Enríquez, R. G., Rangel-López, E., Villeda, J., Rios, M. Y., Navarrete-Vázquez, G., Hurtado-Días, I., Guzmán-Valdivieso, U., Núñez-Urquiza, V., Escobedo-Martínez, C. *Magn. Reson. Chem.* **2017**, *55*, 214-223.

(20) Ono, M.; Takagi-Taki, Y.; Honda-Yamada, F.; Noda, N.; Miyahara, K. *Chem. Pharm. Bull.* **2010**, *58*, 666-672.

(21) Ono, M.; Kishida, M.: Ikegami, Y.; Takaki, Y.; Okawa, M.; Kinjo, J.; Yoshimitsu, H.: Nohara, T.; Miyahara, K. *J. Nat. Med.* **2011**, *65*, 95-102.

(22) Sura, M. B., Ponnapalli, M. G., Annam, S. C. V. A. R., Bobbili, V. V. P. *J. Nat. Prod.* **2019**, DOI: 10.1021/acs.jnatprod.8b01100.

(23) Cerda-García-Rojas, C. M.; Zamorano, G.; Chávez, M. I.; Catalán, C. A.; Joseph-Nathan P. *Magn. Reson. Chem*. **2000**, *38*, 494-499.

(24) Lawson, E. N.; Jamie, J. F.; Kitching, W. *J. Org. Chem.* **1992**, *57*, 353-358.

CAPÍTULO II

Reversión de la resistencia múltiple a fármacos por las resinas glicosídicas de especies de la familia Convolvulaceae en patógenos bacterianos y células cancerosas humanas

Phytochemistry Reviews

Reversal of multidrug resistance by amphiphilic morning glory resin glycosides in bacterial pathogens and human cancer cells

Jesús Lira-Ricárdez & Rogelio Pereda-Miranda*

Departamento de Farmacia, Facultad de Química, and Programa de Maestría y Doctorado en Ciencias Químicas, Universidad Nacional Autónoma de México, Ciudad Universitaria, Mexico City 04510, Mexico

e-mail: pereda@unam.mx

Abstract

Pathogens that express resistance to multiple drugs are becoming the norm, complicating treatment and increasing human morbidity. Acylsugars or resin glycosides from the morning glory family (Convolvulaceae) are amphipathic modulators of the efflux pumps responsible for the drug-resistant phenotype in prokaryotic and eukaryotic cells. These inhibitory effects could be used to overcome the acquired resistance to common anticancer or antimicrobial drugs by lowering the current effective therapeutic doses, thus decreasing toxic side-effects in refractory malignancies. Active chemosensitizers identified by *in vitro* screening methods have demonstrated the therapeutic potential of resin glycosides for further exploration as coadjuvants to avoid drug resistance and restore the clinical utility of chemotherapy in treating infections and cancer. To date, more than 20 resin glycosides have been documented as inhibitors or modulators of efflux pumps, mainly isolated from species of the genus *Ipomoea*. Resin glycosides have shown the ideal structural features associated with multidrug-resistant efflux pump substrates. An overview is given to the acylsugar diversity and their amphiphilicity properties for bioactivity as leads of efflux pump inhibitors for drug development.

Key Words

Acylsugar diversity, Amphiphilicity, Chemosensitizer, Efflux pump inhibitor, Multidrug-resistance

Abbreviations

EP	Efflux pump
EPI	Efflux pump inhibitor
EtBr	Ethidium bromide
IC_{50}	Half maximal inhibitory concentration
MDR	Multidrug-resistant/resistance
MIC	Minimal inhibitory concentration
NOR	Norfloxacine
P-gp	P-glycoprotein
RES	Reserpine
RG	Resin glycoside
Rh123	Rhodamin-123
VIN	Vinblastine

Introduction

Multidrug resistance (MDR) is a major obstacle in the chemotherapy of refractory malignancies. Multiple resistance mechanisms in cancer and life-threatening infections complicate treatment and increase both human morbidity and financial cost in health-care systems. MDR phenotype is often the overexpression of plasma-membrane-associated translocases that extrude a wide range of structurally and functionally diverse lipophilic and amphipathic antibiotics, anticancer drugs, carcinogens, toxins, and other xenobiotics from inside the cells. This prevents drugs from exerting their cytotoxicity, by decreasing intracellular accumulation below a cell-killing threshold (Du et al. 2018). Cells are resistant when they are not susceptible to the concentration of a clinically used drug; they develop various mechanisms that cause the loss of their initial sensitivity to the treatment. These mechanisms include alteration of drug targets, decrease in drug permeability across membranes, inactivation of drugs, and extrusion of drugs by efflux pumps (EPs), among others (Varela et al. 2017). These translocases are universally expressed, from bacteria to mammals (Higgins 1992).

In mammalian cancer cells, the expression of ATP-dependent EPs, such as P-glycoprotein (MDR protein 1/P-gp) and the breast cancer resistance protein (BCRP/ABCG2) in the superfamily of adenosine triphosphate (ATP)-binding cassette (ABC) transporters (Kathawala 2015; Locher 2016), are the principle responsible for the MDR phenotype (Figure 30). Therefore, inhibition of these EPs is essential in order to avoid drug resistance and potentially restore the clinical utility of chemotherapy (Basha Syed and Selvaraj Coumar 2016).
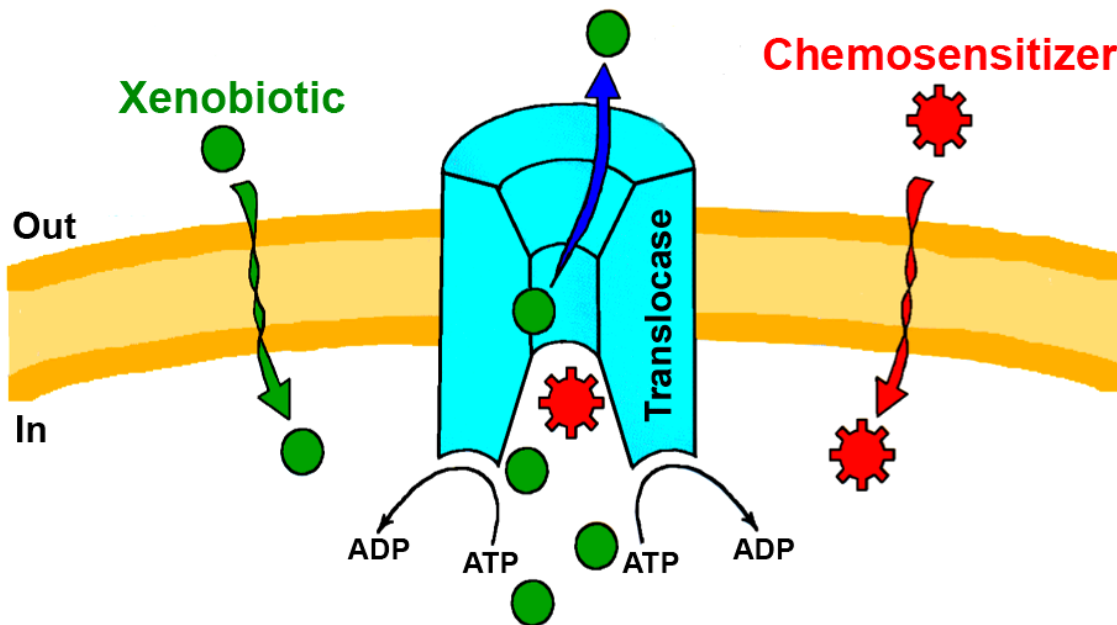
Figure 30. Glycoprotein-P, a unique ATP-dependent membrane transport protein, is one of those key regulators or translocases, which has a diverse tissue distribution in the human body. Over-expression of P-gp leads to decrease intracellular accumulation of many chemotherapeutic agents. Eventually, the effectiveness of these drugs is decreased as well as the toxicity of any xenobiotic. ABC transporter inhibitors or modulators, also known as chemosensitizers, can be used in combination with chemotherapeutic drugs to enhance their efficacy.

Indiscriminate and irrational use of antibiotics has produced an emergence of MDR in pathogenic bacteria. This now has become an important threat to global health because both Gram-positive and Gram-negative bacteria are affected by the expansion of antibiotic MDR (Szakács et al. 2014; Blair et al. 2015; Chandra et al. 2017). When overexpressed, bacterial EPs confer elevated levels of resistance to therapeutically useful antimicrobial agents (Blair et al., 2015). Clinical data indicate that EPs function in drug extrusion and provide virulence and adaptive responses that contribute to drug resistance during infection (Du et al. 2018). Efflux is most effective when working in cooperation with other resistance mechanisms, as seen in nosocomial bacterial strains. Decreasing passive absorption (influx) or increasing active efflux of antibiotics (Nikaido and Pagès 2012) has

contributed to the spread of MDR Gram-negative bacteria in hospitals and other communitary clinical situations. The infections caused by Gram-negative pathogens are difficult to treat due to their higher intrinsic resistance due to the presence of a protective double-layer of lipid membranes –not present in Gram-positive microorganisms– (Venter et al. 2015).

Nowadays, MDR Gram-negative bacteria produce approximately 80% of clinically diagnosed infections. There are few antibiotics that treat infections caused by methicillin-resistant *Staphylococcus aureus* strains (Remschmidt et al. 2017). Resistance to vancomycin, the main antibiotic used clinically, has become more frequent, a cause for considerable concern in hospitals, prisons, and nursing homes (O'Driscoll and Crank 2015; Chiang et al. 2017). Resistance to oxazolidinone (linezolid) and streptogramin-type antibiotics has also been reported for vancomycin-resistant Enterococci (Remschmidt et al. 2017). The acronym ESKAPEE has been created from the names of the organisms identified as the major pathogenic bacteria capable of escaping the biocidal activity of antibiotics: *Enterococcus faecium*, *S. aureus*, *Klebsiella pneumoniae*, *Acinetobacter baumannii*, *Pseudomonas aeruginosa*, *Enterobacter* species, and *Escherichia coli* (Pendleton et al. 2013). Various other organisms have become equally challenging to treat in the clinic, including *Burkholderia cepacia* and *Cryptococcus neoformans* (Nascimento et al. 2017) –invasive life-threatening opportunistic infection of the lungs– and *Neisseria gonorrhoeae* (Ohnishi et al. 2011).

So there is evident and urgent need to recognize new compounds that exhibit a broad spectrum of activities and develop those leads into new, clinically useful drugs. The use of EP chemosensitizers (modulators or inhibitors) co-administered with accessible drugs

could result in a susceptibility equivalent to that of a cell without transporter expression *in vitro* and *in vivo* (Sun et al. 2014; Adamson et al. 2015).

Considering these needs for chemosensitizers, natural bioactive secondary metabolites with modulatory effects offer huge potential for discovering new ways and scaffolds to recognize the function of transporters, apart from avoiding the toxicities shown by synthetic counterparts (Prasch and Bucar 2015; Ayaz et al. 2017; Dewanjee et al. 2017). There is growing evidence that acylsugars or resin glycosides (RGs) from the morning glory family (Convolvulaceae) are amphipathic modulators of the EPs responsible for the MDR phenotype in prokaryotic (Corona-Castañeda and Pereda-Miranda 2012; Pereda-Miranda et al. 2006) and eukaryotic cells (Figueroa-González et al. 2012; Castañeda-Gómez et al. 2013).

This review will give direct information to plant chemists, pharmacognosists, medicinal chemists, and plant biotechnologists working in the field of drug discovery to explore further the therapeutical potential of RGs as chemosensitizers for the treatment of infections and cancer by presenting the importance of the acylsugar diversity and their amphiphilicity properties.

Acylsugar diversity in the Convolvulaceae

The Convolvulaceae family belongs to the order Solanales and is taxonomically related to the Solanaceae family (Eich 2008). Both families are characterized by the presence of a high diversity RGs built on distinct sugar cores (Pereda-Miranda et al. 2010; Kroumova et al. 2016; Moghe et al. 2017). These seem to play important roles in natural pest resistance, providing protection against fungi, insects, herbivores, bacteria, and mechanical damage

such as synergistic antimicrobial (Luu et al. 2017) or insect protective action (Leckie et al. 2016; Liu et al. 2017), as well as offering a chemical defense in plant-plant interactions for the producing species (Lotina-Hennsen et al. 2013). It has been postulated that this natural variability may generate a synergistic antimicrobial or insect protective action to the producing plants that might provide selective adaptive defence advantages.

This diversity allows acylsugars to play important, divergent roles, ranging from cell-surface interactions with important proteins in recognition, differentiation, and proliferation of cells to interactions with another oligo- and polysaccharides that produce the mechanical properties of plants (Prestegard et al. 2017). These structural variations could be the result of promiscuous enzyme activities during the biosynthetic pathways of these bioactive secondary metabolites that provide advantages against abiotic and biotic stress (Moghe et al. 2017).

Several biological activities evident in purgative morning glory species (Convolvulaceae) have been attributed to their RG contents, complex mixtures of acylsugars built on distinct oligosaccharides of monohydroxy and dihydroxy C-14 and C-16 fatty acids (Pereda-Miranda et al. 2010). Their structures are unusual: amphiphilic metabolites, meaning that their structure contains hydrophobic (fatty acid aglycones) as well as hydrophilic (sugar or glycone) moieties. The latter is composed of a heteropolysaccharide with few residues (up to seven) that contain no more than four different monosaccharides. These compounds illustrate how nature creates structural diversity by using simple metabolic building blocks. The sugars are D-glucose and four pentoses: D-fucose, L-rhamnose, D-quinovose, and D-

xylose, all in their pyranose form. Fatty acids with different lengths esterify the oligosaccharide core at variable positions.

The way in which the sugar units assemble to form the glycolipid core produces structures of enormous diversity. The most interesting structural feature is their macrolactone ring formed by the aglycone spanning two or more units of the saccharide backbones. The chemical diversity of these oligosaccharides is further increased by the diverging possibilities of cyclization of the glycosidic acid cores into corresponding macrolactones. In addition, the hyper-diverse RG phenotype caused by acylation of the oligosaccharide cores considerably increases their structural variety.

In fact, on the whole, a large number of RG congeners occur in the Convolvulaceae family, as well as a remarkable number in each species. The amphiphilic (lipophilicity/hydrophilicity balance) properties found in these RGs are crucial to isolate them because they are easily extractable and/or precipitated using methanol. However, the use of reversed phase columns in HPLC, using the recycling mode, proved to be the key to achieving purification of all these polar complex mixtures (Pereda-Miranda et al. 2010). In the purification of the individual constituents both heart-cutting and peak-shaving are used. Each peak collected by either method is recycled to achieve homogeneity to the point of separation of the overlapped components (Pereda-Miranda and Hernández-Carlos 2000). Figure 31 shows a chromatogram obtained during the complete resolution of the diastereomeric mixtures of niloyl esters, involving both enantiomers (levorotatory and dextrorotatory), bonded to the same macrocyclic tetrasaccharide of four major RGs from the Mexican scammony root, *Ipomoea orizabensis* (Pereda-Miranda and Hernández-Carlos
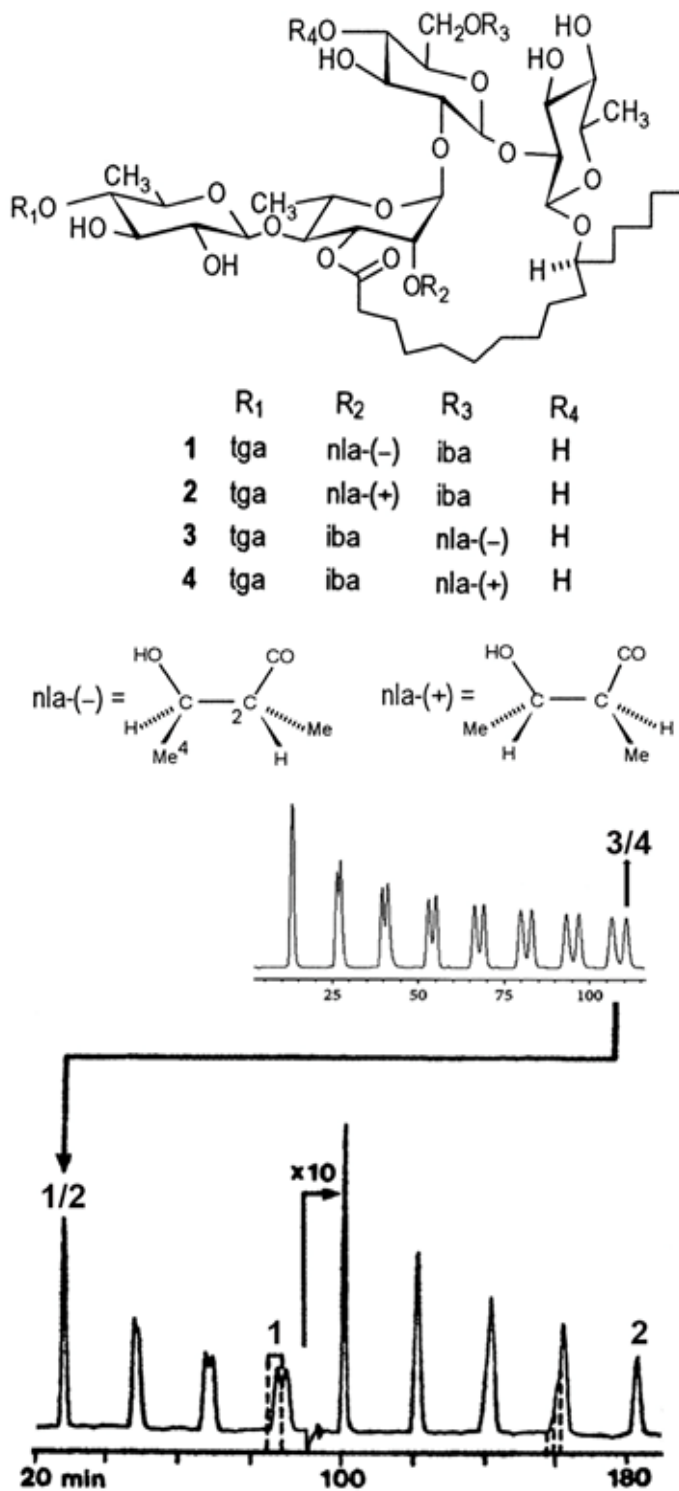
Figure 31. Recycling HPLC separation by heart-cutting and peak shaving of the two mixtures of diastereomeric niloyl (nla) ester pairs, 1/2 and 3/4 (orizabins X/XI and XII/XIII, respectively). The refractometer sensitivity was increased (×10) to optimize peak detection. Column: 150 × 19 mm, μBondapak-amino, 10 μm; mobile phase: CH_3CN-H_2O, 95:5; flow rate 4 ml/min; sample injection: 10 mg/500 μl. Abbreviation: tga, tigloyl; iba, isobutyroyl.

2000). High-resolution mass spectrometry (FAB and ESI) and NMR spectroscopy have been applied during the structural elucidation of RGs. All the steps involved in this characterization have been previously reviewed (Pereda-Miranda and Bah 2003; Pereda-Miranda et al. 2010).

Numerous species of morning glories accumulate acylsugars with a tetrasaccharide or pentasaccharide core with substantial diversity in the number and length of the acyl chain aliphatic acids. The number of acylating chains on the sugar cores normally ranged from one to four with chain lengths from 2 to 12 carbons (Pereda-Miranda et al. 2010; Kroumova et al. 2016). Across the Convolvulaceae, many species incorporate at least one oligosaccharide chain in all their major acylsugars and one common aliphatic acid as an esterifying residue in all their acylsugars, for example, methyl butyric acid in *Ipomoea tricolor*, the Mexican morning glory (Bah and Pereda-Miranda 1996; Castañeda-Gómez et al., 2019); tiglic acid in *Ipomoea alba*, the moon vine (Cruz-Morales et al. 2012; Castañeda-Gómez et al. 2017); and nilic acid (Figure 31) *in I. orizabensis*, the Mexican scammony (Pereda-Miranda and Hernández-Carlos 2002). Long-chain fatty acids were found in multiple species, including decanoic and dodecanoic acids in *Ipomoea pes-caprae*, the beach morning glory (Pereda-Miranda et al. 2005), and sweet potato, *Ipomoea batatas* (Rosas-Ramírez et al. 2011), *inter alia*. So far, the most complex RG structures isolated are the macrocyclic bisdesmosides (Bautista et al. 2014; 2016) and ester-type dimers of acylated tri- (Bah and Pereda-Miranda 1997), tetra- (Rosas-Ramírez et al. 2011), and pentasaccharides (Escalante-Sánchez and Pereda-Miranda 2007). Figure 32 illustrates the structural diversity of the acylsugars from the purgative Mexican jalap root (*Ipomoea purga*). In these, the same

pentasaccharide of jalapinolic acid, operculinic acid A –originally isolated from *Operculina macrocarpa* (Ono 2017)– is incorporated in both the individual macrolactones and the ester-type dimeric structures, while variations are observed in the number and length of the acylating residues of the oligosaccharide core (Castañeda-Gómez and Pereda-Miranda 2011; Castañeda-Gómez et al. 2013).
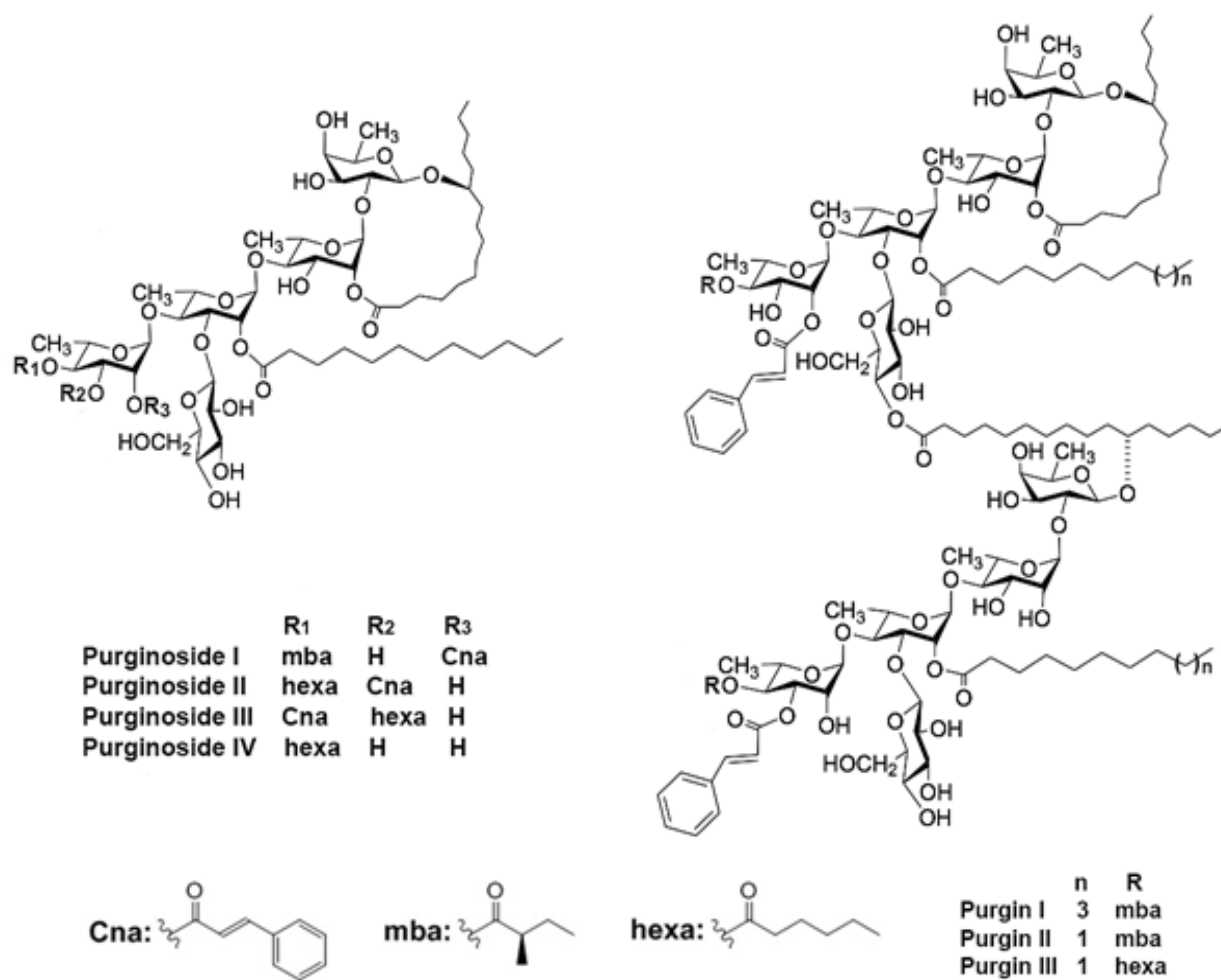
Figure 32. Structural diversity of the acylsugars from the Mexican jalap root (*I. purga*) where the same pentasaccharide of 11S-hydroxyhexadecanoic acid is incorporated in both the individual macrolactones (purginosides) and the ester-type dimeric (purgins) structures, while variation is observed in the number and length of the acylating residues. Abbreviation: mba, methyl butyroyl; Cna, *trans*-cinnamoyl; hexa, hexanoyl.

Amphiphilicity and biological activities

The evolutionary process of acylsugar diversification may have a huge potential in the discovery of new plant bioactive leads for therapeutic applications for the treatment of human diseases. That is because these naturally occurring glycolipids have demonstrated in some cases noteworthy antimicrobial (Pereda-Miranda et al. 2006), cytotoxic (Nagano et al. 2009; Zong et al. 2016), anti-mycobacterial (Rivero-Cruz et al. 2005), anti-diabetic (Rosas-Ramírez et al. 2018), or chemosensitizing properties (Pereda-Miranda et al. 2006; Figueroa-González et al. 2013), as well as other biological activities (Rodriguez et al. 2018).

While the biological activities of acylsugars have not been completely investigated (Yu et al. 2018), inquiry to this kind of amphiphilic plant secondary metabolites seems greatly promising as therapeutic adjuvants for macrophage modulation in the treatment of immune disorders (Schepetkin and Quinn 2006). These active principles are responsible for the purgative action of all the important Convolvulaceous species used in traditional medicine throughout the world since ancient times (Pereda-Miranda et al. 2006).

It has been demonstrated that the macrocyclic structure is an essential requirement for the biological activity of RG. All properties are totally lost, including cytotoxicity and purgative action (Pereda-Miranda 1995), in the glycosidic acid derivative prepared by saponification of intact natural RGs, and suggest both the importance of the overall lipophilicity as essential to the molecule's potency and the need for a macrocyclic structure as the pharmacophore. The macrolide effectively constrains the oligosaccharide core into bioactive conformations (Rodriguez et al. 2018). Since the report on the cytotoxic activity of tricolorin A (P-388: IC$_{50}$ 2.2 μg/ml), a tetrasaccharide of 11S-hydroxyhexadecanoic acid

from *I. tricolor*, the Mexican morning glory (Pereda-Miranda et al. 1993), other research groups have pursued the search for constrained oligosaccharides in order to discover further examples of potent chemotherapeutics (Cao et al. 2005; 2007).

The amphiphilicity is another important feature for the biological activities of these secondary metabolites, which enhanced cell penetration. This is a desirable feature in the process of drug development, through the improvement of the pharmacokinetic profile of bioactive natural products (Govindarajan 2018). The importance of the amphiphilicity in the activity of RGs was first observed in the herbicidal potential of tricolorin A, which inhibited seed germination and radical growth (Pereda-Miranda et al. 1993), acting as a pre- and post-emergence inhibitor of plant growth (Lotina-Hennsen et al. 2013). This principle was also found to be a potent inhibitor of seed respiration and uncoupler of photophosphorylation in spinach chloroplasts, through inhibition of H^+-uptake and adenosine 5'-triphosphate synthesis (Achnine et al. 1999). Saponification of this compound caused the elimination of all esterifying residues, including the opening of the macrolactone, yielding the glycosidic acid core, and resulting in the loss of inhibition of ATP-synthesis, the uncoupling of electron flow by this derivative (tricoloric acid A) and a debilitated potential exhibited by its methyl ester derivative (Figure 33). This macrocyclic oligosaccharide acts as a non-protonophoric uncoupler, probably by interfering directly with the thylakoidal membrane, facilitated by the amphiphilicity derived from the esterification of the constrained oligosaccharide core.

Efforts have been conducted to understand the structural requirements for cytotoxic activity by synthesizing analogues with the same amphipathic properties but lower

molecular weight and cyclic structure (Brito-Arias et al. 2004; Nagano et al. 2009). The results are inconclusive in relation to the structure-activity relationships (Zong and Shi 2017).
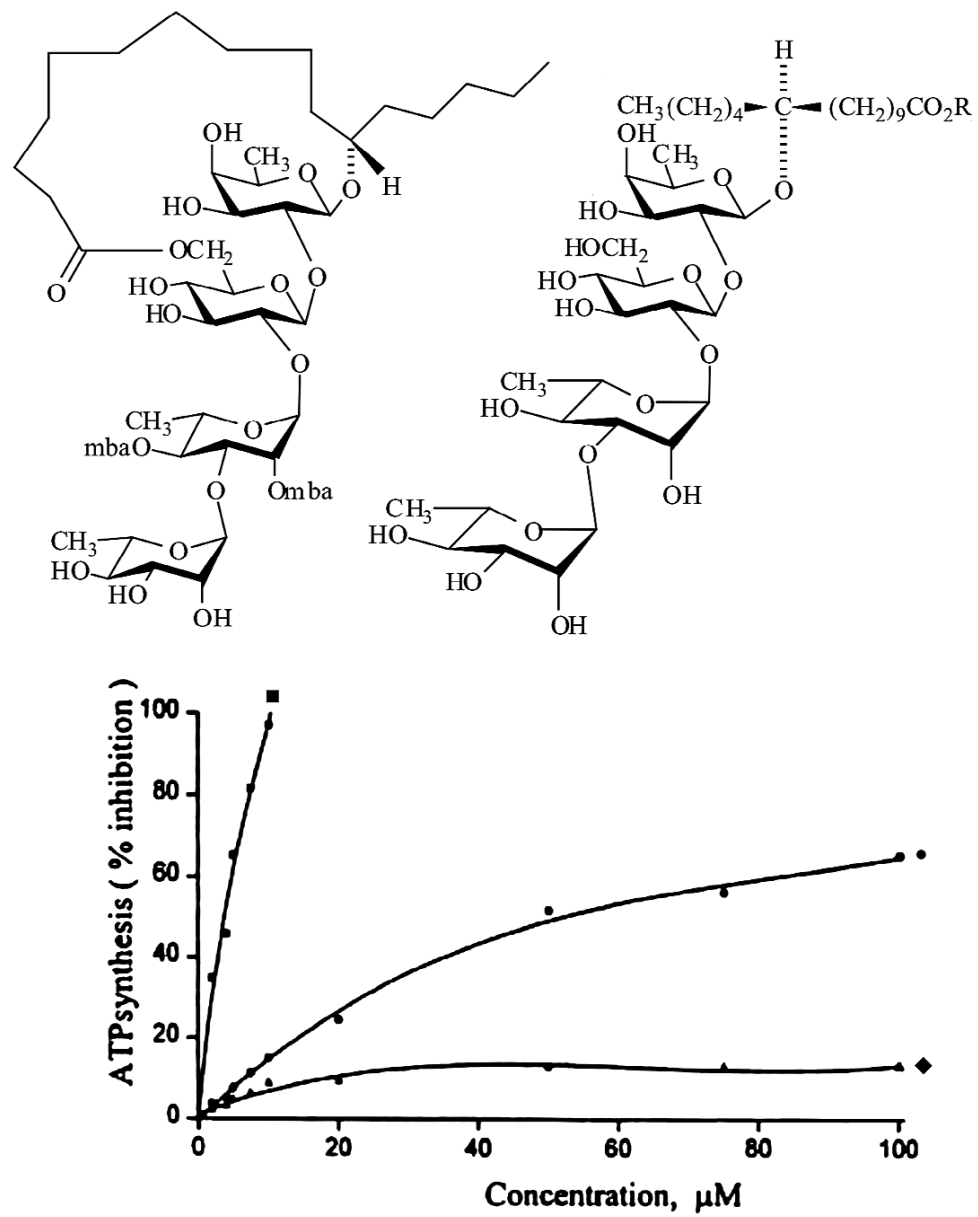
Figure 33. Inhibition of ATP-synthesis by tricolorin A (■) and its saponification derivatives, tricoloric acid A (R = H, •) and methyl ester (R = CH₃, ♦). Loss of inhibitory activity suggested that the amphiphilicity is a requirement for uncoupling activity. Abbreviation: mba, methyl butyroyl.

Most of the RG series of related homologues or diastereoisomers of macrocyclic RGs have been demonstrated to be non-cytotoxic or with a marginal activity (Figueroa-González et at. 2012; Bai et al. 2017). However, the ipomoeassin series (Figure 34) from the leaves of *Ipomoea squamosa* has shown to be extremely potent against multiple cell lines (Cao et al. 2005; 2007). Ipomoeassins D and F exhibited single-digit nanomolar (IC_{50} = 4.2-36 nM) growth-inhibition activity against many cancer cell lines and represent the most cytotoxic RGs isolated so far (Nagano et al. 2009).

	R¹	R²	IC_{50}
ipomoeassin A	H	Ac	0.5 µM
ipomoeassin B	H	H	0.4 µM
ipomoeassin C	OH	Ac	2.9 µM
ipomoeassin D	OAc	Ac	35 nM
ipomoeassin E	OAc	H	3.3 µM

ipomoeassin F

IC_{50} 36 nM
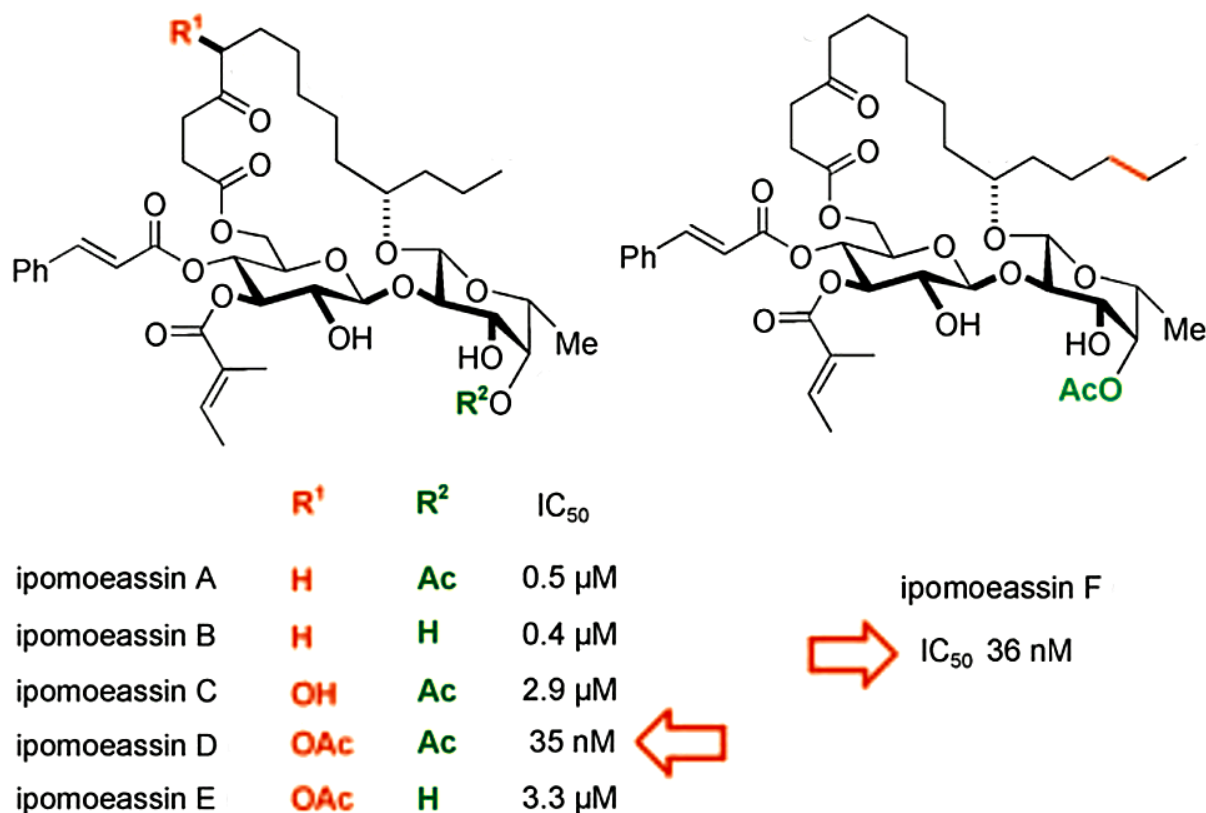
Figure 34. Structures of ipomoeassins A-F and cytotoxicity data (IC_{50}) against the human ovarian cancer cell line (A2780). The lipophilicity/hydrophilicity balance is a critical parameter for cytotoxicity as evident from the IC_{50} values described for ipomoeassins. Reproduced with permission from John Wiley and Sons [ref. Nagano et al., 2009].

Three distinct structural features are present in ipomoeassins A-F: 1) a small sugar core formed by two units: one hexose (D-glucose) and one methylpentose (D-fucose); 2) a ketone functional group at the C-4 position of the macrocyclic aglycone; and 3) a disaccharide core highly acylated with diverse ester functionalities, remarkably two α,β-unsaturated esters (tiglate and cinnamate). The presence of these lipophilic alkylating substituents may facilitate irreversible binding between these acylsugars and its biological targets (Zong et al. 2016; 2017). Ipomoeassin F incorporates two more methylene groups in the macrocyclic alkyl chain than its shorter homologues, ipomoeassins A-E (Figure 34). Thus, it is evident that the lipophilicity/hydrophilicity balance is a critical consideration for cytotoxicity as demonstrated against the human ovarian cancer cell line (A2780) from the IC_{50} values described for ipomoeassins (Nagano et al. 2009; Zong et al. 2016; Zong and Shi 2017). Ring size and aglycone flexibility also demonstrated a substantial influence on the activity; however, the macrocyclic aglycone backbone was proved to be modifiable since the 5-oxo/aza analogues of ipomoeassin F also displayed low nanomolar potential (Zong et al. 2018). Recently, Sec61α (protein transport protein Sec61 subunit alpha isoform 1), the pore-forming subunit of the Sec61 protein translocon, was identified as a direct binding partner of ipomoeassin F in living cells (Zong et al. 2019). This binding is the principal mechanism for its potent cytotoxicity and results in substantial and selective inhibition of protein translocation in vitro and broad-ranging inhibition of protein secretion in live cells (Zong et al. 2019).

Crystals for X-ray analysis of the cytotoxic tricolorin A were obtained by taking advantages of its amphiphilic properties. Its constrained macrocyclic oligosaccharide

preserves a rigid structure in contrast with acyclic oligosaccharides that experience free

rotation in solution around the anomeric linkages. The crystals were grown in the interface

of water as the precipitating agent, together with a mixture of mineral oil and ethanol, by
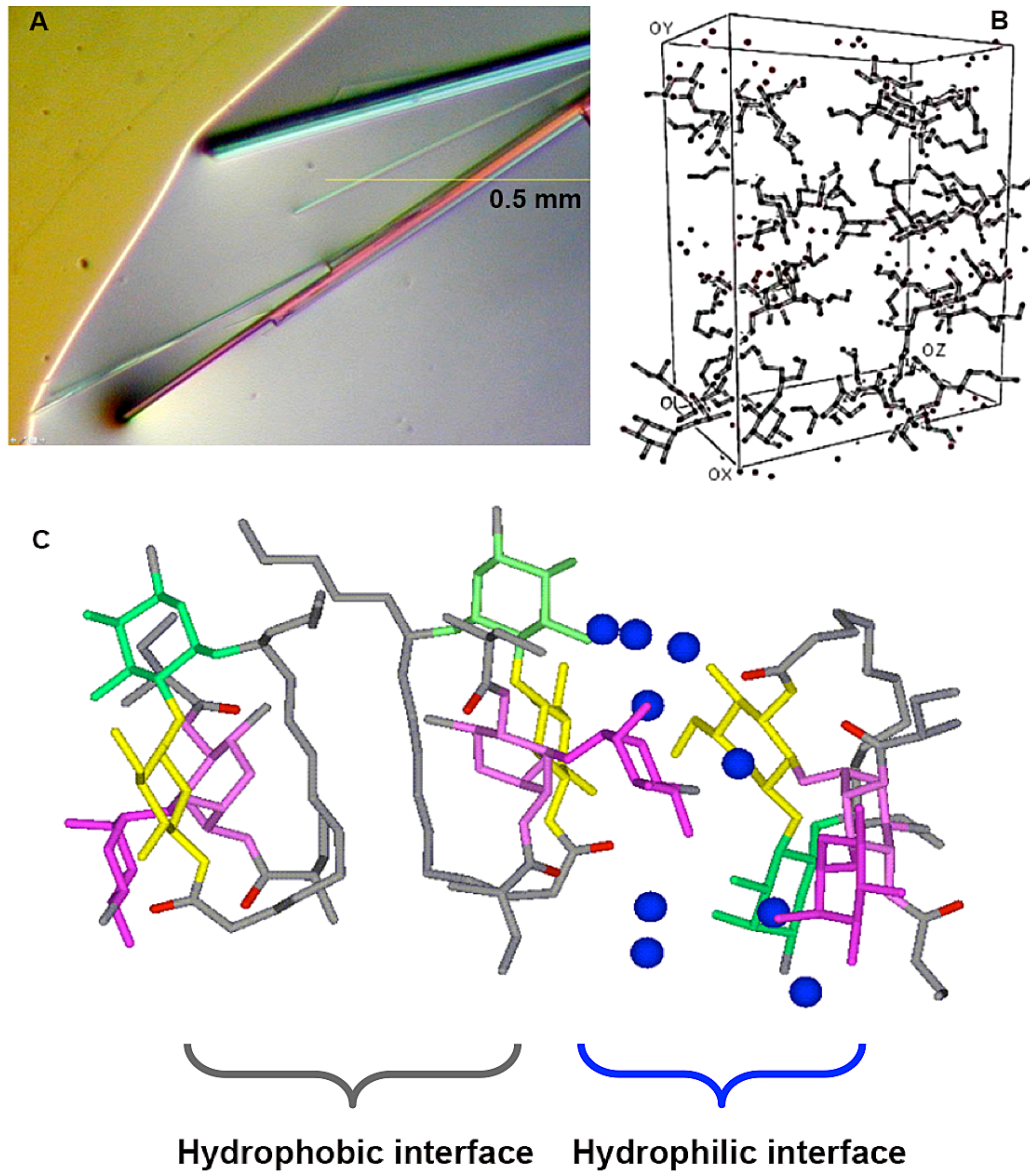
Figure 35. Tricolorin A single crystals. A) Crystals were grown in the interface of water and a mixture of mineral oil and ethanol by the reverse vapor diffusion method; B) tricolorin A packing on a unit cell showing the presence of four independent conformation and eighteen water molecules (represented as spheres) in the monoclinic asymmetric unit cell; C) tricolorin A packing shows an alternance of hydrophilic (tetrasaccharide core) and hydrophobic (macrocylic aglycone) interfaces where water molecules mediate the contact between two glycolipid bilayers.
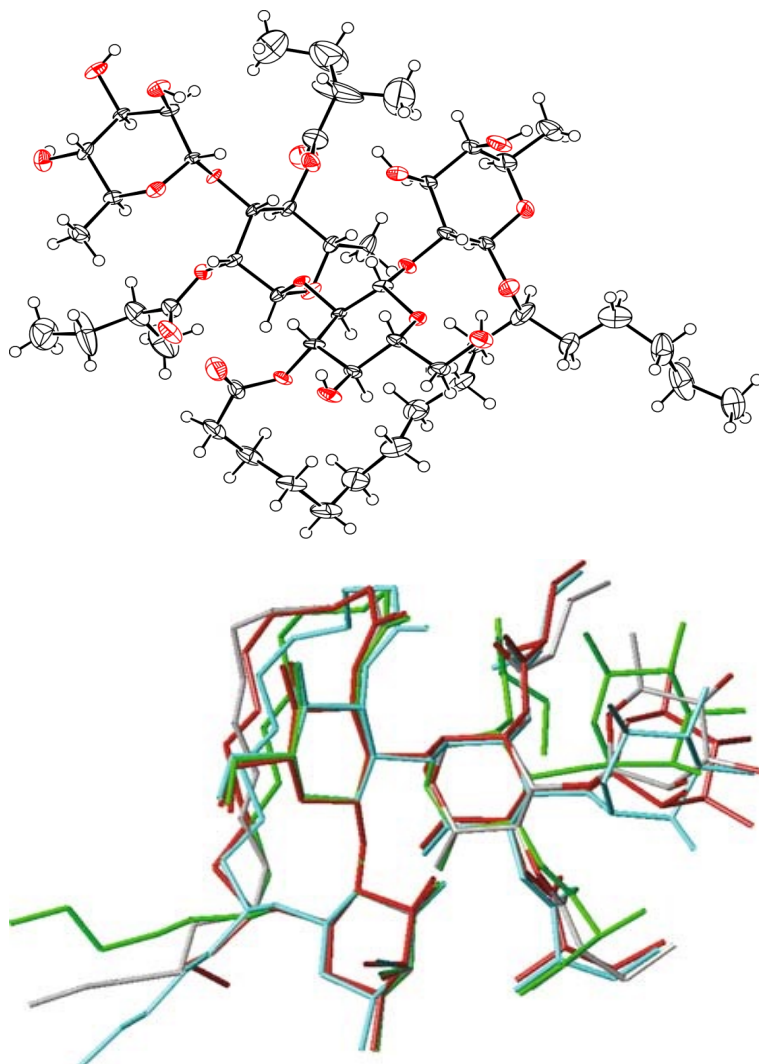
Figure 36. Constrained oligosaccharide structure of tricolorin A, a tetrasaccharide with L-rhamnose-(1→3)-*O*-*α*-L-rhamnose-(1→2)-*O*-*β*-D-glucose-(1→2)-*O*-*β*-D-fucose connectivity, in solid state (above), which is the only resin glycoside that has been characterized crystallographically. Superposition of the four independent molecules (below) showing that the internal trisaccharide has limited conformational flexibility due to its macrolactone structure spaning the *β*-D-glucopyranosyl-(1→2)-*O*-*β*-D-fucopyranoside subunit.

the reverse vapour diffusion method (Rencurosi et al. 2004). In the asymmetric unit cell,

refinement indicated the presence of 18 water molecules in addition to the four independent

tricolorin A conformation. The most notable feature of tricolorin A in the solid state is the

anisotropic repartitioning of the hydrophobic and hydrophilic sections (Figure 35). Four

conformational isomers were found, but all shared the same global arrangements for the

117

trisaccharide subunit, L-rhamnopyranosyl-(1→2)-O-β-D-glucopyranosyl-(1→2)-O-β-D-fuco-pyranoside, imposed by the limited conformational freedom due to its macrolactone that spans the terminal disaccharide units, reducing rotation but allowing flexibility around the externally placed L-rhamnopyranosyl-(1→3)-O-α-L-rhamnopyranoside moiety (Figure 36). This conformational stability would likely be maintained in solution, suggesting that constrained carbohydrates are conformationally stable and that this stability is necessary for biological activity (Rencurosi et al. 2004).

Remarkably, macrocyclic RGs have shown the ability to increase membrane permeability and transport on both cations (Na^+, K^+, and Ca^{2+} ions) and anions (Cl^-), which could trigger an imbalance in cellular homeostasis through pore-forming activity (Pereda-Miranda et al. 2009; Zhu et al. 2019a). This could be the mechanism of action for the cathartic activity of RGs, acting as osmotic laxatives, which cause an increase in water elimination and peristalsis of the intestine via a decreased expression of aquaporin 3 in colon cells and activation of the pro-inflammatory nuclear factor NF-kB and cyclooxygenase (COX-2) pathways (Zhu et al. 2019a).

The lipophilicity/hydrophilicity balance and the need for the macrocyclic structure, as in tricolorin A, were also evident from the inability to disrupt the membrane by tricoloric acid A and its methyl ester derivative. This can be directly correlated with the lack of cytotoxicity previously found for all glycosidic acids derived from natural macrocyclic RGs (Pereda-Miranda and Bah 2003). These highly polar glycosidic acids are likely incapable of forming conjugates due to the lack of alternating hydrophilic and hydrophobic surfaces needed for membrane insertion and pore formation (Pereda-Miranda et al. 2009). This was

proved to be the basis for the inhibition of the proliferation of cancer cells via G_0/G_1 cell cycle arrest regulated by related proteins CDK4/6, cyclin D/E and p21, and mitochondria-mediated apoptosis induction by RGs (Fan et al. 2014; 2015). Also, the cytotoxic effect of RGs in cancer cells was a consequence of paraptosis mediated by activation of chloride intracellular channel-1 (Zhu et al. 2019b).

These mixtures of amphiphilic acylsugars from the morning glory family have been recently described as sources of inhibitory compounds of EPs, which play an important role in extruding xenobiotics outside the cells providing a protective means responsible for the MDR phenotype in Gram-positive (Pereda-Miranda et al. 2006) and -negative bacteria (Corona-Castañeda and Pereda-Miranda 2012), as well as in mammalian cancer cells (Figueroa-González et al. 2012; Castañeda-Gómez et al. 2013), which could have therapeutically important benefits for the introduction of new of alternatives for the treatment of refractory malignancies.

Screening for chemosensitizers: an overview

EPs are transport proteins (translocases) that mediate their function through energy-dependent mechanisms, which can facilitate a reduced influx into the cytosol and increased efflux from the cell of drugs and toxic substances (Figure 30), including drugs, thereby reducing the attainment of therapeutic concentrations and subsequently leading to resistance (Ayaz et al. 2017).

Some of these translocases resulted in a high drug specificity, while others are non-specific and primarily responsible for MDR. Among these transporters, ATP is employed as

the energy source for the process (ATP-binding cassette transporters or ABC transporters) and these proteins are termed primary transporters. In an alternative group of transporters, drug efflux is coupled to an electrochemical ionic difference across the cell membrane (Na^+/H^+ driven active anti-porters), commonly known as secondary transporters. In eukaryotes, primary transporters frequently carry out the efflux process, whereas prokaryotes mainly employ secondary active anti-porters (Ayaz et al. 2017). Multidrug transporters are grouped within five superfamilies: (a) the ATP-binding cassette transporters (ABC), (b) the resistance-nodulation-cell division transporters (RND), (c) the small multi-drug resistant transporters (SMR), (d) the multiple antimicrobial extrusion proteins (MATE), and (e) the major facilitator superfamily (MFS).

Several methods have been developed to identify potential chemosensitizers through the induction and activation of EPs (Prasch and Bucar 2015; Stavri et al. 2007). In order to succeed as an EPI in both bacteria and human cancer cells, a natural product must be able to satisfy the following criteria: 1) the chemosensitizers must potentiate the activity to which a microorganism strain or a mammalian cell line has developed resistance by the expression of a drug EP and not affect sensitive strains; 2) the chemosensitizers should increase the accumulation and decrease the extrusion of EP substrates; and 3) the chemosensitizers must not affect the proton gradient across the cell membranes (Lomovskaya and Watkins 2001).

The modulation assay is an easy method for screening EPIs in both bacteria and cancer cells. An initial study of the antibacterial or cytotoxic activities of a plant extract, crude fraction or pure compounds to determine the MIC (antimicrobial assay) or IC_{50} (cytotoxic

assay) of the test sample is necessary to protect against false-positive results, the main criterion for selecting subsequent assays.

The absence of antimicrobial or cytotoxic activities is an important and indispensable prerequisite to carry out trials of modulation and differentiate clearly any effect of potentiation (by inhibition of EPs) of a possible synergy between an active compound and the selected drug to be extruded (Figueroa-González et al. 2012; Pereda-Miranda et al. 2006). A subinhibitory concentration of the tested fraction or compound is preferred when performing a modulation assay; usually, a concentration fourfold lower than the MIC (Stavri et al. 2007; Venter et al. 2015). Depending on the sample solubility, they can be dissolved in DMSO, deionized water, or ethanol.

Most samples can be dissolved and stored in DMSO; therefore, in primary screening, samples are prepared in 100% DMSO, and final concentrations of the sample and the DMSO of 50 mg/ml and 0.5% (vol/vol) are diluted in culture media (Vichai and Kirtikara 2006). Serial doubling dilutions of a drug known to be a substrate for an efflux transporter, such as norfloxacin for the NorA protein in antimicrobial assays (Pereda-Miranda et al. 2006) or vinblastine for P-gp in cytotoxic assays (Figueroa-González et al. 2012), is added and then interpreted in the same manner as MIC or IC_{50} determinations, respectively. The use of an EPI as positive control is highly recommended for comparison, e.g., reserpine (RES), a plant-derived drug used as an antihypertensive (Schillaci et al. 2017).

The methods for measuring EP activity of substrates to intracellular or extracellular drug concentration can be divided into two categories; efflux assays that directly measure the EP substrate extruded out of the cell and accumulation assays that measure the intracellular

accumulation of an EP substrate inside the cell. Both methods are based on either fluorescence or radiometric measurements. Normally, dyes are used with a differential intracellular or extracellular fluorescence, such as ethidium bromide (EtBr), a DNA-intercalating dye that produces fluorescence when it accumulates within the cell if efflux is reduced (Blair and Piddock 2016; Spengler et al. 2017). Berberine efflux has also been used to determine active transport (Stermitz et al. 2000; Tegos et al. 2002). Accumulation studies in microorganisms have been performed with various substrates, including norfloxacin (NOR) and novobiocin (Baranova and Nikaido 2002; Kaatz et al. 2002). An increase in drug accumulation only in the presence of an inhibitor indicates that the chemosensitizer is a blocker of an efflux mechanism.

In cancer cells, accumulation assays of P-gp substrates (Silva et al. 2015) like the fluorescent dyes rhodamine 123, hoechst 33342, and calcein AM (calcein acetoxymethyl ester) –in the presence or in the absence of a P-gp inhibitor– have been evaluated fluorimetrically and by flow cytometry (Haynes et al. 2018); thus, it is also possible to use naturally fluorescent clinically relevant drugs, e.g., fluoroquinolones for antimicrobial assays and doxorubicin for cytotoxic compounds. Radioactive analogues have been described for many drugs in bacterial assays, including quinolones, tetracyclines, chloramphenicol, β-lactams, and rifampin (Blair and Piddock, 2016). Drug efflux studies have also been performed by incubating cells with [^{3}H]-vinblastine, [^{3}H]-colchicine, or [^{3}H]-digoxin, with the amount of the extruded drug in the medium determined by scintillation counting.

Plant extracts and some fluorescent pure compounds can produce false negative results due to optical interference. Also, the limitation of radio-labelled compounds and the lack of a fluorescent chromophore for many novel active EPIs have resulted in alternative mass spectrometry-based approaches implemented for the quantitative measurement of unlabeled EPIs (Brown et al. 2015; Dumont et al. 2018). Protein expression of P-gp has been determined by the use of mouse monoclonal anti-P-gp or rabbit polyclonal anti–P-gp antibodies by Western blot, flow cytometry, quantitative real-time polymerase chain reaction and immunocytochemistry (Silva et al. 2015). Random *in vitro* screening has been primarily performed for the search of new chemosensitizers.

These assays to evaluate the transport and interactions of new chemical entities with EPs are expensive and time-consuming. Consequently, several *in silico* models, which offer inexpensive and fast screening approaches, have been developed to identify EP substrates or inhibitors. In actuality, numerous computational models, based on structure-activity relationship analyses (QSAR), pharmacophore modeling, and molecular docking techniques have been developed to detect EP substrates and inhibitors (Cacciotto et al. 2018; Chen et al. 2012; Desai et al. 2013; Ramaswamy et al. 2017; Thai et al. 2015; Volpe and Qosa 2018). Subsequent molecular dynamics simulations have also found that partitioning into the lipid membrane is the rate-limiting step for the interaction of a substrate with EPs (Bhaskar et al. 2016). Thus, some physicochemical characteristic features, such as the amphiphilicity balance, hydrogen-bonding ability, and surface area may contribute to the substrate binding ability to EPs.

Resin glycosides as chemosensitizers

As an evolutionary strategy, the MDR phenotype is the result of a variation in a regular translocase where the EP simply broadened the substrate spectrum (Higgins 1992). This substrate promiscuity provides the cells with a successful defence against toxins until they acquire resistance by developing more specific adaptive mechanisms. This was the rationale for testing RGs as potential modulators in Gram-positive and Gram-negative bacteria, in addition to human breast-cancer cells, since plant-derived metabolites have proved to be important chemosensitizers to restore the efficacy of clinically useful drugs (Abreu et al. 2012, Basha Syed and Selvaraj Coumar 2016; Lamut et al. 2019; Mahmood et al. 2016; Rao et al. 2018; Silva et al. 2015; Tegos et al. 2002).

The first series of RGs subjected to a screening process for the identification of potential chemosensitizers were the orizabins from the Mexican scammony (*I. orizabensis*). These tetrasaccharides were evaluated for activity against a panel of *S. aureus* strains possessing specific efflux pumps (Pereda-Miranda et al. 2006). Predominantly, NorA, a member of the major facilitator superfamily of efflux pumps, is the basic EP in *S. aureus*. NorA is a drug/ proton antiporter (SA-1199B, NOR: MIC 64 µg/ml) that extrudes a broad spectrum of antimicrobic compounds such as phenothiazines, fluoroquinolones, rhodamine, acridines, and EtBr, *inter alia*.

The tested orizabins, 13 compounds in total, are highly lipophylic tetrasaccharides due to the acylation in various degrees of their saccharide core (Figure 31), and the majority of these RGs did have no intrinsic antibacterial activity (Pereda-Miranda et al. 2006). Therefore, they were selected for further evaluation of their modulatory effects. When

tested in combination with NOR, two orizabins were able to restore the antibacterial susceptibility to strain SA-1199B better than did RES, the EPI used as a positive control. Orizabin XIX at the concentration of 25 mg/ml caused a 16-fold reduction in the MIC value of NOR from 64 to 4 µg/ml while orizabin IX at 1 µg/ml completely inhibited SA-1199B growth in the presence of 2 µg/ml of NOR (Figure 37). The modulatory effects of RGs on resistant *S. aureus* were used as the basis to characterize these types of compounds as EP substrates.
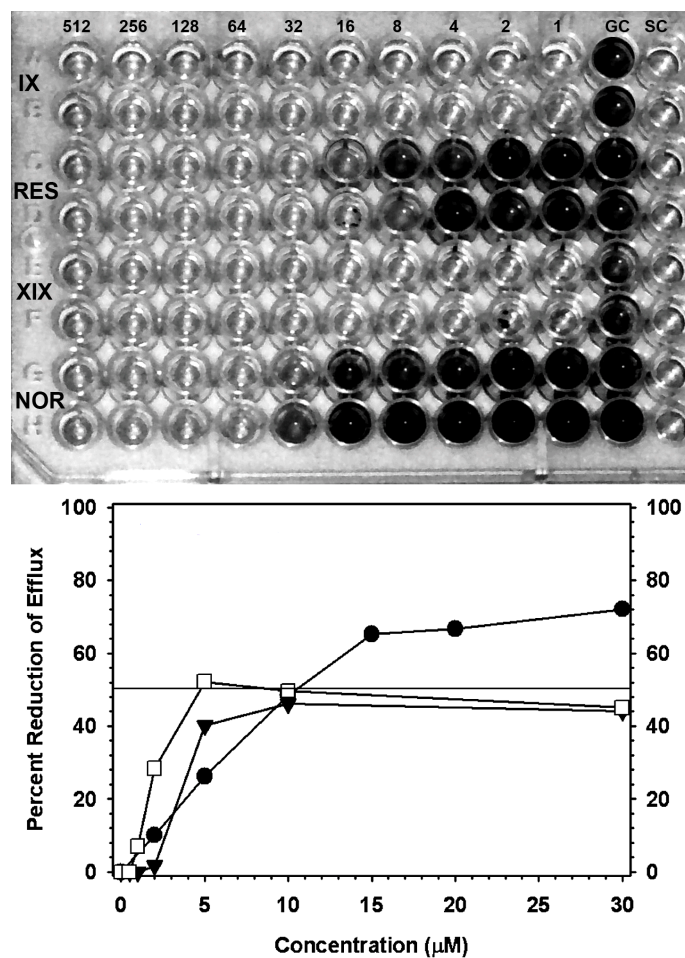
Figure 37. Potentiation effect of orizabins IX (1 µg/ml) and XIX (25 µg/ml) on norfloxacin (NOR; 2 µg/ml) sensitivity against the resistant strain of *Staphylococcus aureus* SA-1199B, overexpressing the transporter NorA (above). Ethidium efflux inhibition assay from SA-1199B cells: (●) reserpine (RES); (▼) orizabin IX [R_1 = tga; R_2 = mba; R_3 = H; R_4 = nla-(−)], (□) orizabin XIX [R_1 = mba; R_2 = nla-(+); R_3 = mba; R_4 = H] (below). See, Figure 31 for the oligosaccharide core of orizabins.

Experiments were performed of efflux inhibition using EtBr on the strain SA-1199B overexpressing the Nor-A transporter. At low concentrations (< 10 µM), both orizabins IX and XIX were more effective than RES (Figure 37). However, at 10 µM or higher, their effects reached a state of no change. This reduction in EtBr efflux inhibition was due to solubility problems of the tested chemosensitizer, since above 30 µM, precipitation of the test compound was clearly observed (Pereda-Miranda et al. 2006).

All members of the murucoidin series, isolated from *Ipomoea murucoides*, exerted a potentiation effect of NOR against the NorA overexpressing *S. aureus* strain SA-1199B by increasing the activity fourfold (8 µg/ml from 32 µg/ml) at concentrations of 25 µg/ml (Chérigo et al. 2008; 2009). The non-cytotoxic pescaprein series, isolated from beach morning glory (*I. pes-caprae*), potentiated the action of norfloxacin against the NorA overexpressing strain in the same fashion as the murucoidins (Escobedo-Martínez et al. 2010). These RGs were found to be macrolactones of tetrasaccharides and pentasaccharides of jalapinolic acid with different fatty acids esterifying the oligosaccharide cores. The modulatory activity of two diastereoisomeric tetrasaccharides, tricolorins A and E (SA-1199B, MIC 8 µg/ml) –the latter with a quinovose instead of a fucose in the sugar core– and their peracetylated derivatives (SA-1199B, MIC >256 µg/ml) was tested to compare their effects with those obtained for the orizabin and murucoidin series. The antimicrobial tricolorins and their peracetylated derivatives exhibited no modulatory activity at the subinhibitory concentration of 2 µg/ml for the natural products and 25 µg/ml for the derivatives. The loss of activity for the highly acylated compounds is comparable to the inactivity recorded for their saponified polar analogue (tricoloric acid A) since the cellular

uptake is not facilitated, probably in this case, by the formation of complex aggregates or micelles that could induce membrane perturbation. The amphiphilic properties of these compounds resulting from the partial acylation of the oligosaccharide core and the lipophilic alkyl chains of their aglycones seem to be important to facilitate interaction with their EP target. Therefore, compounds that are nonpolar will not interact with the membrane EPs, and those that are too polar are poorly membrane-soluble.

Thirty-two microbiologically inactive RGs (MIC > 512 μg/ml) were tested for resistance modulatory activity against selected Gram-negative bacteria (Corona-Castañeda and Pereda-Miranda 2012; Corona-Castañeda et al. 2016). Minimum inhibitory concentration values for antibiotics and RGs were registered against the Rosetta-gami effluxing strain of *Escherichia coli* and two epidemic strains of *Shigella flexneri* and *Salmonella typhi*. These compounds exerted a potentiation effect on the clinically useful antibiotics tetracycline, kanamycin, and chloramphenicol by increasing antibiotic susceptibility up to 32-fold at concentrations of 25 μg/ml (Corona-Castañeda and Pereda-Miranda 2012). The modulation of antibiotic activity on MDR Gram-negative strains was similar to that observed for RES, an EPI positive control.

The complexity of the machinery and mechanisms of multidrug efflux in Gram-negative pathogens causes the major difference observed in potency for modulatory activity of the tested glycolipids against both Gram-positive and -negative bacteria, the latter of which are enveloped within a protective double-layer of lipid membranes. Noxious compounds are expelled across these membranes by active transport, providing the pathogens with a permeability barrier to hydrophilic compounds like antibiotics (Stavri et al. 2007). The more

complex structure of multidrug EPs in Gram-negative strains includes an inner membrane transporter and a periplasmic fusion protein, as well as an outer membrane channel (Mahmood et al. 2016). This tripartite EP system, therefore, confers MDR bacteria with the capacity to occupy lethal ecological niches by avoiding the cytotoxic effects of antibiotics and drastically limits the clinical use of these drugs (Corona-Castañeda et al. 2013).

With these results in mind, the reversal effects as modulators of RGs were further investigated using VIN-resistant breast carcinoma cells (MCF-7/Vin) overexpressing P-gp. Our current research program aims to identify amphipathic efflux pump inhibitors considering their lack of antibiotic and cytotoxic activities for differentiating a real drug potentiation in modulation assays (Corona-Castañeda and Pereda-Miranda 2012; Figueroa-González et al. 2012). The first step in these evaluations was the development of a resistant counterpart to VIN from sensitive human breast carcinoma cells (MCF-7) through continual exposure to this drug for three years. To maintain drug resistance, cells were cultured in medium containing VIN (MCF-7/Vin[+]). At the same time, a stock of resistant cells was maintained in VIN-free medium (MCF-7/Vin[-]). These cells were found to express the MDR phenotype (Figueroa-González et al. 2012), due to their cross-resistance to adriamycin, colchicine, camptothecin, and ellipticine as displayed in experiments of cytotoxicity using the sulforhodamine B colourimetric assay (Vichai and Kirtikara 2006). Modulation assays of VIN cytotoxicity using both sensitive (MCF-7) and resistant cells (MCF-7/Vin) showed that all tested non-cytotoxic compounds displayed modulation of VIN susceptibility by onefold to more than 1906-fold at tested concentrations of 5 and 25 µg/ml (Corona-Castañeda et al. 2016; Cruz-Morales et al. 2016; Figueroa-González et al. 2012).

These screenings also yielded the identification of four compounds with a positive response ($RF_{MCF-7/Vin-}$ >255-fold) from preliminary screening assays of 40 RGs, superior to that observed for RES ($RF_{MCF-7/Vin+}$: fourfold), the drug used as a positive reversal agent (Cruz-Morales et al. 2012; Castañeda-Gómez et al. 2017; Figueroa-González et al. 2012). These four compounds were (Figure 39): murucoidin V from *I. murucoides* (Figueroa-González et al. 2012), jalapinoside I (Bautista et al. 2014) and purgin II (Figure 32) from *I. purga* (Castañeda-Gómez et al. 2013), and albinoside III from *I. alba* (Cruz-Morales et al. 2016).
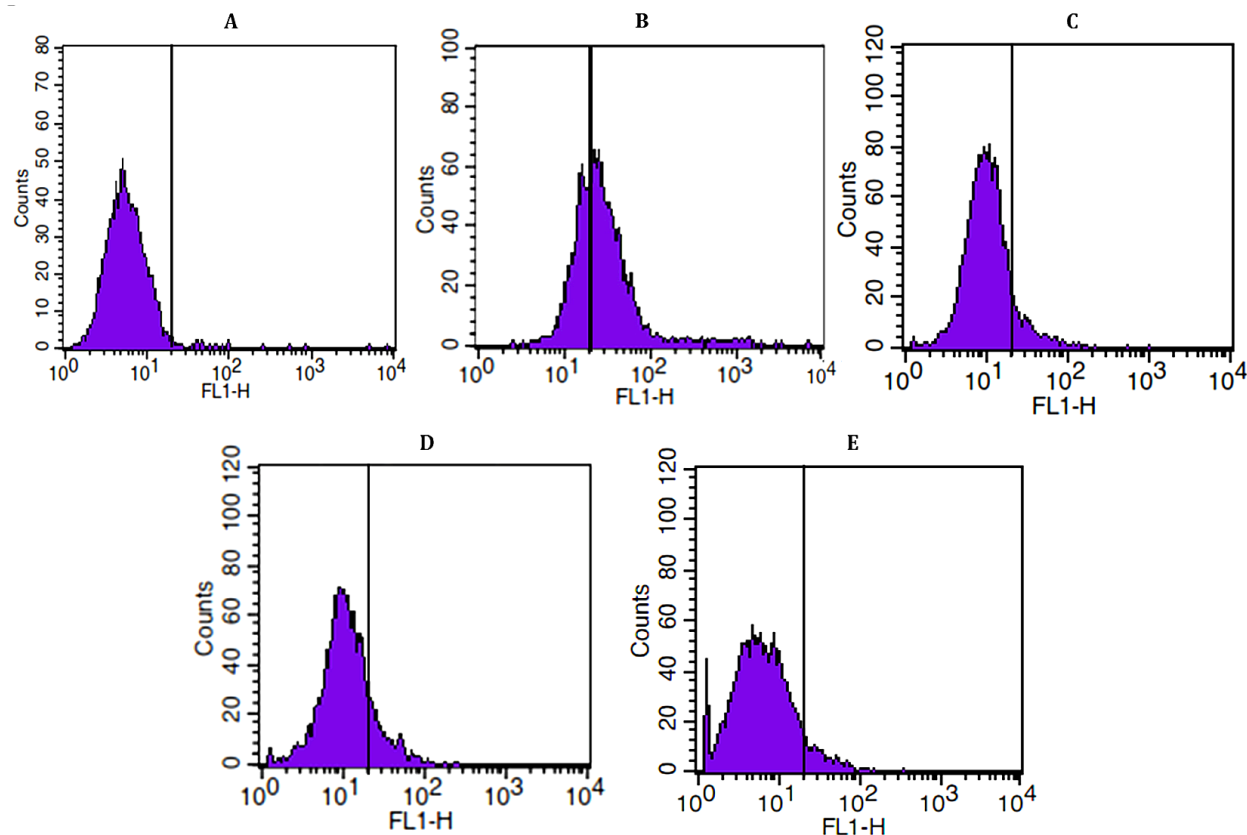
Figure 38. Mediated P-gp expression by purgin II and murucoidin V in drug-sensitive MCF-7 cells and multidrug-resistant MCF-7/Vin$^+$ cells after incubating with UIC2 anti-P-gp monoclonal antibody: (A) untreated MCF-7 cells; (B) untreated MCF-7/Vin$^+$; (C) MCF-7/Vin$^+$ treated with purgin II (25 µg/ml); (D) MCF-7/Vin$^+$ treated with murucoidin V (25 µg/ml); (E) MCF-7/Vin$^+$ treated with reserpine (5 µg/ml). The percentage area to the right indicates the relative quantity of P-gp expression.

Murucoidin V and purgin II were chosen to explore further their inhibitory effect on both P-gp function and its expression of the resistant phenotype by flow cytometry (Figueroa-González et al. 2012). Murucoidin V, a non-cytotoxic branched acylated pentasaccharide, displayed a stronger potentiation effect on VIN than does RES ($RF_{MCF-7/Vin+}$: eightfold). In the experiment on the intracellular efflux of Rh123, a rapid decrease was observed in the levels of this fluorescent compound after incubation in a Rh123-free medium. However, in the presence of murucoidin V, Rh123 efflux was suppressed. This result was almost equipotent to the effect observed for RES, the positive control (Figueroa-González et al. 2012). It would appear that this cellular uptake of RGs is facilitated by their amphipathic properties, resulting in an easy interaction with P-gp.

Purgin II is an ester-type dimer having three different acylating residues in both monomeric units (Figure 32). Reversal of multidrug resistance evaluation for purgin II resulted in enhancing VIN activity more than 2000-fold (MCF-7/Vin$^+$) when incorporated at 25 µg/ml. This modulatory activity was also higher than that registered for murucoidin V. Based on flow cytometry, purgin II significantly increased the intracellular accumulation of Rh123. Incubation of MCF-7/Vin cells with this RG caused an increase in uptake and notably lowered the efflux rate of Rh123 when compared with untreated MCF-7/Vin, in a way similar to murucoidin V (Castañeda-Gómez et al. 2013). In the presence of purgin II, Rh123 efflux was suppressed in MCF-7/Vin$^+$ in an almost equipotent manner to RES.

Decreased expression of P-gp by murucoidin V and purgin II was detected by immunofluorescence and measured by flow cytometry (Figure 38) after incubating with the UIC2 anti-MDR1 mouse monoclonal antibody, specific for an extracellular conformational

epitope of P-gp (Figueroa-González et al. 2012). The fluorescence intensity obtained for the sensitive MCF-7 line was used as a reference (Figure 38A). In these experiments, the expression of P-gp is understood as an antigen-antibody recognition reaction between the glycoprotein expressed in the cell membranes with its specific antibody. Therefore, the decrease in fluorescence will reflect the inhibition of this interaction due to the conformational changes induced by the tested RG, as a possible substrate of the EP.
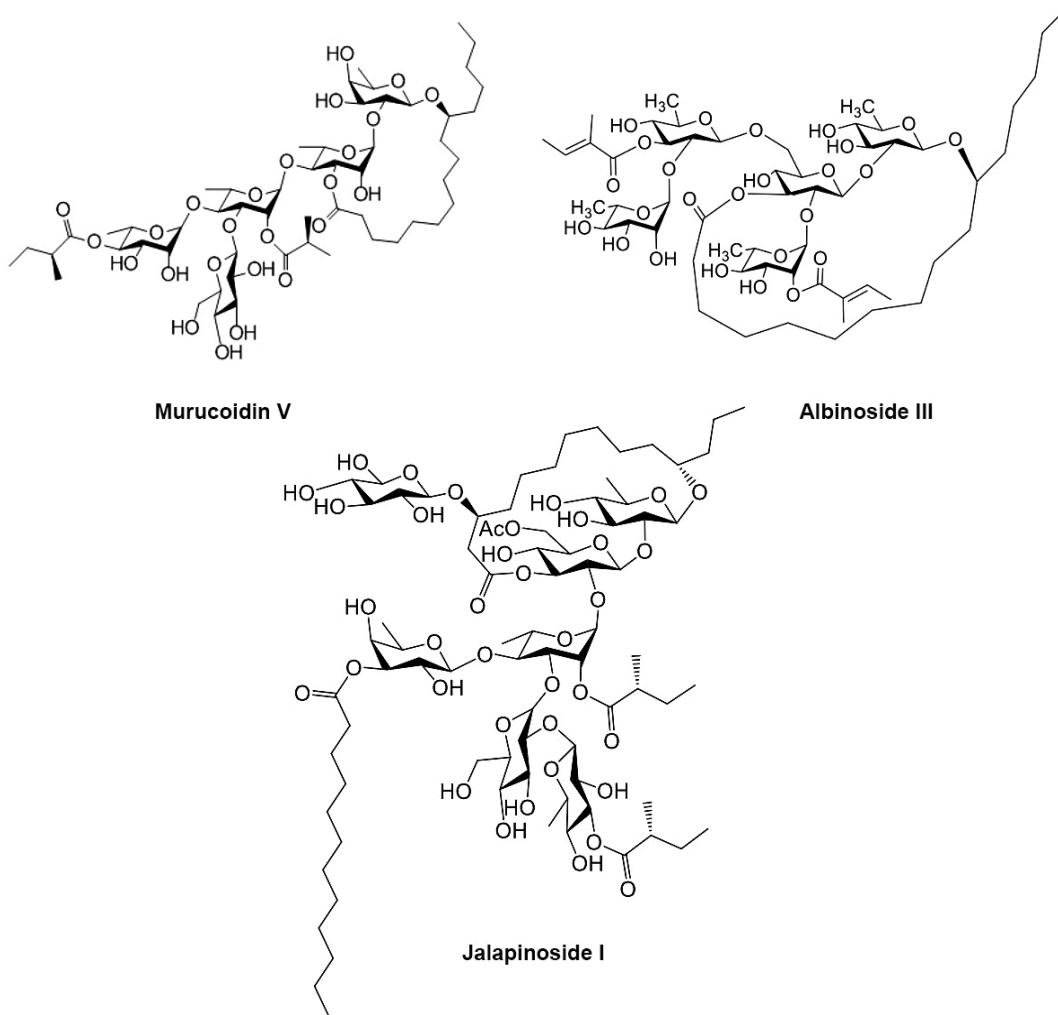
Figure 39. Chemical structures of non-cytotoxic resin glycosides identified as efflux pump inhibitors in bacterial pathogens and human cancer cells.

The MDR cell line MCF-7/Vin$^+$ showed a high intensity in fluorescence that corresponds to the expression of the transporter in large quantities (Figure 38B). After 30 minutes of incubation with purgin II at the concentration of 5 μg/ml, the level of expression of the P-gp decreased significantly with respect to the cells MCF-7/Vin$^+$ without treatment (Figure 38C). The same response was obtained for murucoidin V (Figure 38D). This percentage is noteworthy when compared with the reduction obtained with RES as a positive control at 5 μg/ml (Figure 38E). Therefore, these results provided additional evidence to support the potential of non-cytotoxic RGs as inhibitory substrates of P-gp (Figueroa-González et al. 2012).

In terms of the relationship between the chemical structure and the observed modulatory activity, none could be deduced. Neither the size of the lactone ring nor the lengths of the oligosaccharide were crucial for activity. Therefore, it has been suggested that the only common property among RGs, as EP substrates, was their relative amphiphilic nature (Figure 39).

Nonetheless, these active glycolipids have shown some of the ideal structural features recognized for EPIs or substrates, various hydrophobic units, which are represented by the glycosidic acid aglycone, in addition to the esterifying residues, sometimes containing aromatic rings, and various H-bond acceptors and H-bond donor centres at the oligosaccharide core. Therefore, both covalent and non-covalent interactions will modulate the three-dimensional EP protein structure, resulting in conformational changes, which are associated with a loss or reduction in the effluxing activity.

Thus, Convolvulaceous plants may elaborate an array of amphipathic mixtures of

acylsugars with very similar logP values, which can cause non-specific membrane disruption. However, if this were their mechanism of action, all RGs would be active, and the modulating activity could not be observed. Lastly, the large structural diversity of known potential EPIs reflects the low substrate specificity of EPs, as demonstrated for NorA and P-glycoprotein (Lamut et al. 2019).

Conclusions

MDR is regarded as one of the impediments to successful clinical treatment for many chemotherapeutic agents. Pathogens that express multiple resistance are becoming the norm, complicating treatment and increasing human morbidity. The most important result from the viewpoint of the potential use of RGs, which are substrates for MDR pumps, is that by combining these plant non-cytotoxic products with common anticancer or antimicrobial drugs - and thereby lowering current effective therapeutic doses and decreasing toxic side-effects in refractory malignancies - the treatment of these diseases could be improved.

The use of bacterial resistance modifiers such as this type of complex oligosaccharides as prototypes for new EPIs could facilitate the reintroduction into the clinical use of antibiotics that have become therapeutically ineffective and might contribute to the suppression of the emergence of new MDR bacterial strains, a major cause of infections in clinical settings. Plant standardized on these mixtures of RGs could also prove useful in developing antiseptic adjuvants to replace or be used as synergistic agents in combination therapies.

A greater understanding of drug recognition and transport by multidrug EPs is needed to develop clinically useful inhibitors, given the breadth of molecules that can be effluxed

by these systems. The results reviewed in this manuscript provide an insight into the therapeutical potential of these complex acylsugars and open the possibility of using RGs as starting points for the development of more potent chemosensitizers of multidrug EPs, as competitive and non-competitive adjuvants to reduce resistance. This possible therapeutical application of EPIs has attracted significant attention although no plant-derived or synthetic compounds have successfully reached the clinic as yet –in spite of their potential benefits– because of their high toxicity and low efficacy *in vivo*.

References

Abreu A, McBain A, Simoes M (2012) Plants as sources of new antimicrobials and resistance-modifying agents. Nat Prod Rep 29:1007-1021

Achnine, L, Pereda-Miranda, R, Iglesias-Prieto, R, Moreno-Sánchez, R, Lotina-Hennsen, B (1999) Tricolorin A, a potent natural uncoupler and inhibitor of photosystem ii

acceptor side of spinach chloroplasts. Physiologia Plantarum 106:246-252

Adamson D, Krikstopaityte V, Coote P (2015) Enhanced efficacy of putative efflux pump inhibitor/antibiotic combination treatments versus MDR strains of *Pseudomonas aeruginosa* in a *Galleria mellonella* in vivo infection model. J Antimicrob Chemother 70:2271-2278

Ayaz, M, Subhan, F, Sadiq, A, Ullah, F, Ahmed, J, Sewell, RD (2017) Cellular efflux transporters and the potential role of natural products in combating efflux mediated drug resistance. Frontiers In Bioscience 22:732-756

Bah, M, Pereda-Miranda, R (1996) Detailed FAB-mass spectrometry and high resolution NMR investigations of tricolorins A-E, individual oligosaccharides from the resins of *Ipomoea tricolor* (Convolvulaceae). Tetrahedron 52:13063-13080

Bah, M, Pereda-Miranda, R (1997) Isolation and structural characterization of new glycolipid ester type dimers from the resins of *Ipomoea tricolor* (Convolvulaceae). Tetrahedron 53: 9007-9022

Bai, LJ, Luo, JG, Chen, C, Kong, LY (2017) Pharesinosides A-G, acylated glycosidic acid methyl esters derivatized by NH2 silica gel on-column catalyzation from the crude resin glycosides of Pharbitis Semen. Tetrahedron 73(20):2863-2871

Baranova, N, Nikaido, H (2002) The baeSR two-component regulatory system activates transcription of the yegMNOB (mdtABCD) transporter gene cluster in *Escherichia coli* and increases its resistance to novobiocin and deoxycholate. J Bacteriol 184:4168-4176

Basha Syed, S, Selvaraj Coumar, M (2016) P-glycoprotein mediated multidrug resistance reversal by phytochemicals: a review of SAR and future perspective for drug design. Curr Top Med Chem 16(22):2484-2508

Bautista, E, Fragoso-Serrano, M, Pereda-Miranda, R (2014) Jalapinoside, a macrocyclic bisdesmoside from the resin glycosides of *Ipomoea purga*, as a modulator of multidrug resistance in human cancer cells. J Nat Prod 78(1):168-172

Bautista, E, Fragoso-Serrano, M, Pereda-Miranda, R (2016) Jalapinoside II, a bisdesmoside resin glycoside, and related glycosidic acids from the officinal jalap root (*Ipomoea purga*). Phytochem Lett 17:85-93

Bhaskar, BV, Babu, TMC, Reddy, NV, Rajendra, W (2016) Homology modeling, molecular dynamics, and virtual screening of NorA efflux pump inhibitors of *Staphylococcus aureus*. Drug Des Dev Ther 10:3237-3252

Blair, JM, Webber, MA, Baylay, AJ, Ogbolu, DO, Piddock, LJ (2015) Molecular mechanisms of antibiotic resistance. Nat Rev Microbiol 13(1):42-51

Blair, JM, Piddock, LJ (2016) How to measure export via bacterial multidrug resistance efflux pumps. mBio 7(4). DOI 10.1128/mBio.00840-16

Brito-Arias, M, Pereda-Miranda R, Heathcock, CH (2004) Synthesis of tricolorin F. J Org Chem 69(14):4567-4570

Brown, AR, Ettefagh, KA, Todd, D, Cole, PS, Egan, JM, Foil, DH, Graf, TN, Schindler, BD, Kaatz, GW, Cech, NB (2015) A mass spectrometry-based assay for improved quantitative measurements of efflux pump inhibition. PloS One 10. DOI 10.1371/journal.pone.0124814

Cacciotto P, Ramaswamy VK, Malloci G, Ruggerone P, Vargiu AV (2018) Molecular modeling of multidrug properties of resistance nodulation division (RND) transporters. In: Yamaguchi A, Nishino K (eds) Bacterial multidrug exporters. Methods in molecular biology, vol 1700. Humana Press, New York, NY, pp179-219

Cao, S, Guza, RC, Wisse, JH, Miller, JS, Evans, R, Kingston, DG (2005) Ipomoeassins A–E, cytotoxic macrocyclic glycoresins from the leaves of *Ipomoea squamosa* from the Suriname rainforest. J Nat Prod 68(4):487-492

Cao, S, Norris, A, Wisse, JH, Miller, JS, Evans, R, Kingston, DG (2007) Ipomoeassin F, a new cytotoxic macrocyclic glycoresin from the leaves of *Ipomoea squamosa* from the Suriname rainforest. Nat Prod Res 21(10):872-876

Castañeda-Gómez, J, Pereda-Miranda, R (2011) Resin glycosides from the herbal drug jalap (*Ipomoea purga*). J Nat Prod 74(5):1148-1153

Castañeda-Gómez, J, Figueroa-González, G, Jacobo, N, Pereda-Miranda, R (2013) Purgin II, a resin glycoside ester-type dimer and inhibitor of multidrug efflux pumps from *Ipomoea purga*. J Nat Prod 76:64-71

Castañeda-Gómez, J, Rosas-Ramírez, D, Cruz-Morales, S, Fragoso-Serrano, M, Pereda-Miranda, R (2017) HPLC-MS profiling of the multidrug-resistance modifying resin glycoside content of *Ipomoea alba* seeds. Rev Bras Farmacogn 27:434-439

Castañeda-Gómez, J, Lavias-Hernández, P, Fragoso-Serrano, M, Lorence, A, Pereda-Miranda, R (2019) Acylsugar diversity in the resin glycosides from *Ipomoea tricolor* seeds as chemosensitizers in breast cancer cells. Phytochemistry Letters 32:77-82.

Chandra, H, Bishnoi, P, Yadav, A, Patni, B, Mishra, AP, Nautiyal, AR (2017) Antimicrobial resistance and the alternative resources with special emphasis on plant-based antimicrobial: a review. Plants 6(2):6-16. DOI 10.3390/plants6020016

Chen, L, Li, Y, Yu, H, Zhang, L, Hou, T (2012) Computational models for predicting substrates or inhibitors of P-glycoprotein. Drug Discov Today 17(7-8):343-351

Chérigo, L, Pereda-Miranda, R, Fragoso-Serrano, M, Jacobo-Herrera, N, Kaatz, GW, Gibbons, S (2008) Inhibitors of bacterial multidrug efflux pumps from the resin glycosides of *Ipomoea murucoides*. J Nat Prod 71(6):1037-1045

Chérigo, L, Pereda-Miranda, R, Gibbons, S (2009) Bacterial resistance modifying tetrasaccharide agents from *Ipomoea murucoides*. Phytochemistry 70(2):222-227

Chiang HY, Perencevich EN, Nair R, Nelson RE, Samore M, Khader K, Chorazy ML, Herwaldt LA, Blevins A, Ward MA, Schweizer, ML (2017) Incidence and outcomes associated with infections caused by vancomycin-resistant Enterococci in the United States: systematic literature review and meta-analysis. Infect Cont Hosp Ep 38(2):203-215

Corona-Castañeda, B, Pereda-Miranda, R (2012) Morning glory resin glycosides as modulators of antibiotic activity in multidrug-resistant Gram-negative bacteria. Planta Med 78:128-131

Corona-Castañeda, B, Chérigo, L, Fragoso-Serrano, M, Gibbons, S, Pereda-Miranda, R (2013) Modulators of antibiotic activity from *Ipomoea murucoides*. Phytochemistry 95:277-283

Corona-Castañeda, B, Rosas-Ramírez, D, Castañeda-Gómez, J, Aparicio-Cuevas, MA, Fragoso-Serrano, M, Figueroa-González, G, Pereda-Miranda, R (2016) Resin glycosides from *Ipomoea wolcottiana* as modulators of the multidrug resistance phenotype in vitro. Phytochemistry 123:48-57

Cruz-Morales, S, Castañeda-Gómez, J, Figueroa-González, G, Mendoza-García, AD, Lorence, A, Pereda-Miranda, R (2012) Mammalian multidrug resistance lipopentasaccharide inhibitors from *Ipomoea alba* seeds. J Nat Prod 75:1603-1611

Cruz-Morales, S, Castañeda-Gómez, J, Rosas-Ramírez, D, Fragoso-Serrano, M, Figueroa-González, G, Lorence, A, Pereda-Miranda, R (2016) Resin glycosides from *Ipomoea alba* seeds as potential chemosensitizers in breast carcinoma cells. J Nat Prod 79:3093-3104

Desai, PV, Sawada, GA, Watson, IA, Raub, TJ (2013) Integration of in silico and in vitro tools for scaffold optimization during drug discovery: predicting P-glycoprotein efflux. Mol Pharmaceutics 10(4):1249-1261

Dewanjee, S, Dua, T, Bhattacharjee, N, Das, A, Gangopadhyay, M, Khanra, R, Joardar, S, Riaz, M, Feo, V, Zia-Ul-Haq, M (2017) Natural products as alternative choices for P-glycoprotein (P-gp) inhibition. Molecules 22(6):871

Du, D, Wang-Kan, X, Neuberger, A, van Veen, HW, Pos, KM, Piddock, LJ, Luisi, BF (2018) Multidrug efflux pumps: structure, function and regulation. Nat Rev Microbiol 16:523-539

Dumont, E, Vergalli, J, Conraux, L, Taillier, C, Vassort, A, Pajović, J, Réfrégiers, M, Mourez, M, Pagès, JM (2018) Antibiotics and efflux: combined spectrofluorimetry and mass spectrometry to evaluate the involvement of concentration and efflux activity in antibiotic intracellular accumulation. J Antimicrob Chemoth 74(1):58-65

Escalante-Sánchez, E, Pereda-Miranda, R (2007) Batatins I and II, ester-type dimers of acylated pentasaccharides from the resin glycosides of sweet potato. J Nat Prod 70(6):1029-1034

Escobedo-Martínez, C, Cruz-Morales, S, Fragoso-Serrano, M, Rahman, MM, Gibbons, S, Pereda-Miranda, R (2010) Characterization of a xylose containing oligosaccharide, an inhibitor of multidrug resistance in *Staphylococcus aureus*, from *Ipomoea pes-caprae.* Phytochemistry 71(14-15):1796-1801

Eich E (2008) Solanaceae and Convolvulaceae: Secondary Metabolites. Springer, Berlin Heidelberg

Fan, BY, Gu, YC, He, Y, Li, ZR, Luo, JG, Kong, LY, (2014) Cytotoxic resin glycosides from *Ipomoea aquatica* and their effects on intracellular Ca^{2+} concentrations. J Nat Prod 77(10):2264-2272

Fan, BY, Li, ZR, Ma, T. Gu, YC, Zhao, H., Luo, JG, Kong, LY (2015) Further screening of the resin glycosides in the edible water spinach and characterisation on their mechanism of anticancer potential. J Funct Food 19:141-154

Figueroa-González, G, Jacobo-Herrera, N, Zentella-Dehesa, A, Pereda-Miranda, R (2012) Reversal of multidrug resistance by morning glory resin glycosides in human breast cancer cells. J Nat Prod 75:93-97

Govindarajan, M (2018) Amphiphilic glycoconjugates as potential anti-cancer chemotherapeutics. Eur J Med Chem 143:1208-1253

Haynes, MK, Garcia, M, Peters, R, Waller, A, Tedesco, P, Ursu, O, Bologa, CG, Santos, RG, Pinilla, C, Wu, TH, Lovchik, JA, Oprea, TI, Sklar, LA, Tegos, GP (2018) High-throughput flow cytometry screening of multidrug efflux systems. In: Yamaguchi A,

Nishino K (eds) Bacterial multidrug exporters. Methods in molecular biology, vol 1700. Humana Press, New York, NY, pp. 293-318

Higgins, CF (1992) ABC transporters: from microorganisms to man. Annu Rev Cell Biol 8(1):67-113

Kathawala, RJ, Gupta, P, Ashby Jr, CR, Chen, ZS (2015) The modulation of ABC transporter-mediated multidrug resistance in cancer: a review of the past decade. Drug Resist Update 18:1-17

Kaatz, GW, Moudgal, VV, Seo, SM (2002) Identification and characterization of a novel efflux-related multidrug resistance phenotype in *Staphylococcus aureus*. J Antimicrob Chemother 50: 833-838

Kroumova, AB, Zaitlin, D, Wagner, GJ (2016) Natural variability in acyl moieties of sugar esters produced by certain tobacco and other Solanaceae species. Phytochemistry 130:218-227

Lamut, A, Peterlin Mašič, L, Kikelj, D, Tomašič, T (2019) Efflux pump inhibitors of clinically relevant multidrug resistant bacteria. Med Res Rev; 1-45. DOI 10.1002/med.21591

Leckie, BM, D'Ambrosio, DA, Chappell, TM, Halitschke, R, De Jong, DM, Kessler, A, Kennedy, GG, Mutschler, MA (2016) Differential and synergistic functionality of acylsugars in suppressing oviposition by insect herbivores. PLoS One 11. DOI 10.1371/journal.pone.0153345

Liu, X, Enright, M, Barry, CS Jones, AD (2017) Profiling, isolation and structure elucidation of specialized acylsucrose metabolites accumulating in trichomes of *Petunia* species. Metabolomics 13:85. DOI 10.1007/s11306-017-1224-9

Locher, KP (2016) Mechanistic diversity in ATP-binding cassette (ABC) transporters. Nat Struct Mol Biol 23:487-493

Lomovskaya, O, Watkins, W (2001) Inhibition of efflux pumps as a novel approach to combat drug resistance in bacteria. J. Mol. Microb. Biotech 3:225-236

Lotina-Hennsen, B, King-Díaz, B, Pereda-Miranda, R (2013) Tricolorin A as a Natural Herbicide. Molecules 18:778-788

Luu, VT, Weinhold, A, Ullah, C, Dressel, S, Schoettner, M, Gase, K, Gaquerel, E, Xu, S, Baldwin, IT. (2017) *O*-acyl sugars protect a wild tobacco from both native fungal pathogens and a specialist herbivore. Plant Physiology 174:370-386

Mahmood, HY, Jamshidi, S, Sutton, JM, and Rahman, KM (2016) Current advances in developing inhibitors of bacterial multidrug efflux pumps. Curr Med Chem 23(10):1062-1081

Moghe, GD, Leong, BJ, Hurney, SM, Jones, AD, Last, RL (2017) Evolutionary routes to biochemical innovation revealed by integrative analysis of a plant-defense related specialized metabolic pathway. eLife 6. DOI 10.7554/eLife.28468.001

Nagano, T, Pospíšil, J, Chollet, G, Schulthoff, S, Hickmann, V, Moulin, E, Herrmann, J, Müller, R, Fürstner, A (2009) Total synthesis and biological evaluation of the cytotoxic resin glycosides ipomoeassin A–F and analogues. Chem-Eur J 15(38):9697-9706

Nascimento, E, Vitali, LH, Kress, MRVZ, Martinez, R (2017) *Cryptococcus neoformans* and *C. gattii* isolates from both HIV-infected and uninfected patients: antifungal susceptibility and outcome of cryptococcal disease. Rev Inst Med Trop SP 59. DOI 10.1590/s1678-9946201759049

Nikaido, H, Pagès, JM (2012) Broad-specificity efflux pumps and their role in multidrug resistance of Gram-negative bacteria. FEMS Microbiol Rev 36(2):340-363

O'Driscoll T, Crank CW (2015) Vancomycin-resistant enterococcal infections: epidemiology, clinical manifestations, and optimal management. Infect Drug Resist 8:217-230

Ono, M (2017) Resin glycosides from Convolvulaceae plants. J Nat Med 71(4):591-604

Ohnishi M, Golparian D, Shimuta K, Saika T, Hoshina S, Iwasaku K, Nakayama, SI, Kitawaki, J, Unemo, M (2011). Is *Neisseria gonorrhoeae* initiating a future era of untreatable gonorrhea?: Detailed characterization of the first strain with high-level resistance to ceftriaxone. Antimicrob Agents Chemother. 55 (7):3538-3545

Pendleton, JN, Gorman, SP, Gilmore, BF (2013) Clinical relevance of the ESKAPE pathogens. Expert Rev Anti-Infe 11(3):297-308

Pereda-Miranda, R, Bah, M (2003) Biodynamic constituents in the Mexican morning glories: purgative remedies transcending boundaries. Curr Top Med Chem 3(2):111-131

Pereda-Miranda, R, Escalante-Sánchez, E, Escobedo-Martínez, C (2005) Characterization of lipophilic pentasaccharides from beach morning glory (*Ipomoea pes-caprae*). J Nat Prod 68:226-230

Pereda-Miranda, R, Hernández-Carlos, B (2002) HPLC Isolation and structural elucidation of diastereomeric niloyl ester tetrasaccharides from Mexican scammony root. Tetrahedron 58:3145-3154

Pereda-Miranda, R, Kaatz GW, Gibbons S (2006) Polyacylated oligosaccharides from medicinal Mexican morning glory species as antibacterials and inhibitors of multidrug resistance in *Staphylococcus aureus*. J Nat Prod 2006 69(3):406-409

Pereda-Miranda, R, Mata, R, Anaya, AL, Wickramaratne, DM, Pezzuto, JM, Kinghorn, AD (1993) Tricolorin A, major phytogrowth inhibitor from *Ipomoea tricolor*. J Nat Prod 56:571-582

Pereda-Miranda, R, Rosas-Ramírez, D, Castañeda-Gómez, J (2010) Resin glycosides from the morning glory family. In: Kinghorn, A, Falk, H, Kobayashi, J (eds) Progress in the chemistry of organic natural products, vol. 92. Springer Verlag. New York, pp. 77-153

Pereda-Miranda, R, Villatoro-Vera, R, Bah, M, Lorence, A (2009) Pore-forming activity of morning glory resin glycosides in model membranes. Rev Latinoamer Quim 37:144-154.

Prasch, S, Bucar, F (2015) Plant derived inhibitors of bacterial efflux pumps: an update. Phytochem Rev 14(6):961-974

Prestegard, JH, Liu, J, Widmalm, G (2017) Oligosaccharides and polysaccharides. In: Varki A, Cummings RD, Esko JD, et al., editors. Essentials of glycobiology [Internet], 3rd edn. Cold Spring Harbor Laboratory Press, New York

Rao, M, Padyana, S, Dipin, KM, Kumar, S, Nayak, BB, Varela, MF (2018) Antimicrobial compounds of plant origin as efflux pump inhibitors: new avenues for controlling multidrug resistant pathogens. J Antimicrob Agents 4:159. DOI:10.4172/2472-1212.1000159

Ramaswamy, VK, Cacciotto, P, Malloci, G, Vargiu, AV, Ruggerone, P (2017) Computational modelling of efflux pumps and their inhibitors. Essays Biochem 61(1):141-156

Rencurosi, A, Mitchell, EP, Cioci, G, Pérez, S, Pereda-Miranda, R, Imberty, A (2004) Crystal structure of tricolorin A: molecular rationale for the biological properties of resin glycosides found in some Mexican herbal remedies. Angew Chem Int Edit 43(44):5918-5922

Remschmidt, C, Schneider, S, Meyer, E, Schroeren-Boersch, B, Gastmeier, P, Schwab, F (2017) Surveillance of antibiotic use and resistance in intensive care units (SARI): a 15-year cohort study. Dtsch Arztebl Int 114(50):858-865

Rodriguez, J, O'Neill, S, Walczak, MA (2018) Constrained saccharides: a review of structure, biology, and synthesis. Nat Prod Rep 35(3):220-229

Rosas-Ramírez, D, Escalante-Sánchez, E, Pereda-Miranda, R (2011) Batatins III-VI, glycolipid ester-type dimers from *Ipomoea batatas*. Phytochemistry 72:773-780

Rosas-Ramírez, D, Escandón-Rivera, S, Pereda-Miranda, R (2018) Morning glory resin glycosides as α-glucosidase inhibitors: in vitro and in silico analysis. Phytochemistry 148:39-47

Rivero-Cruz, I, Acevedo, L, Guerrero, JA, Martínez, S, Pereda-Miranda, R, Mata, R, Bye, R, Franzblau, S Timmermann, BN (2005) Antimycobacterial agents from selected Mexican medicinal plants. J Pharm Pharmacol 57(9):1117-1126

Schepetkin, IA, Quinn, MT (2006) Botanical polysaccharides: macrophage immunomodulation and therapeutic potential. Int Immunopharmacol 6(3):317-333

Schillaci, D, Spanò, V, Parrino, B, Carbone, A, Montalbano, A, Barraja, P, Diana, P, Cirrincione, G, Cascioferro, S (2017) Pharmaceutical approaches to target antibiotic resistance mechanisms. J Med Chem, 60(20):8268-8297

Silva, R, Vilas-Boas, V, Carmo, H, Dinis-Oliveira, RJ, Carvalho, F, de Lourdes Bastos, M, Remião, F (2015) Modulation of P-glycoprotein efflux pump: induction and activation as a therapeutic strategy. Pharmacol Therapeut 149:1-123

Spengler, G, Kincses, A, Gajdács, M, Amaral, L (2017) New roads leading to old destinations: efflux pumps as targets to reverse multidrug resistance in bacteria. Molecules 22(3):468. DOI:10.3390/molecules22030468

Stavri, M, Piddock, LJ, Gibbons, S (2007) Bacterial efflux pump inhibitors from natural sources. J Antimicrob Chemoth 59(6):1247-1260

Stermitz, FR, Lorenz, P, Tawara, JN, Zenewicz, LA, Lewis, K (2000) Synergy in a medicinal plant: antimicrobial action of berberine potentiated by 5′-methoxyhydnocarpin, a multidrug pump inhibitor. P Natl Acad Sci USA 97(4):1433-1437

Sun J, Deng Z, Yan A (2014) Bacterial multidrug efflux pumps: mechanisms, physiology and pharmacological exploitations. Biochem Bioph Res Co 453:254–267

Szakács, G, Hall, MD, Gottesman, MM, Boumendjel, A, Kachadourian, R, Day, BJ, Baubichon-Cortay, H, Di Pietro, A (2014) Targeting the Achilles heel of multidrug-resistant cancer by exploiting the fitness cost of resistance. Chem Rev 114(11):5753-5774

Tegos, G, Stermitz, FR, Lomovskaya, O, Lewis, K (2002) Multidrug pump inhibitors uncover remarkable activity of plant antimicrobials. Antimicrob Agents Ch 46(10):3133-3141

Thai, KM, Ngo, TD, Phan, TV, Tran, TD, Nguyen, NV, Nguyen, TH Le, MT (2015) Virtual screening for novel *Staphylococcus aureus* NorA efflux pump inhibitors from natural products. Med Chem 11(2):135-155

Varela, MF, Andersen, JL, Ranjana, KC, Kumar, S, Sanford, LM, Hernandez, AJ (2017) Bacterial resistance mechanisms and inhibitors of multidrug efflux pumps belonging to the major facilitator superfamily of solute transport systems. In Rahman, A, Choudhary, MI (eds) Frontiers in anti-infective drug discovery, vol 5. Bentham Science Publishers, Sharjah. pp. 109

Venter, H, Mowla, R, Ohene-Agyei, T, Ma, S (2015) RND-type drug efflux pumps from Gram-negative bacteria: molecular mechanism and inhibition. Front Microbiol 6. DOI 0.3389/fmicb.2015.00377

Vichai, V, Kirtikara, K (2006) Sulforhodamine B colorimetric assay for cytotoxicity screening. Nat Protoc 1:1112-1116

Volpe, DA, Qosa, H (2018) Challenges with the precise prediction of ABC-transporter interactions for improved drug discovery. Expert Opin Drug Dis 13(8):697-707

Yu, Y, Shen, M, Song, Q, Xie, J (2018) Biological activities and pharmaceutical applications of polysaccharide from natural resources: A review. Carbohyd Polym 183:91-101

Zong, G, Aljewari, H, Hu, Z, Shi, WQ (2016) Revealing the pharmacophore of ipomoeassin F through molecular editing. Org Lett 18(7):1674-1677

Zong, G, Whisenhunt, L, Hu, Z Shi, WQ (2017) Synergistic contribution of tiglate and cinnamate to cytotoxicity of ipomoeassin F. J Org Chem 82(9):4977-4985

Zong, G, Shi, WQ (2017) Total synthesis of ipomoeassin F and its analogs for biomedical research. In Harmata, M (ed) Strategies and tactics in organic synthesis, vol 13. Academic Press, London San Diego Cambridge Oxford. pp. 81

Zong, G, Sun, X, Bhakta, R, Whisenhunt, L, Hu, Z, Wang, F, Shi, WQ (2018) New insights into structure-activity relationship of ipomoeassin F from its bioisosteric 5-oxa/aza analogues. Eur J Med Chem 144:751-757

Zong, G, Hu, Z, O'Keefe, S, Tranter, D, Iannotti, MJ, Baron, L, Hall, B, Corfield, K, Paatero, AO, Henderson, MJ, Roboti, P, Zhou, J, Sun, X, Govindarajan, M, Rohde, JM, Blanchard, N, Simmonds, R, Inglese, J, Du, Y, Demangel, C, High, S, Paavilainen, VO, Shi, WQ (2019) Ipomoeassin F binds Sec61α to inhibit protein translocation J. Am. Chem. Soc 141(21):8450-8461

Zhu, D, Chen, C, Bai, L, Kong L, Luo, J (2019a) Downregulation of aquaporin 3 mediated the laxative effect in the rat colon by a purified resin glycoside fraction from Pharbitis Semen. Evid-Based Compl Alt. DOI: 10.1155/2019/9406342

Zhu, D, Chen, C, Xia, Y, Kong, LY, Luo, J (2019b) A purified resin glycoside fraction from Pharbitidis Semen induces paraptosis by activating chloride intracellular channel-1 in human colon cancer cells. Integr Cancer Ther 18(1):1-13

CAPÍTULO III

Evaluación del potencial modulador de las resinas glicosídicas de *O. macrocarpa* sobre la resistencia múltiple a fármacos

Brazilian Journal of Pharmacognosy

Is the lipophilicity-hydrophilicity balance of macrocyclic resin glycosides important for their chemosensitizer activity in multidrug-resistant cells?

Jesús Lira-Ricárdez,[†] Mabel Fragoso-Serrano,[†]

Suzana Guimarães Leitão,[§] and Rogelio Pereda-Miranda*[,†]

[†]Departamento de Farmacia, Facultad de Química and Programa de Maestría y Doctorado en Ciencias Químicas, Universidad Nacional Autónoma de México, Ciudad Universitaria, Mexico City 04510, Mexico

[§]Faculdade de Farmácia, Universidade Federal do Rio de Janeiro, CCS, Bloco A, Ilha do Fundão, 21941-902, Rio de Janeiro, Brazil

ABSTRACT: High-polar resin glycosides from MeOH-soluble the Brazilian jalap root extract, *Operculina macrocarpa* (L.) Urb. (Convolvulaceae), and some derivatives were evaluated as chemosensitizers of vinblastine in multidrug-resistance human breast carcinoma cells (MCF-7/Vin$^+$). The potentiation of the modulatory activity of these glycolipids was found to be directly associated to the constrained macrolactone structure, as well as to their amphiphilicity, as demonstrated by the peracetyl operculinic acid H macrolactone, which enhances vinblastine susceptibility with a reversal factor of 20-fold when incorporated at 25 μg/ml, in comparison with the non-cyclic macrocarposidic acids A-C (3-fold) and macrocarposidic acid C methyl ester (7-fold). The lipophilicity-hydrophilicity balance of macrocyclic resin glycosides seems to be important to facilitate interactions with their efflux pump targets.

INTRODUCTION

Human ATP-binding cassette (ABC) transporters are an important family of around 50 transmembrane glycoproteins, which decrease the intracellular accumulation of many therapeutic agents. Eventually, the effectiveness of these drugs is decreased as well as the toxicity of any xenobiotic, including environmental contaminants. The most important member of this family is P-glycoprotein (P-gp) or multidrug-resistance factor-1 (MDR1), which is expressed on excretory, glandular, and visceral tissues, but also highly expressed in human cancer cells as part of the defensive mechanism against chemotherapeutic agents, such as taxanes, epipodophyllotoxins, vinca alkaloids, among other anti-cancer drugs (Arana and Altenberg, 2019, Kathawala et al. 2015).

In recent years, P-gp inhibition has been considered as a potential target for new medicinal options to counteract chemotherapy resistance. Usually, P-gp substrate affinity includes molecules with weak amphipathic and rather hydrophobic behavior, aromatic groups or positively charged amino groups at normal pH (Arana and Altenberg, 2019). For the discovery and developing of selective P-gp inhibitors, some molecular and physicochemical requirements have also to be considered, such as lipophilicity, higher partition constant (LogP ≥ 2.91), a high E_{homo} value, the presence of a positively ionizable group (tertiary amine group, predominantly), and 18 atoms long or large molecular axis (Palmeira et al., 2012). Most of these characteristics have been found in some natural products with P-gp inhibitory activity like alkaloids (e.g., berberine, reserpine and

yohimbine), coumarins (e.g., bergamottin), flavonoids (e.g., galangin and quercetin), and terpenoids (e.g., ophiobolin A and thymol), *inter alia* (Dewanjee et al, 2016).

Resin glycosides are another important group of natural products that have shown an *in-vitro* high P-gp modulating activity in chemotherapy-resistant human cancer cells which displayed cross-resistance to adriamycin, vinblastine, colchicine, camptothecin, and ellipticine (Figueroa-González et al., 2012). Particularly, macrocyclic compounds like tricolorin A from *Ipomoea tricolor* (reversal fold value: $RF_{MCF-7/Vin+}$ = IC_{50} vinblastine/IC_{50} vinblastine in the presence of glycolipid; RF_{MCF-7/Vin^+} 2164-fold) (Castañeda-Gómez et al., 2019), murucoidin V from *I. murucoides* (RF_{MCF-7/Vin^+} >255-fold) (Figueroa-González et al., 2012), albinosides III, VIII, and IX from *I. alba* (RF_{MCF-7/Vin^+} >2140-fold) (Cruz-Morales et al., 2016), and purgin II and jalapinoside I from *I. purga* (RF_{MCF-7/Vin^+} >1906-fold) (Bautista et al., 2012; Castañeda-Gómez et al., 2013). This antigen-antibody recognition reaction between the glycoprotein expressed in the cell membranes with its specific antibody reflects the conformational changes induced by resin glycosides, as a possible substrate of this efflux pumps.

As part of our continuing interest to analyze the importance of the resin glycoside structure-activity relationships for uncovering novel glycolipids as chemosensitizers in mammalian cells, this article describes the modulation of the multidrug-resistance phenotype of intact resin glycosides and their derivatives from the Brazilian jalap root (*Operculina macrocarpa*) on vinblastine-resistant human breast cancer cells.

MATERIAL AND METHODS

General experiment procedures: Isolation and structural characterization of macrocarposidic acids A-C (**1-3**) and peracetyl operculinic acid H macrolactone (**4**) were previously described (Lira-Ricárdez et al., 2019).

Esterification of macrocarposidic acid C (3): Macrocarposidic acid C (3 mg) was diluted in a small volume of MeOH and reacted with diazomethane in Et_2O until the liberation of N_2 ceased. The reaction mixture was evaporated in vacuum to obtain compound **3a** (3.5 mg). Macrocarposidic acids C methyl ester (**3a**) white powder; mp 146–148 °C; $[\alpha]^{25}_D$ –21.0 (*c* 1.0, MeOH); HRFABMS m/z 1697.8157 $[M + H]^+$. This derivative was identified by comparison of their physical and spectroscopic constants with published values (Ono et al., 2017).

Chemical and cell lines: RPMI 1640 medium and fetal bovine serum were purchased from Gibco (Life Technologies, Carlsbad, CA) and sulforhodamine B (SRB), colchicine, reserpine, and vinblastine from Sigma-Aldrich (St. Louis, MO). Breast (MCF-7), cervix (HeLa), and colon (HCT-15) carcinoma cell lines were acquired from the American Type Culture Collection. The resistant counterpart MCF-7/Vin$^+$ has been subcultured for eight years. To maintain drug resistance, MCF-7/Vin$^+$ cells were cultured in medium containing 0.192 μg/mL vinblastine. At the same time, a stock of MCF-7/Vin$^-$ cells was maintained in vinblastine-free medium (Figueroa-González et al., 2012).

Cytotoxicity and modulation of multidrug-resistance assays: Cytotoxicity of compounds was determined by using the SRB assay (Vichai and Kirtikara, 2006). Cell lines were maintained in RPMI 1640 medium supplemented with 10% fetal bovine serum and cultured at 37 °C in 5% CO_2 in air (100% humidity) and harvested at log phase of their growth cycle and were treated in triplicate with various concentrations of the test samples. MCF-7/Vin$^+$ cells were cultured in medium containing 0.192 μg/ml vinblastine. A stock of MCF-7/Vin cells was also maintained in vinblastine-free medium (MCF-7/Vin$^-$). Cells at log phase were treated in triplicate with test samples (0.2–25 μg/ml) and incubated for 72 h. For the reversal effects, sensitive MCF-7 and MDR MCF-7/Vin cells were seeded into 96-well plates and treated with various concentrations of vinblastine (0.00064–10 μg/ml) in the presence or absence of glycolipids (25 μg/ml) for 72 h. The ability of glycolipids to potentiate vinblastine cytotoxicity was measured by calculating the IC_{50} (Figueroa-González et al., 2012).

RESULTS AND DISCUSSION

Macrocarposidic acids A-C (**1-3**) were the major resin glycosides isolated from the MeOH-soluble extract of *O. macrocarpa* roots. These oligosaccharides of operculinolic acid (3*S*,12*S*-dihydroxyhexadecanoic acid) are composed by a hexasaccharide core, containing two unit of rhamnose and four units of glucose (operculinic acid H) with different acylating moieties including exogonic, 3-methyl butyric, and tiglic acids. These examples of non-macrolactone-type resin glycosides exhibit an amphiphilic behavior which was useful for their isolation by precipitation with water (Lira-Ricárdez et al., 2019). Natural compounds

1-3 were first evaluated for cytotoxicity, considering that the lack of activity for test samples in sensible cancer human cells is an important requirement for further exploring their efflux pump modulatory activity (Lira-Ricárdez and Pereda-Miranda, 2019). As previously demonstrated for most of the evaluated resin glycosides from the morning glory family (Figueroa-González et al., 2012), compounds **1-3** were inactive against breast cancer human cells (MCF-7) with an IC_{50} > 25 μg/mL, in contrast with the activity of positive controls, colchicine (IC_{50} = 0.008 μg/mL) and vinblastine (IC_{50} = 0.038 μg/mL).

	R₁	R₂	R₃	R₄	R₅
1:	Iva	Tga	H	Tga	H
2:	Iva	Tga	Iva	H	H
3:	Iva	Tga	H	Iva	H
3a:	Iva	Tga	H	Iva	CH₃

Iva :

Tga :
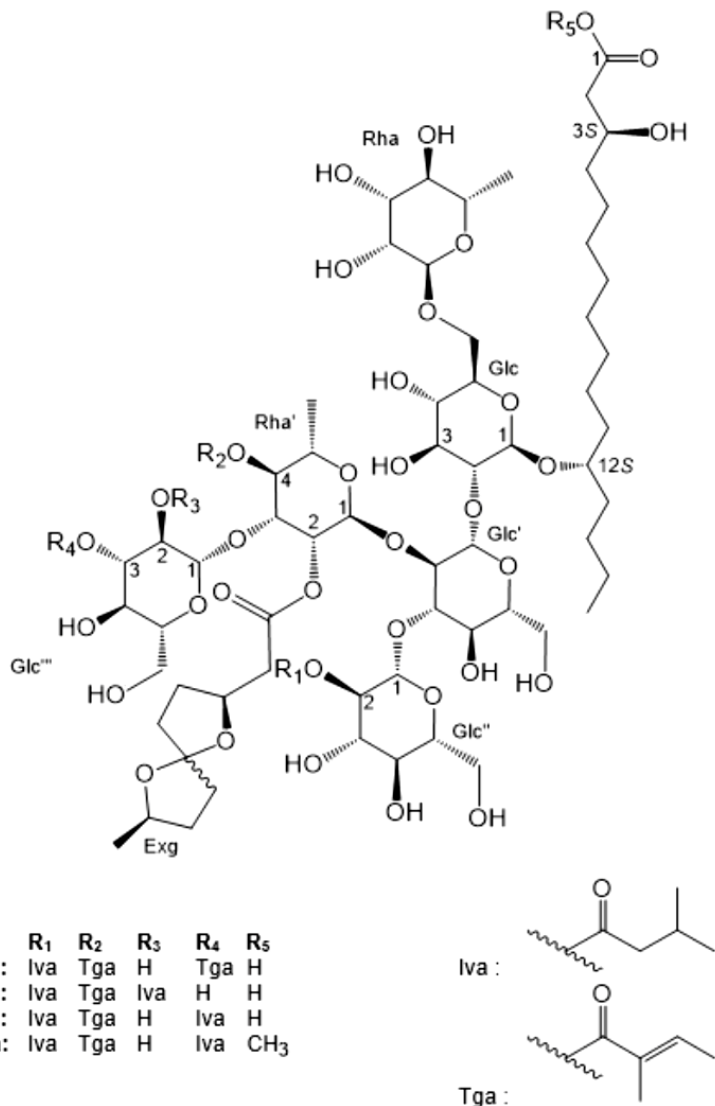
Table 9. Cytotoxicity of macrocarposidic acids A-C (**1-3**), macrocarposidic acid C methyl ester (**3a**) and peracetyl operculinic acid H macrolactone (**4**)

	IC$_{50}$ (μg/mL)		
Compound	**MCF-7**	**HeLa**	**HCT15**
1	>25	>25	>25
2	>25	>25	>25
3	>25	>25	>25
3a	>25	NE	NE
4	>25	NE	NE
Colchicine	0.008	0.0045	0.010
Vinblastine	0.038	0.009	0.015

MCF-7 = breast carcinoma; HeLa = cervix carcinoma, HCT-15 = colon carcinoma.

Table 10. Modulation of Vinblastine Cytotoxicity in Drug Sensitive MCF-7 and Multidrug-Resistant MCF-7/Vin by macrocarposidic acids A-C (**1-3**), macrocarposidic acid C methyl ester (**3a**) and peracetyl operculinic acid H macrolactone (**4**)

	IC$_{50}$ (μg/mL)			reversal fold[c]		
compound[a]	**MCF-7/Vin⁻**	**MCF-7/Vin⁺**	**MCF-7 sens**	**RF$_{MCF-7/Vin^-}$**	**RF$_{MCF-7/Vin^+}$**	**RF$_{MCF-7\ sens}$**
Vinblastine	1.279 ± 0.085	1.385 ± 0.027	0.038 ± 0.014			
1	0.561 ± 0.204	0.414 ± 0.105	0.015 ± 0.006	2	3	3
2	0.416 ± 0.106	0.522 ± 0.150	0.006 ± 0.003	3	3	6
3	0.496 ± 0.130	0.835 ± 0.049	0.0003 ± 0.0001	3	2	127
3a	0.209 ± 0.065	0.186 ± 0.049	0.00015 ± 0.0001	6	7	253
4	0.078 ± 0.009	0.068 ± 0.022	<0.000128	16	20	297
Reserpine[b]	0.013 ± 0.003	0.065 ± 0.033	0.003 ± 0.0007	98	21	13

In order to evaluate the importance of the entire lipophilicity as a crucial requirement for the molecule's potency as a chemosensitizer and the need for a macrocyclic structure, two derivatives were included in the subsequent modulation screening: the macrocarposidic acid C methyl ester (**3a**) and the peracetyl operculinic H macrolactone (**4**). Both derivatives presented significant changes in the lipophilicity-hydrophilicity balance in relation to the non-cyclic glycosidic acids **1-3**. This change in amphiphilicity was an important characteristic reflected in their efflux pump modulatory activities, as a consequence of enhancement in both cell penetration and pharmacokinetic profile of these samples (Lira-Ricárdez and Pereda-Miranda, 2019). Thus, esterification of the carboxylic acid moiety in glycosidic acid **3** increased the solubility in non-protic organic solvents (e.g., CHCl3) of derivative **3a**, while the macrocyclic structure of derivative **4** provided evidence for the implication of a macrolide, which effectively would constrain the oligosaccharide core into a limited number of bioactive conformations. The conformational analysis by crystallography (Rencurosi et al., 2004) of the tetrasaccharide macrolactone-type structure of tricolorin A, a potent efflux pump inhibitor (Castañeda-Gómez et al., 2019), offered an understanding for the constrained rigid structure of its macrocyclic disaccharide portion, as opposed to the free rotation experienced in solution around the anomeric linkages in the acyclic disaccharide segment (Rencurosi et al., 2004), as it would be expected for linear compounds **1-3**. It has been demonstrated that oligossacharides avoid the entropic costs of their conformational flexibility by generating multivalent interactions with their target proteins (Rodriguez et al., 2018). The main structural features of the amphiphilic resin

glycosides, which include the presence of numerous hydrophobic units (represented by the glycosidic acid core) containing various H-bond acceptors and H-bond donor centers, in addition to the esterifying residues, sometimes holding aromatic rings, are responsible for the lipophilicity-hydrophilicity balance, which facilitates the multivalent interactions with membrane efflux pumps.

Efflux pump modulatory evaluation was performed with these compounds against multidrug resistant breast cancer human cells cultivated in vinblastine-free medium (MCF-7/Vin$^-$) and vinblastine-supplemented medium (MCF-7/Vin$^+$). Compounds **1-3** exerted a low potentiation to vinblastine susceptibility in both cell lines with a limited response (RF$_{\text{MCF-7/Vin}}^-$ and RF$_{\text{MCF-7/Vin}}^+$ ≤ 3-fold) in comparison to reserpine used as a positive control for reversion (RF$_{\text{MCF-7/Vin}}^-$ 98-fold and RF$_{\text{MCF-7/Vin}}^+$ 21-fold). The hydrophilic character of the aglycone's carboxyl group of **1-3** decreases the whole molecule lipophilicity and produced a poor interaction with the membrane efflux pumps, as demonstrated for the slight increment of the modulatory activity for derivative **3a** (RF$_{\text{MCF-7/Vin}}^-$ 6-fold and RF$_{\text{MCF-7/Vin}}^+$ 7-fold). Esterification of aglycone restricted the hydrophilic character and the ionizable carboxyl group tendency in the extracellular space, which provided a subtle compensation for the lipophilicity for **3**. This weak modulatory activity of efflux pumps was only comparable with that previously displayed by another group of naturally non-macrocyclic resin glycosides, such as dichondrins A-C (Song et al., 2015), merremin F (Wang et al., 2014), and pescaprosides A-B (Figueroa-González et al., 2012).
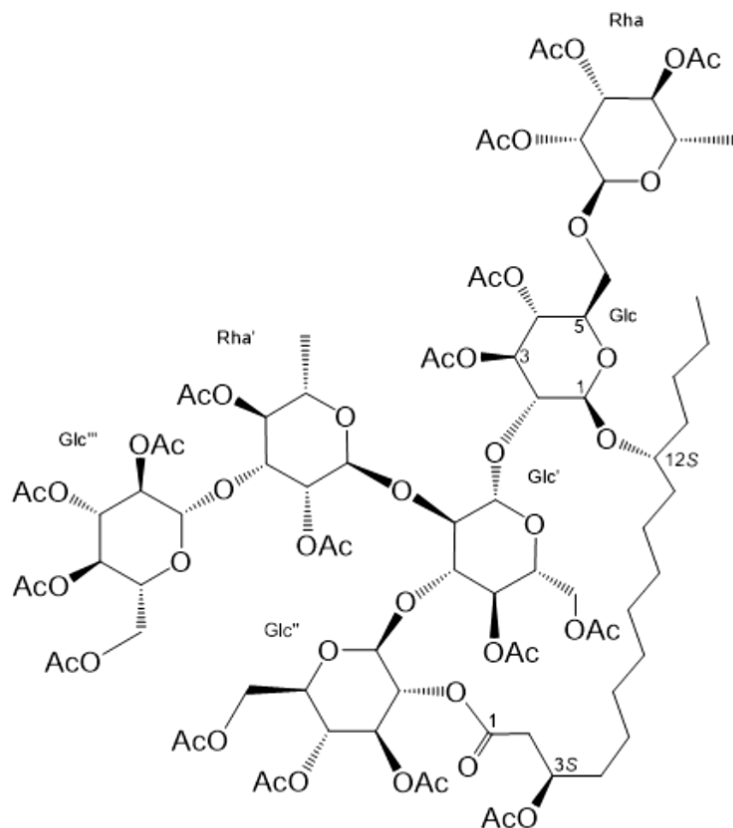
4

The modulatory activity of **4** showed an enhanced increment in both cell lines with a reversal fold ten times higher (RF$_{\text{MCF-7/Vin}}^{+}$ 20-fold) than compounds **1-3**, which was comparable to reserpine. This artifact from the peracetylation of operculinic acid H is a highly lipophilic hexasaccharide with an intramolecular macrocyclic structure between the carboxylic acid of the aglycone and the OH group at C-2 of the third glucose unit (Glc″) (Lira-Ricárdez et al., 2019). The presence of a constrained macrocyclic structure for derivative **4** definitely conferred high conformational stability which provided a better fitting interaction with the efflux pump active sites, like those of the P-gp, as indicated the increment in its modulatory potential.

Therefore, it is possible to conclude that lipophilicity and constrained-configurational stability of the oligosaccharide core of resin glycosides are fundamental properties that are involved in the biological activity as chemosensitizers. Amphiphilic properties of resin glycosides resulting from partial acylation of their oligosaccharide cores and the lipophilic alkyl chains of their fatty acid aglycones seem to be important to facilitate interaction with their efflux pump targets. Therefore, substantially non-polar molecules (highly acylated) will not efficiently interact with the membrane efflux pumps and those that are extremely polar are poorly membrane-soluble, thus difficulting the interaction with the membrane efflux pumps. Therefore, both covalent and non-covalent interactions will modulate the three-dimensional efflux pump structure, resulting in conformational changes associated with a reduction in their effluxing potential. These notable structural characteristics of resin glycosides modify the lipophilicity-hydrophilicity balance of these non-cytotoxic macrocyclic natural products, which will impact their potential use in combinatorial chemotherapies by reducing current effective therapeutic doses and diminishing noxious side-effects in refractory malignancies.

ACKNOWLEDGMENTS

AUTHORSHIP

JLR performed the isolation of novel compounds, prepared derivatives, completed their structure elucidation, and wrote the first draft of this manuscript which is based on his Ph.D. thesis (Posgrado en Ciencias Químicas, UNAM). MFS performed the bioassays and supervised experimental general procedures. SGL supplied the plant material and recorded NMR spectra. RPM planned the study and made a critical reading of the manuscript. All authors contributed to the revision of the manuscript final version.

REFERENCES

Arana, M. R., Altenberg, G. A., 2019. ATP-binding Cassette Exporters: Structure and Mechanism with a Focus on P-glycoprotein and MRP1. Curr. Med. Chem. 26, 1062-1078.

Bautista, E., Fragoso-Serrano, M., Pereda-Miranda, R. 2014. Jalapinoside, a macrocyclic bisdesmoside from the resin glycosides of *Ipomoea purga*, as a modulator of multidrug resistance in human cancer cells. J Nat Prod 78, 168-172.

Castañeda-Gómez, J., Figueroa-González, G., Jacobo, N., Pereda-Miranda, R. 2013. Purgin II, a resin glycoside ester-type dimer and inhibitor of multidrug efflux pumps from *Ipomoea purga*. J Nat Prod 76:64-71

Castañeda-Gómez, J., Lavias-Hernández, P., Fragoso-Serrano, M., Lorence, A., Pereda-Miranda, R. 2019. Acylsugar diversity in the resin glycosides from *Ipomoea tricolor* seeds as chemosensitizers in breast cancer cells. Phytochem. Lett. 32, 77-82.

Cruz-Morales, S., Castañeda-Gómez, J., Rosas-Ramirez, D., Fragoso-Serrano, M., Figueroa-González, G., Lorence, A., Pereda-Miranda, R. 2016. Mammalian multidrug resistance lipopentasaccharide inhibitors from *Ipomoea alba* seeds. J. Nat. Prod. 79, 3093-3104.

Dewanjee, S., Dua, T., Bhattacharjee, N., Das, A., Gangopadhyay, M., Khanra, R., Joardar, S., Riaz, M., Feo, V., Zia-Ul-Haq, M. 2017. Natural products as alternative choices for P-glycoprotein (P-gp) inhibition. Molecules 22, 871.

Figueroa-González, G., Jacobo-Herrera, N., Zentella-Dehea, A., Pereda-Miranda, R. 2011. Reversal of multidrug resistance by morning glory resin glycosides in human breast cancer cells. J. Nat. Prod. 75, 93-97.

Kathawala, R.J., Gupta, P., Ashby Jr, C.R., Chen, Z.S., 2015. The modulation of ABC transporter-mediated multidrug resistance in cancer: a review of the past decade. Drug Resist Update 18, 1-17.

Lira-Ricárdez, J., Pereda-Miranda, R., 2019. Reversal of multidrug resistance by amphiphilic morning glory resin glycosides in bacterial pathogens and human cancer cells. Phytochem. Rev. in press.

Lira-Ricárdez, J., Pereda-Miranda, R., Castañeda-Gómez, J., Fragoso-Serrano, M., Costa Simas, R, Guimarães Leitão, S. 2019. Resin Glycosides from the roots of *Operculina macrocarpa* (Brazilian Jalap) with Purgative Activity. J. Nat. Prod., https://doi.org/10.1021/acs.jnatprod.9b00222.

Palmeira, A., Sousa, E., H Vasconcelos, M., M Pinto, M. 2012. Three decades of P-gp inhibitors: skimming through several generations and scaffolds. Curr. Med. Chem. 19, 1946-2025.

Rencurosi, A., Mitchell, E.P., Cioci, G., Pérez, S., Pereda-Miranda, R., Imberty, A. 2004. Crystal structure of tricolorin A: molecular rationale for the biological properties of resin glycosides found in some Mexican herbal remedies. Angew Chem Int Edit 43(44):5918-5922

Rodriguez, J, O'Neill, S, Walczak, MA (2018) Constrained saccharides: a review of structure, biology, and synthesis. Nat Prod Rep 35(3):220-229

Song, W.B., Wang, W.Q., Zhang, S.W., Xuan, L.J. 2015. Multidrug resistance–reversal effects of resin glycosides from *Dichondra repens*. Bioorg. Med. Chem. Lett. 25(4), 795-798.

Vichai, V, Kirtikara, K. 2006. Sulforhodamine B colorimetric assay for cytotoxicity screening. Nat Protoc 1, 1112-1116.

Wang, W. Q., Song, W. B., Lan, X. J., Huang, M., & Xuan, L. J. 2014. Merremins A–G, resin glycosides from *Merremia hederacea* with multidrug resistance reversal activity. J. Nat. Prod. 77, 2234-2240.

CONCLUSIONES

1. La fracción rica en resinas glicosídicas solubles en metanol se analizó, fraccionó y resolvió mediante la técnica de cromatografía de líquidos de alta resolución en fase reversa. De esta manera, se obtuvieron tres productos lipohexasacáridos designados como ácidos macrocarposídicos A-C, cuyas estructuras químicas se establecieron como análogos acilados del ácido operculínico H. Estos produtos natuales exhiben enlaces tipo éster en la cadena oligosacárida con residuos de los ácidos tíglico, isovalérico y exogónico, el cual, se encuentra presente en sus dos formas epiméricas (*E,E* 3*S*,6*S*,9*R* y *Z,Z* 3*S*,6*R*,9*R)*; por ello, los compuestos descritos se encuentran formando una mezcla inseparable y proporcional de dichos diastereoisómeros.

2. La saponificación de dicha fracción produce una mezcla compleja de lipooligosacáridos, que fue analizada mediante el uso de técnicas analíticas instrumentales de separación (cromatografía de líquidos de alta resolución y cromatografía de gases), espectroscópicas (resonancia magnética nuclear en 1D y 2D) y espectrométricas (espectrometría de masas), en conjunto con una serie de reacciones químicas de derivatización. Se reconoce al ácido operculínico H, hexasacárido constituido por cuatro unidades de glucosa, dos unidades de ramnosa y una unidad de ácido operculinólico, como el ácido glicosídico principal de esta fracción, y el análisis complementario de los ácidos volátiles obtenidos de la reacción coincidieron con la presencia de los ácidos tíglico, isovalérico, 2-metilbutírico y exogónico, previamente descritos en estudios anteriores de esta fracción altamente polar de resinas glicosídicas.

3. Los compuestos glicolípidicos minoritarios de la mezcla de reacción de saponificación se aislaron y purificaron mediante las técnicas de reciclaje de pico, rasurado de pico y corte de núcleo. Se realizó una extensa labor exploratoria de los espectros de resonancia magnética nuclear homonuclear

para evaluar los desplazamintos químicos de ^{1}H y ^{13}C y bidimensional (como los métodos homonucleares COSY y TOCSY y heteronucleares HSQC y HMBC) con el fin de completar la elucidación estructural de los ácidos glicosídicos aislados.

4. Se reconoció un par de lipohexasacáridos novedosos designados como los ácidos operculínicos I y J, los cuales están constituidos por la misma cadena oligosacárida del ácido operculínico H y enlazados a un residuo de los ácidos 12S-hidroxihexadecanoico y 11S-hidroxihexadecanoico, respectivamente.

5. El proceso de acetilación realizado a la mezcla lipooligosacárida saponificada dió lugar a la formación de un par de artefactos de reacción del ácido operculínico H: un primer compuesto peracetilado α, β-instaturado derivado de la deshidratación del grupo hidroxilo presente en la posición C-3 del ácido operculinólico –la aglicona– y un segundo compuesto peracetilado macrocíclico tipo lactona entre el ácido operculinólico y el grupo hidroxilo de la posición C-2 de la tercera unidad de glucosa de la cadena oligosacárida, este último asemejándose a las estructuras distintivas de tipo macrocíclico características de las resinas glicosídicas de las convolvuláceas.

6. Del mismo modo que los análogos del ácido operculínico H y sus congéneres, fue posible el aislamiento del ácido púrgico A, un lipohexasacárido previamente aislado y analizado de la fracción soluble en metanol de la raíz de la jalapa mexicana (*Ipomoea purga*), utilizada tradicionalmente en la herbolaria mexicana como remedio purgante, junto con el aislamiento de un monosacárido novedoso designado como el ácido operculínico K, conformado por una unidad de quinovosa y una unidad del ácido (−)-7R-hidroxidecanoico, relacionado como una unidad esterificante de otros núcleos oligosacáridos en especies afines.

7. La diversidad química de las resinas glicosídicas presentes en la fracción insoluble en éter (convolvulina) de las raíces de las jalapas mexicana y brasileña sustenta la presencia de oligómeros de alto peso molecular, principalmente hexasacáridos acíclicos, divergiendo en la longitud de sus agliconas.

8. En cuanto a la relación entre la estructura química de las resinas glicosídicas y la actividad moduladora de las bombas de eflujo relacionadas a la resistencia múltiple a fármacos (e.g., glicoproteína-P), los resultados indican que la naturaleza anfifílica producto de un determinado grado de esterificación, complementada con la presencia de un sistema macrocíclico que restringe la libertad conformacional del núcleo oligosacárido, permite una mejor interacción con el sitio de acción de las bombas de eflujo y la generación de un efecto modulador significativamente alto. Lo anterior quedó demostrado con los resultados sobre la reversión de la actividad de dicho factor de resistencia a la vinblastina en células de carcinoma mamario por la macrolactona del ácido operculínico H peracetilada, cuya actividad moduladora fue cuantitativamente mayor que la observada para las estructuras acíclicas de los ácidos macrocarposídicos A-C y el éster metílico del ácido macrocarposídico C.

9. Estos glicolípidos presentan algunas de las características estructurales reconocidas para las inhibidores o sustratos de las bombas de eflujo, como son la presencia de varias unidades hidrófobas, que están representadas por las agliconas, además de los residuos de esterificación, que a veces contiene anillos aromáticos y varios aceptores y donadores de H^+ en los núcleos oligosacáridos. Por lo tanto, interacciones covalentes y no covalentes modulan la estructura tridimensional de las bombas de eflujo, resultando en cambios conformacionales, que se asocian con la pérdida o reducción en la actividad de extrusión celular de agentes xenobióticos.

Glycosidic Acid Content of the Brazilian Jalap, Roots of *Operculina macrocarpa* with Purgative Activity

José de Jesús Lira-Ricárdez,[†] Rogelio Pereda-Miranda,*,[†] Jhon Castañeda-Gómez,[‡]

Mabel Fragoso-Serrano,[†] Rosineide Costa Simas,[§] and Suzana Guimarães Leitão[§]

[†]Departamento de Farmacia, Facultad de Química, Universidad Nacional Autónoma de México, Ciudad Universitaria, Mexico City 04510, Mexico

[‡]Grupo Químico de Investigación y Desarrollo Ambiental. Programa de Licenciatura en Ciencias, Facultad de Educación. Universidad Surcolombiana, Nieva, Colombia

[§]Faculdade de Farmacia, Universidade Federal do Rio de Janeiro, CCS, Bloco A, Ilha do Fundão, 21941-590, Rio de Janeiro, Brazil

Table of contents Page

Figure S1. Brazilian jalap root: crude drug, powders, and phytopharmaceuticals. Brazilian jalap continues to be extensively traded for medicinal purposes in the Brazilian Northern regions as crude drug, in addition to many products made with the roots and the resin glycoside contents: A) Roots; B) Dried-roots cut into slices; C) Commercialized powders, pulverized "batatão" and "jalapa" for sale in a public market; D) Syrup of batatão (Hypolito), hydro-alcoholic extracts (Sobral Pharmaceutical Industry) and pills. All products were purchased at the Mercado 2000, Santarém, Pará, Brazil in september 2015.
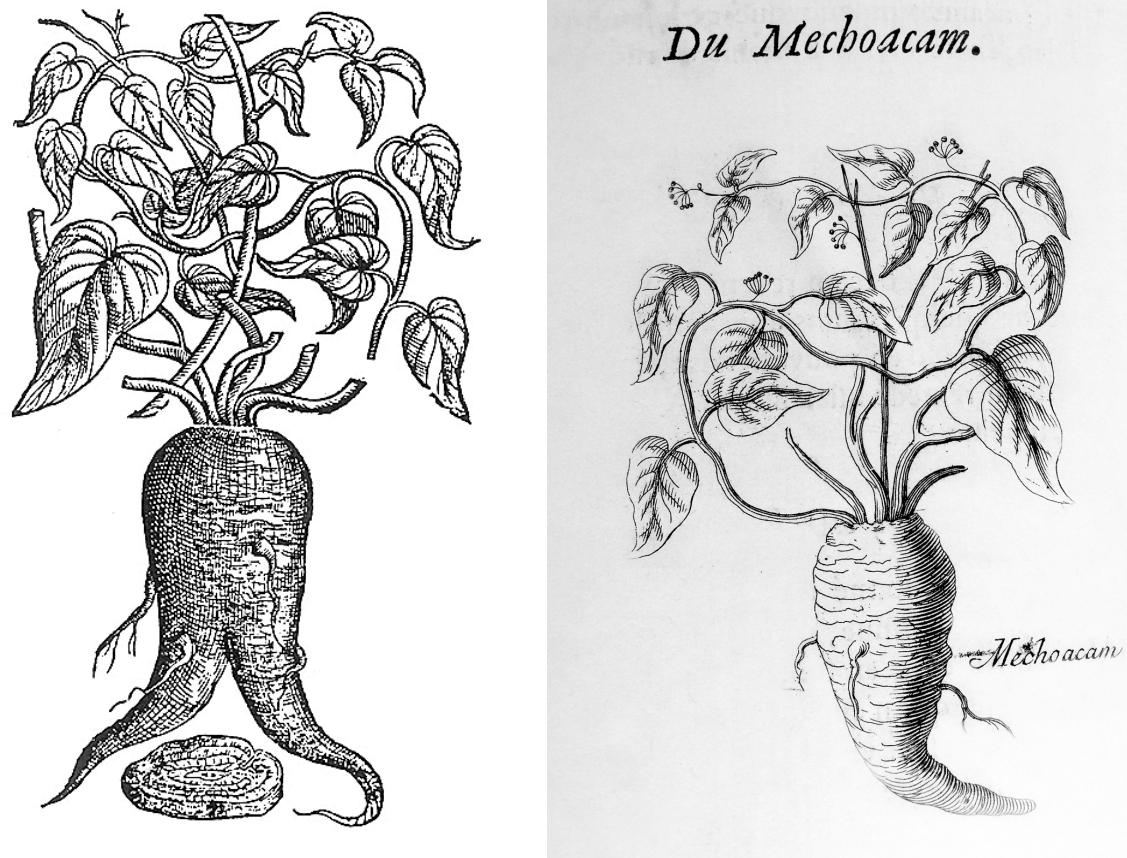
Figure. S2. Illustrations of the root of Michoacan in European herbals. Left: XVI century European woodcut print of the root of Michoacan (*Ipomoea jalapa*) which because of the mildness of its effects became popular in herbal medicine as a New World substitute for the drastic purgative scammony (From Gerald's *Herbal*. London. J. Norton, 1597). Right: The root of Michoacan (Mechoacam) is described among the Brazilian medicinal plants by the French naturalist Pierre Pomet in his work *Histoire Générale des Drogues, Traitant de Plantes, des Animaux, & des Mineraux* (1694). In the Descriptive Collection of Plants from Ceará (*Coleção Descritiva das Plantas da Capitania do Ceará*) published by J. S. Feijó in 1799, the use of jalap root is indicated by the vernacular name of michoacam; thus, this reference is one of the oldest on the traditional utilization of "batata de purga" in Northeastern Brazil.

Figure S3. TLC analysis of the peracetylated saponified convolvulin fractions from various commercial Brazilian jalap root crude drugs and powders: **1**, Authentic plant material for *Operculina hamiltonii* collected at Varre-Vento, Oriximiná, Pará, Brazil; **2**, Authentic plant material *Operculina macrocarpa* from the Pharmacognosy Drug Collection Dispensary, UFRJ; **3**, *Operculina hamiltonii* provided by Sobral Pharmaceutical Industry; **4**, Commercialized powder "jalapa" purchased at the Mercado 2000, Santarém, Pará; **5**, *Operculina hamiltonii* collected at Rurópolis, Pará.
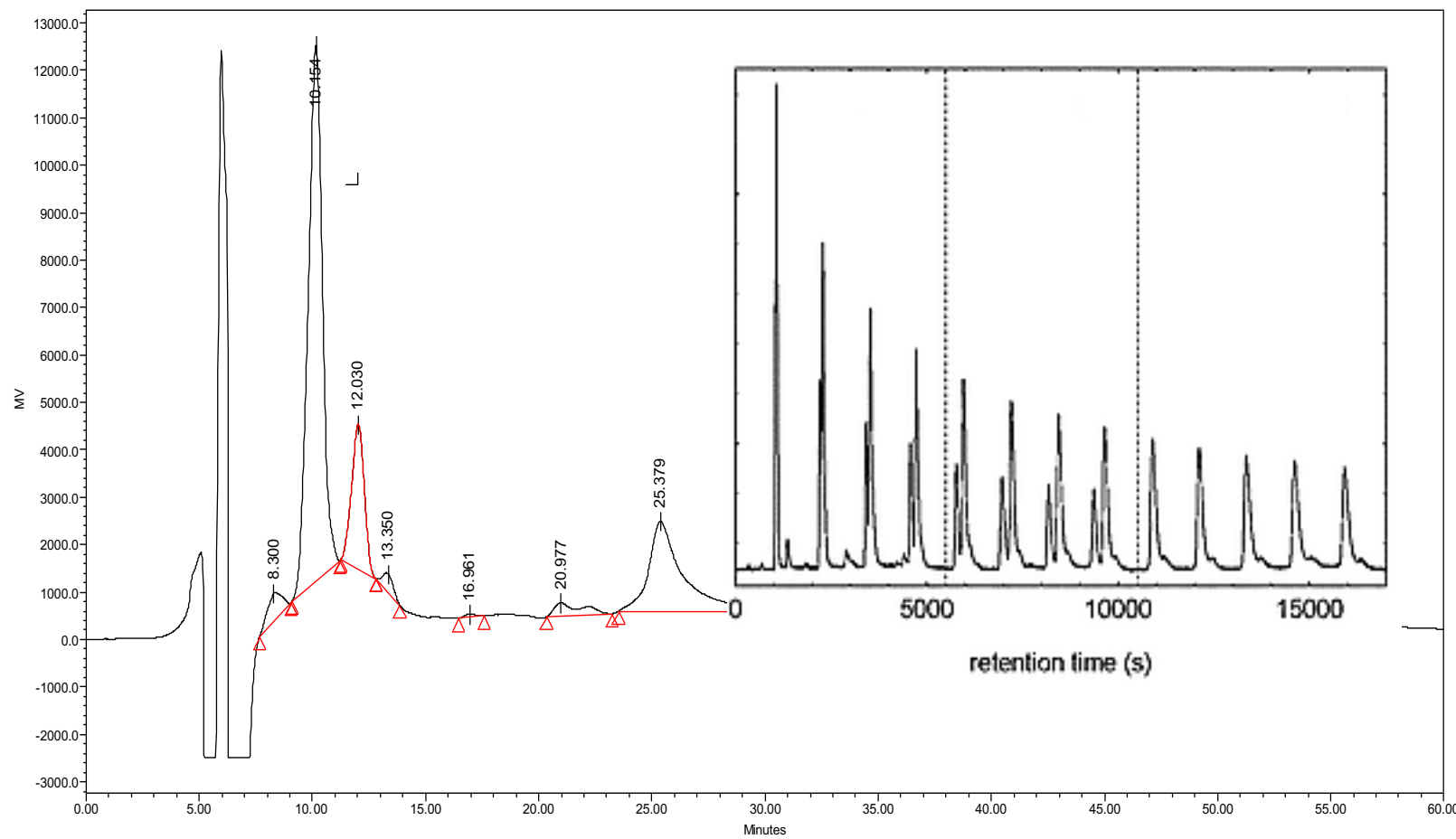
Figure S4. HPLC separation of peracetylated operculinic acids H-M (**6-10**). Colum: Waters SymmetryPrep C_{18} (19 × 300 mm; 7 μm); isocratic elution, $CH_3CN–H_2O$ (9:1); flow rate = 8 mL/min: **12** (t_R = 10.15 min), **14** (t_R = 13.35 min), **15** (t_R = 20.97 min), and **17** (t_R = 25.37 min). The insert illustrates the recycling procedure to achieve total purification of derivatives **13** (after 13 cycles) and **18** (after 8 cycles).
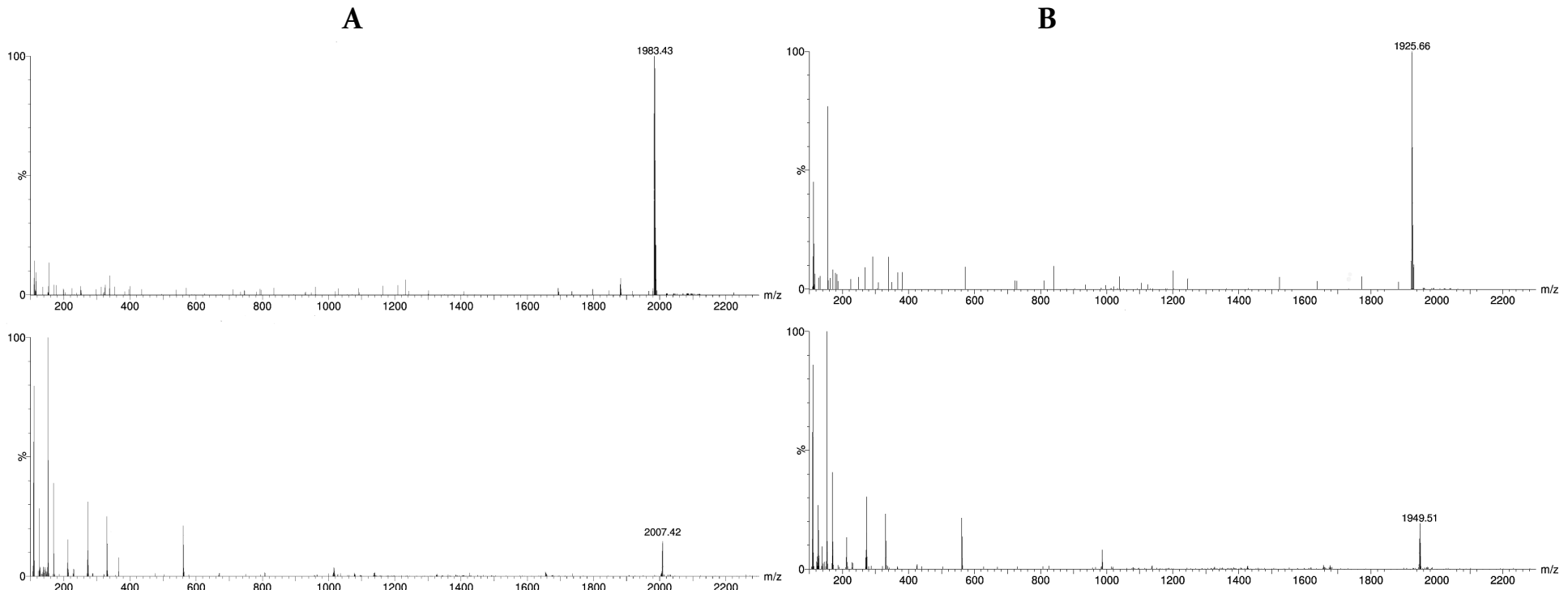
Figure S5. Low resolution electrospray ionization mass spectra for derivatives **12** (**A**: negative mode, *m/z* 1983 [M – H]⁻ and positive mode, *m/z* 2007 [M + Na]⁺) and **13** (**B**: negative mode, *m/z* 1925 [M – H]⁻ and positive mode, *m/z m/z* 1949 [M + Na]⁺).
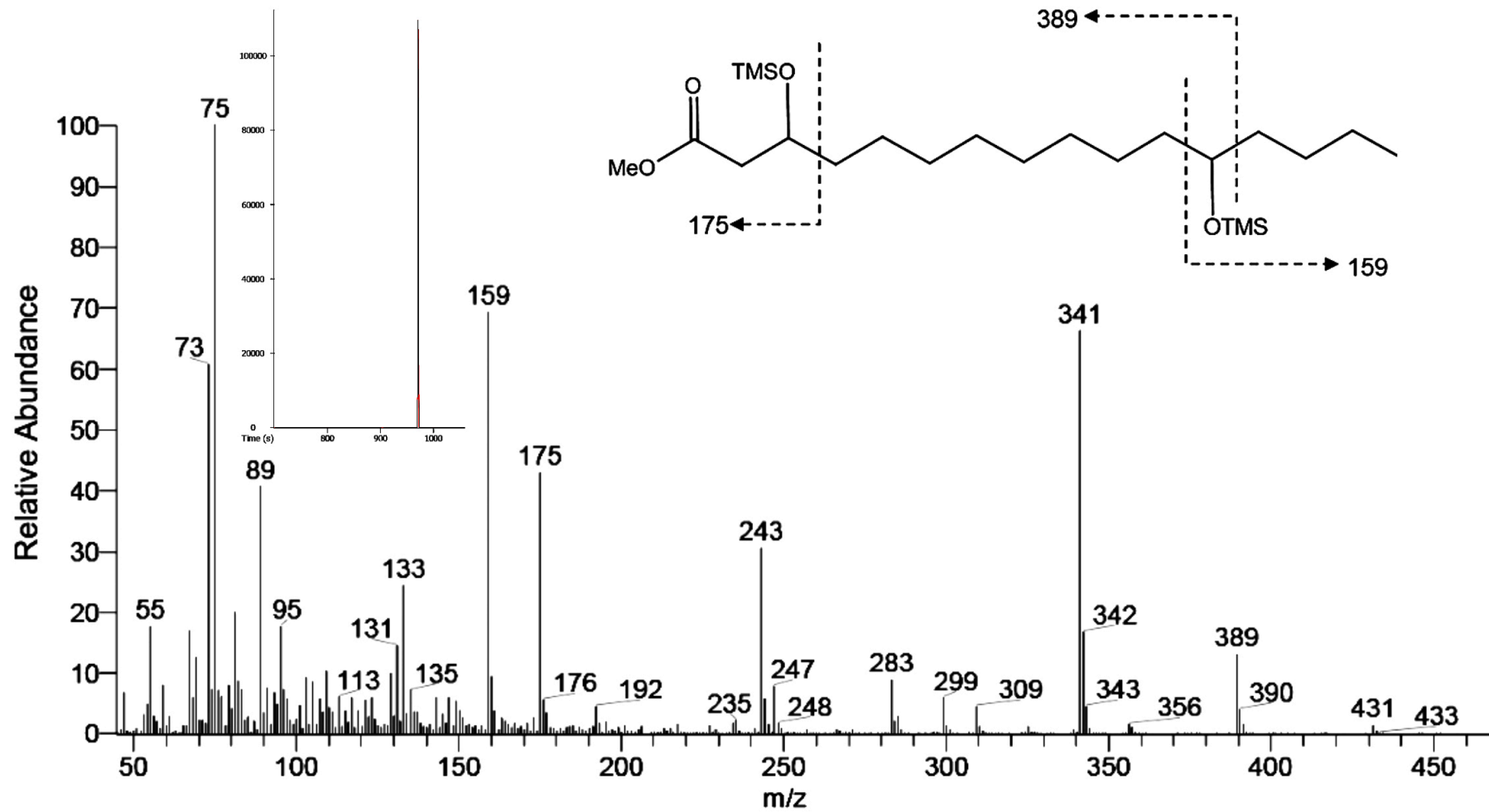
Figure S6. GC-EIMS of silylated aglycone methyl ester liberated from operculinic acid H (**1**); selected ion chromatogram (insert) and fragmentation pattern: 3S,12S-dihydroxyhexadecanoic (operculinolic) acid methyl ester, t_R 16.1 min.
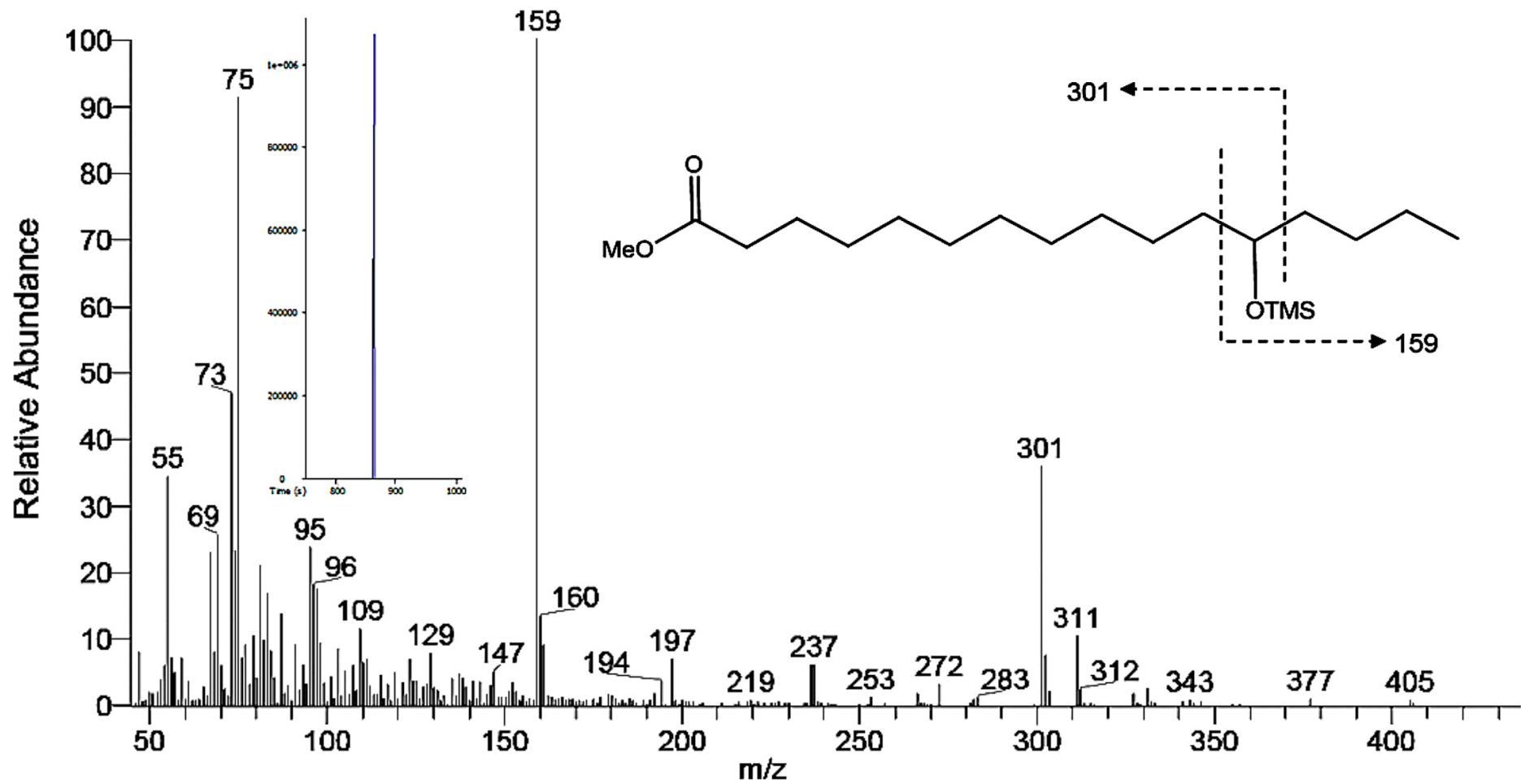
Figure S7. GC-EIMS of silylated aglycone methyl ester liberated from operculinic acid I (**2**); selected ion chromatogram (insert) and fragmentation pattern: 12-hydroxyhexadecanoic acid methyl ester, t_R 14.5 min.
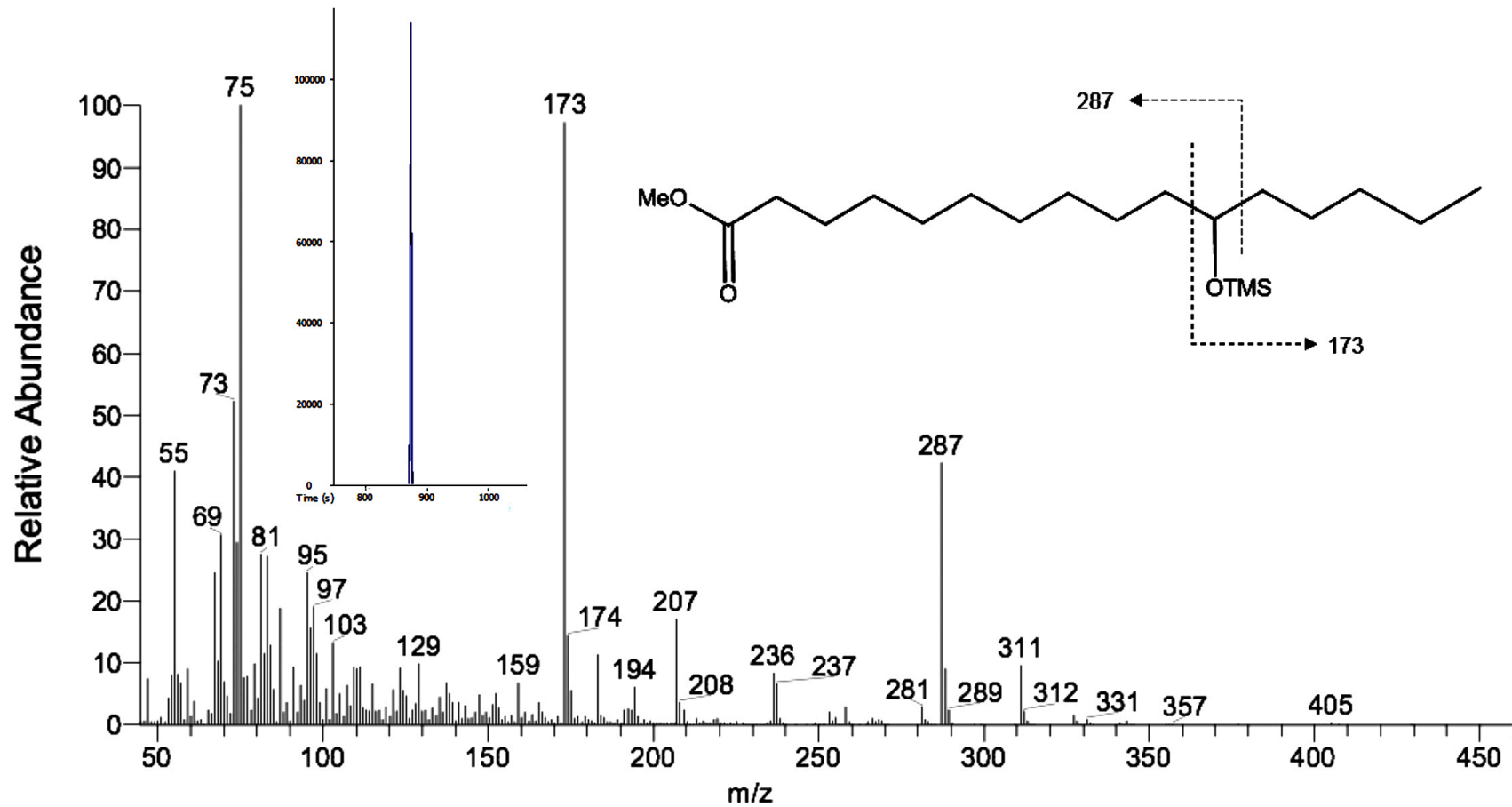
Figure S8. GC-EIMS of silylated aglycone methyl ester liberated from operculinic acid J (**3**); selected ion chromatogram (insert) and fragmentation pattern: 11-hydroxyhexadecanoic acid methyl ester, t_R 14.7 min.
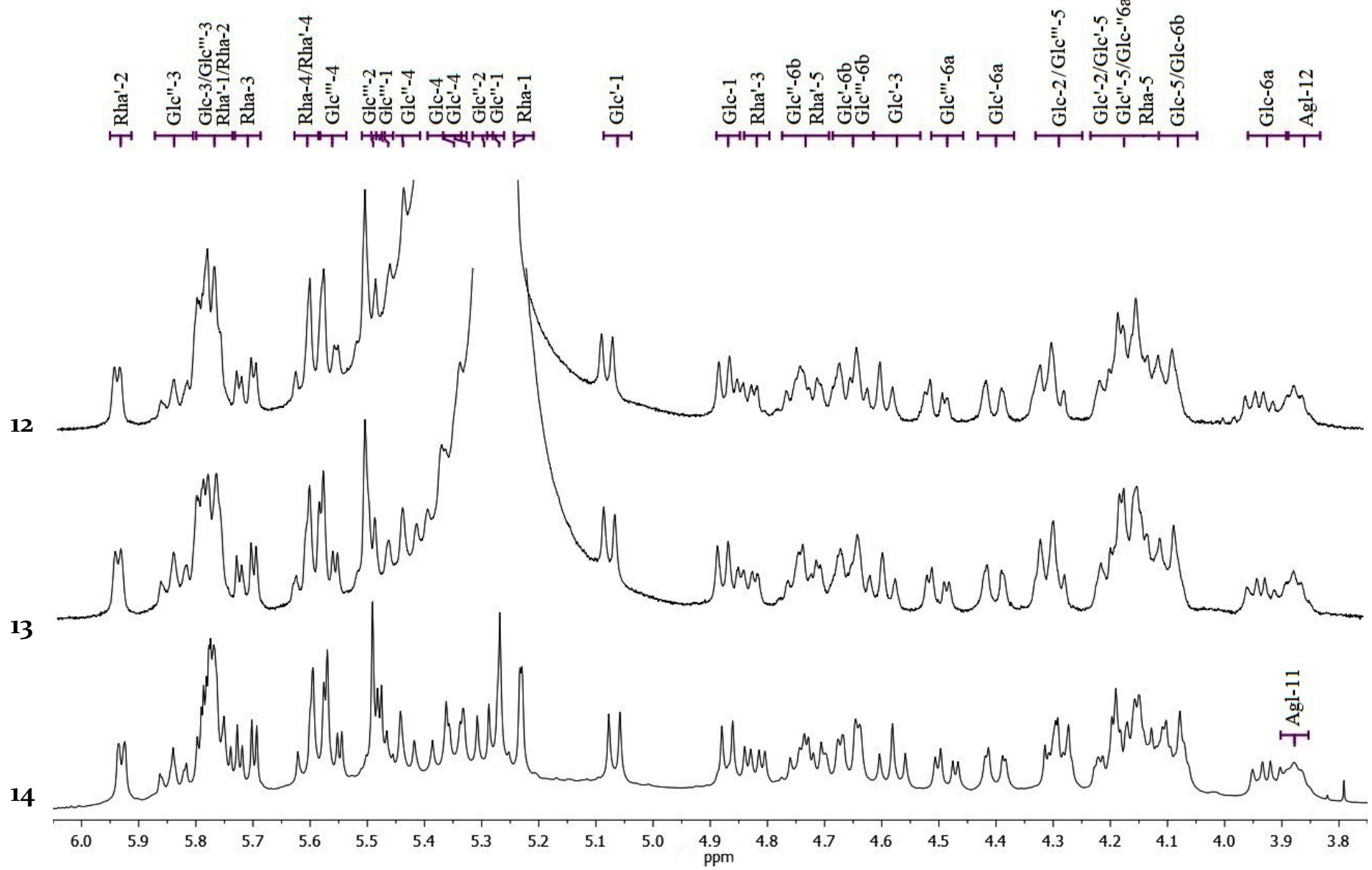
Figure S9. ¹H NMR spectra (500 MHz) of peracetylated derivatives **12-14** in pyridine-d_5 (δ=3.8–6.0).

S16
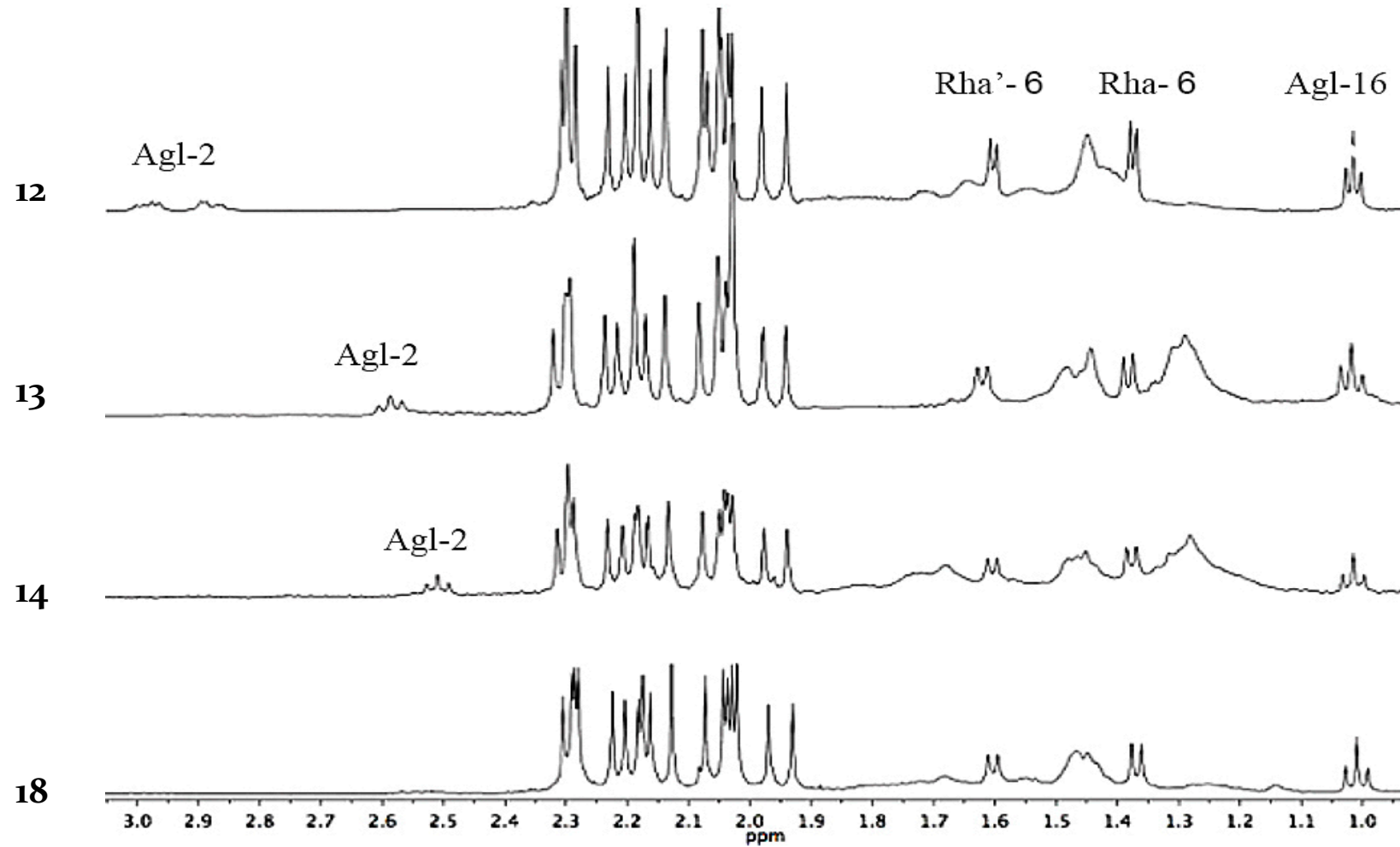
Figure S10. ¹H NMR spectra (δ 0.9-3.1) of peracetylated derivatives **12-14** and **18** in pyridine-d_5.
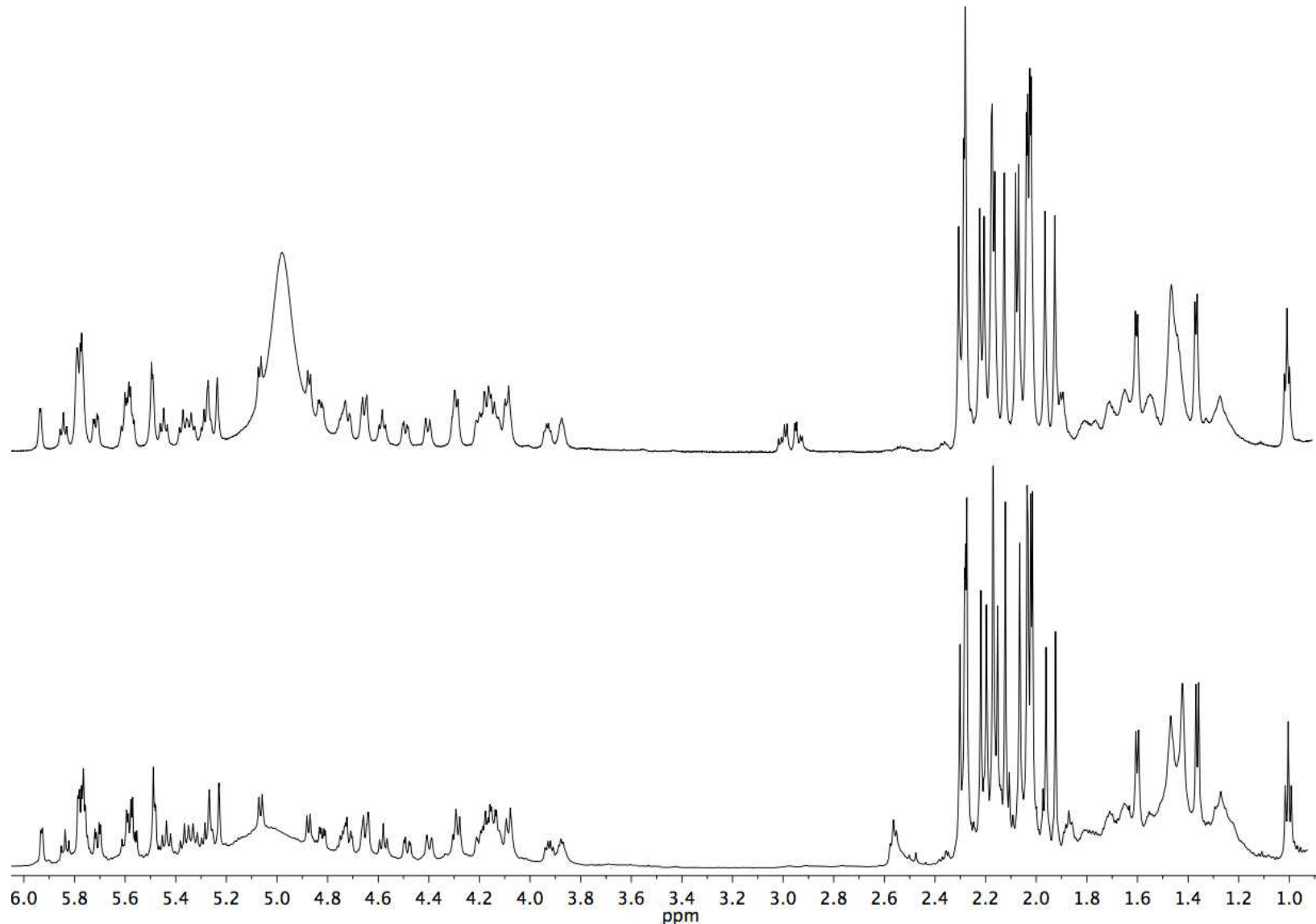
Figure S11. ^{1}H NMR spectra (600 MHz) of peracetylated derivatives **12** and **13** in pyridine-d_5
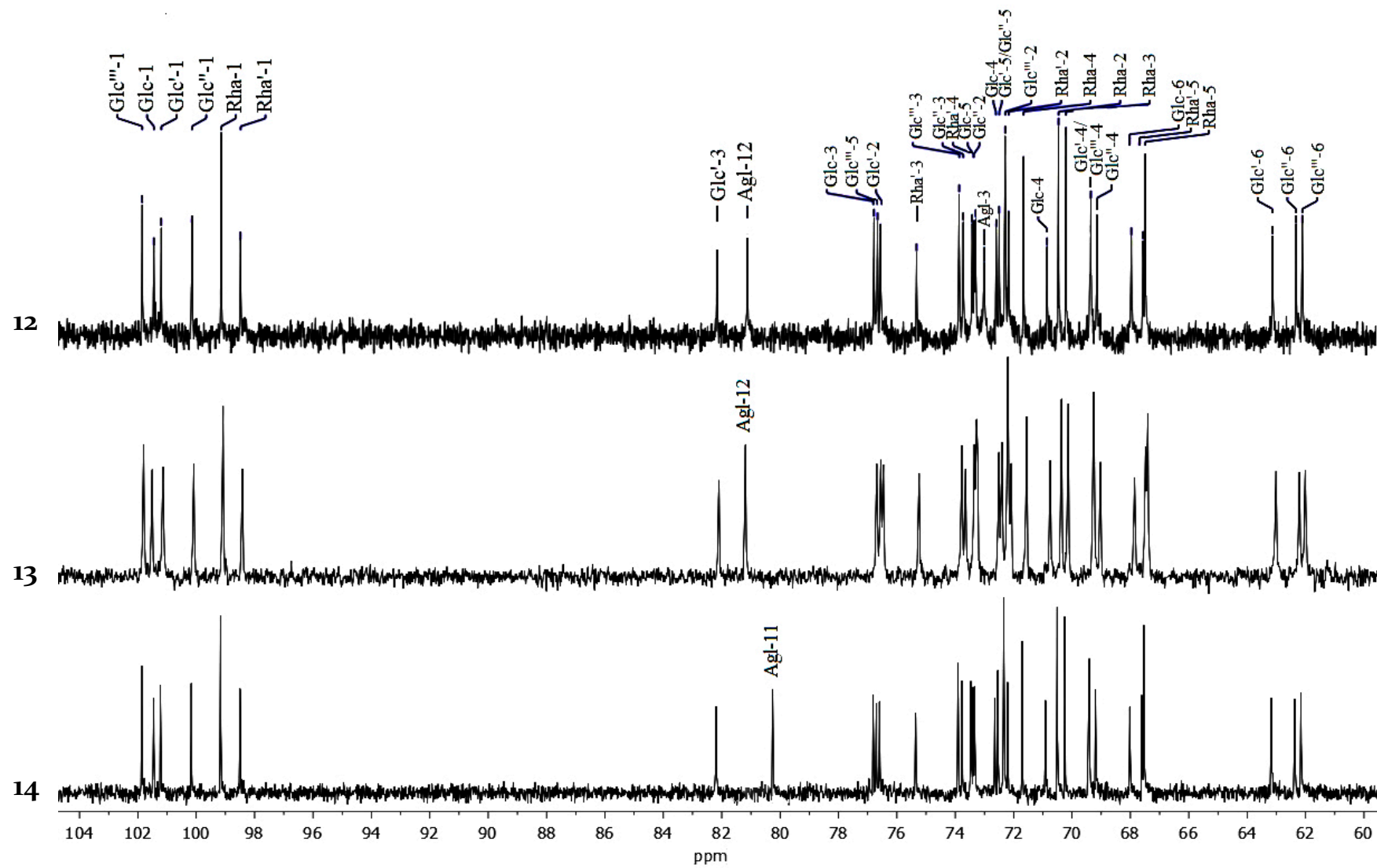
Figure S12. ^{13}C NMR spectra (125 MHz) of peracetylated derivatives **12-14** in pyridine-d_5. Peracetylated operculinic acid H (**12**) displayed an additional signal for the acetyloxyl substituted methine at C-3 (δ_C 72.9) of the aglycone.

S19
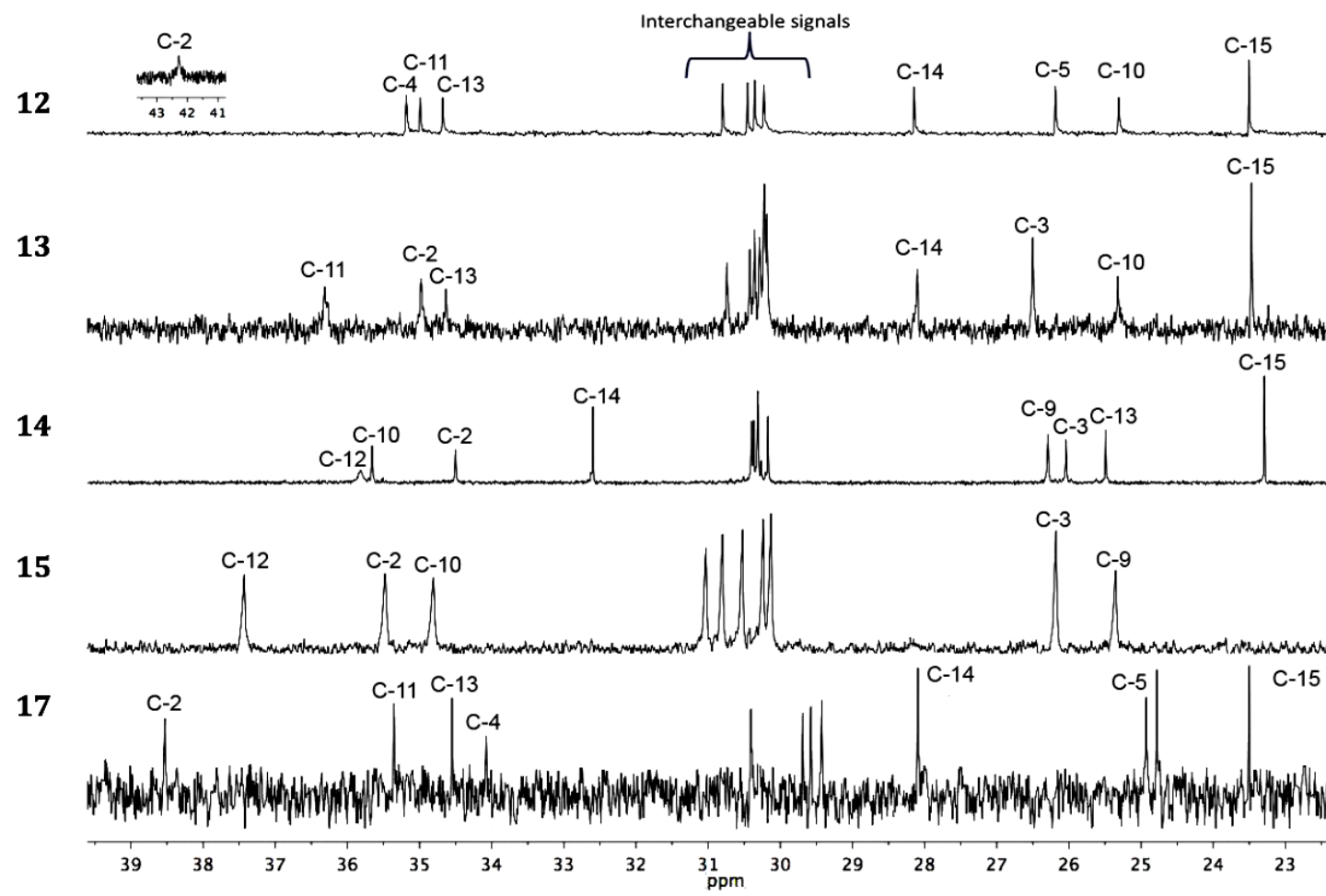
Figure S13. ^{13}C NMR spectra for the aglycone methylenes of derivatives: **12** (3*S*,12*S*-dihydroxyhexadecanoyl moiety), **13** (12*S*-hydroxyhexadecanoyl moiety), **14** (11*S*-hydroxyhexadecanoyl moiety), **15** (11*S*-hydroxytetradecanoyl moiety), and **17** (3*S*,12*S*-dihydroxyhexadecanoyl moiety) in pyridine-d_5.
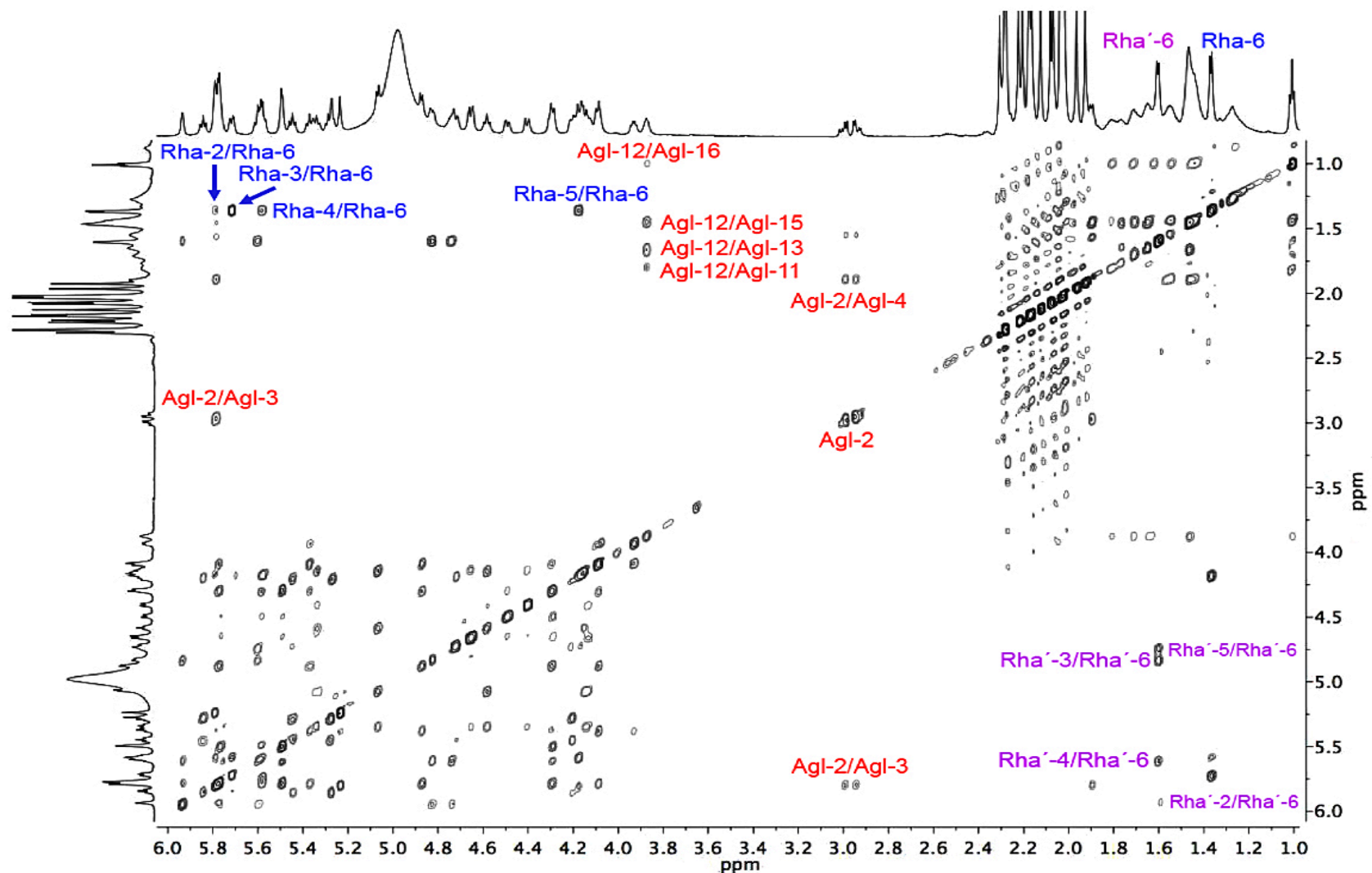
Figure S14. ¹H-Detected homonuclear total correlation (TOCSY) spectrum for the peracetylated derivative of operculinic acid H (**12**) with high resolution 1D projections (700 MHz) in pyridine-d_5.
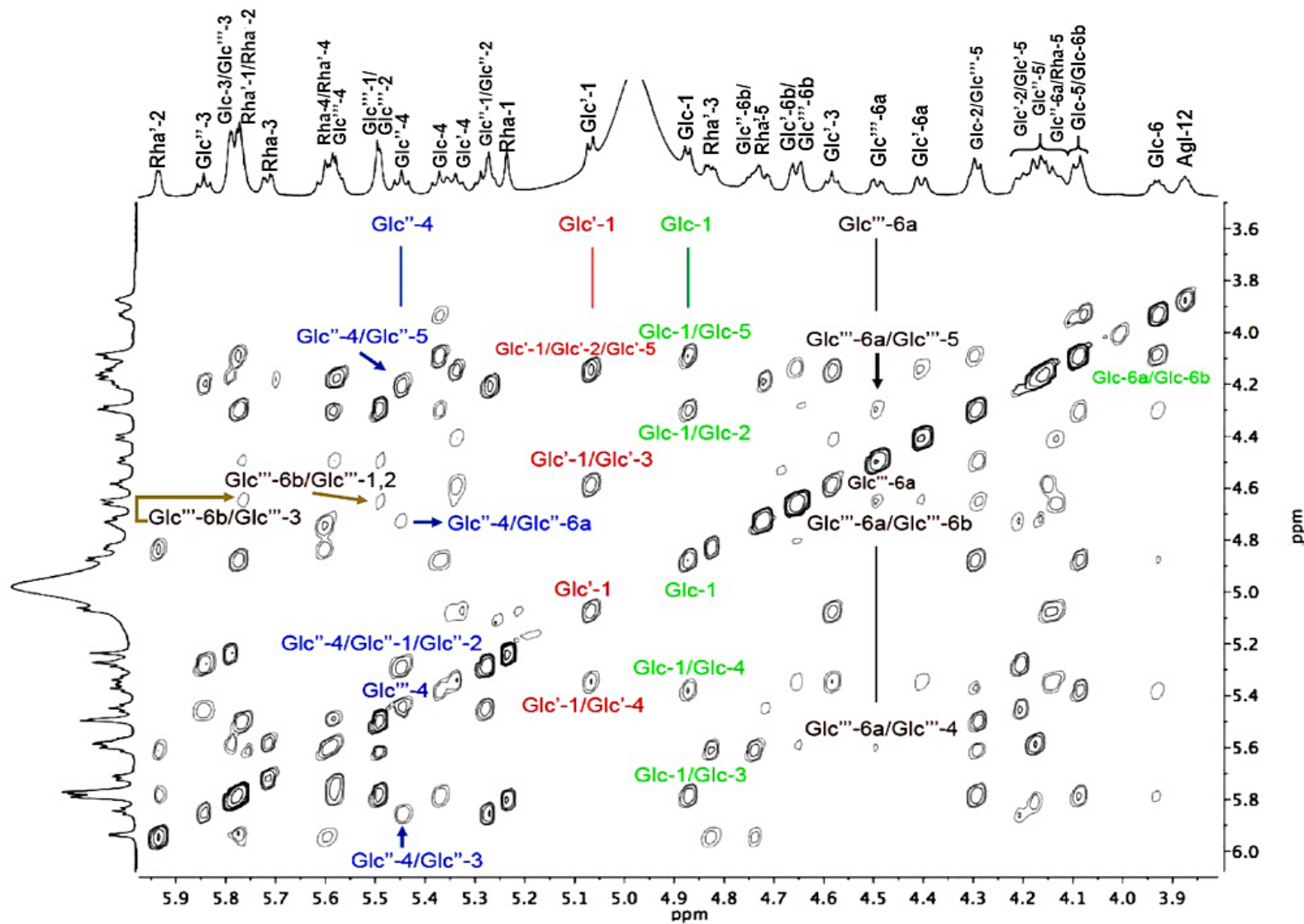
Figure S15. Expanded oligosaccharide core region of the ¹H-detected homonuclear total correlation (TOCSY) spectrum for the peracetylated derivative of operculinic acid H (**12**) with high resolution 1D projections (700 MHz) in pyridine-d_5.
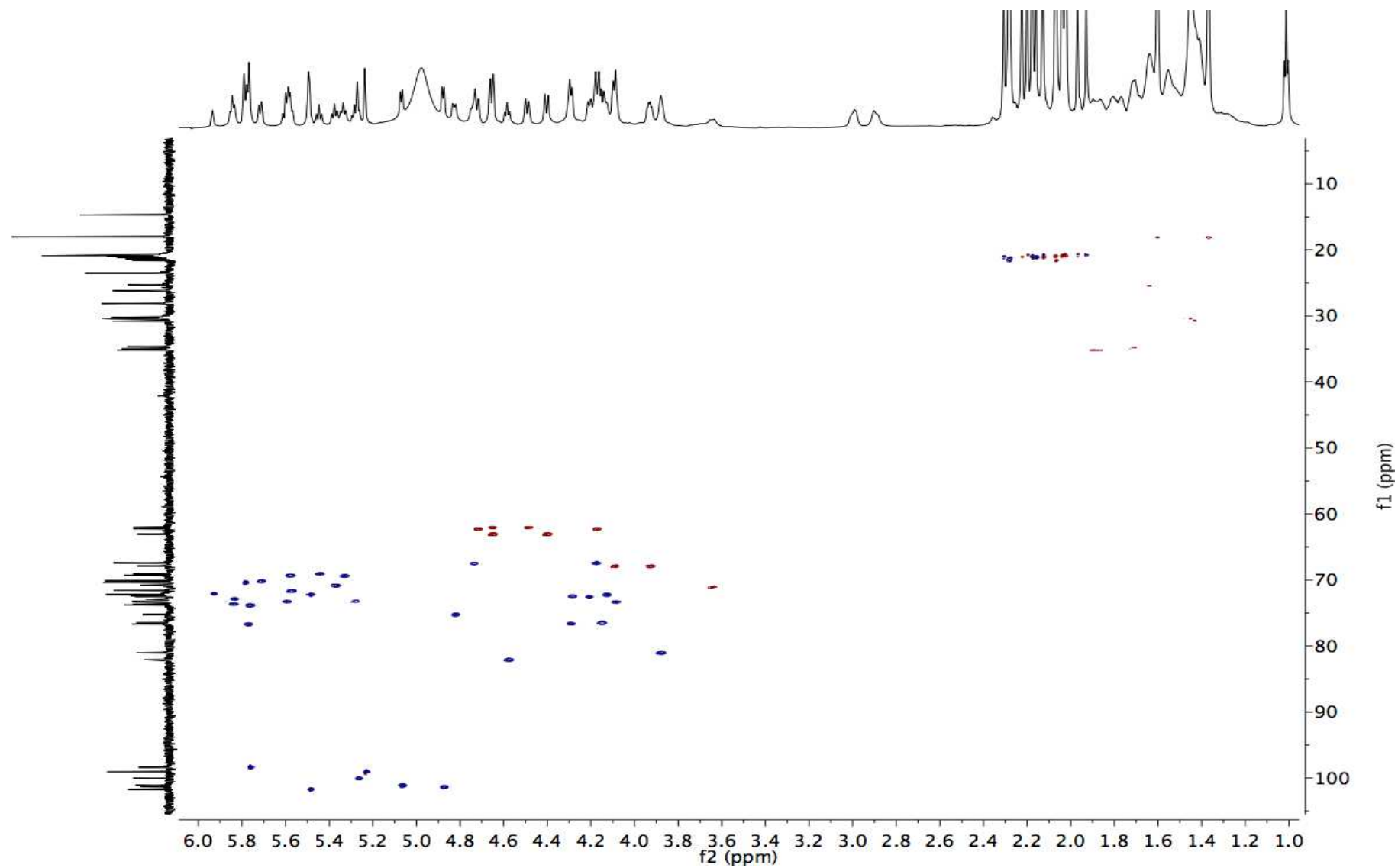
Figure S16. ^{1}H-Detected heteronuclear ($^1J_{CH}$) correlation (HSQC) spectrum for the peracetylated derivative of operculinic acid H (**12**) with high resolution 1D ^{1}H projection (700 MHz) and ^{13}C (175 MHz) projections in pyridine-d_5.
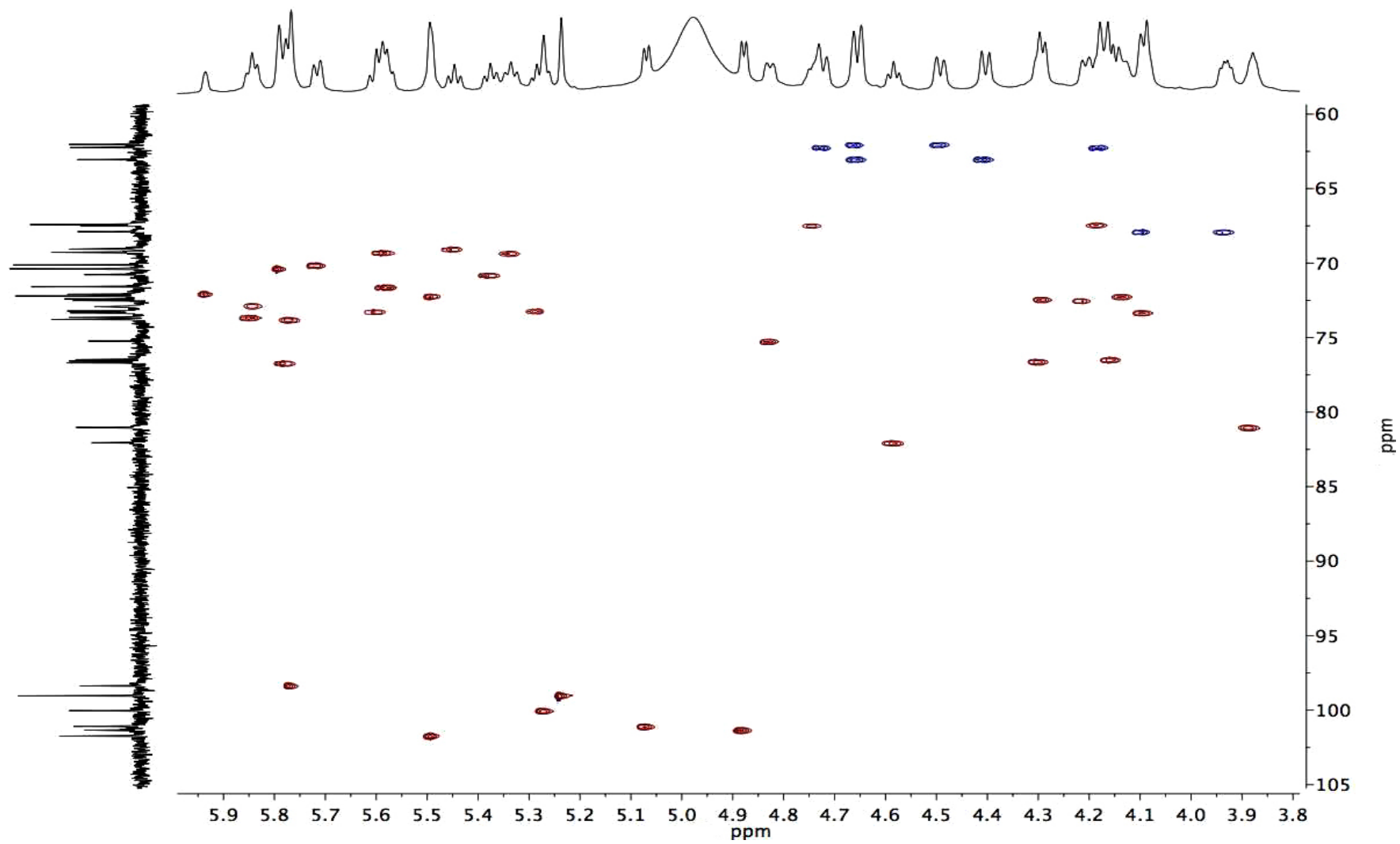
Figure S17. Expanded oligosaccharide core region of the ¹H-Detected heteronuclear ($^1J_{CH}$) correlation (HSQC) spectrum for the peracetylated derivative of operculinic acid H (**12**) with high resolution 1D ¹H projection (700 MHz) and ¹³C (175 MHz) projections in pyridine-d_5. See Figure S18 for cross-peak assignments.
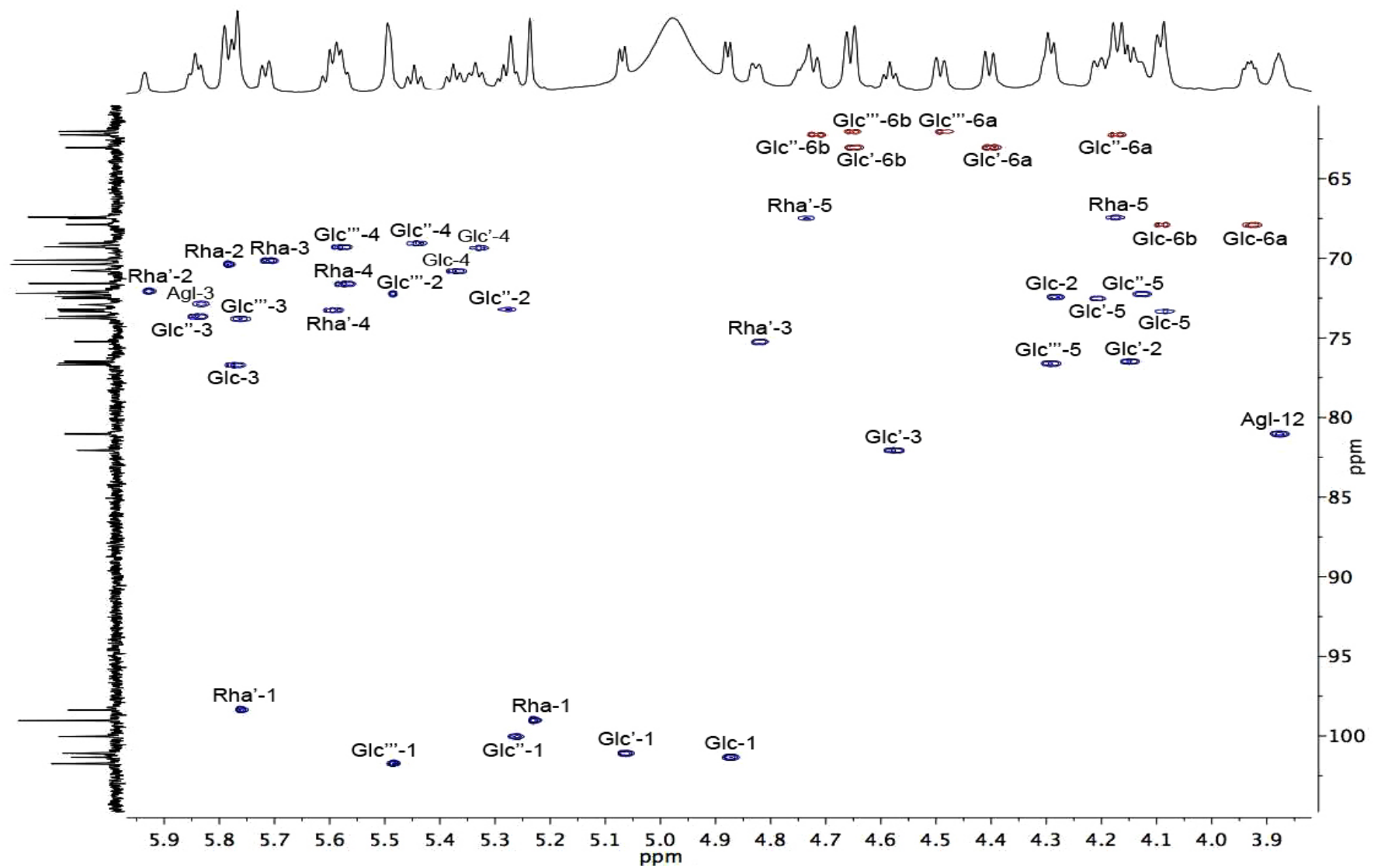
Figure S18. Assigned expanded oligosaccharide core region of the ^{1}H-Detected heteronuclear ($^{1}J_{CH}$) correlation (HSQC) spectrum for the peracetylated derivative of operculinic acid H (**12**) with high resolution 1D ^{1}H projection (700 MHz) and ^{13}C (175 MHz) projections in pyridine-d_5.
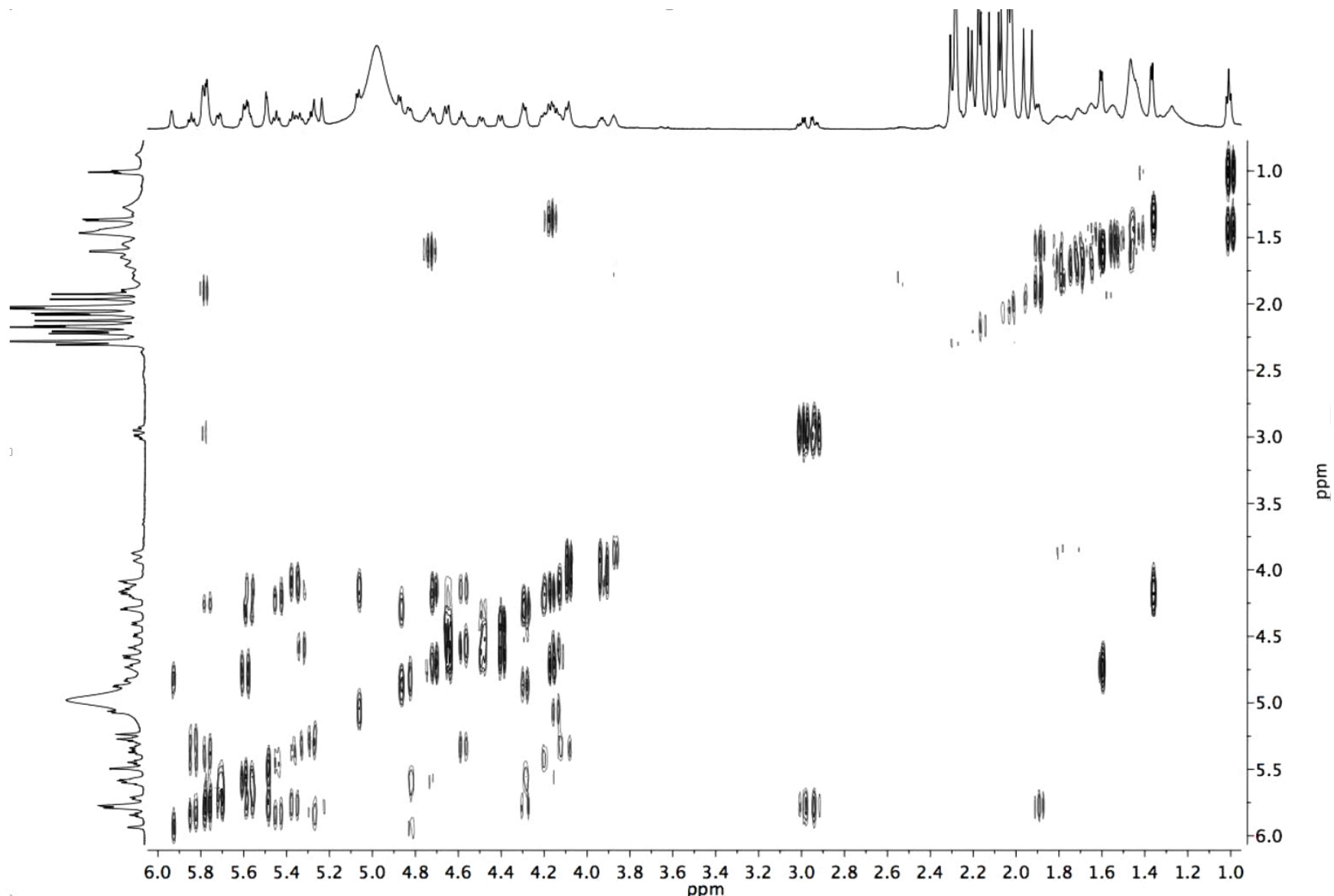
Figure S19. ¹H-Detected homonuclear ($^3J_{HH}$) correlation (COSY) spectrum for the peracetylated derivative of operculinic acid H (**12**) with high resolution 1D projections (700 MHz) in pyridine-d_5.

S26
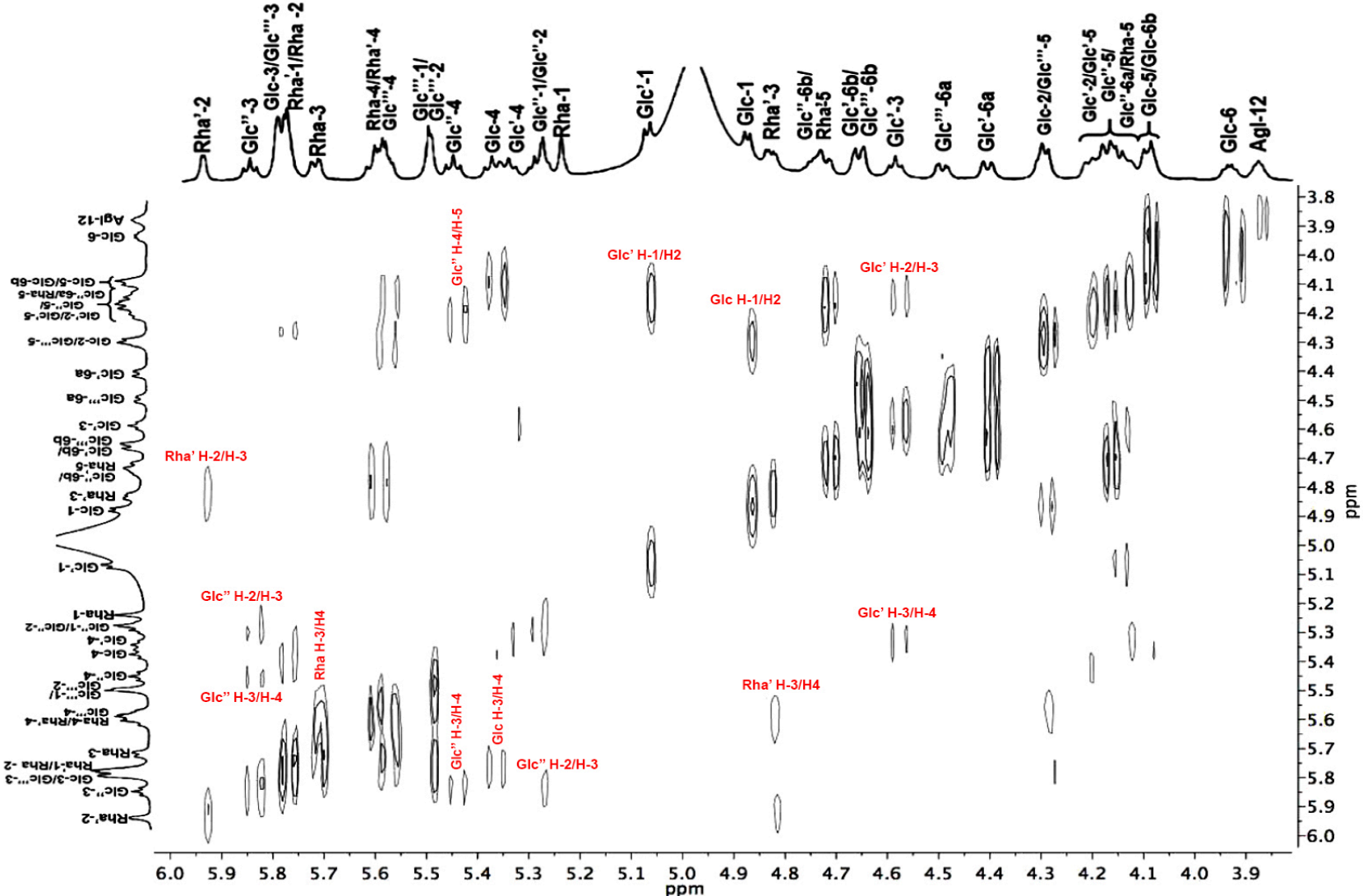
Figure S20. Expanded oligosaccharide core region of the ¹H-detected homonuclear ($^{3}J_{HH}$) correlation (COSY) spectrum for the peracetylated derivative of operculinic acid H (**12**) with high resolution 1D projections (700 MHz) in pyridine-d_5.
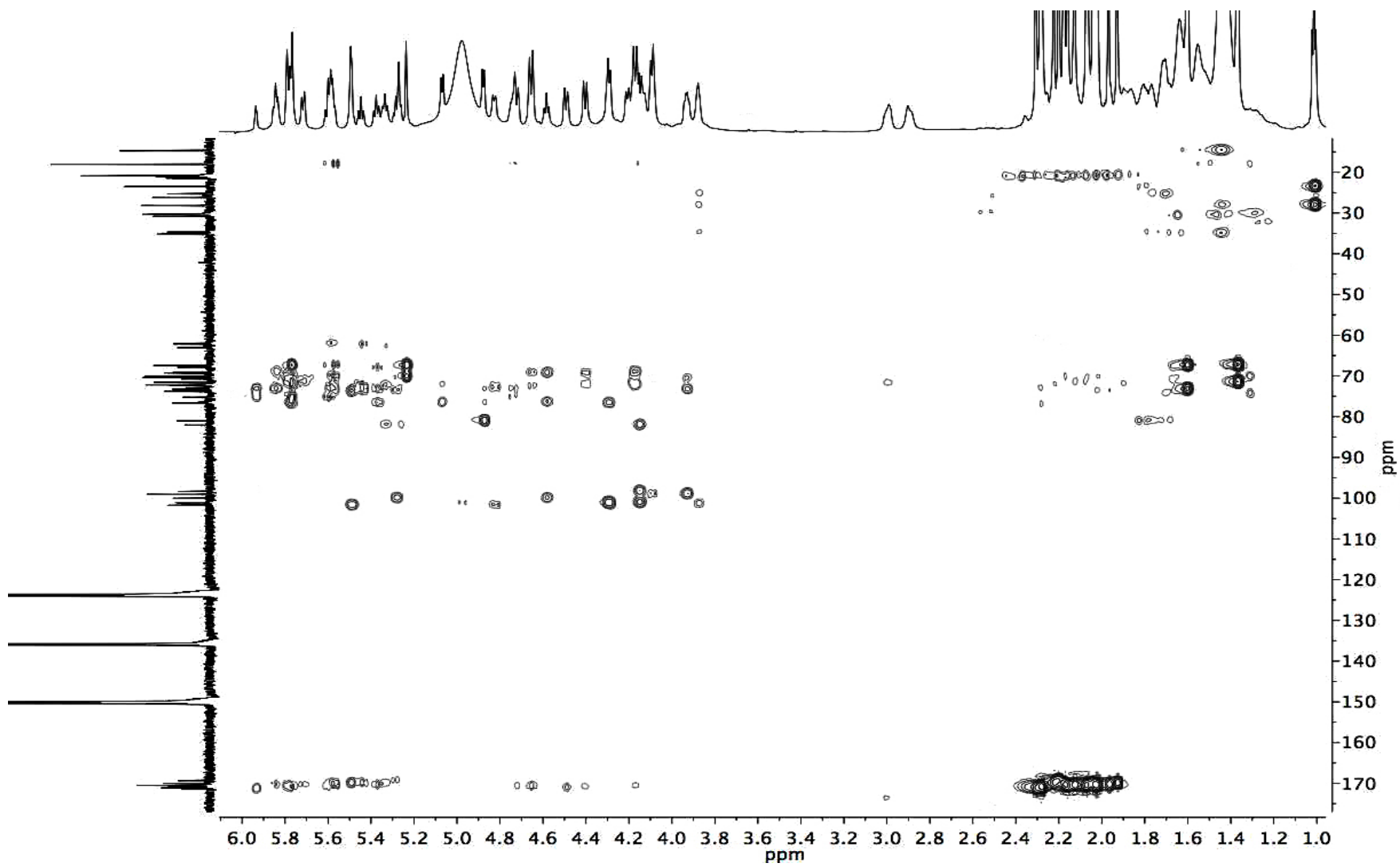
Figure S21. [1]H-detected heteronuclear ($^{2,3}J_{CH}$) correlation (HMBC) spectrum for the peracetylated operculinic acid H (**12**) with high-resolution 1D [1]H (700 MHz) and [13]C (175 MHz) projections in pyridine-d_5.
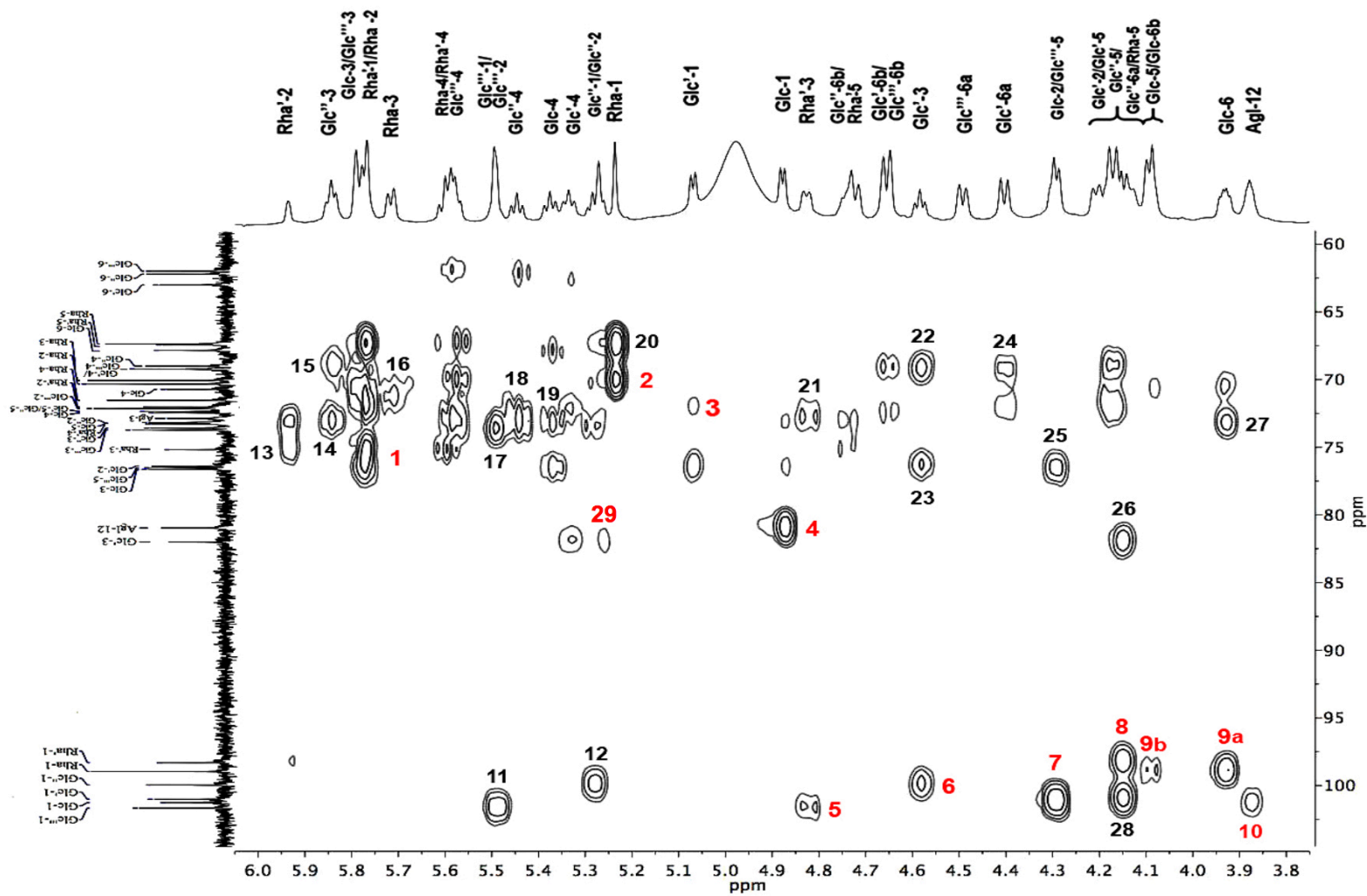
**Figure S22.** ^{1}H-detected heteronuclear ($^{2,3}J_{CH}$) correlation (HMBC) spectrum for the peracetylated operculinic acid H (**12**) with high-resolution 1D ^{1}H (700 MHz) and ^{13}C (175 MHz) projections in pyridine-d_5. Connectivity assignments for the glycosylation sequence ($^3J_{CH}$): **1**, H$_1$-Rha'/C$_2$-Glc'; **2**, C$_6$-Glc/H$_1$-Rha; **3**, H$_1$-Glc'/C$_2$-Glc; **4**, H$_1$-Glc/C$_{12}$-Agl; **5**, H$_3$-Rha'/C$_1$-Glc'''; **6**, C$_1$-Glc''/H$_3$-Glc'; **7**, C$_1$-Glc'/H$_2$-Glc; **8**, C$_1$-Rha'/H$_2$-Glc'; **9**, H$_6$-Glc/C$_1$-Rha; **10**, H$_{12}$-Agl/C$_1$-Glc, **29**, C$_3$-Glc'/ H$_1$-Glc''; Additional cross-peaks, $^2J_{CH}$: **11**, C$_1$-Glc'''/H$_2$-Glc'''; **12**, C$_1$-Glc''/H$_2$-Glc''; **13**, H$_2$-Rha'/C$_3$-Rha'; **14**, C$_2$-Glc''/H$_3$-Glc''; **15**, C$_4$-Glc''/H$_3$-Glc''; **16**, H$_3$-Rha/ C$_4$-Rha; **17**, H$_2$-Glc'''/C$_3$-Glc'''; **18**, C$_3$-Glc''/H$_4$-Glc''; **19**, H$_4$-Glc/C$_3$-Glc; **20**, H$_1$-Rha/C$_5$-Rha; **21**, H$_3$-Rha'/C$_4$-Rha'; **22**, H$_3$-Glc'/C$_4$-Glc'; **23**, H$_3$-Glc'/C$_2$-Glc'; **24**, H$_{6a}$-Glc'/C$_5$-Glc'; **25**, H$_2$-Glc/C$_3$-Glc; **26**, H$_2$-Glc'/C$_3$-Glc'; **27**, H$_6$-Glc/C$_5$-Glc; **28**, H$_2$-Glc'/C$_1$-Glc'.

S29

Formula: $[C_{86}H_{126}O_{48}Na]^+$
Exact mass: 1949.73107
Accurate mass: 1949.72595
Mass accuracy: −2.6 ppm
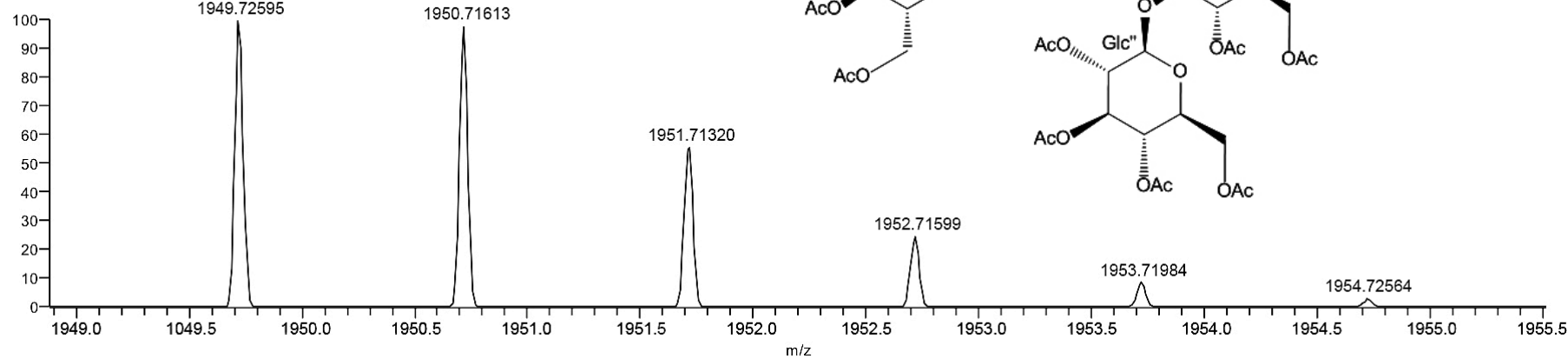
Figure S23. High-resolution positive ion mode ESI mass spectrum of peracetylated operculinic acid I (**13**) showing isotopic distribution and relative abundances of the sodium adduct ion $[C_{86}H_{126}O_{48}Na]^+$.
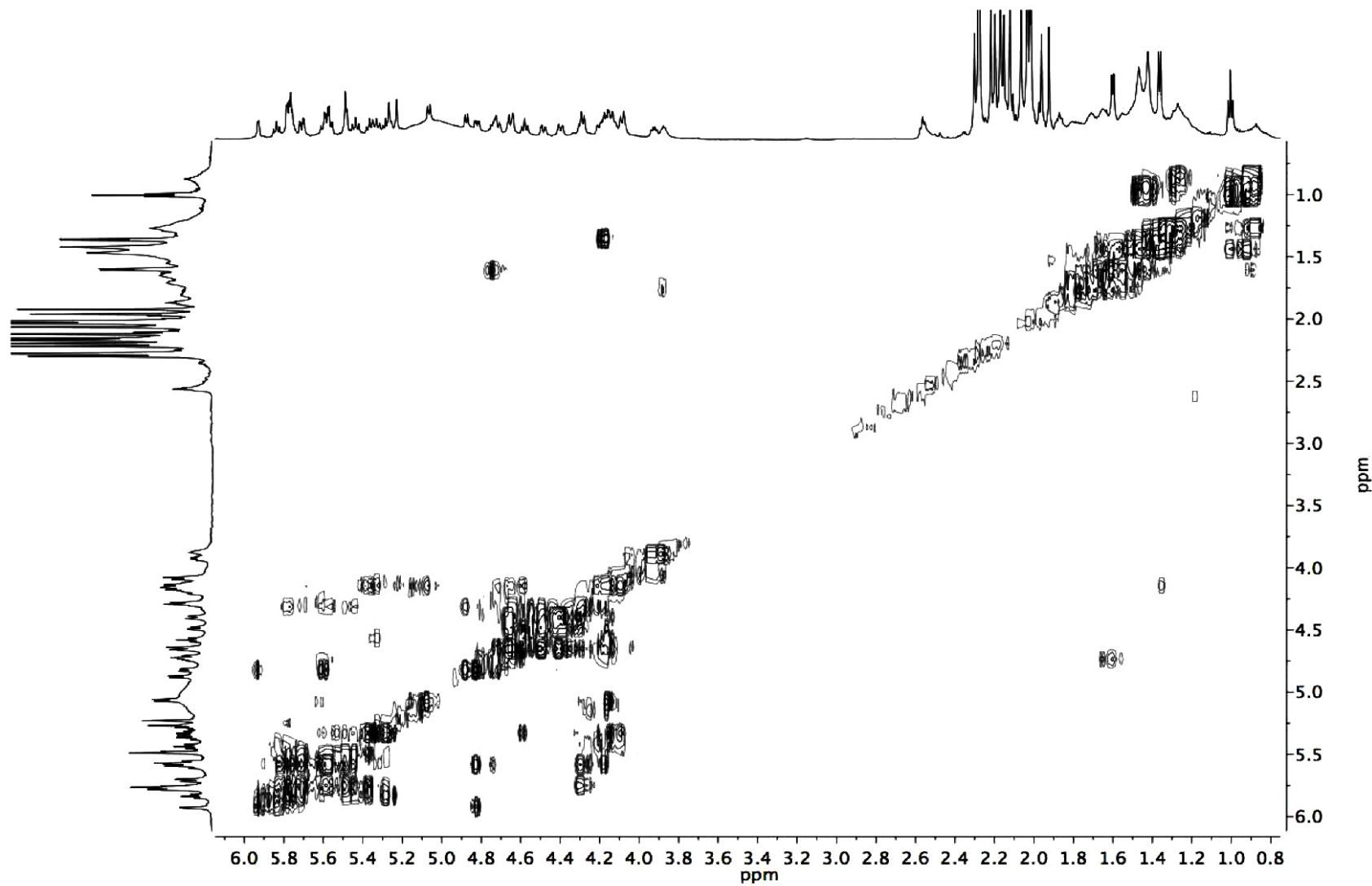
Figure S24. ^{1}H-Detected homonuclear ($^3J_{HH}$) correlation (COSY) spectrum for the peracetylated derivative of operculinic acid I (**13**) with high resolution 1D projections (600 MHz) in pyridine-d_5.
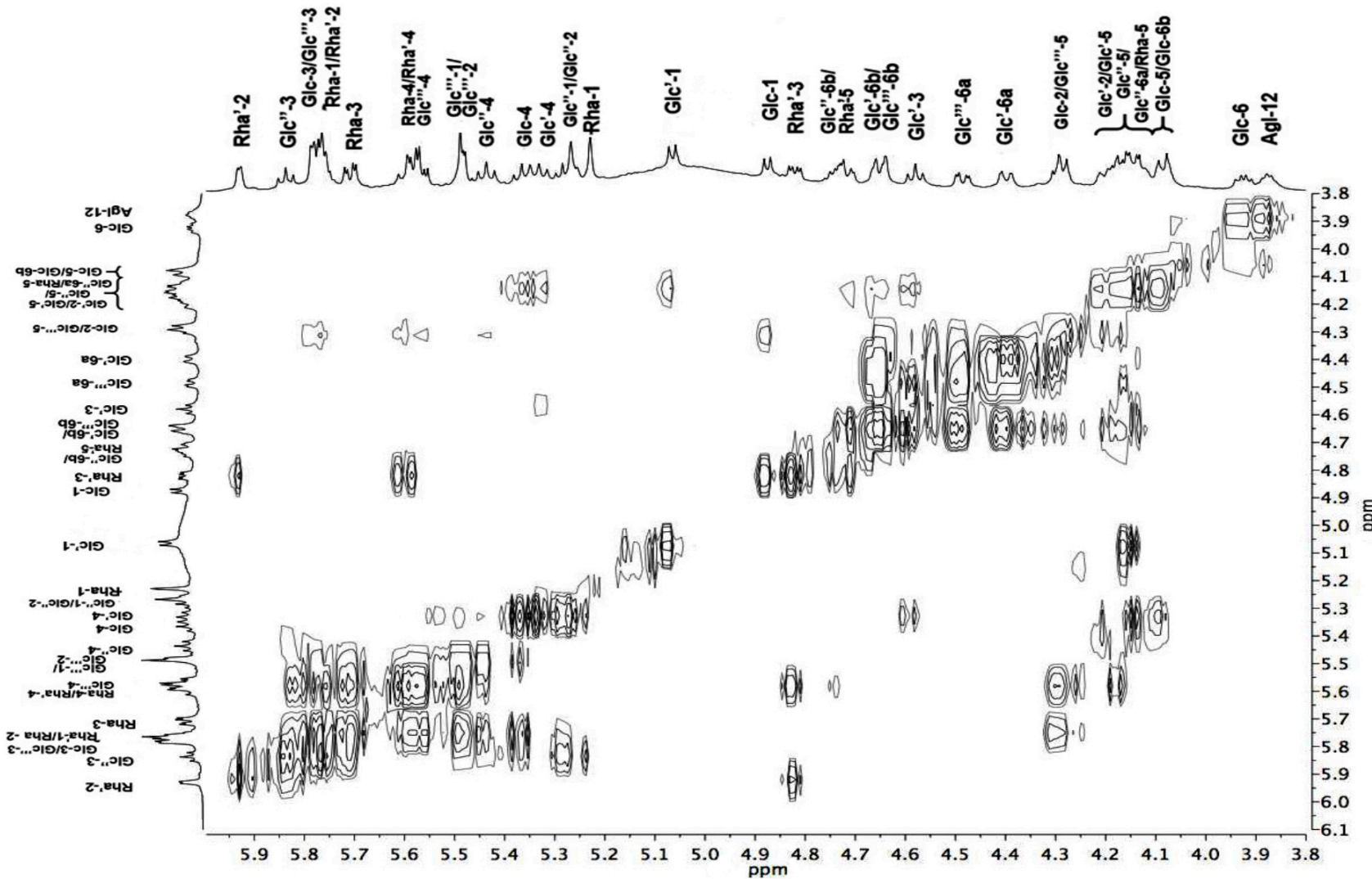
Figure S25. Expanded oligosaccharide core region of the ¹H-detected homonuclear ($^3J_{HH}$) correlation (COSY) spectrum for the peracetylated derivative of operculinic acid I (**13**) with high resolution 1D projections (600 MHz) in pyridine-d_5. See Figure S20 for cross-peak assignments.
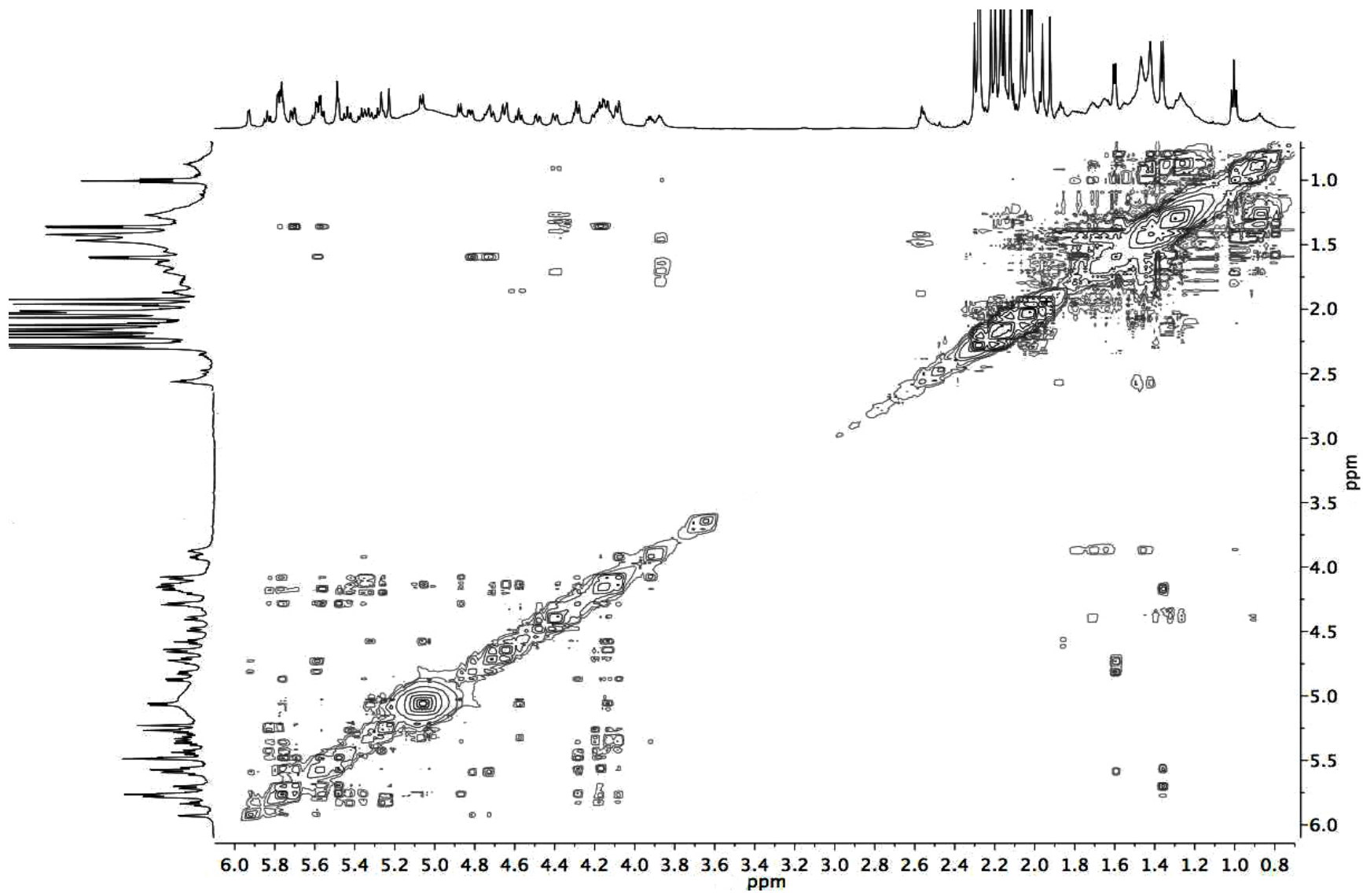
Figure S26. ^{1}H-Detected homonuclear total correlation (TOCSY) spectrum for the peracetylated derivative of operculinic acid I (**13**) with high resolution 1D projections (600 MHz) in pyridine-d_5.

S33
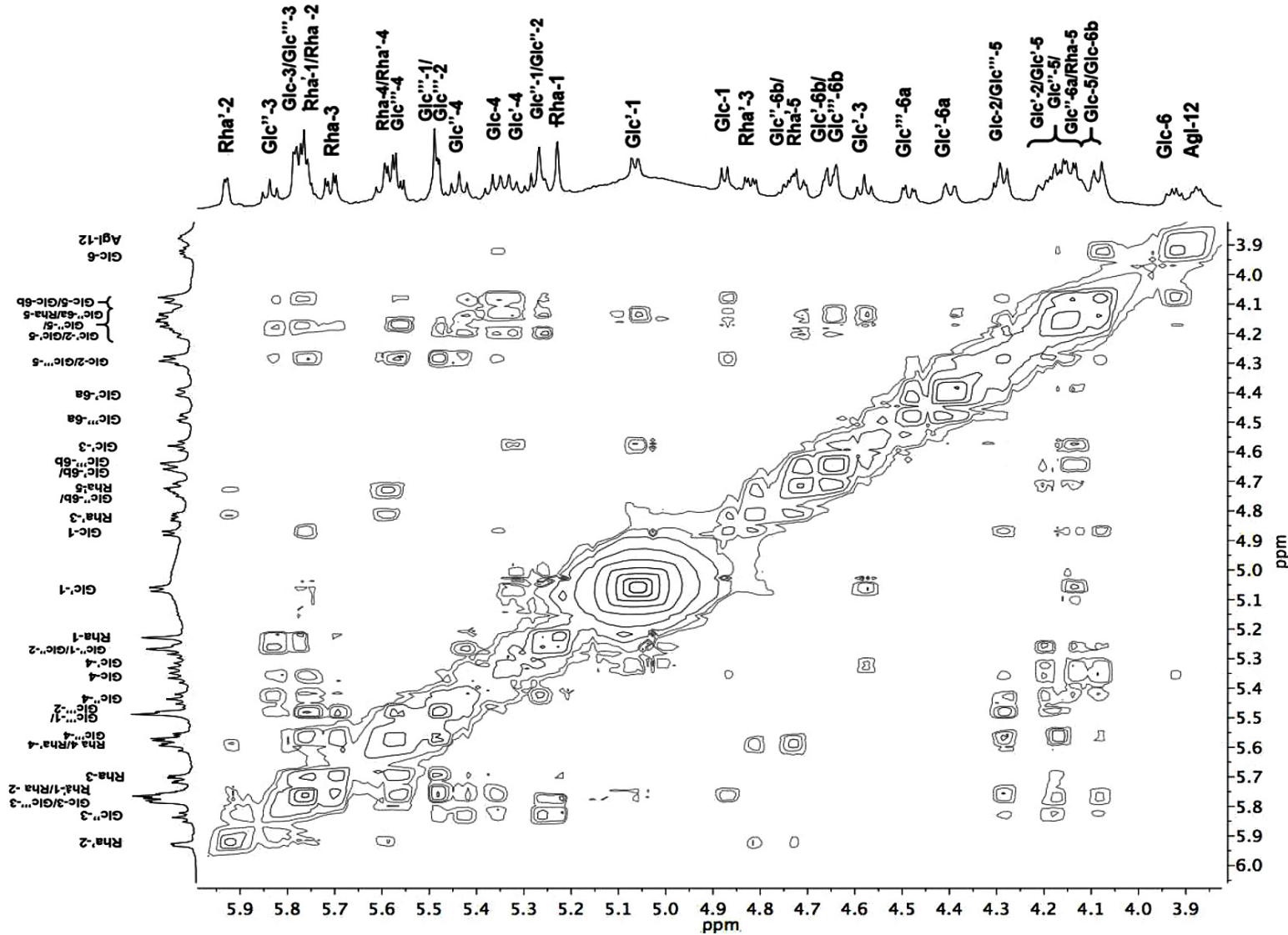
Figure S27. Expanded oligosaccharide core region of the ¹H-detected homonuclear total correlation (TOCSY) spectrum for the peracetylated derivative of operculinic acid I (**13**) with high resolution 1D projections (600 MHz) in pyridine-d_5. See Figure S15 for cross-peak assignments.
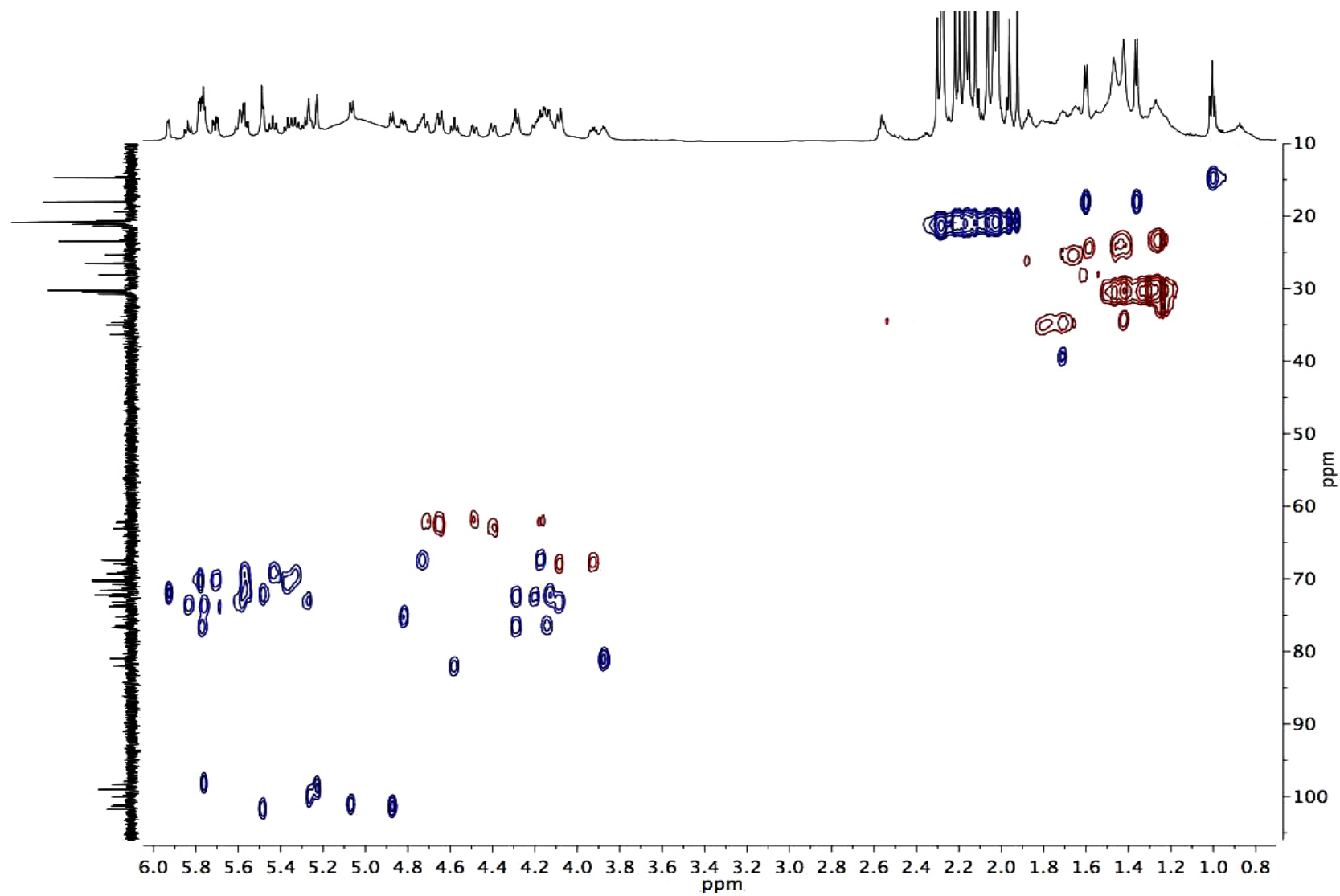
Figure S28. ^{1}H-Detected heteronuclear ($^1J_{CH}$) correlation (HSQC) spectrum for the peracetylated derivative of operculinic acid I (**13**) with high resolution 1D ^{1}H projection (600 MHz) and ^{13}C (150 MHz) projections in pyridine-d_5.
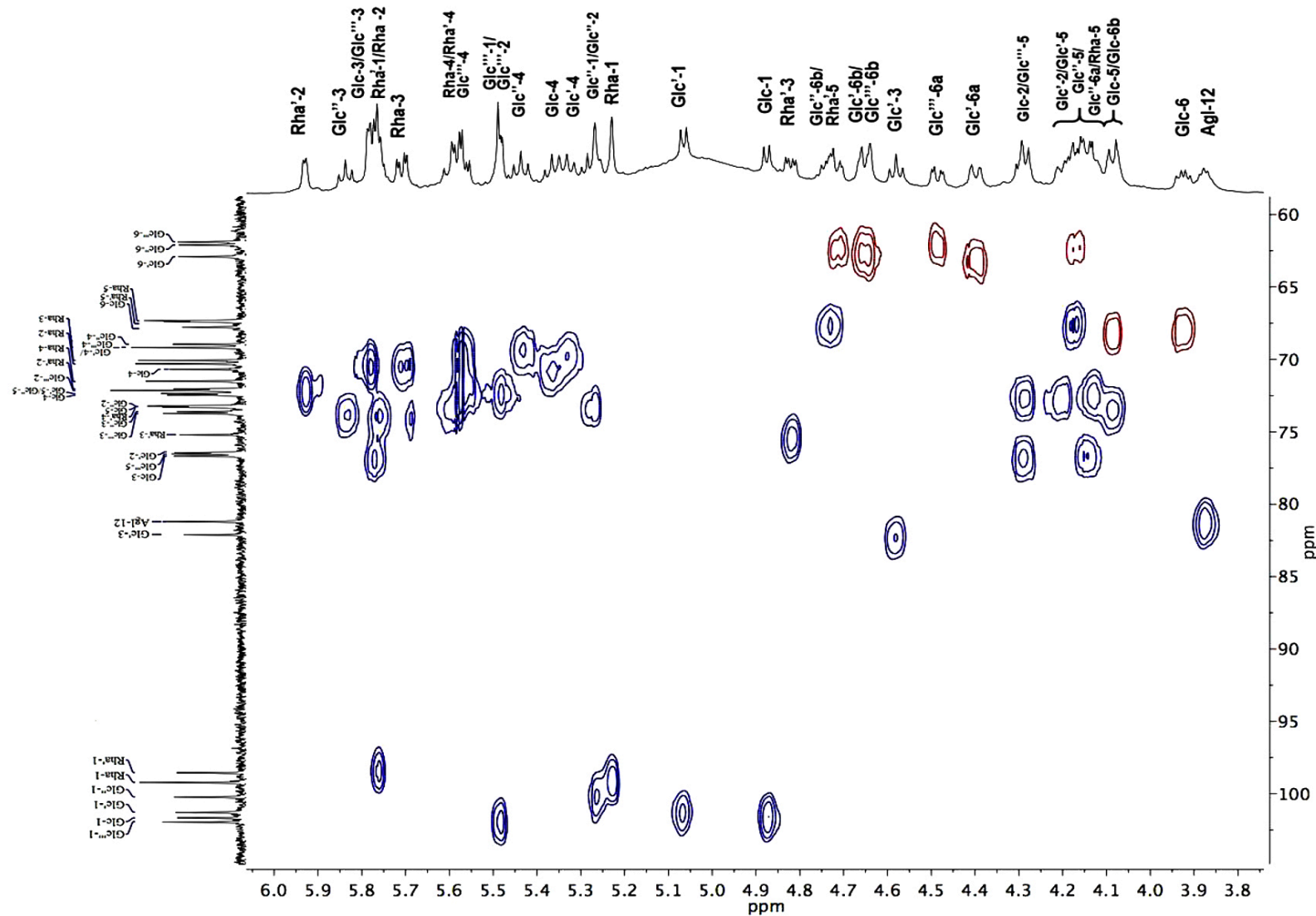
Figure S29. Expanded oligosaccharide core region of the ($^1J_{CH}$) correlation (HSQC) spectrum for the peracetylated derivative of operculinic acid I (**13**) with high resolution 1D ^{1}H projection (600 MHz) and ^{13}C (150 MHz) projections in pyridine-d_5. See Figure S18 for cross-peak assignments.
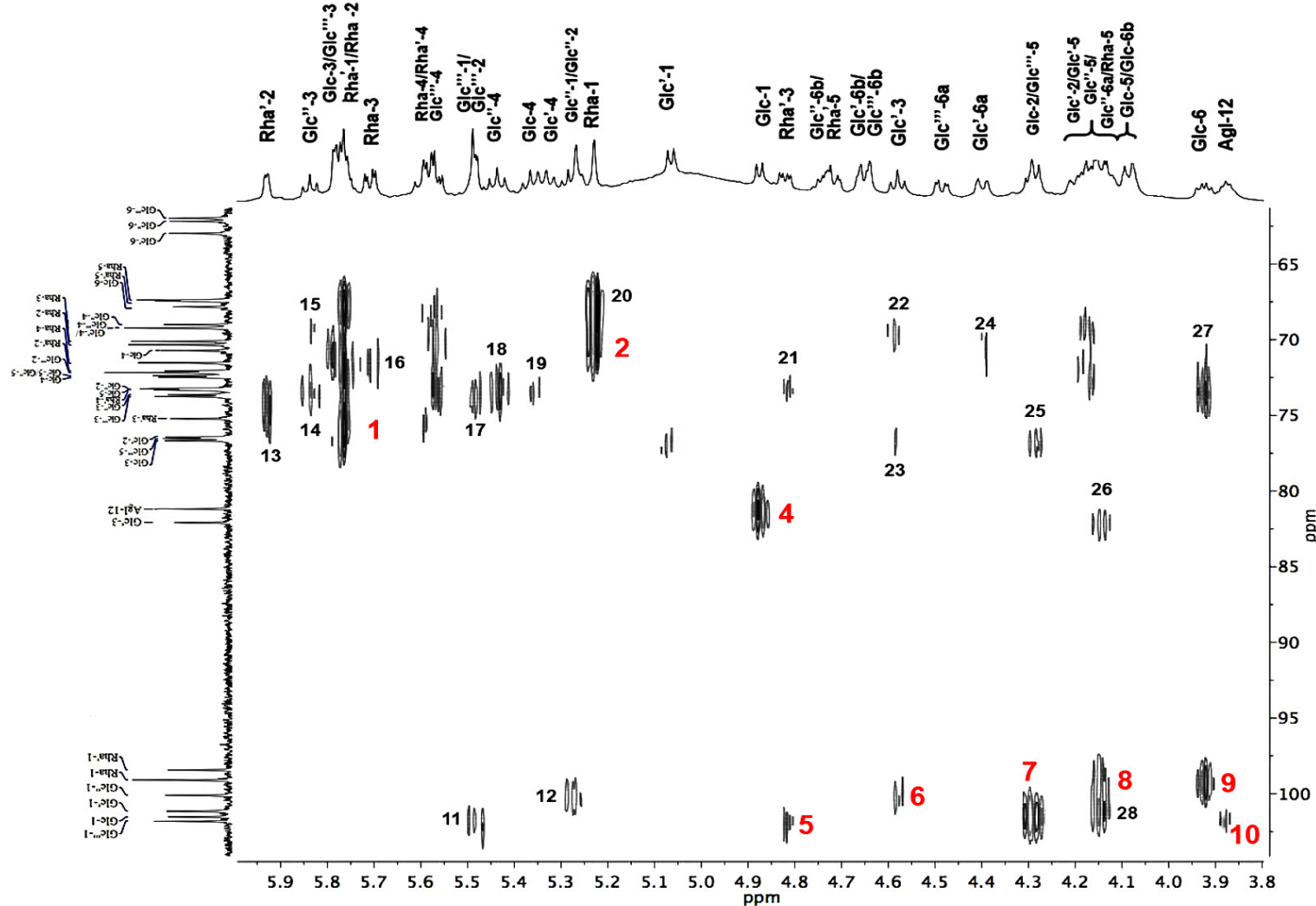
Figure S30. Expanded oligosaccharide core region of the ^{1}H-detected heteronuclear ($^{2,3}J_{CH}$) correlation (HMBC) spectrum for the peracetylated operculinic acid I (**13**) with high-resolution 1D ^{1}H (600 MHz) and ^{13}C (150 MHz) projections in pyridine-d_5. See Figure S22 for cross-peak assignments.

Formula: $[C_{86}H_{126}O_{48}Na]^+$
Exact mass: 1949.73107
Accurate mass: 1949.72618
Mass accuracy: −2.5 ppm
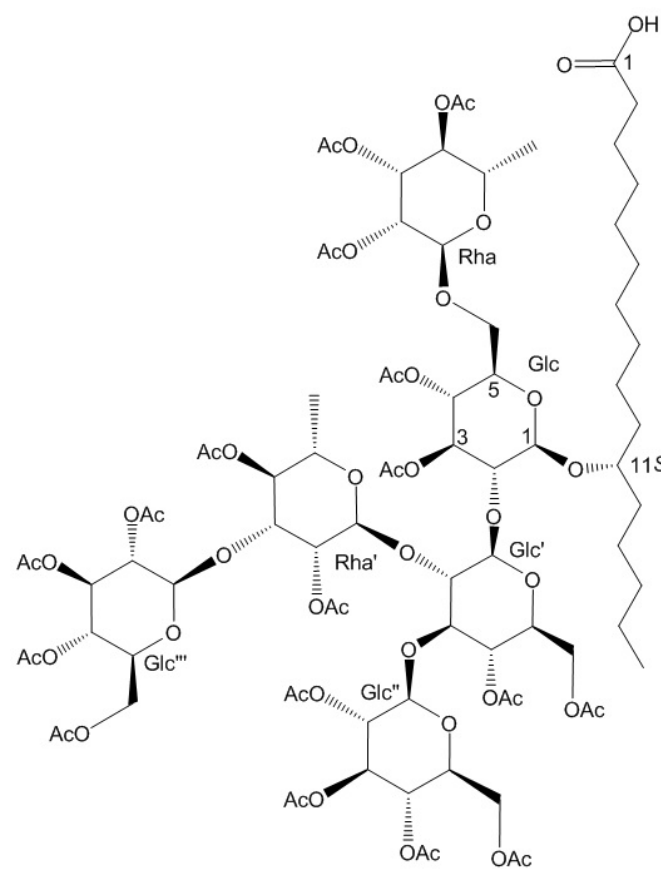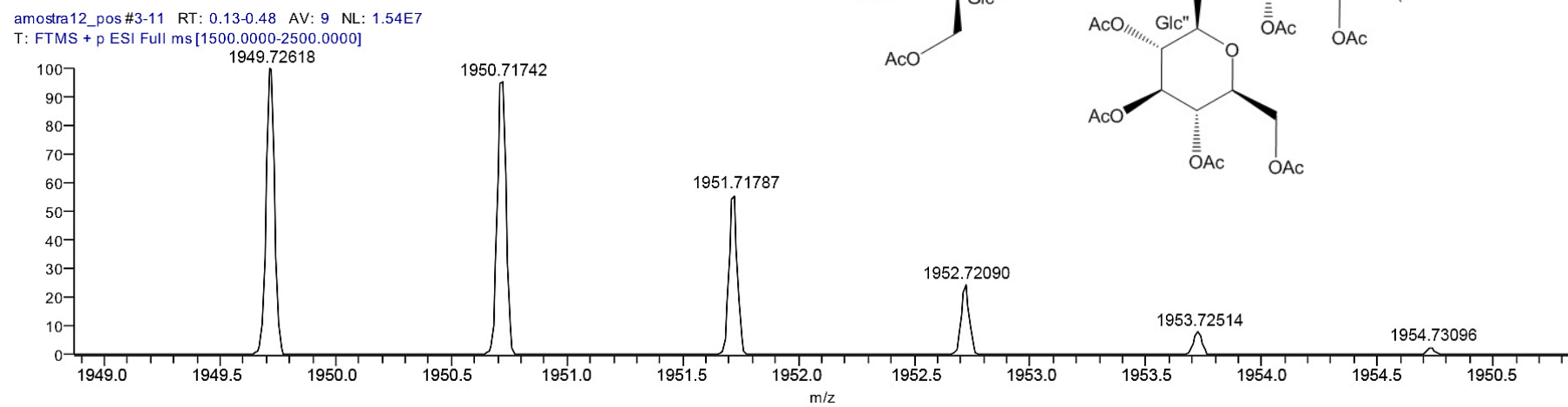
Figure S31. High-resolution positive ion mode ESI mass spectrum of peracetylated operculinic acid J (**14**) showing isotopic distribution and relative abundances of the sodium adduct ion $[C_{86}H_{126}O_{48}Na]^+$.
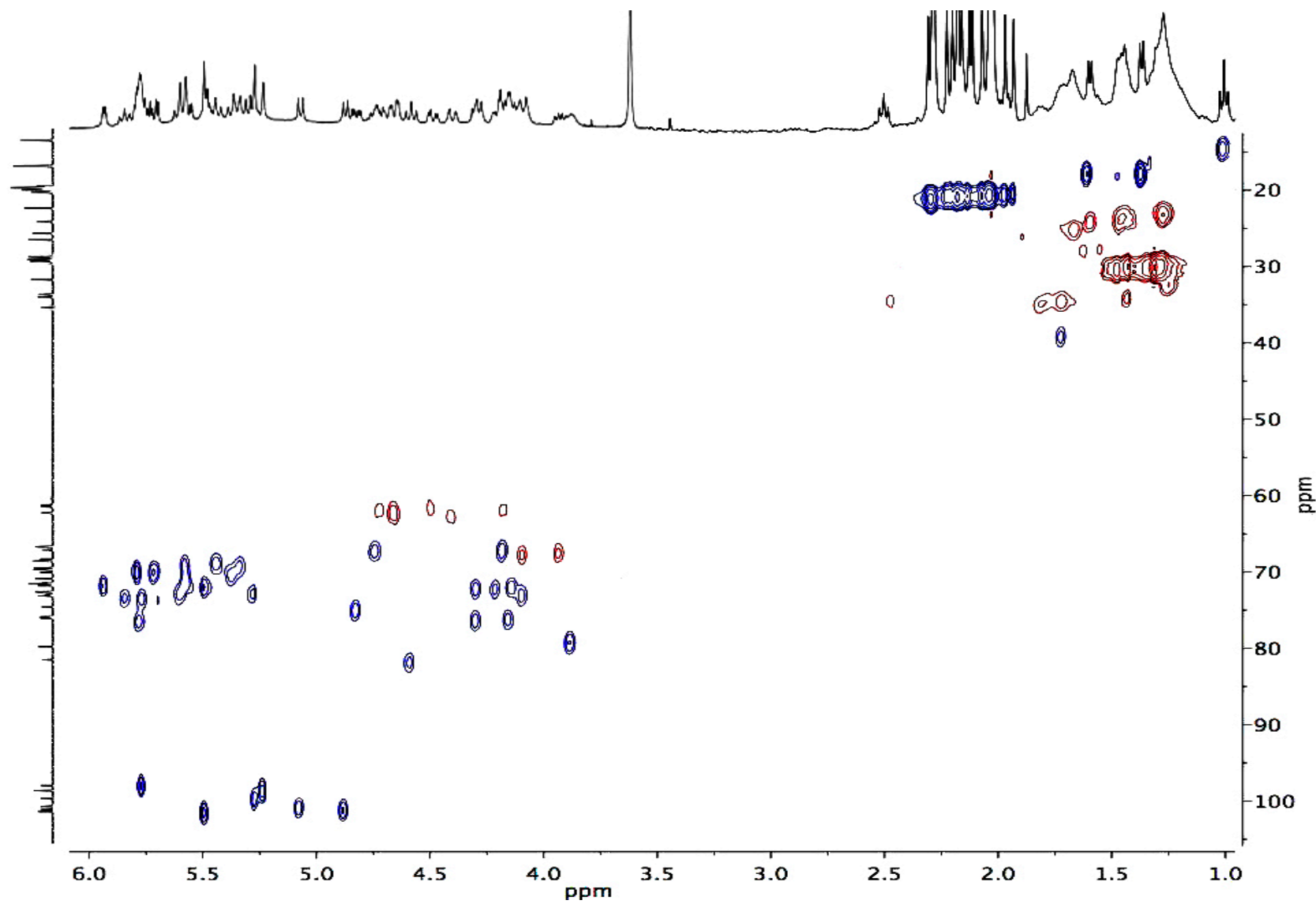
Figure S32. ¹H-Detected heteronuclear ($^1J_{CH}$) correlation (HSQC) spectrum for the peracetylated derivative of operculinic acid J (**14**) in pyridine-d_5.
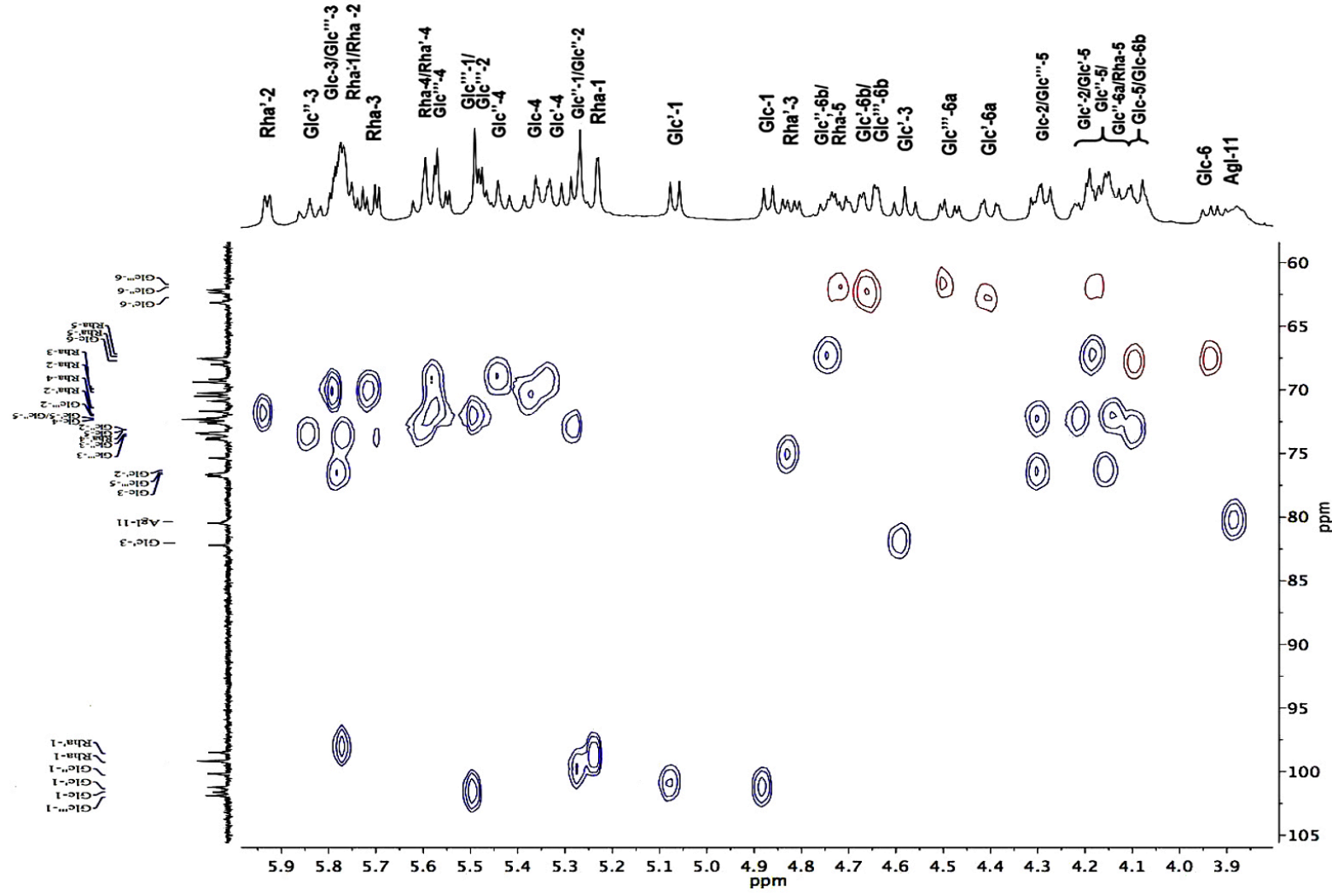
Figure S33. Expanded oligosaccharide core region of the ($^1J_{CH}$) correlation (HSQC) spectrum for the peracetylated derivative of operculinic acid J (**14**) with high resolution 1D ^{1}H projection (400 MHz) and ^{13}C (100 MHz) projections in pyridine-d_5. See Figure S18 for cross-peak assignments.
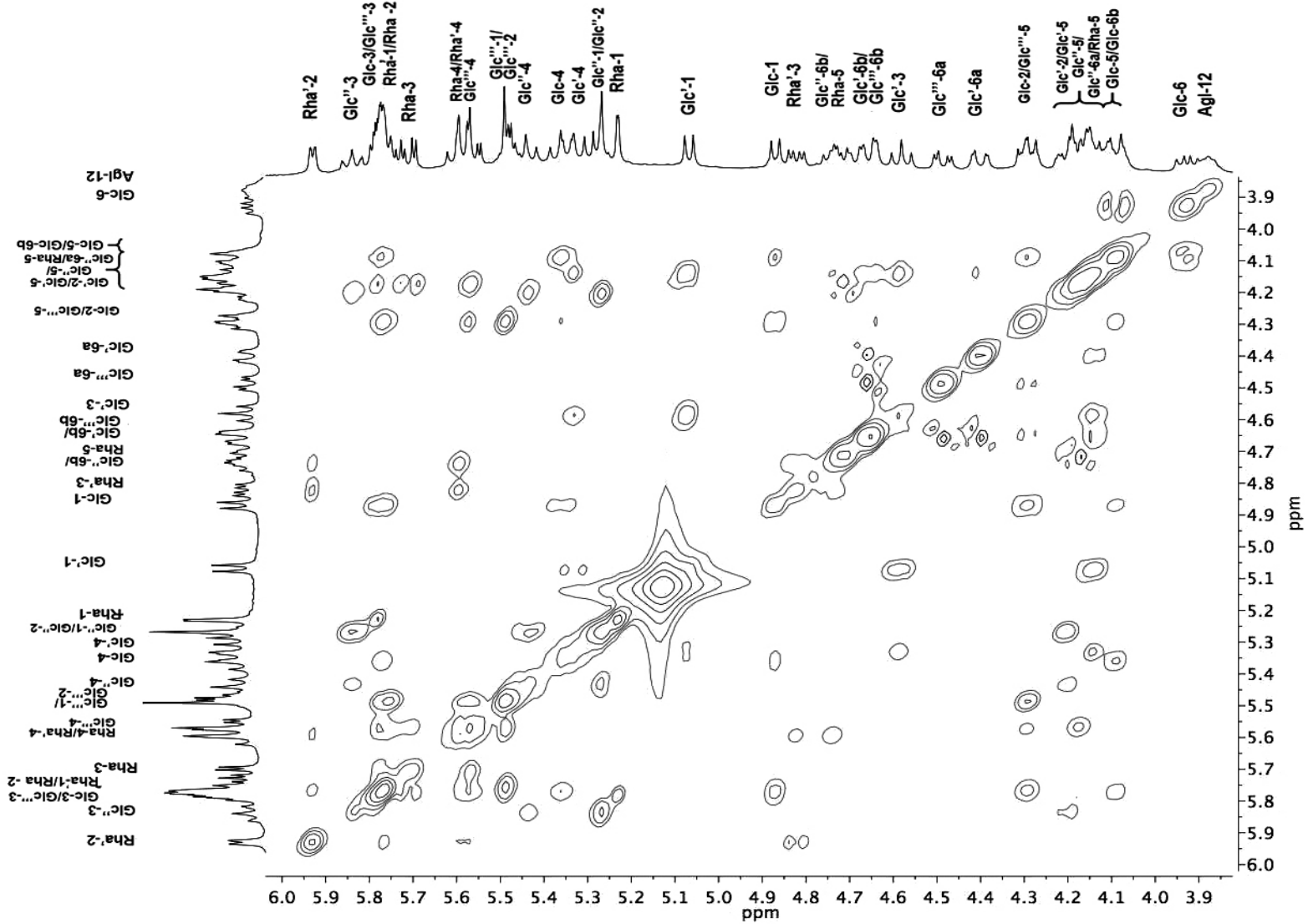
Figure S34. Expanded oligosaccharide core region of the ¹H-detected homonuclear total correlation (TOCSY) spectrum for the peracetylated derivative of operculinic acid J (**14**) with high resolution 1D projections (400 MHz) in pyridine-d_5. See Figure S15 for cross-peak assignments.
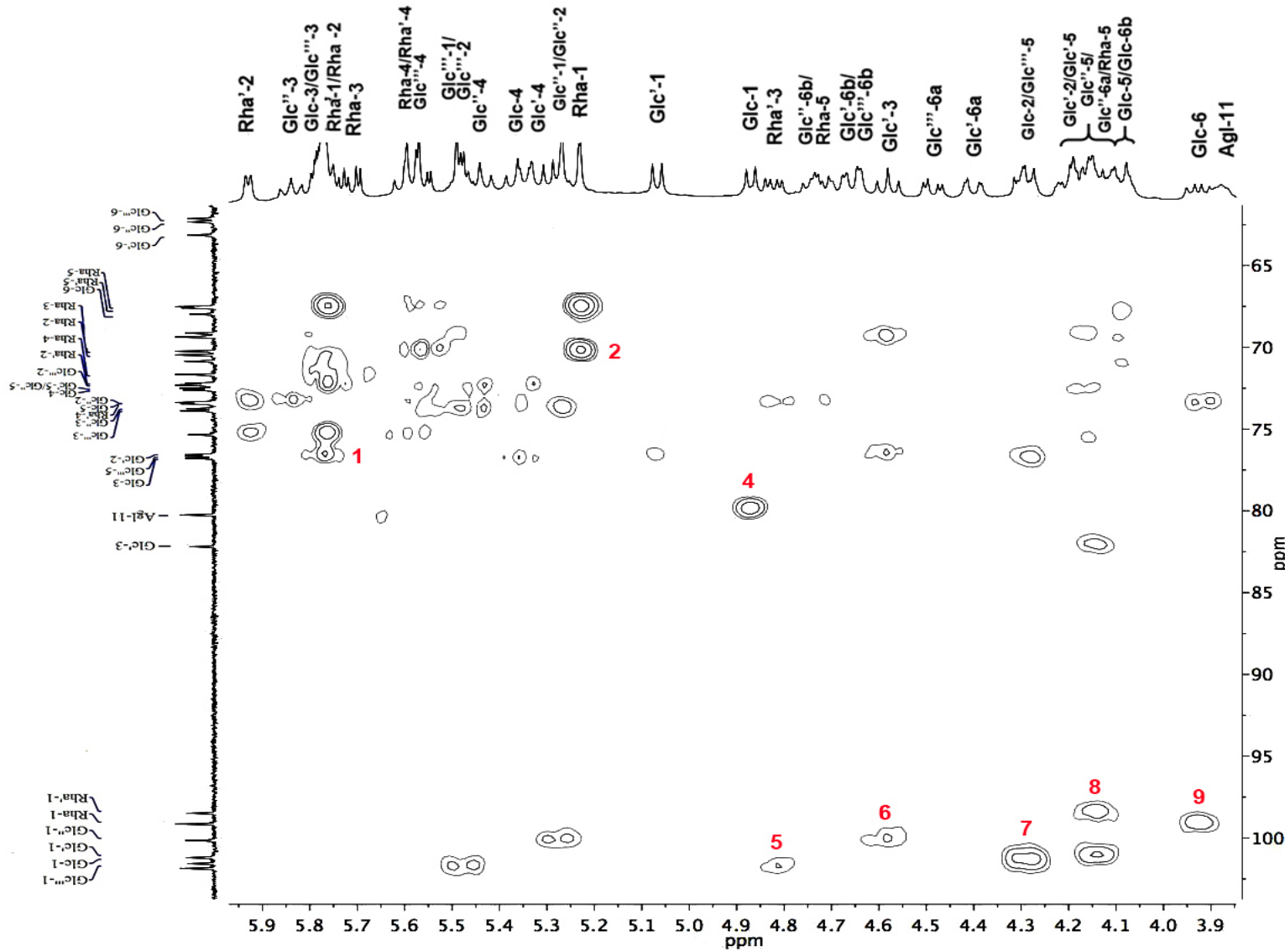
Figure S35. Expanded oligosaccharide core region of the ^{1}H-detected heteronuclear ($^{2,3}J_{CH}$) correlation (HMBC) spectrum for the peracetylated operculinic acid J (**14**) with high-resolution 1D ^{1}H (400 MHz) and ^{13}C (100 MHz) projections in pyridine-d_5. See Figure S22 for cross-peak assignments.
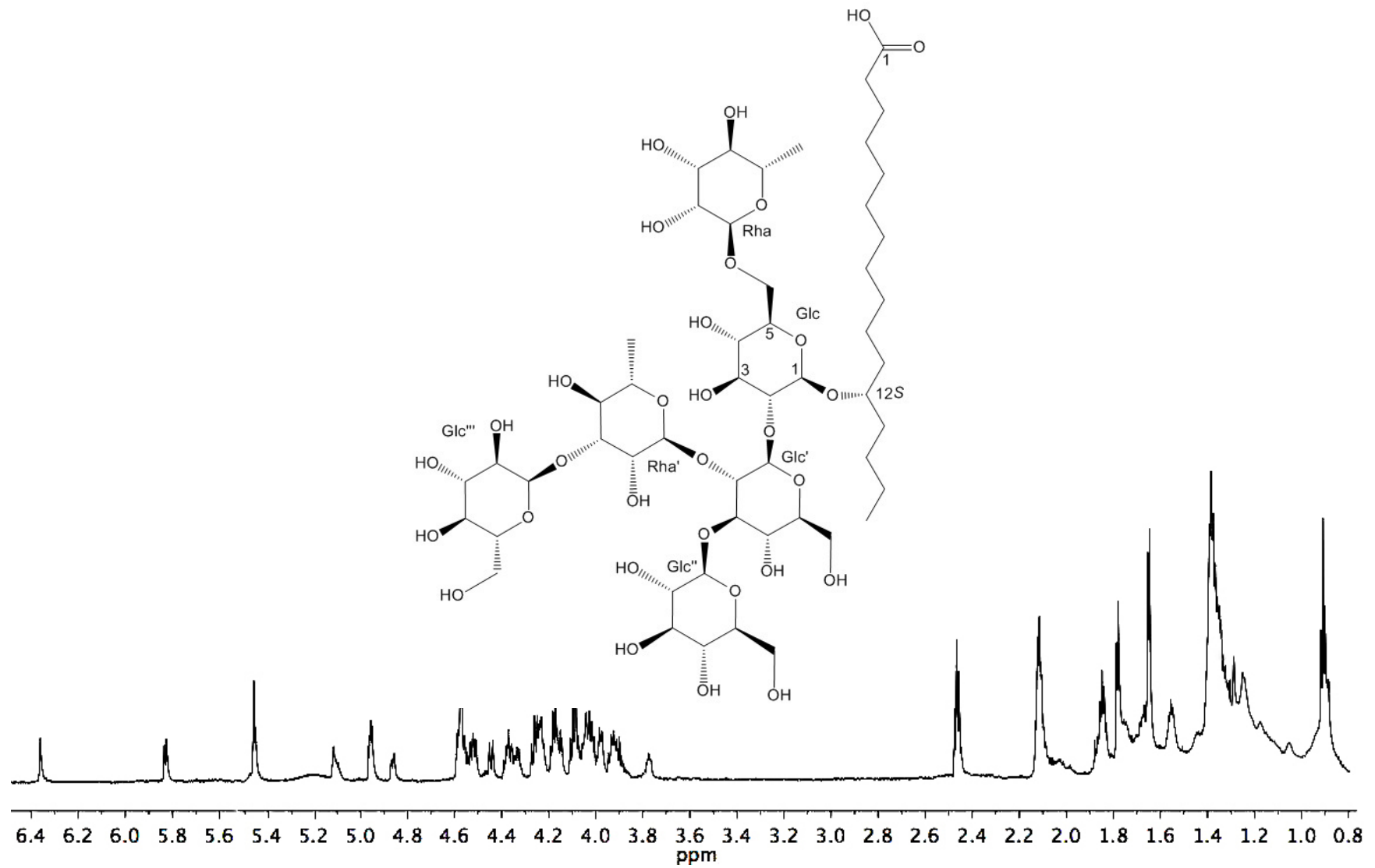
Figure S36. ^{1}H NMR spectrum (800 MHz) of operculinic acid I (**2**) in pyridine-d_5.

S43
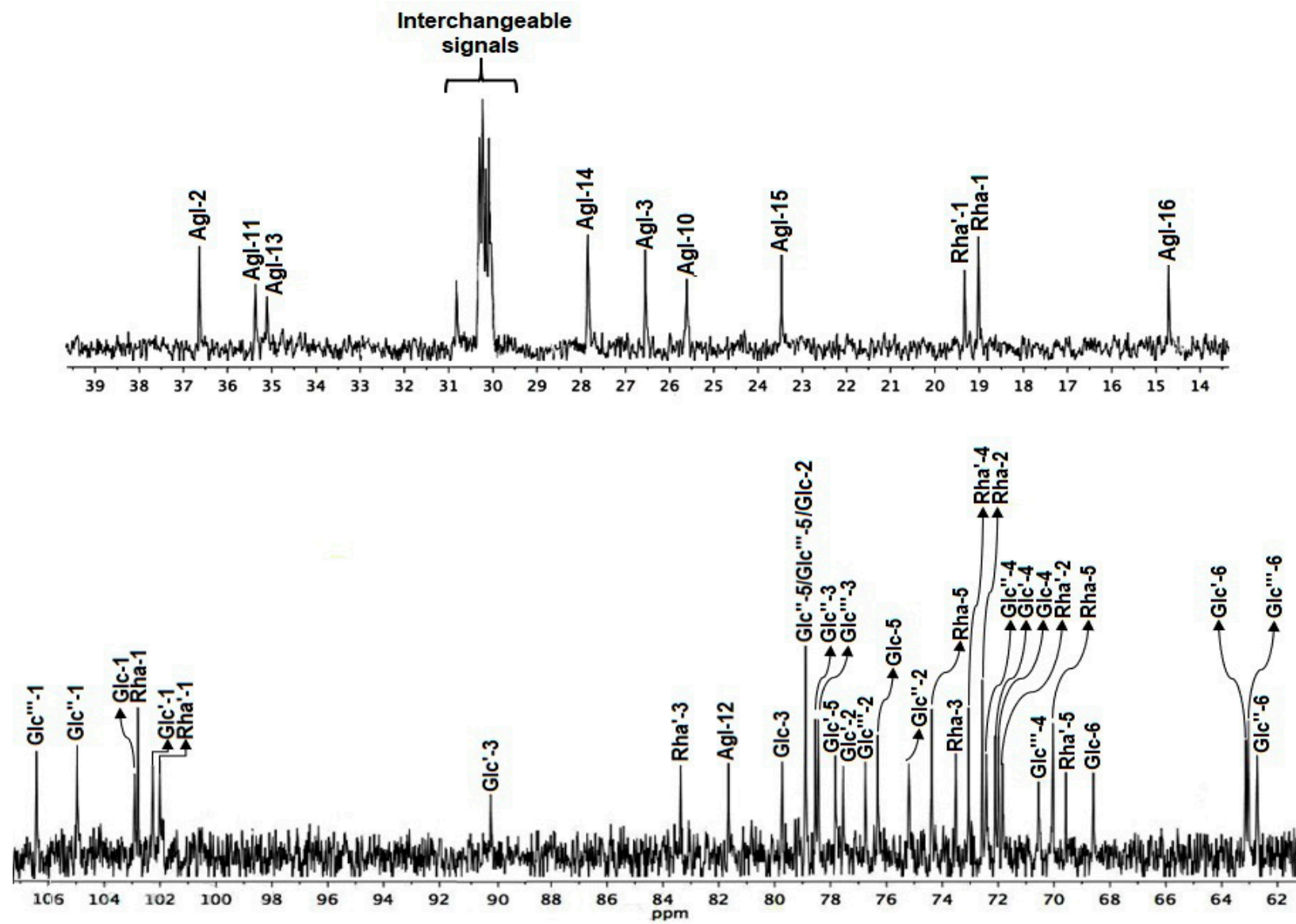
Figure S37. ^{13}C NMR spectrum (200 MHz) of operculinic acid **I** (**2**) in pyridine-d_5.
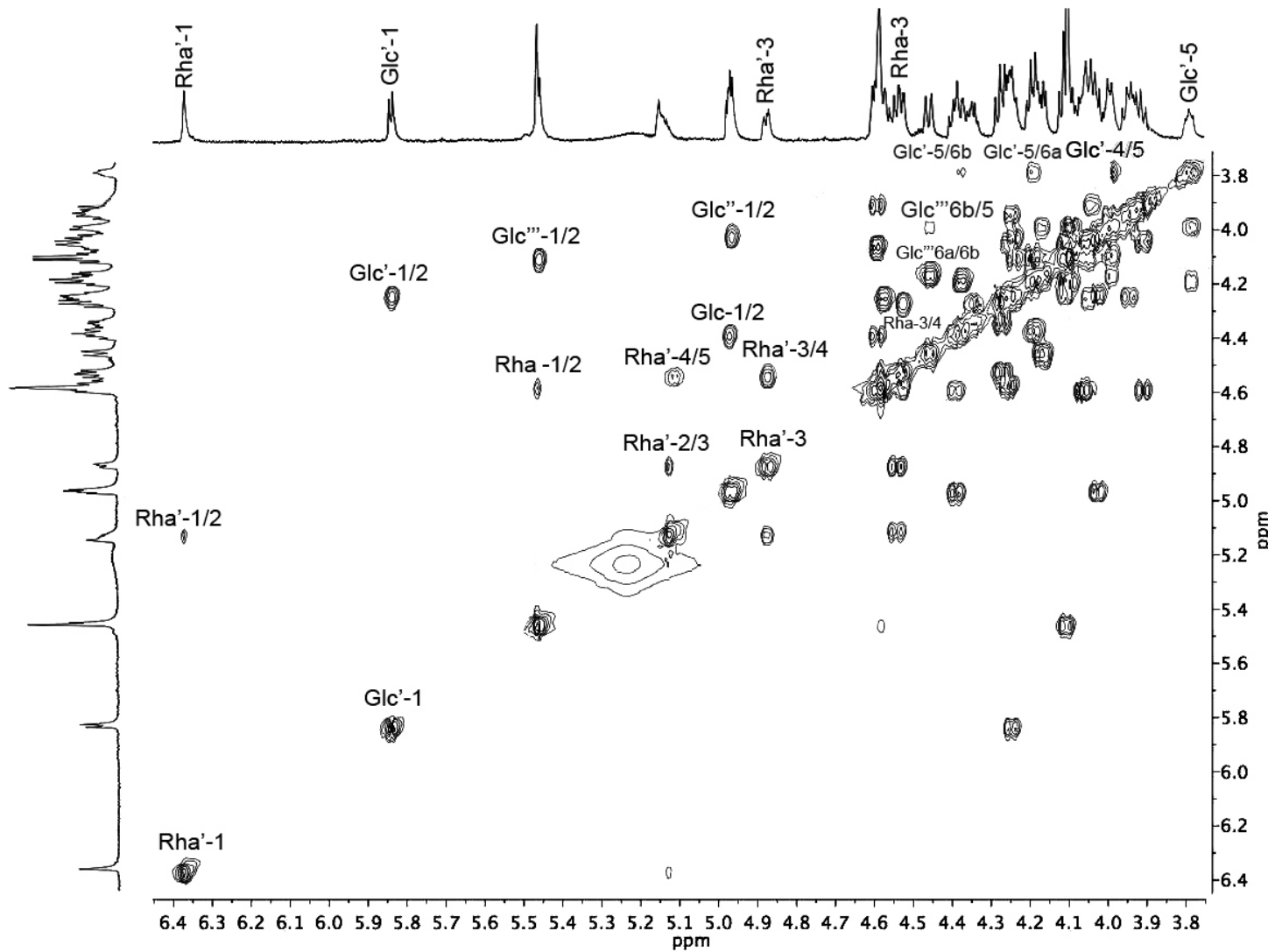
Figure S38. Expanded oligosaccharide core region of the ¹H-detected homonuclear $^3J_{HH}$ correlation (COSY) spectrum for operculinic acid I (**2**) with high resolution 1D projections (800 MHz) in pyridine-d_5.

S45
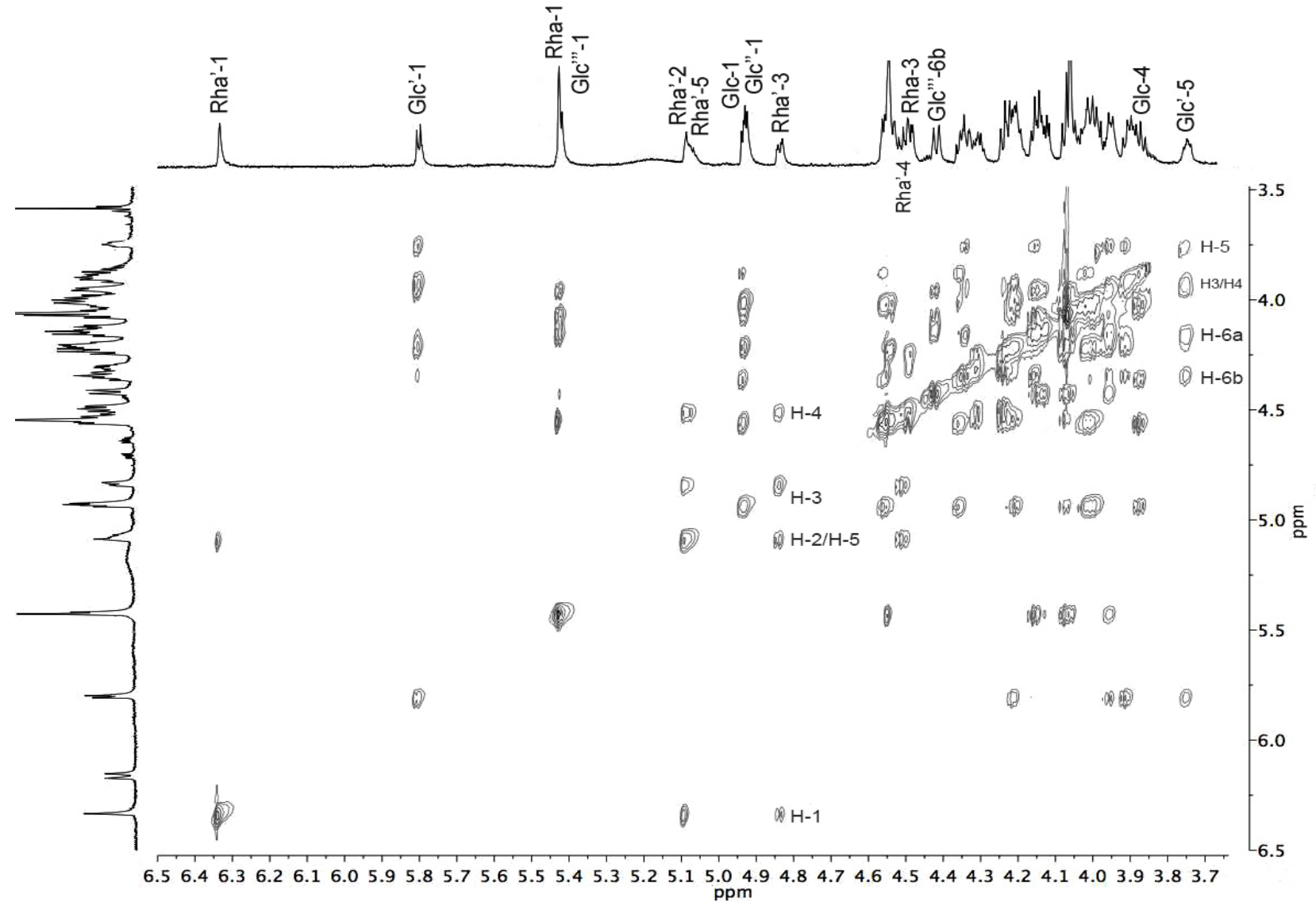
Figure S39. Expanded oligosaccharide core region of the ¹H-detected homonuclear total correlation (TOCSY) spectrum for operculinic acid I (**2**) with high resolution 1D projections (800 MHz) in pyridine-d_5.
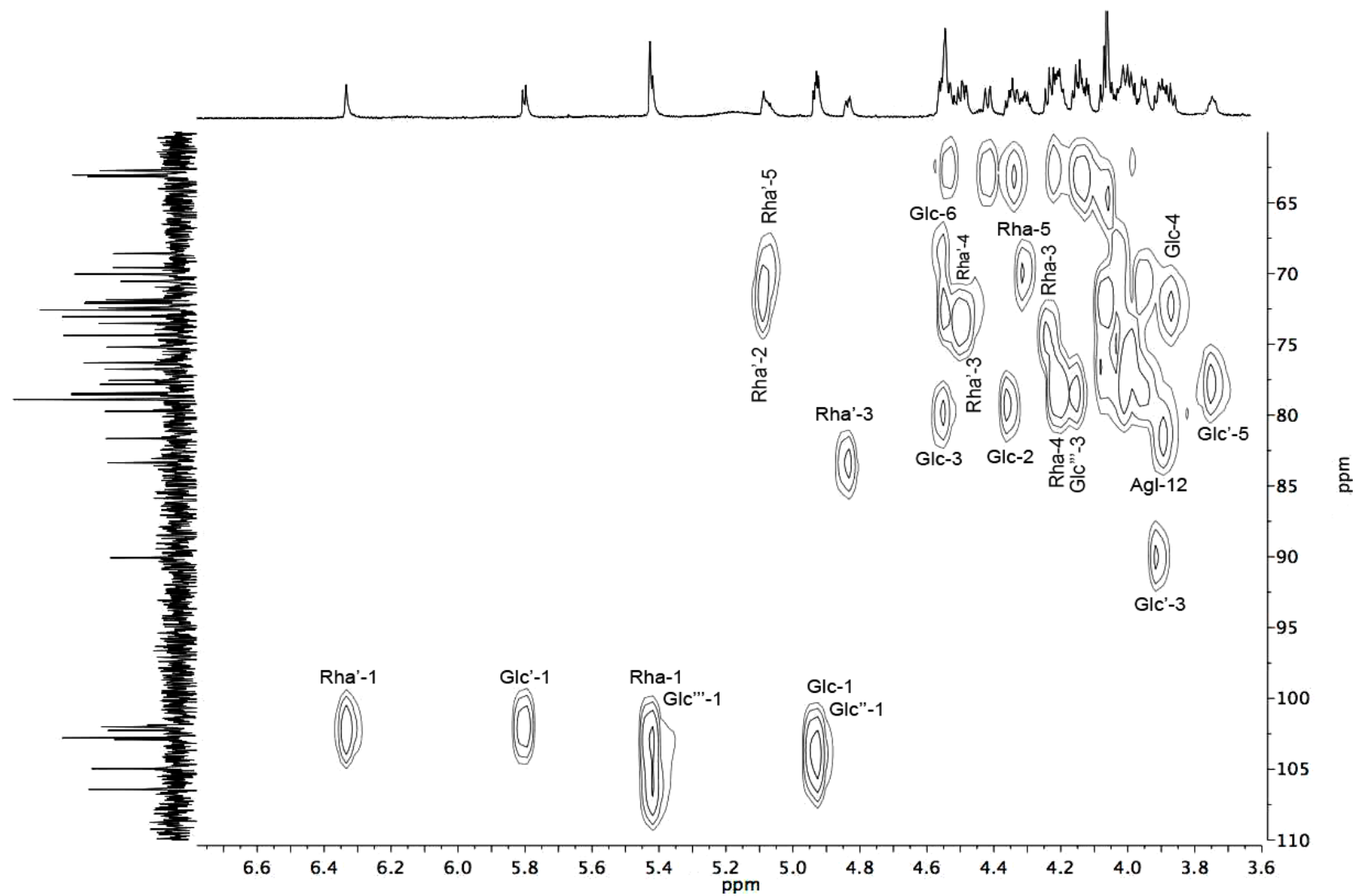
Figure S40. Expanded oligosaccharide core region of the ¹H-detected heteronuclear ($^1J_{CH}$) correlation (HSQC) spectrum for the operculinic acid I (**2**) with high-resolution 1D ¹H (800 MHz) and ¹³C (200 MHz); anomeric region) projections in pyridine-d_5.
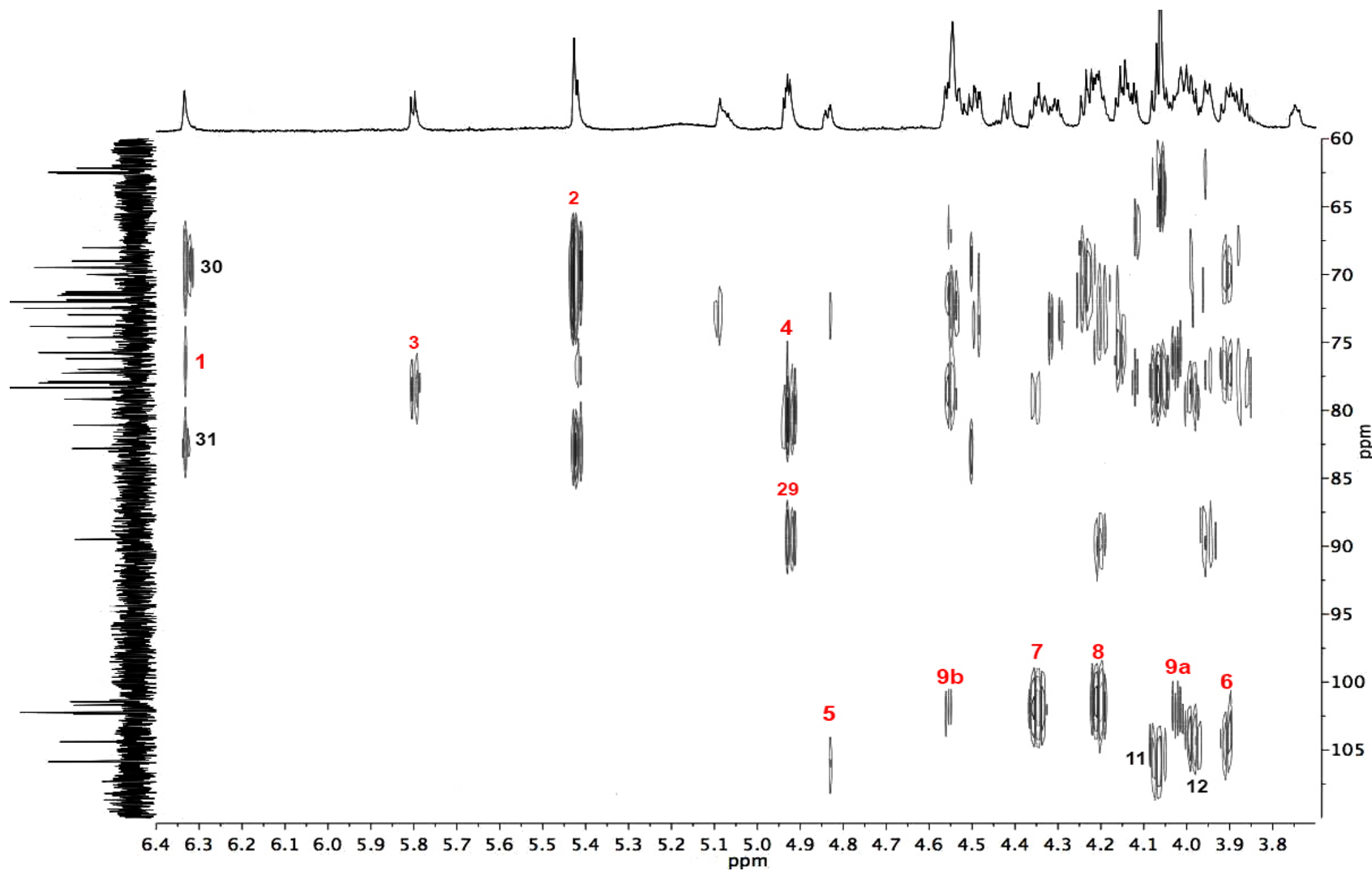
Figure S41. Expanded oligosaccharide core region of the ^{1}H-detected heteronuclear ($^{2,3}J_{CH}$) correlation (HMBC) spectrum for operculinic acid I (**2**) with high-resolution 1D ^{1}H (800 MHz) and ^{13}C (200 MHz) projections in pyridine-d_5. See Figure S22 for cross-peak assignments; additional cross peaks $^3J_{CH}$: **30**, H$_1$-Rha'/C$_5$-Rha'; **31**, H$_1$-Rha'/C$_3$-Rha'.

Formula: $[C_{86}H_{126}O_{48}Na]^+$
Exact mass: 1805.68882
Accurate mass: 1805.69141
Mass accuracy: +1.4 ppm
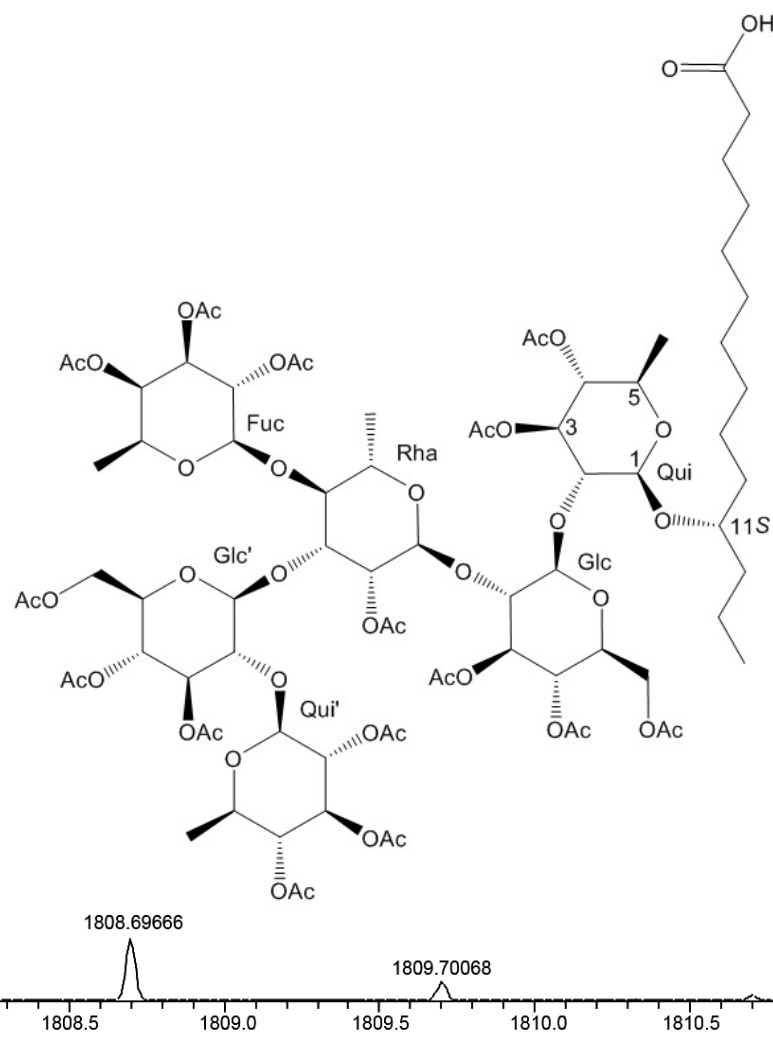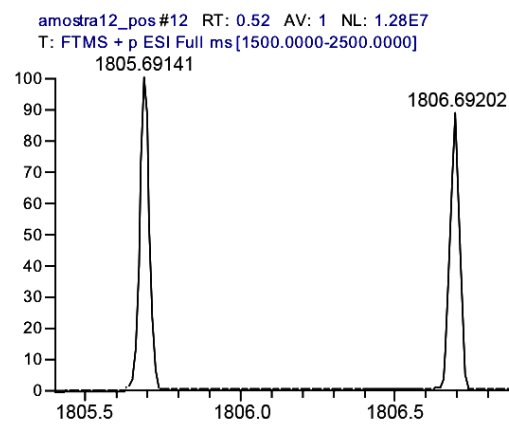
Figure S42. High-resolution positive ion mode ESI mass spectrum of peracetylated purgic acid A (**15**) showing isotopic distribution and relative abundances of the sodium adduct ion $[C_{86}H_{126}O_{48}Na]^+$.
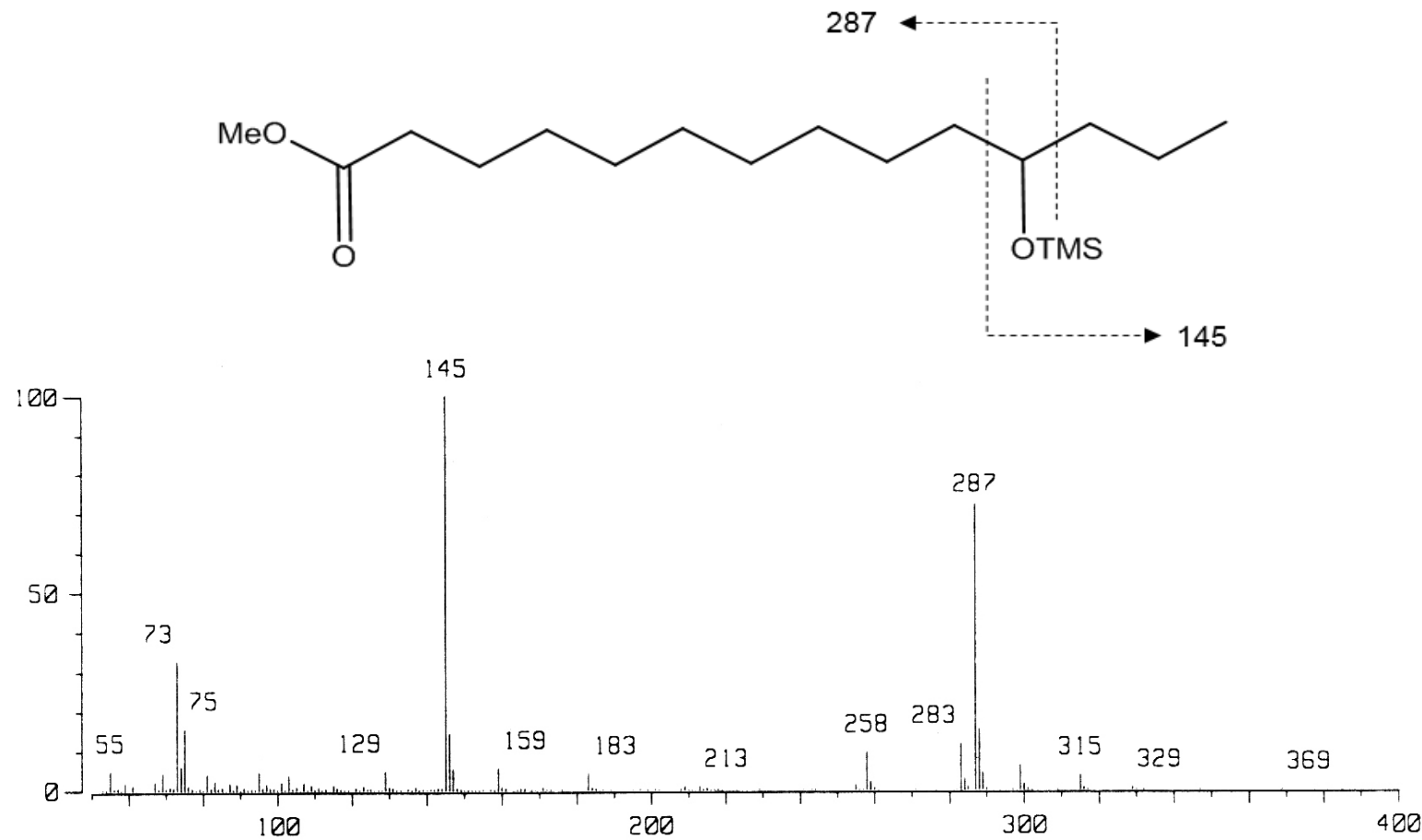
Figure S43. EIMS of silylated 11-hydroxytetradecanoic acid methyl ester liberated from purgic acid A (**4**): m/z 299 (45, $[C_{13}H_{22}O_3TMS]^+$) and 159 (100, $[C_5H_{10}OTMS]^+$).
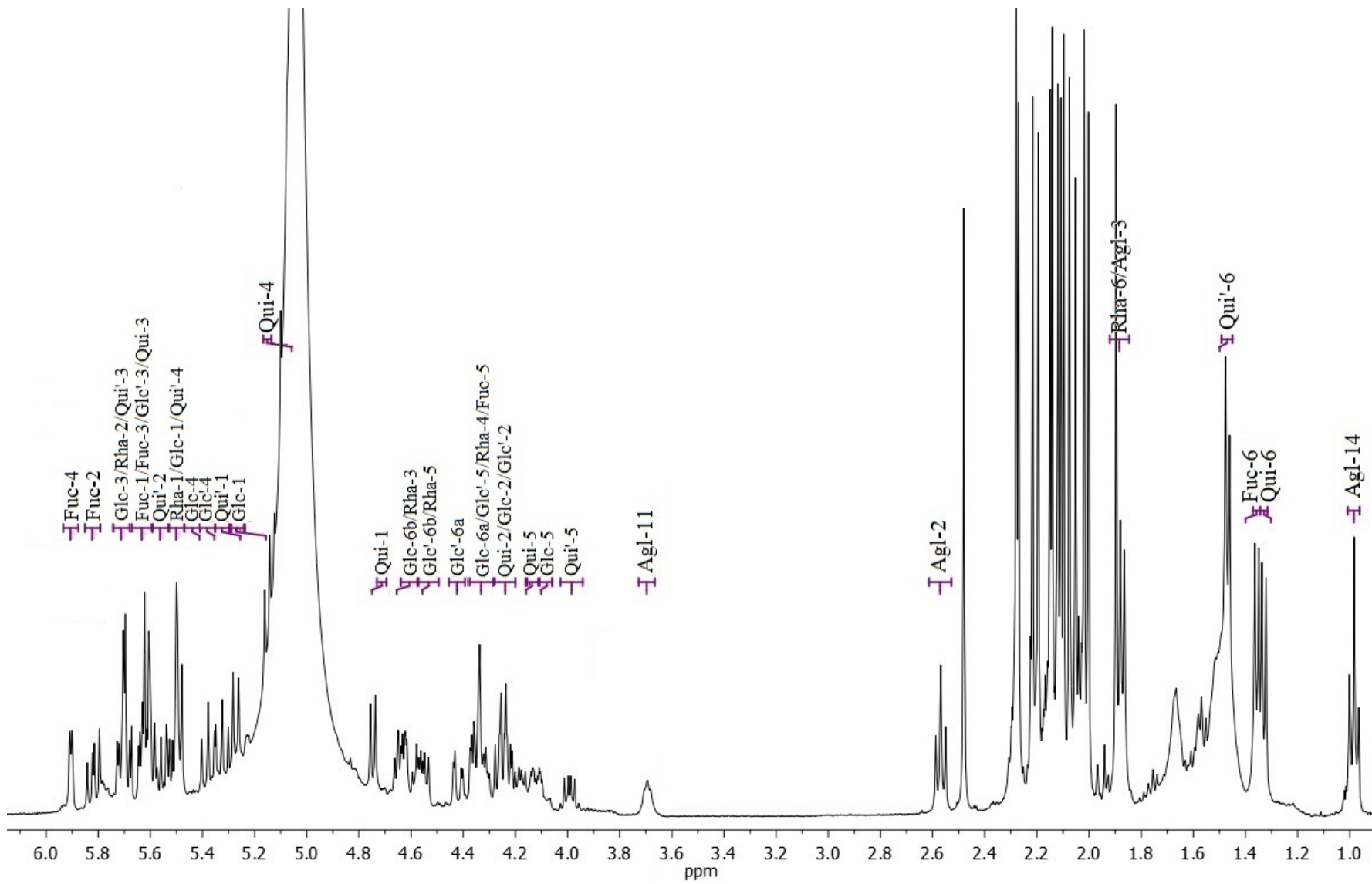
Figure S44. ^{1}H NMR spectrum (400 MHz) of the peracetylated derivative of purgic acid A (**15**) in pyridine-d_5
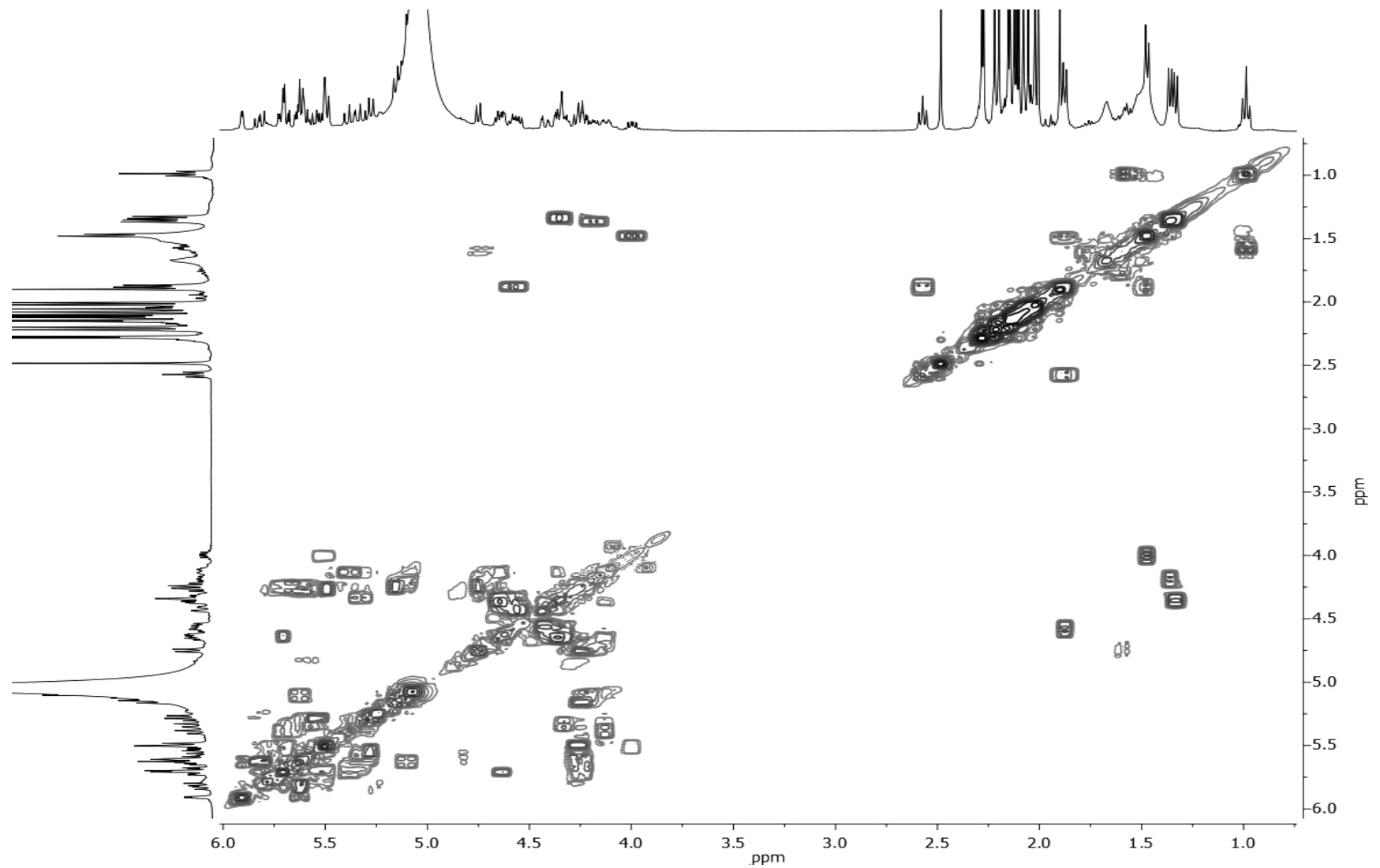
Figure S45. ^{1}H-Detected homonuclear total correlation (COSY) spectrum for the peracetylated derivative of purgic acid A (**15**) with high resolution 1D projections (400 MHz) in pyridine-d_5.
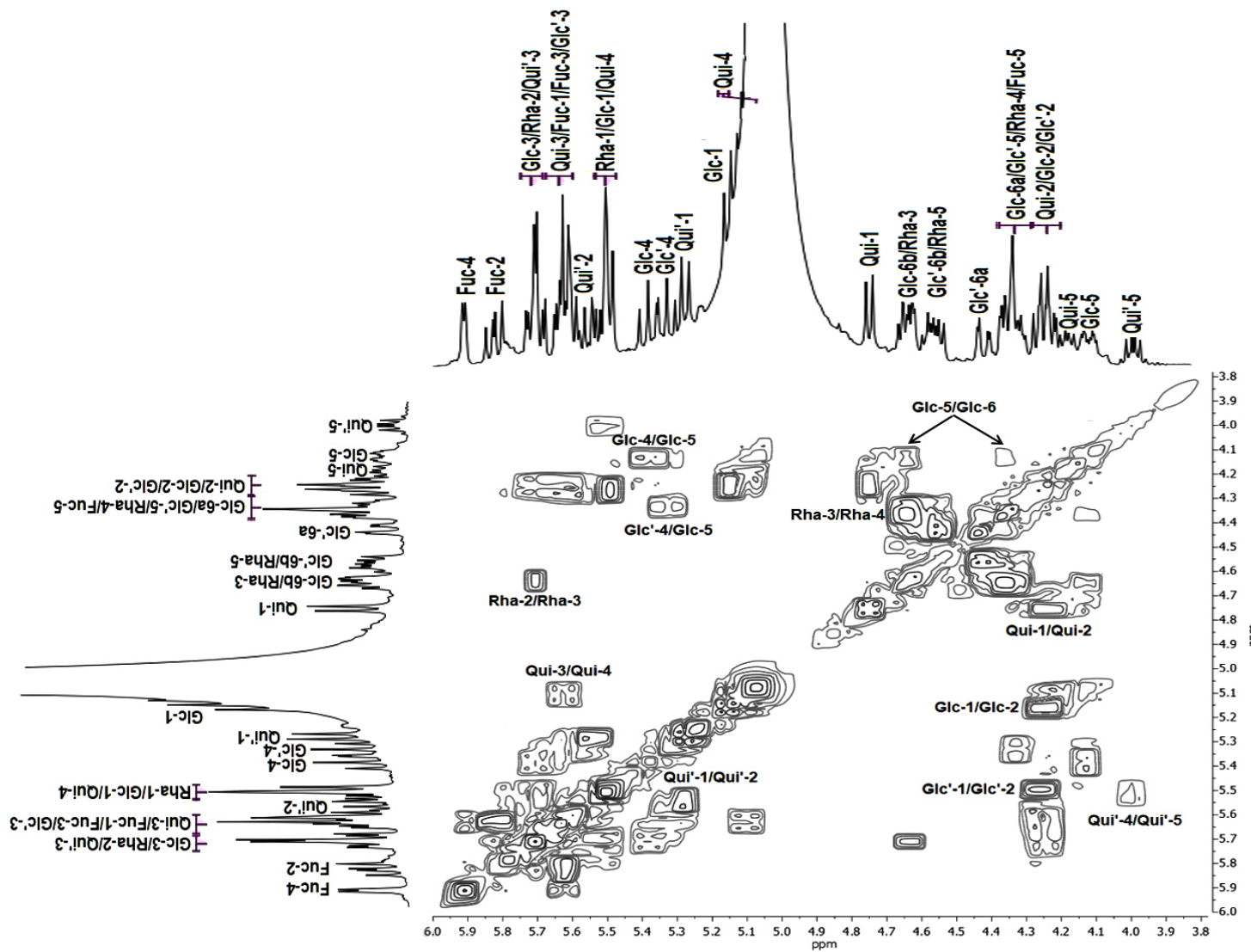
Figure S46. Expanded oligosaccharide core region of the ^{1}H-detected homonuclear ($^3J_{HH}$) correlation (COSY) spectrum for the peracetylated derivative of purgic acid A (**15**) with high resolution 1D projections (400 MHz) in pyridine-d_5.
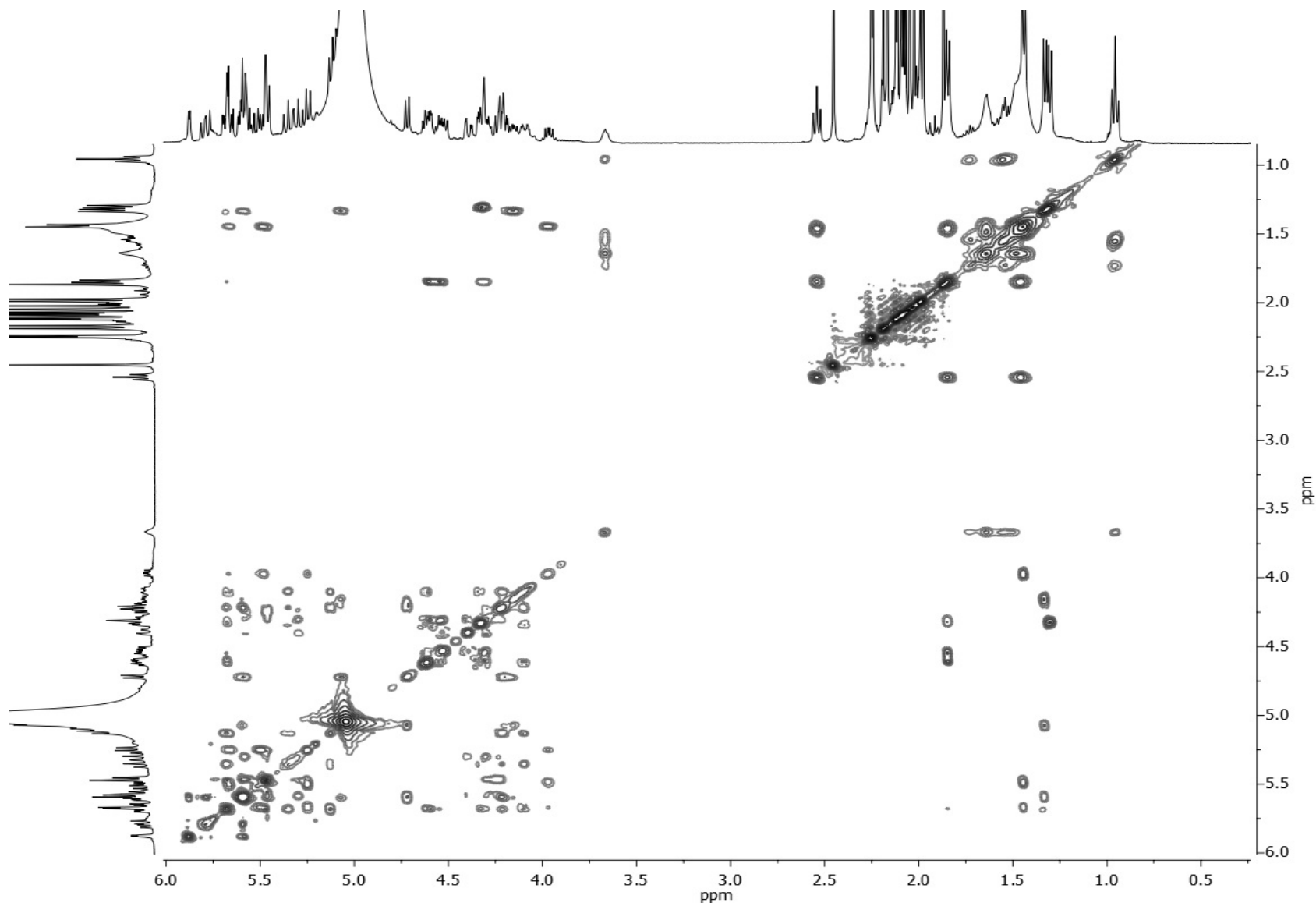
Figure S47. ¹H-Detected homonuclear total correlation (TOCSY) spectrum for the peracetylated derivative of purgic acid A (**15**) with high resolution 1D projections (400 MHz) in pyridine-d_5.
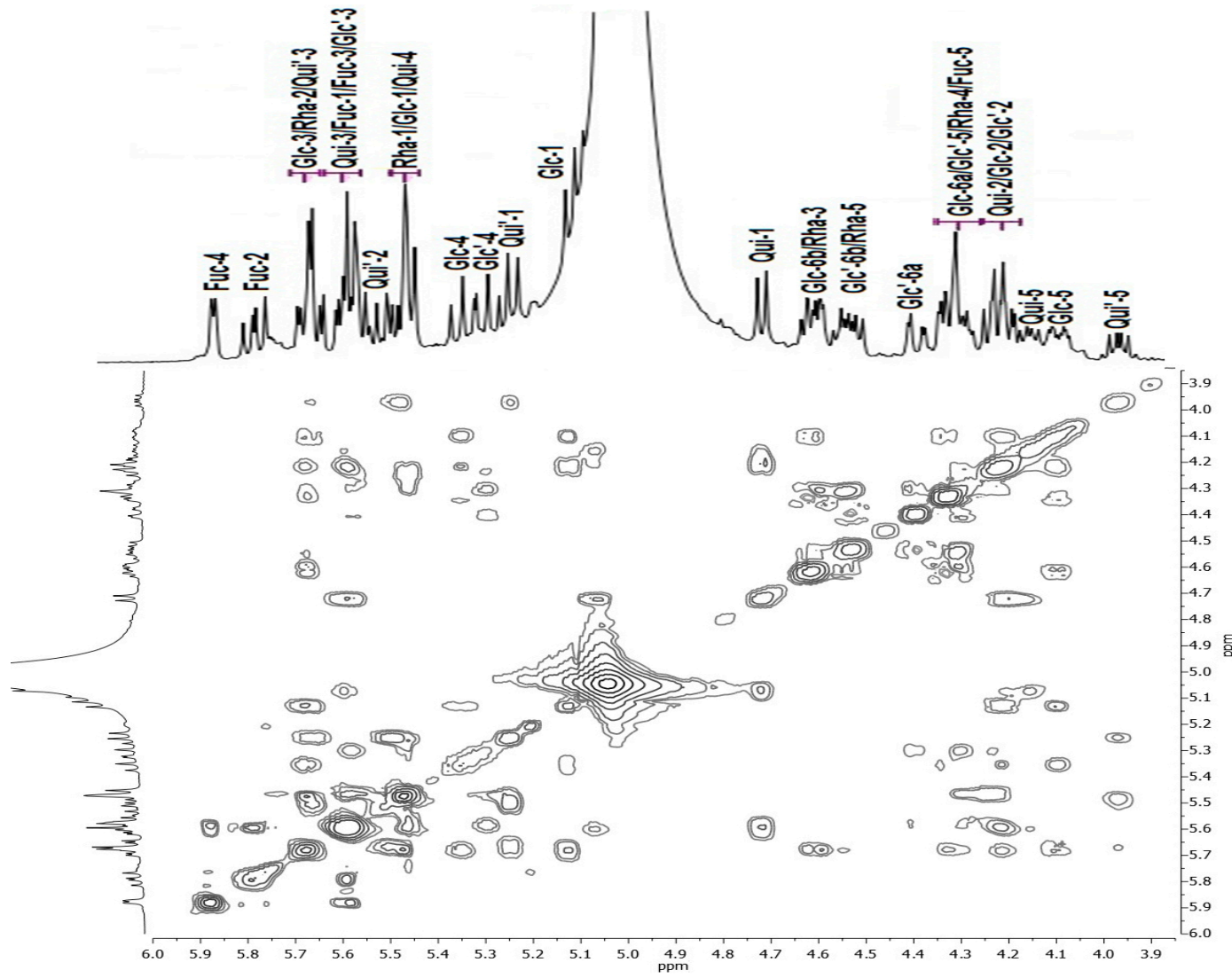
Figure S48. Expanded oligosaccharide core region of the ¹H-detected homonuclear total correlation (TOCSY) spectrum for the peracetylated derivative of purgic acid A (**15**) with high resolution 1D projections (400 MHz) in pyridine-d_5.
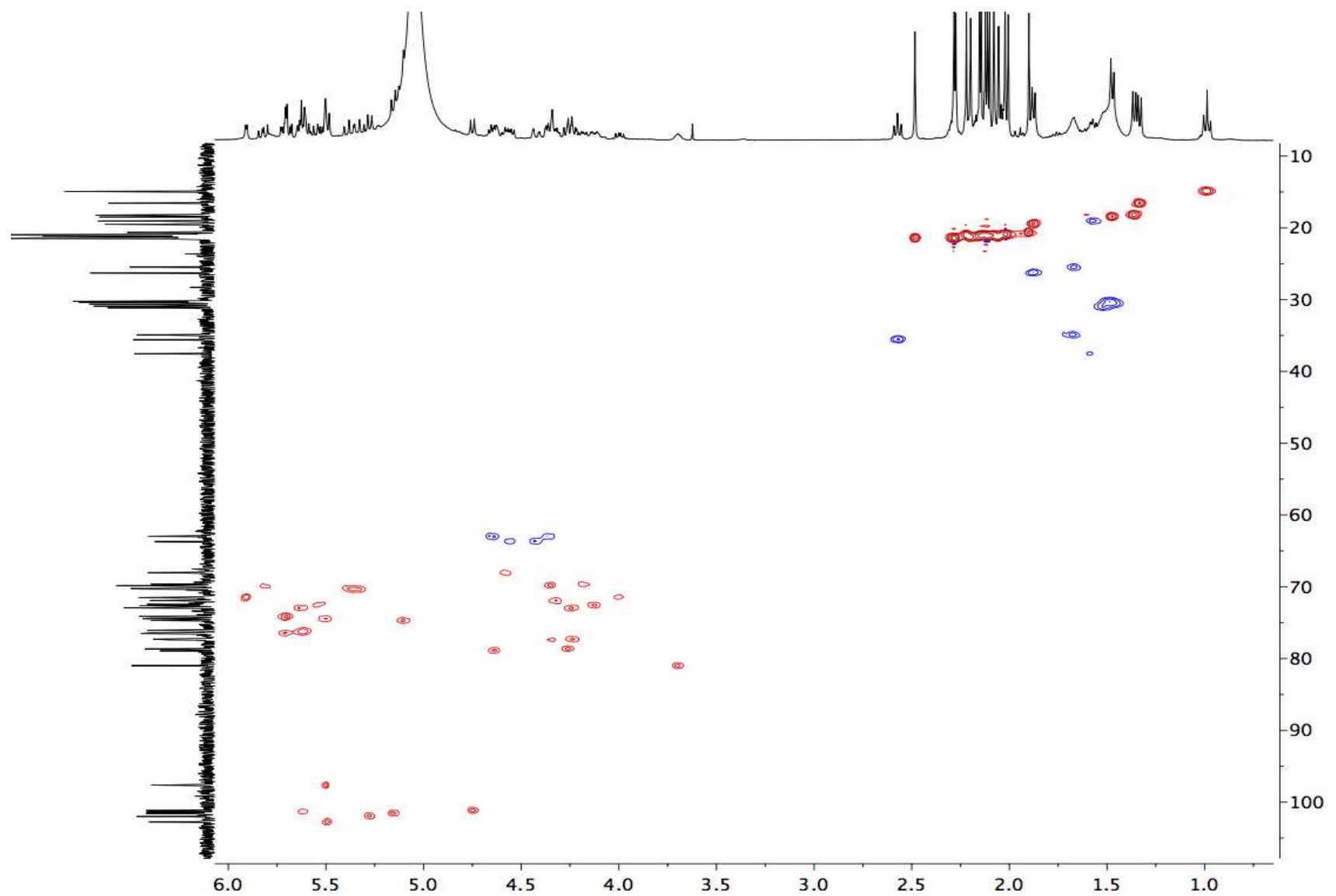
Figure S49. ^{1}H-Detected heteronuclear ($^1J_{CH}$) correlation (HSQC) spectrum for the peracetylated derivative of purgic acid A (**15**) with high resolution 1D ^{1}H (400 MHz) and ^{13}C (100 MHz) projections in pyridine-d_5.
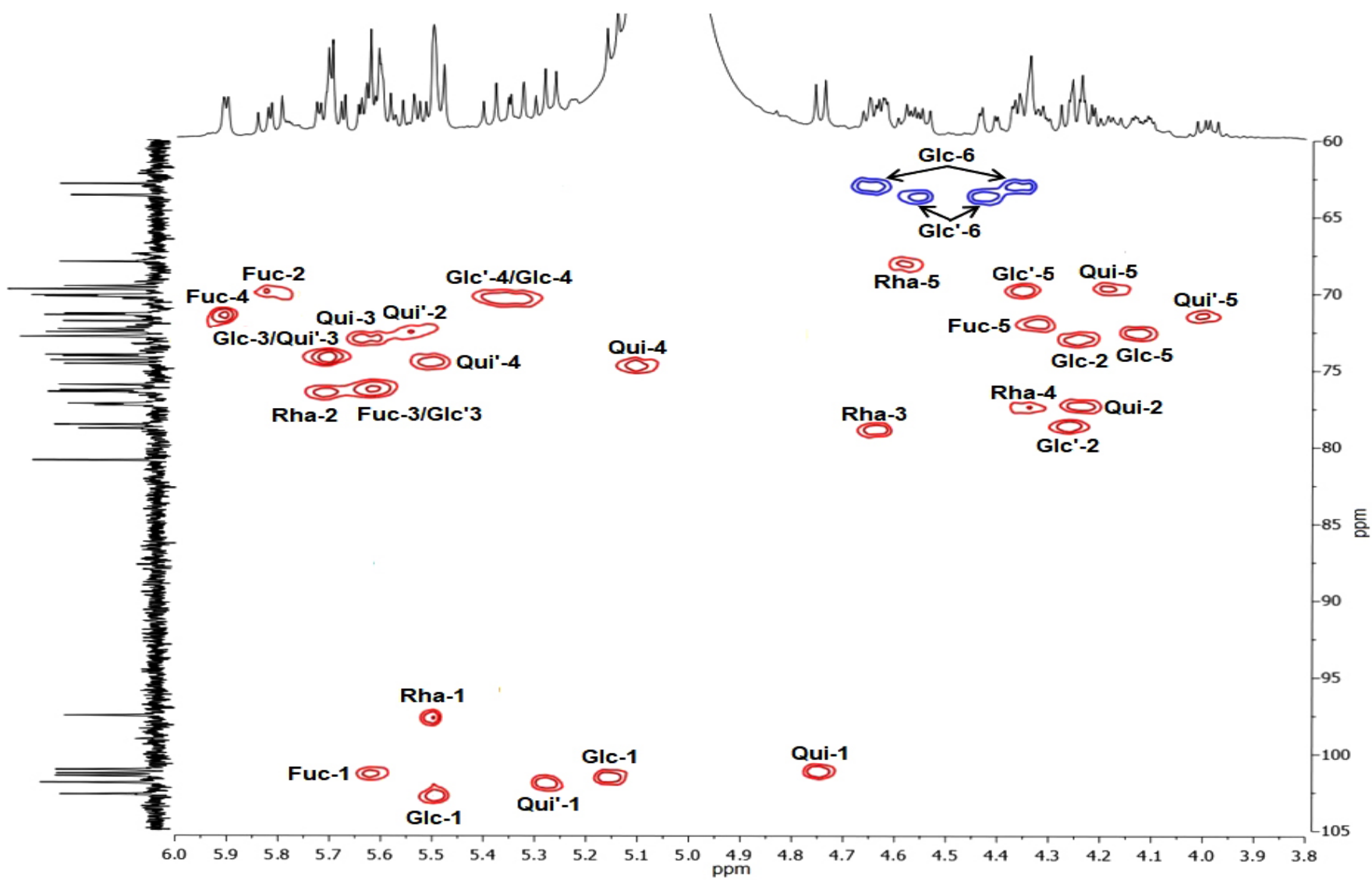
Figure S50. Expanded oligosaccharide core region of the ¹H-detected heteronuclear ($^1J_{CH}$) correlation (HSQC) spectrum for the peracetylated derivative of purgic acid A (**15**) with high resolution 1D ¹H (400 MHz) and ¹³C (100 MHz) projections in pyridine-d_5.

Formula: [C₂₂H₃₆O₁₀Na]⁺
$$[C_{22}H_{36}O_{10}Na]^+$$

Formula: $[C_{22}H_{36}O_{10}Na]^+$

Exact mass: 483.22006

Accurate mass: 483.22120

Mass accuracy: +2.3 ppm
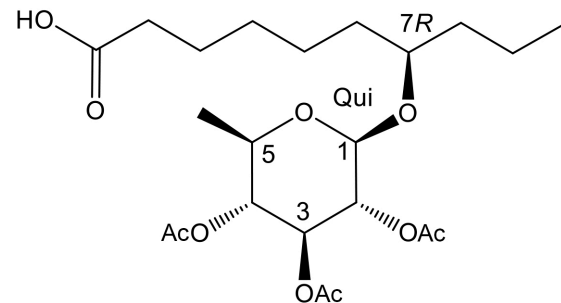
AMOSTRA18_pos #3-11 RT: 0.13-0.48 AV: 9 NL: 7.87E7
T: FTMS + p ESI Full ms [400.0000-600.0000]
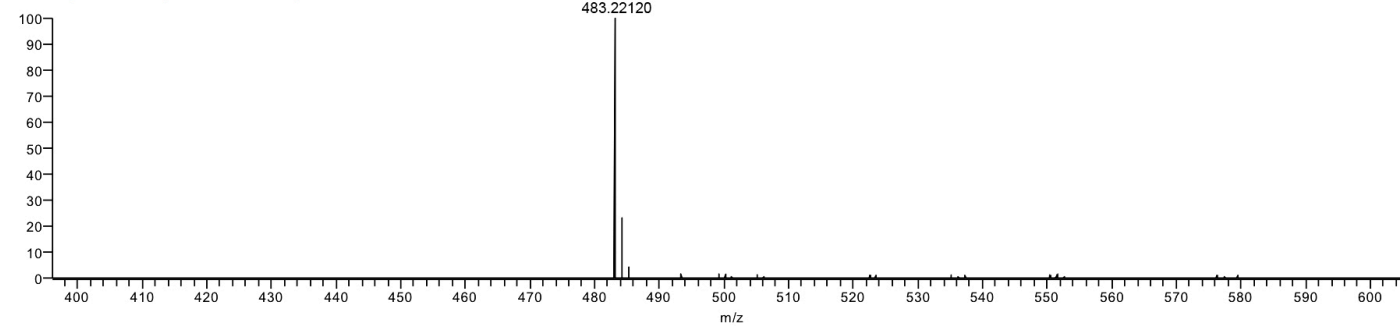
483.22120

AMOSTRA18_pos #3-11 RT: 0.13-0.48 AV: 9 NL: 7.87E7
T: FTMS + p ESI Full ms [400.0000-600.0000]

483.22120

484.21756

485.21693
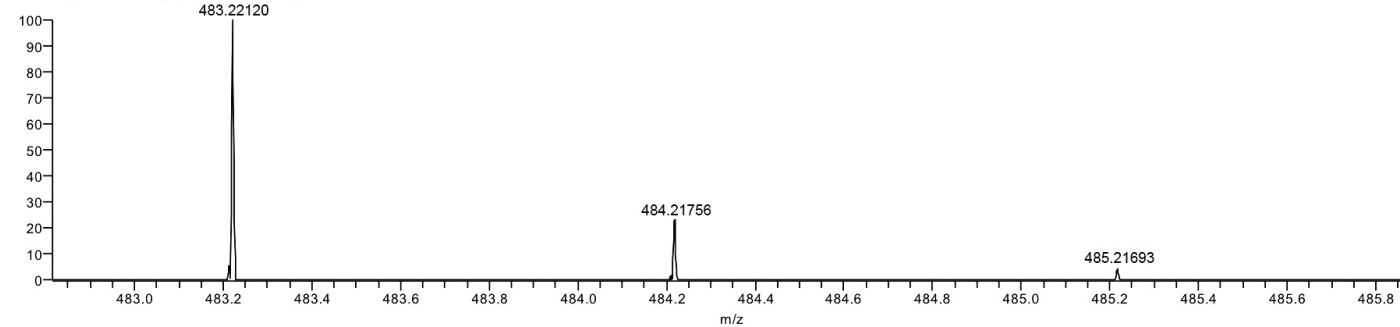
Figure S51. High-resolution positive ion mode ESI mass spectrum of peracetylated operculinic acid K (**16**) showing its sodium adduct ion with accurate mass at m/z 483.22120 (above) and isotopic distribution of the ion signals of $[C_{22}H_{36}O_{10}Na]^+$ (below).
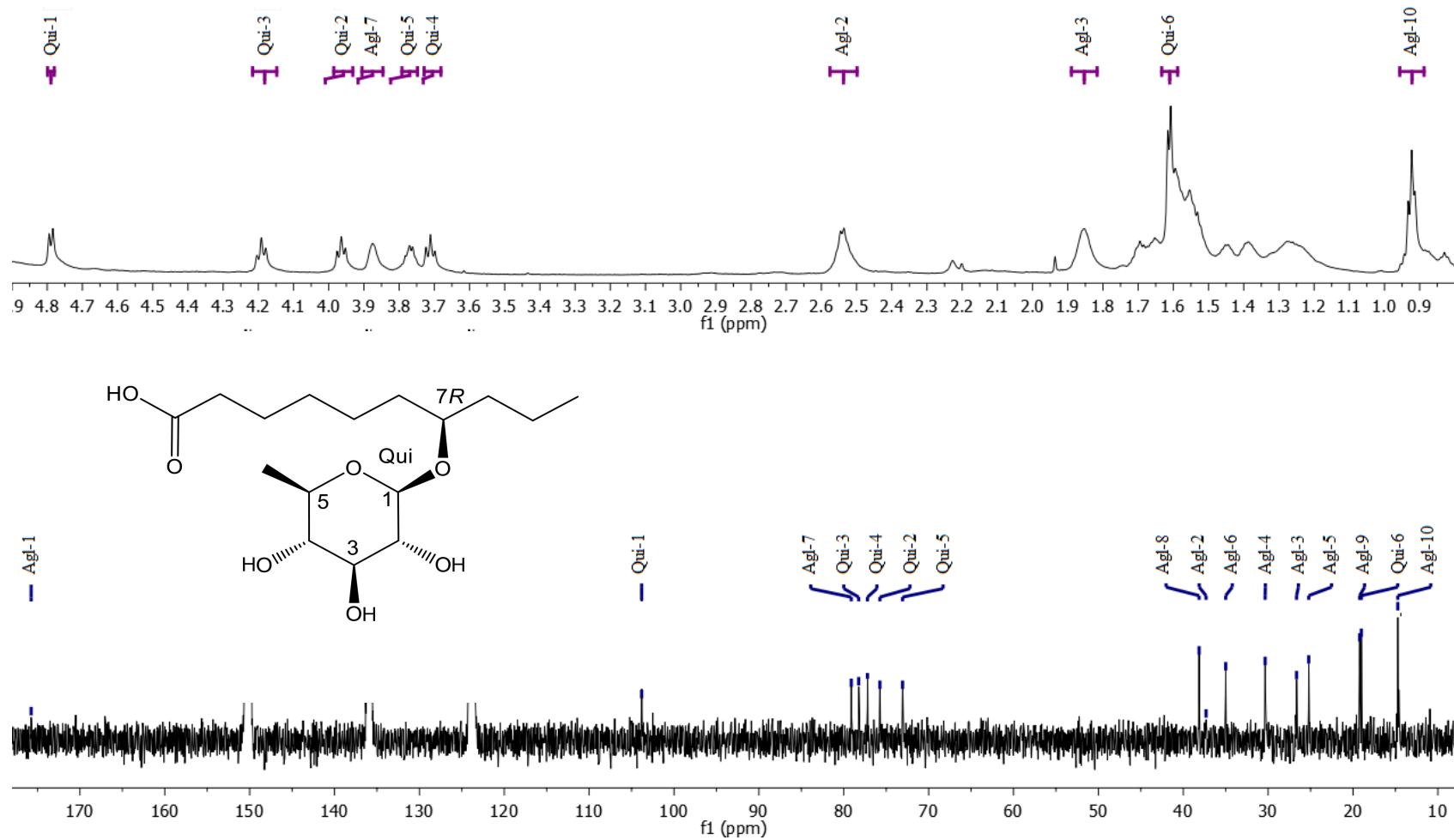
Figure S52. ¹H NMR (700 MHz) and ¹³C NMR spectra (175 MHz) of operculinic acid K (**5**) in pyridine-d_5.
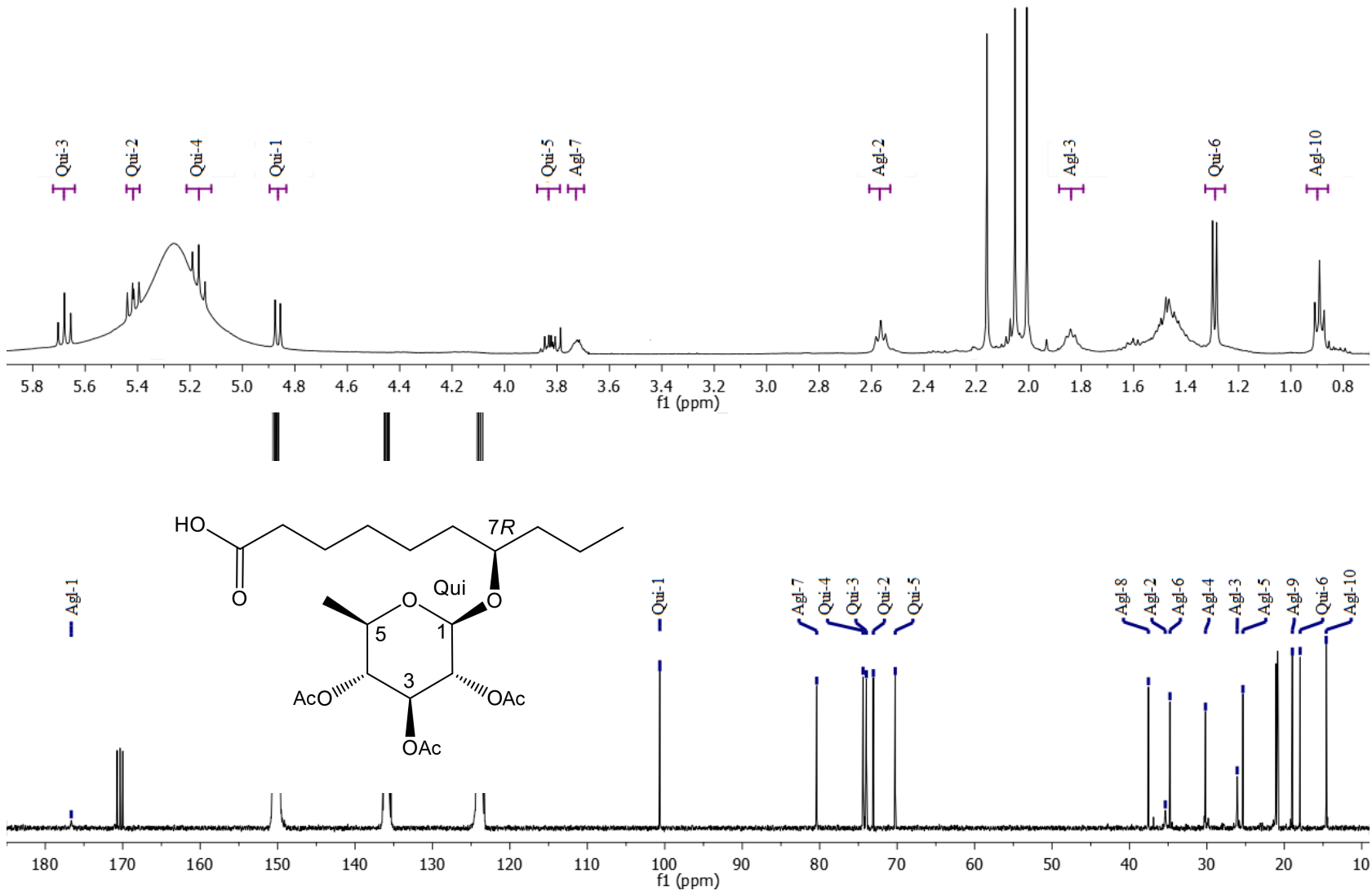
Figure S53. ¹H NMR (400 MHz) and ¹³C NMR spectra (100 MHz) of peracetylated operculinic acid K (**16**) in pyridine-d_5.
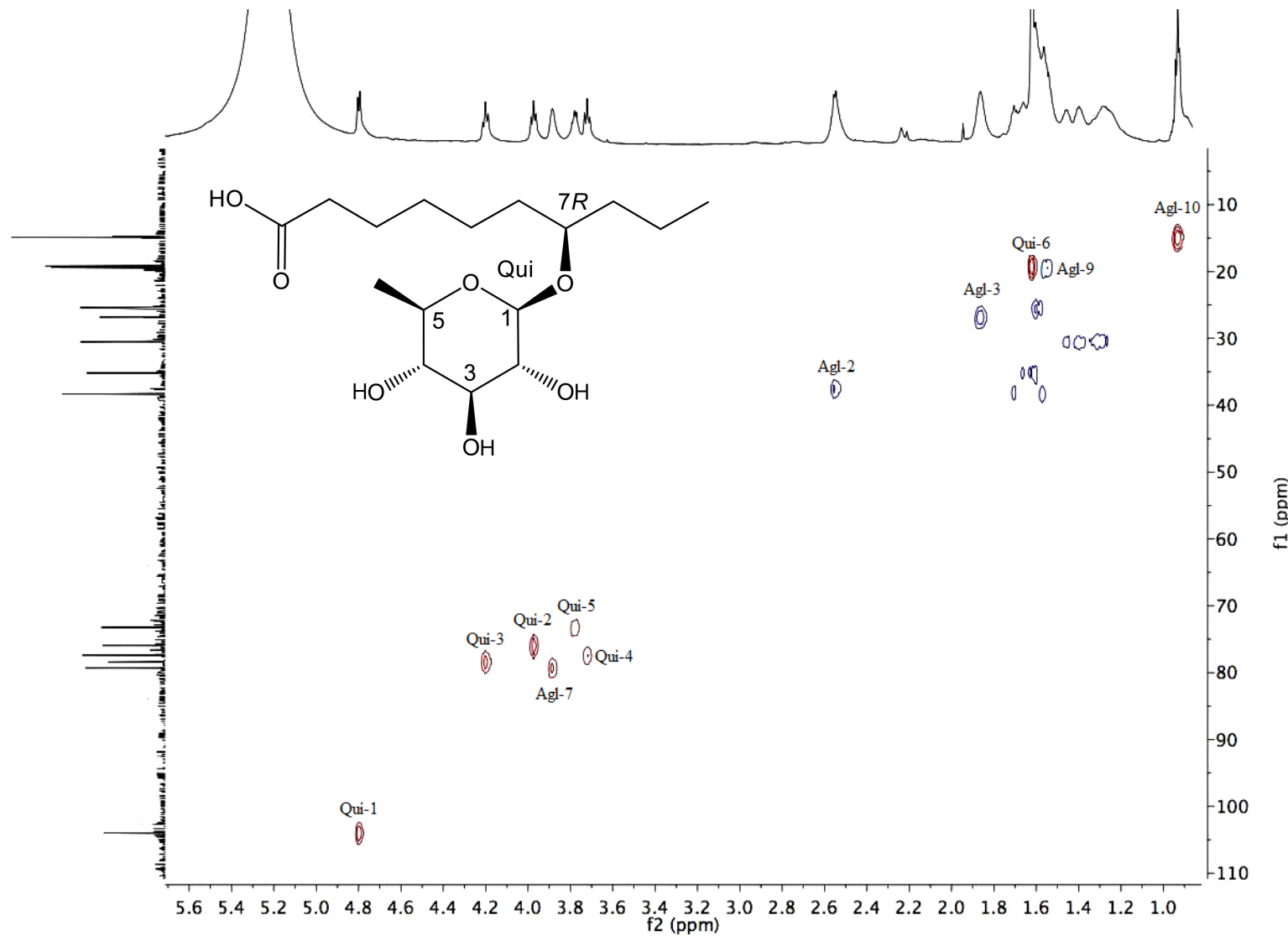
Figure S54. ¹H-Detected heteronuclear (¹J_{CH}) correlation (HSQC) spectrum for operculinic acid K (**5**) with high-resolution 1D ¹H (700 MHz) and ¹³C (175 MHz; anomeric region) projections in pyridine-d_5.
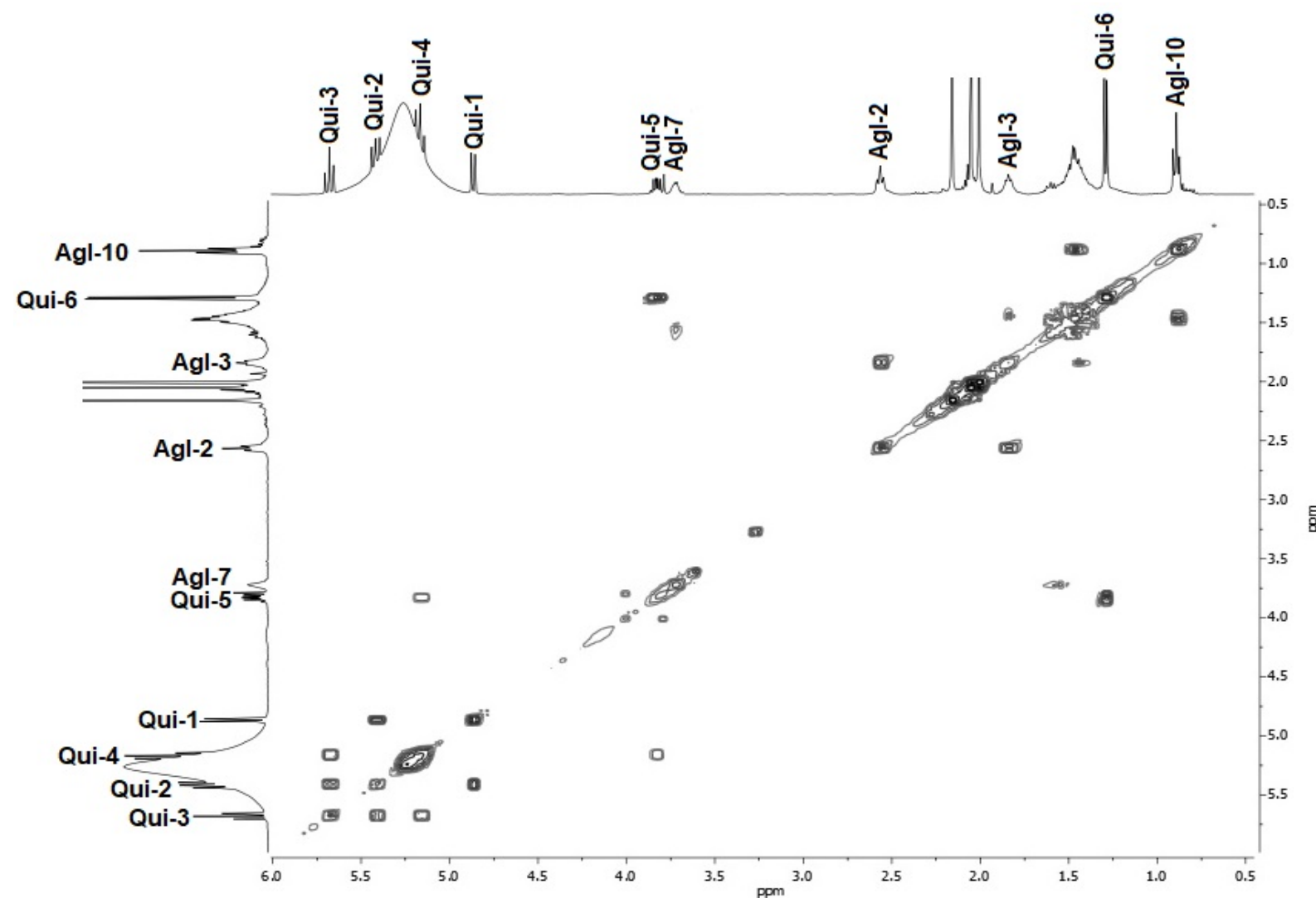
Figure S55. ¹H-Detected homonuclear total correlation (COSY) spectrum for the peracetylated derivative of operculinic acid K (**16**) with high resolution 1D projections (400 MHz) in pyridine-d_5.

S62

**Figure S56.** ^{1}H-Detected heteronuclear ($^1J_{CH}$) correlation (HSQC) spectrum for the peracetylated derivative of operculinic acid K (**16**) with high-resolution 1D ^{1}H (400 MHz) and ^{13}C (100 MHz) projections in pyridine-d_5.

S63
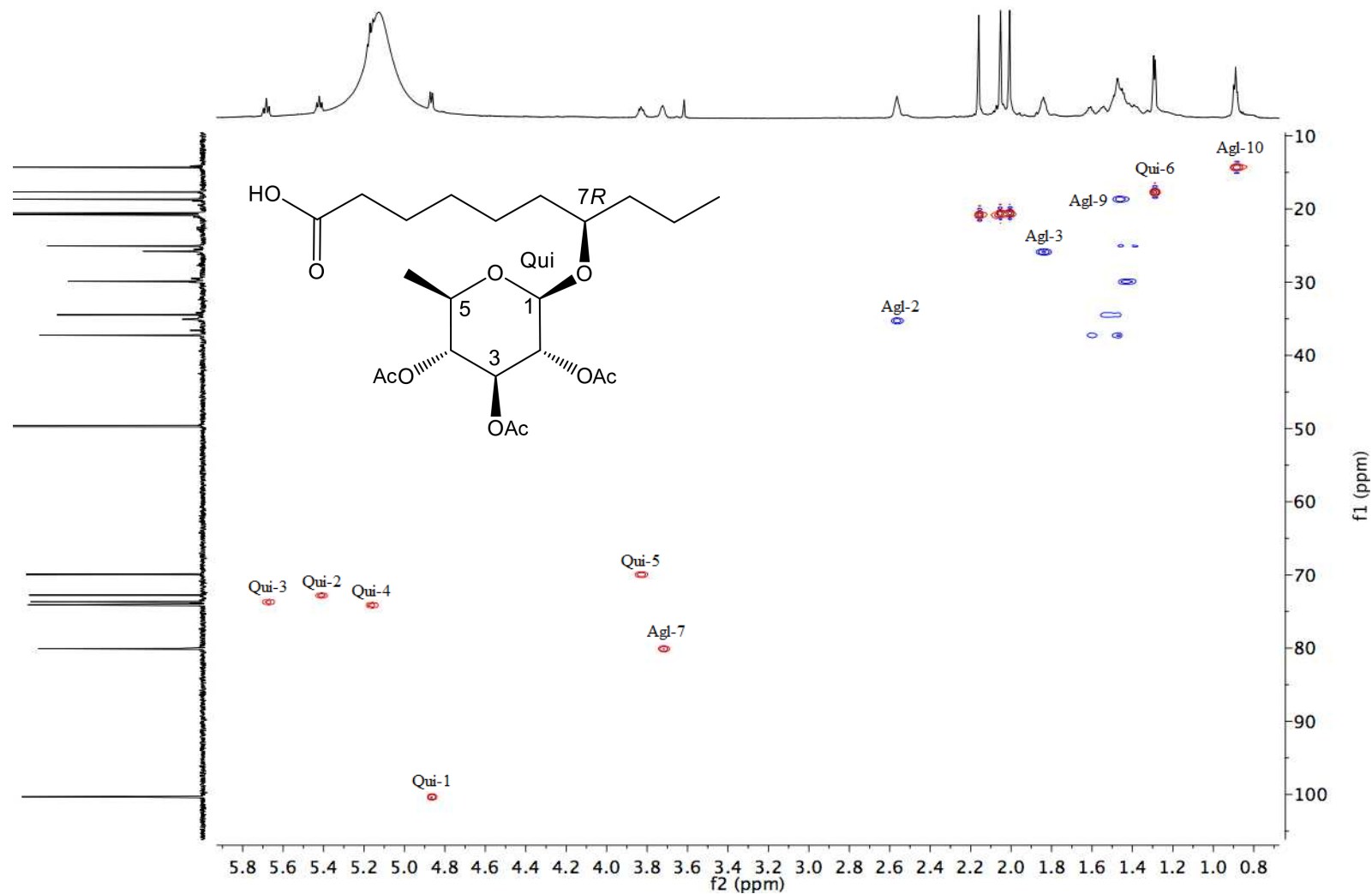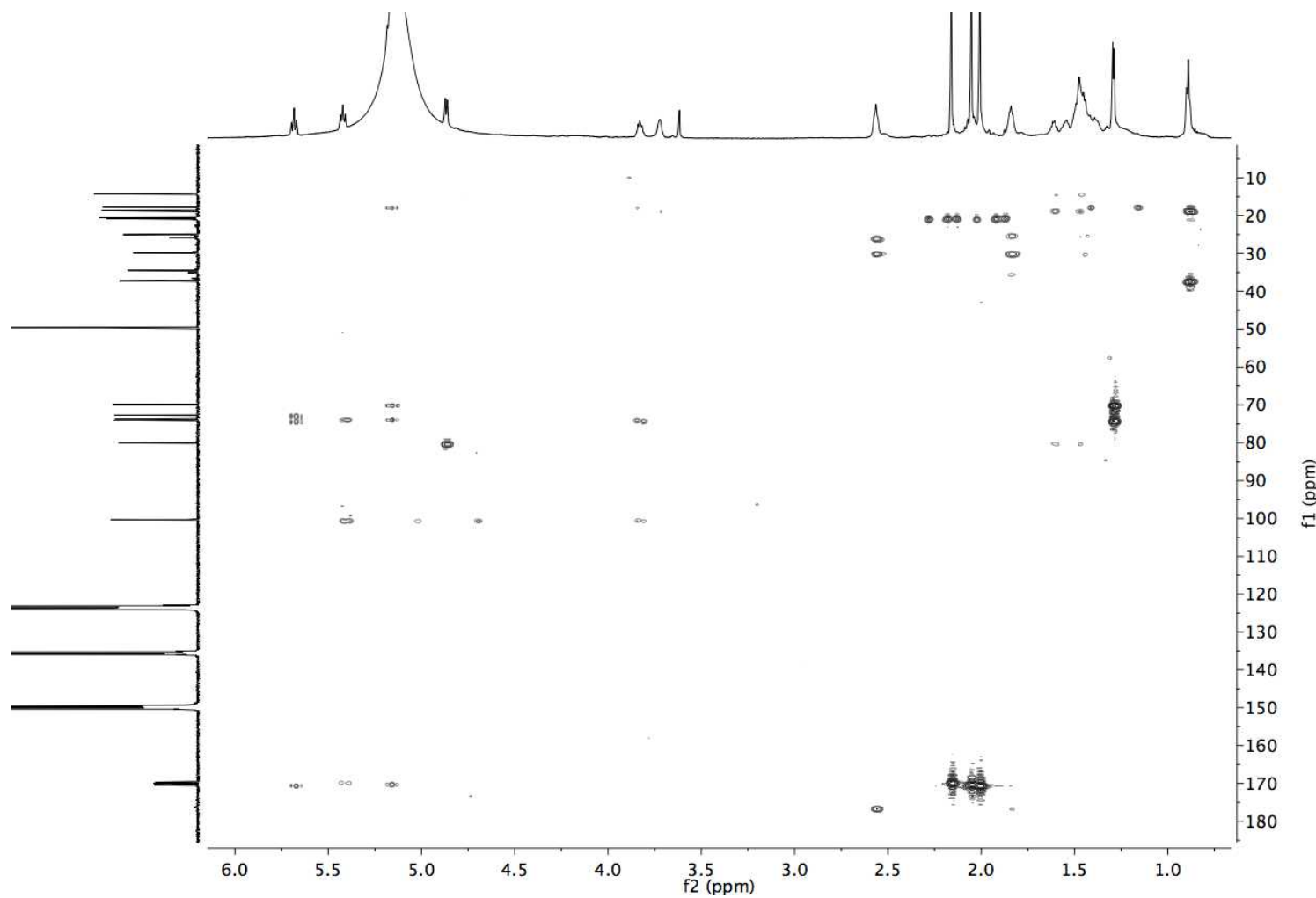
Figure S57. ¹H-detected heteronuclear ($^{2,3}J_{CH}$) correlation (HMBC) spectrum for the peracetylated derivative of operculinic acid K (**16**) with high-resolution 1D ¹H (400 MHz) and ¹³C (100 MHz) projections in pyridine-d_5.
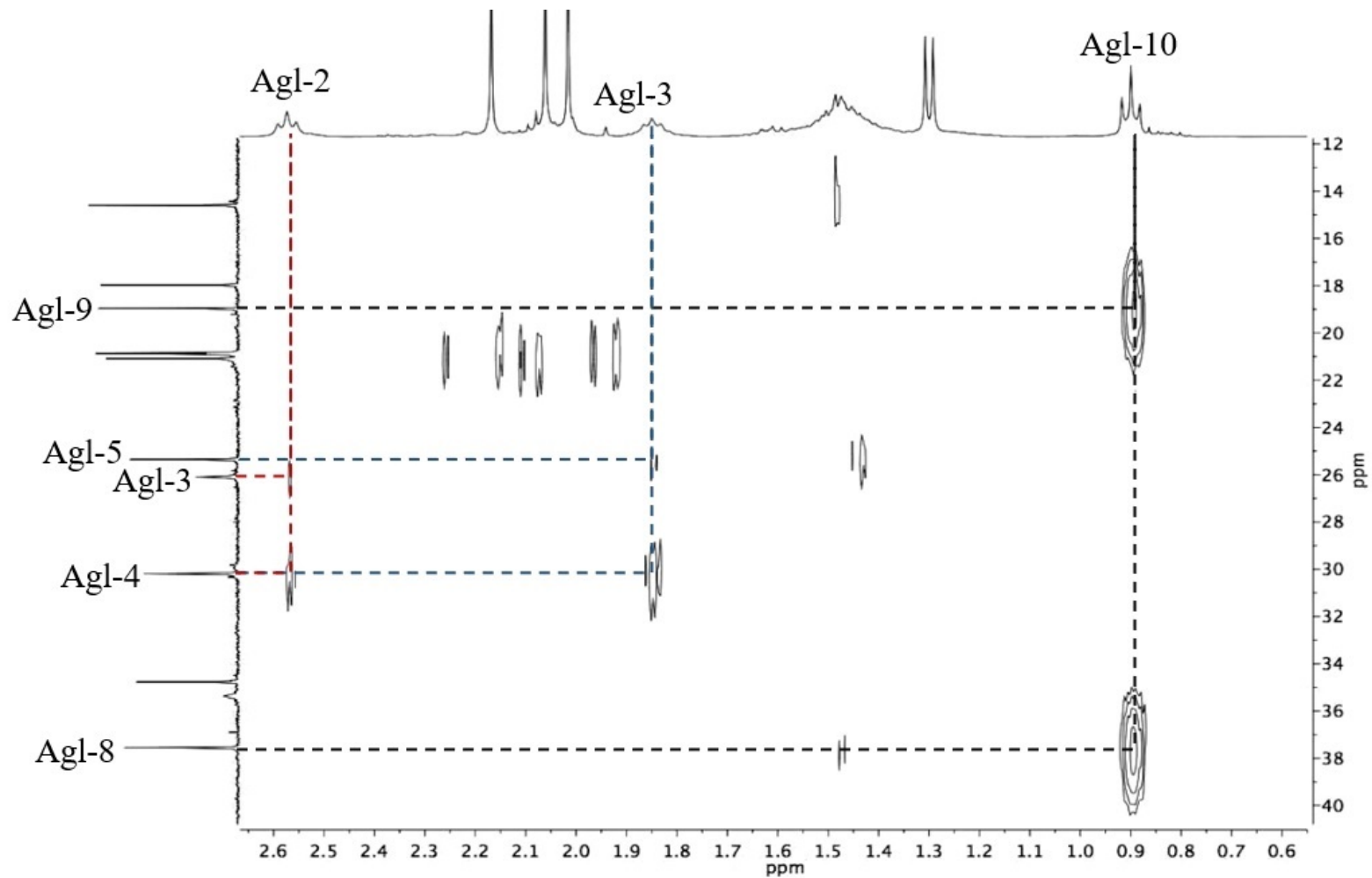
Figure S58. Expanded aglycone region of the ¹H-detected heteronuclear (³J_{CH}) correlation (HMBC) spectrum for the peracetylated derivative of operculinic acid K (**16**) with high-resolution 1D ¹H (400 MHz) and ¹³C (100 MHz) projections in pyridine-d_5.

Formula: $[C_{86}H_{124}O_{48}Na]^+$
Exact mass: 1947.71542
Accurate mass: 1947.71159
Mass accuracy: −1.9 ppm
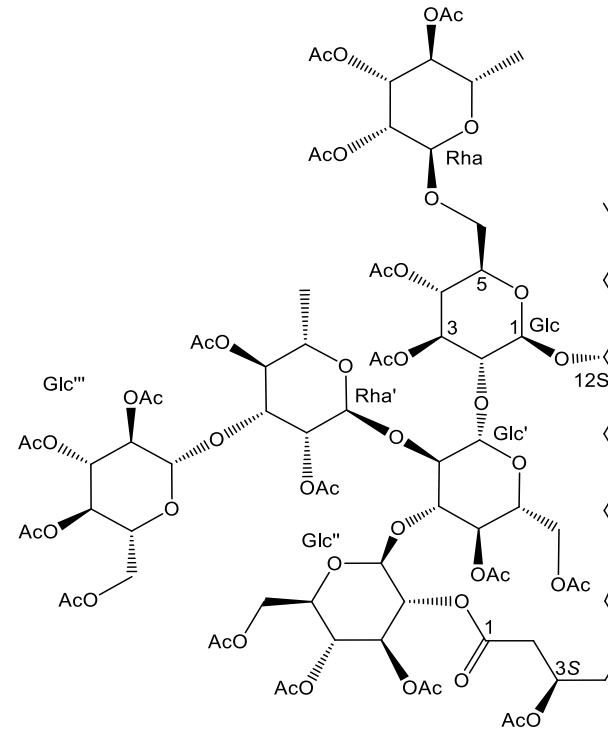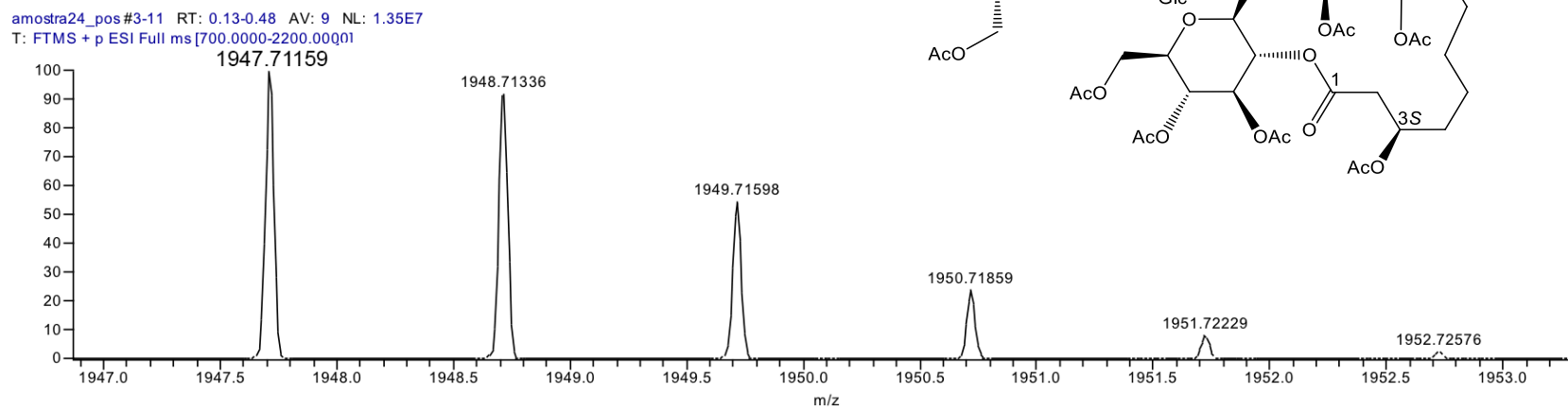
Figure S59. High-resolution positive ion mode ESI mass spectrum of peracetylated lactone derivative of operculinic acid H (**17**) showing isotopic distribution and relative abundances of the sodium adduct ion $[C_{86}H_{124}O_{48}Na]^+$.
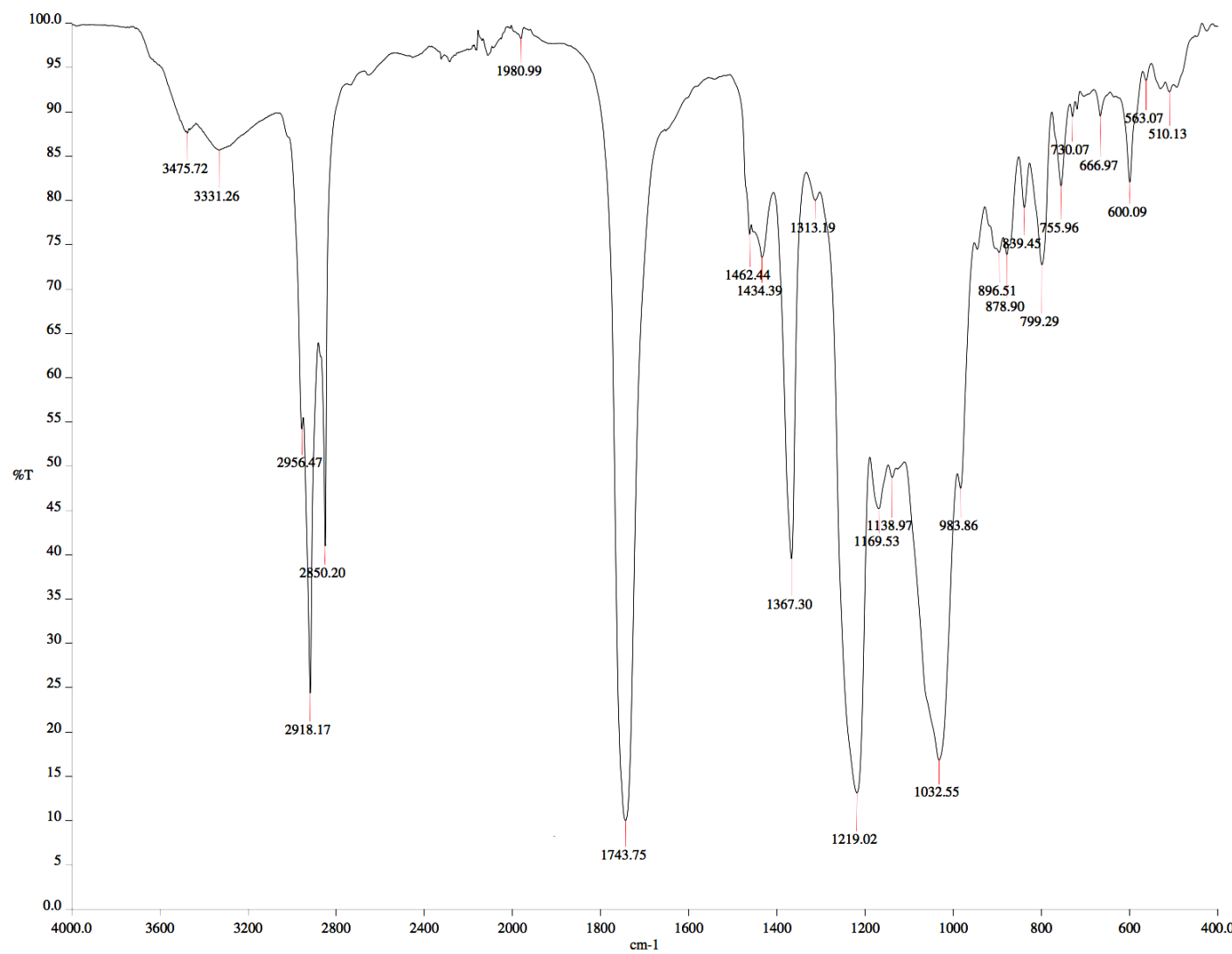
Figure S60. FTIR spectrum of the peracetylated lactone derivative of operculinic acid H (**17**) in CHCl₃.
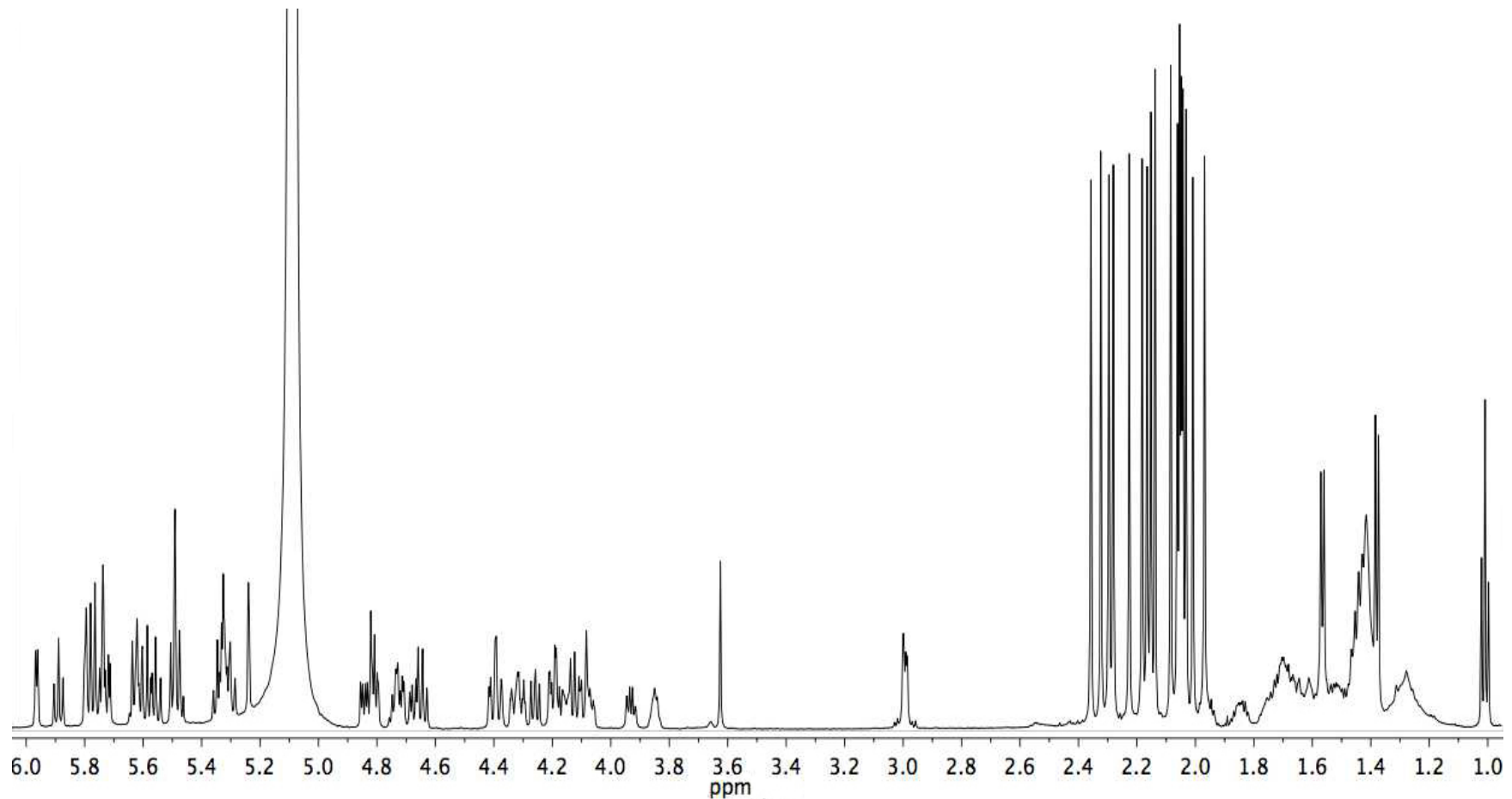
Figure S61. ¹H NMR spectra (600 MHz) of the peracetylated lactone derivative of operculinic acid H (**17**) in pyridine-d_5
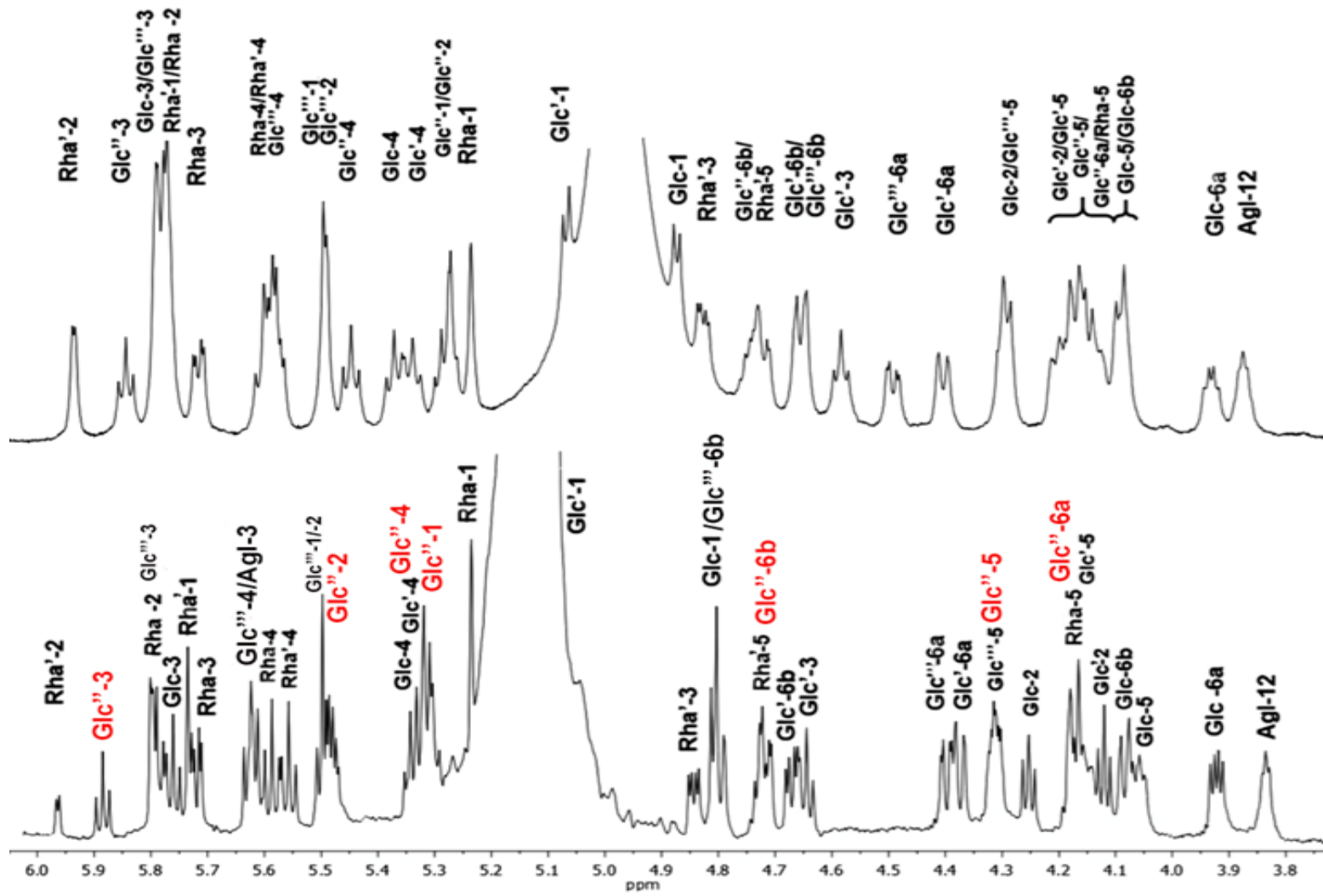
Figure S62. ¹H NMR spectra for the oligosaccharide core of peracetylated derivatives of operculinic acids H (**12**, 700 MHz; above) and peracetylated lactone derivative of operculinic acid H (**17**, 800 MHz, below) in pyridine-d_5.
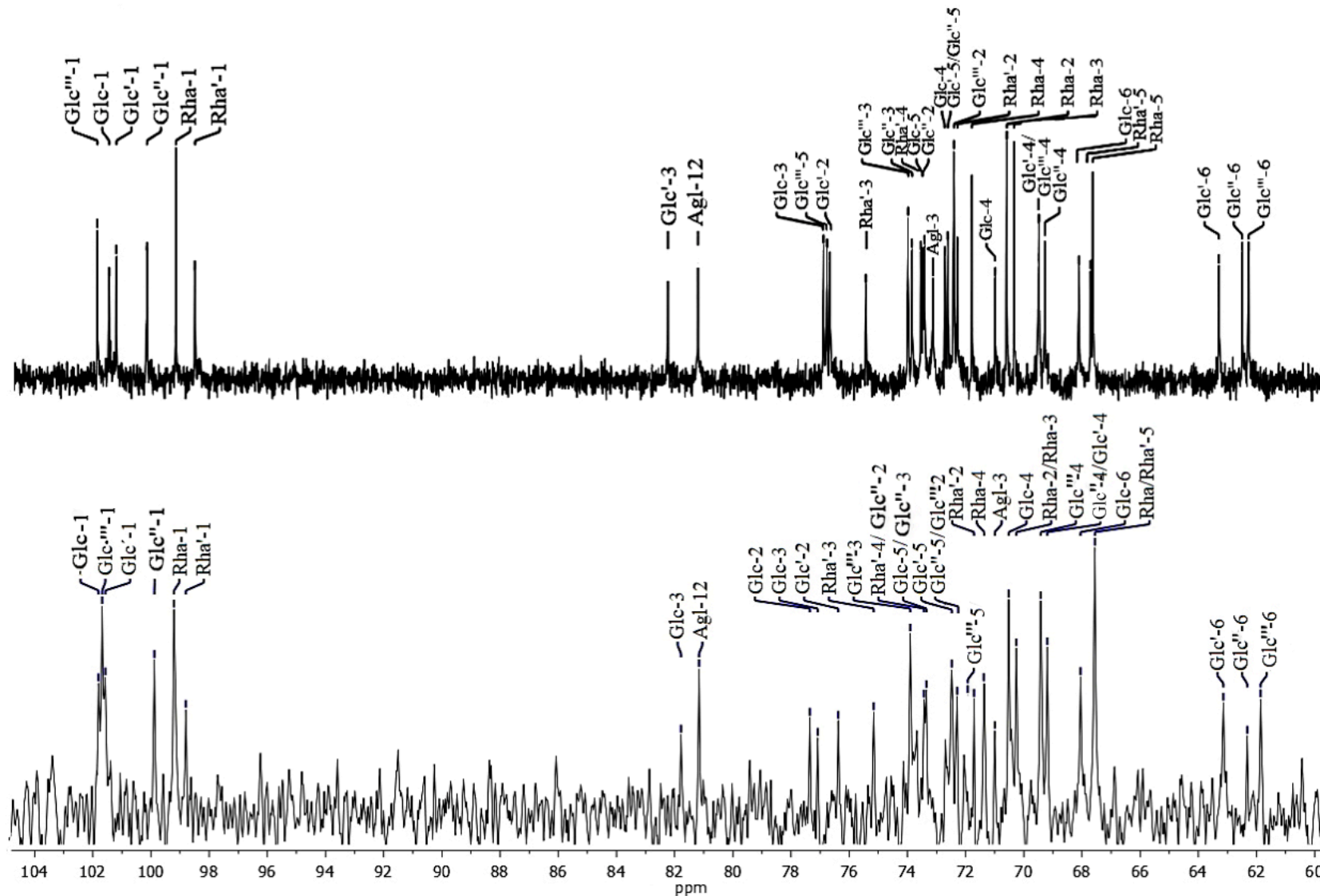
Figure S63. ^{13}C NMR spectra for the oligosaccharide core (δ 105-60 ppm) of peracetylated derivatives of operculinic acids H (**12**, 175 MHz, above) and peracetylated lactone derivative of operculinic acid H (**17**, 200 MHz, below) in pyridine-d_5.
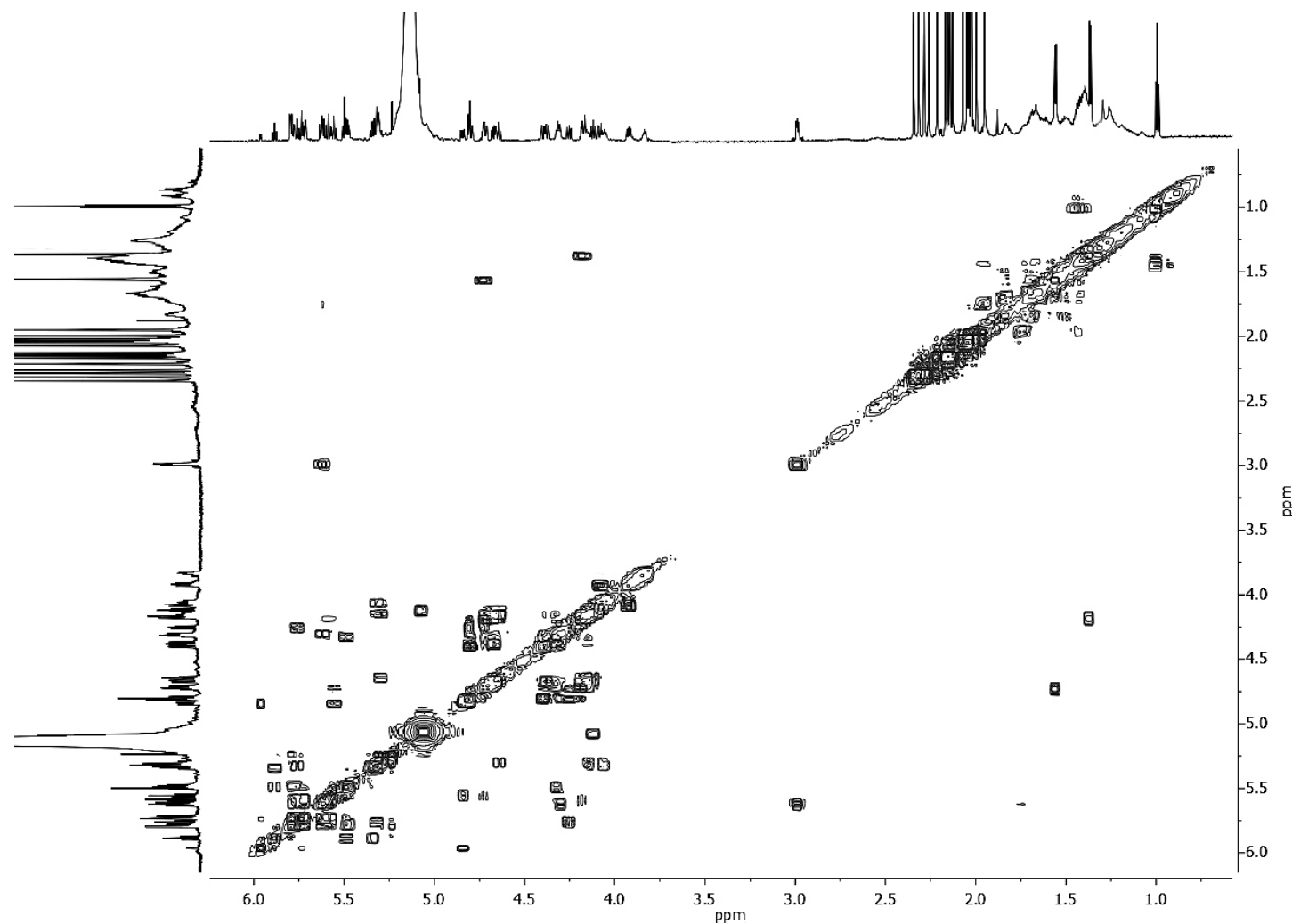
Figure S64. ^{1}H-Detected homonuclear $^3J_{HH}$ correlation (COSY) spectrum for the peracetylated lactone derivative of operculinic acid H (**17**) with high resolution 1D projections (800 MHz) in pyridine-d_5
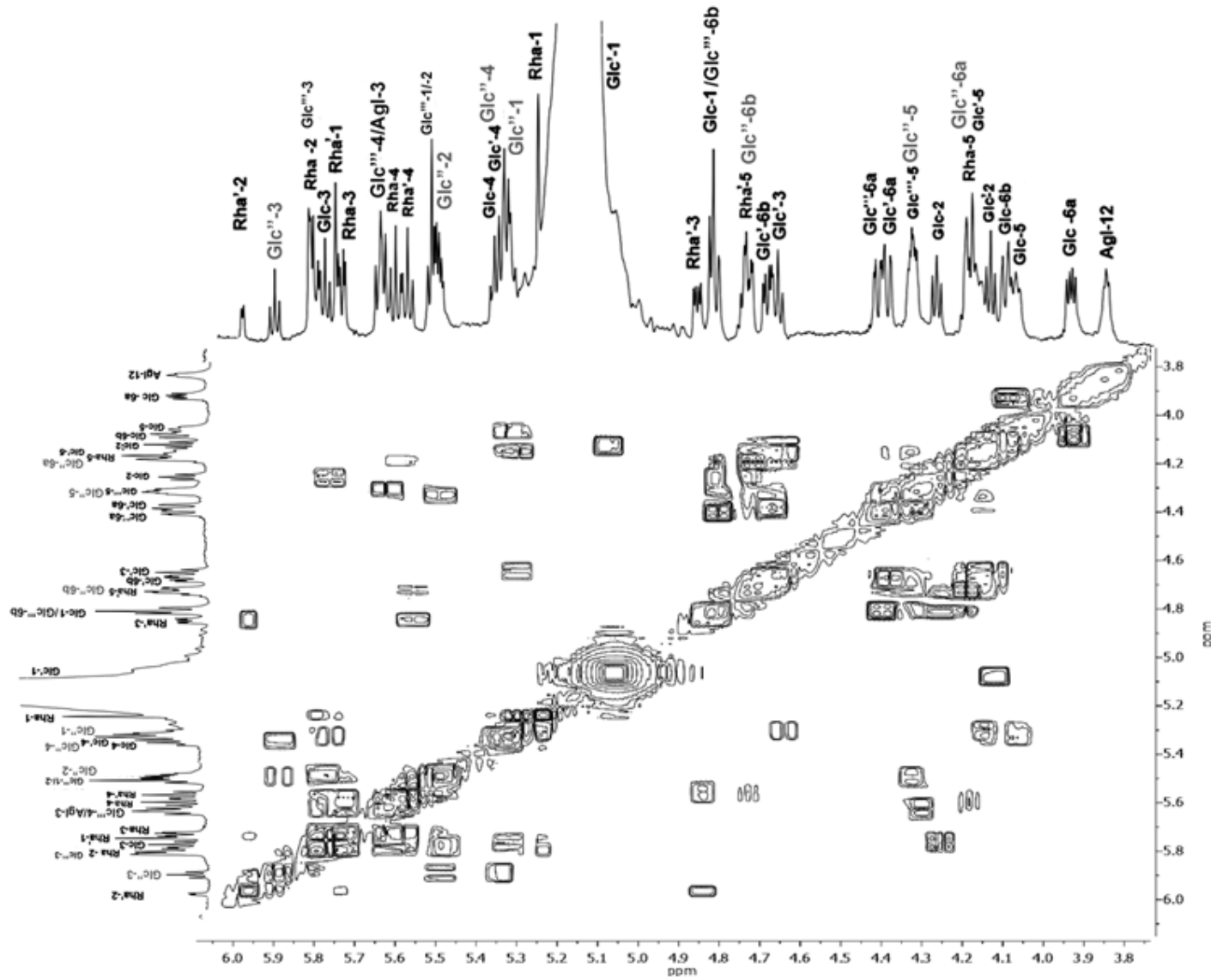
Figure S65. Expanded oligosaccharide core region of the ¹H-detected homonuclear ($^3J_{HH}$) correlation (COSY) spectrum the peracetylated lactone derivative of operculinic acid H (**17**) with high resolution 1D projections (800 MHz) in pyridine-d_5.
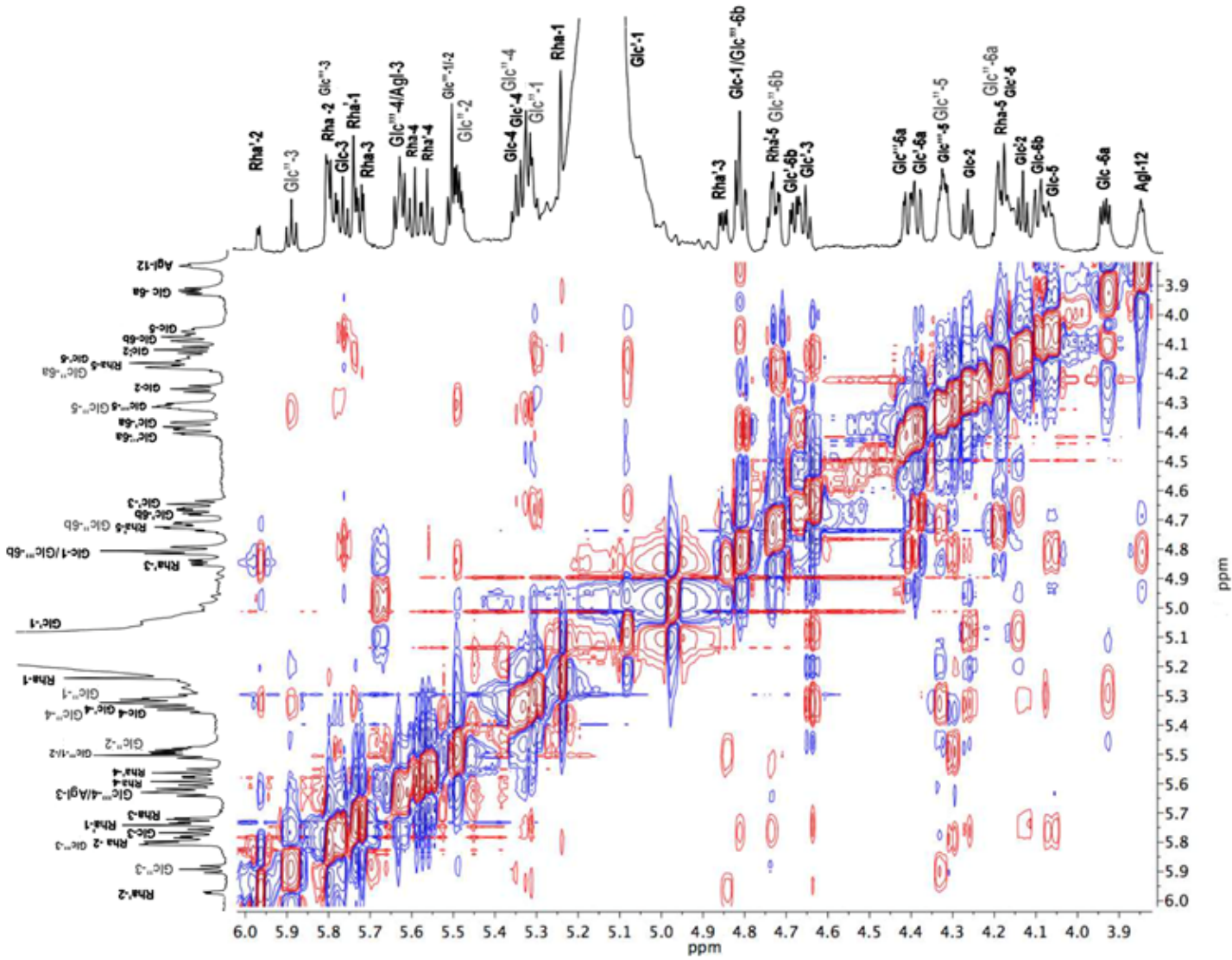
Figure S66. Expanded oligosaccharide core region of the ¹H-detected homonuclear ($^{3}J_{HH}$) correlation (NOESY) spectrum the peracetylated lactone derivative of operculinic acid H (**17**).
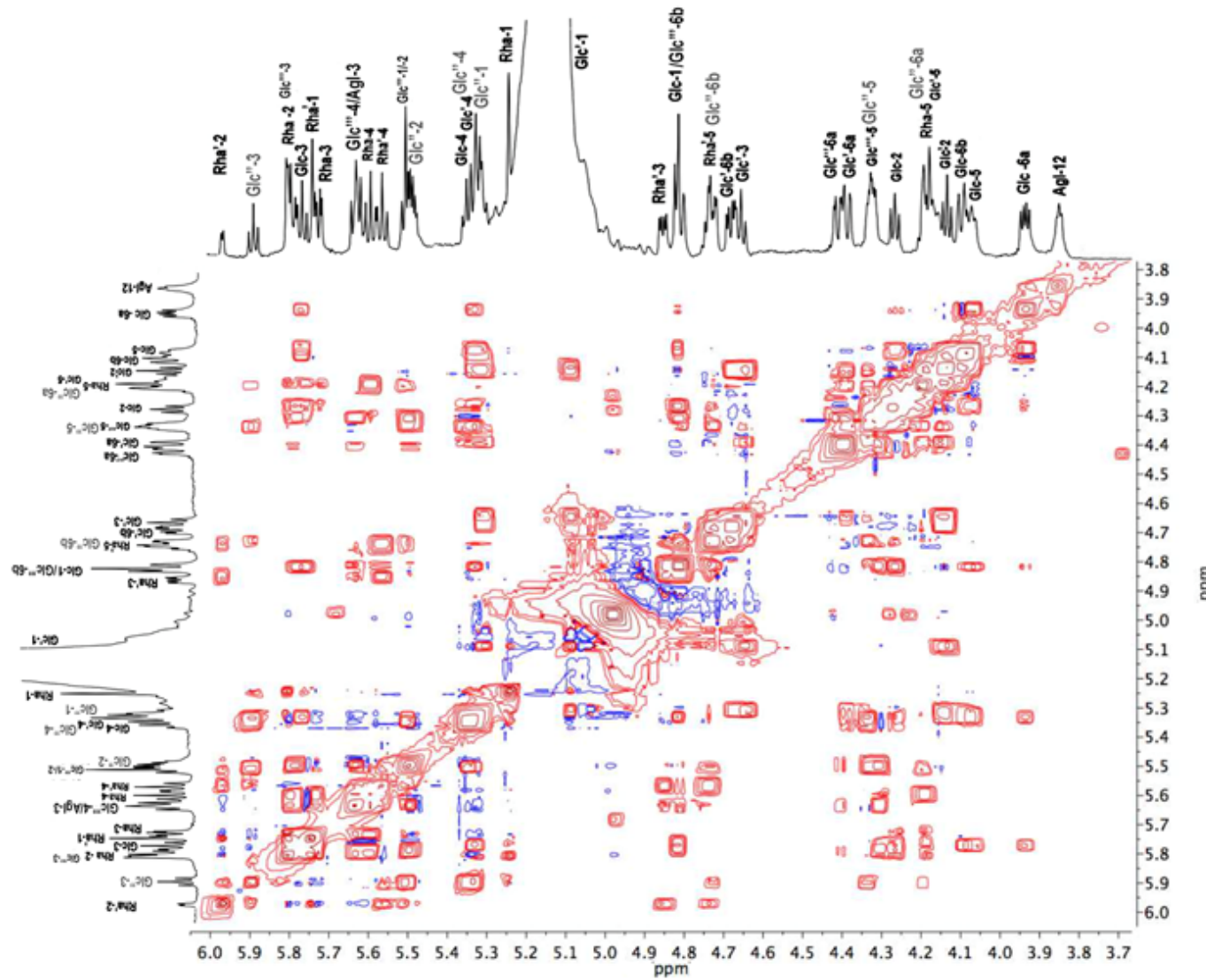
**Figure S67.** Expanded oligosaccharide core region of the ¹H-detected homonuclear total correlation (TOCSY) spectrum for the peracetylated derivative of operculinic acid K (**17**) with high resolution 1D projections (800 MHz) in pyridine-d_5.
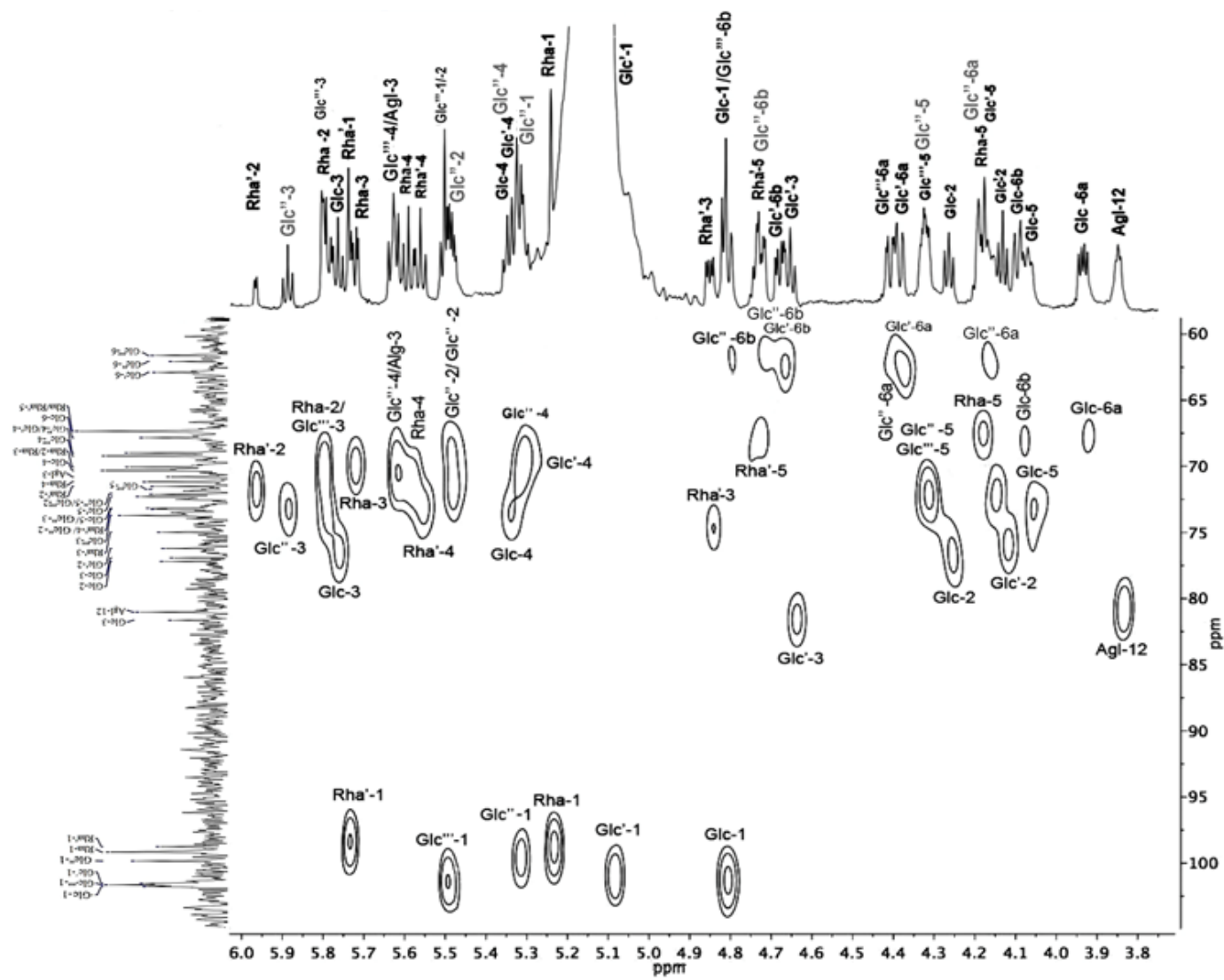
Figure S68. Expanded oligosaccharide core region of the ¹H-detected heteronuclear ($^1J_{CH}$) correlation (HSQC) spectrum for the peracetylated lactone derivative of operculinic acid H (**17**) with high-resolution 1D ¹H (800 MHz) and ¹³C (200 MHz) projections in pyridine-d_5.
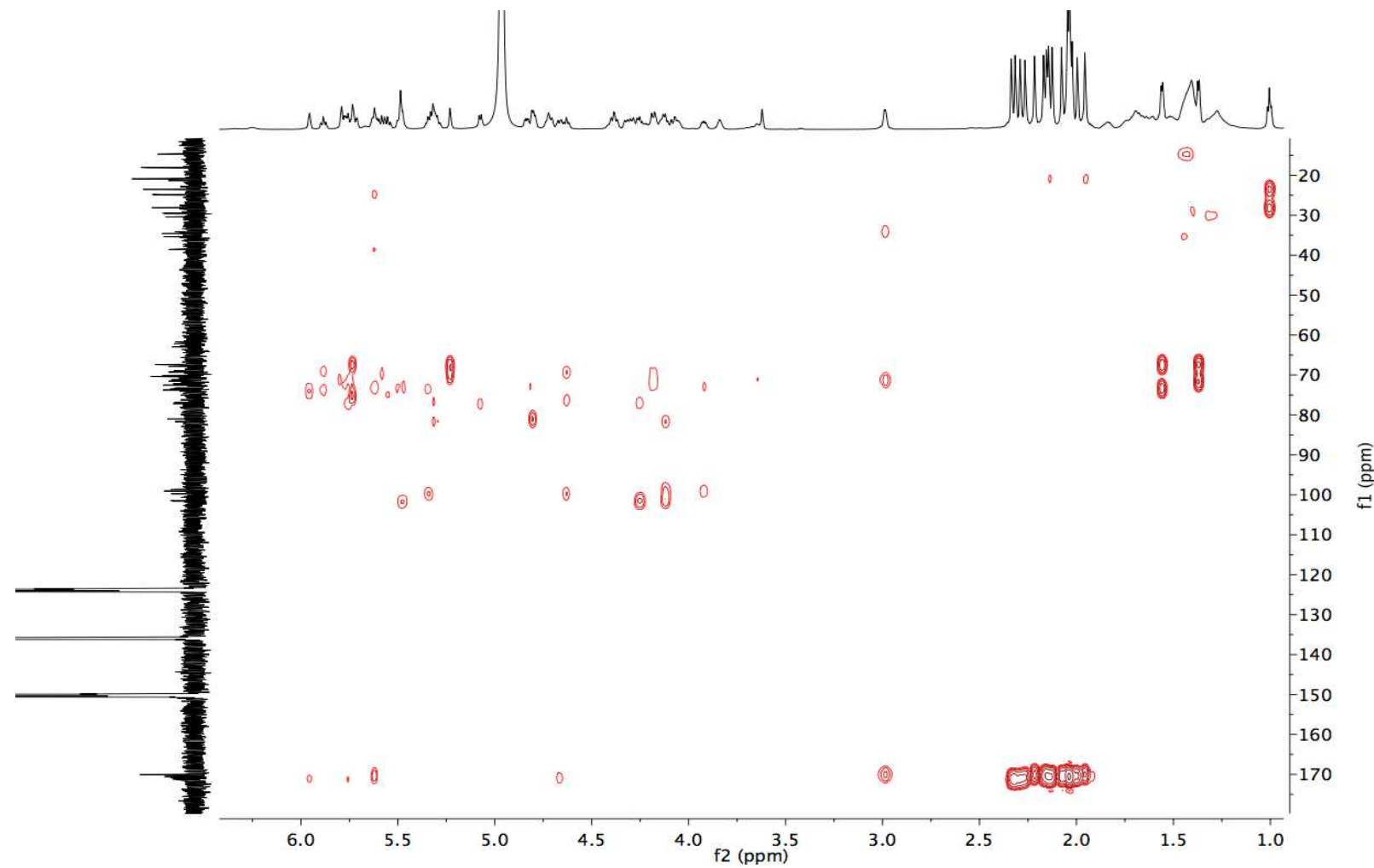
Figure S69. ^{1}H-detected heteronuclear ($^{2,3}J_{CH}$) correlation (HMBC) spectrum for the peracetylated lactone derivative of operculinic acid H (**17**) with high-resolution 1D ^{1}H (700 MHz) and ^{13}C (175 MHz) projections in pyridine-d_5.
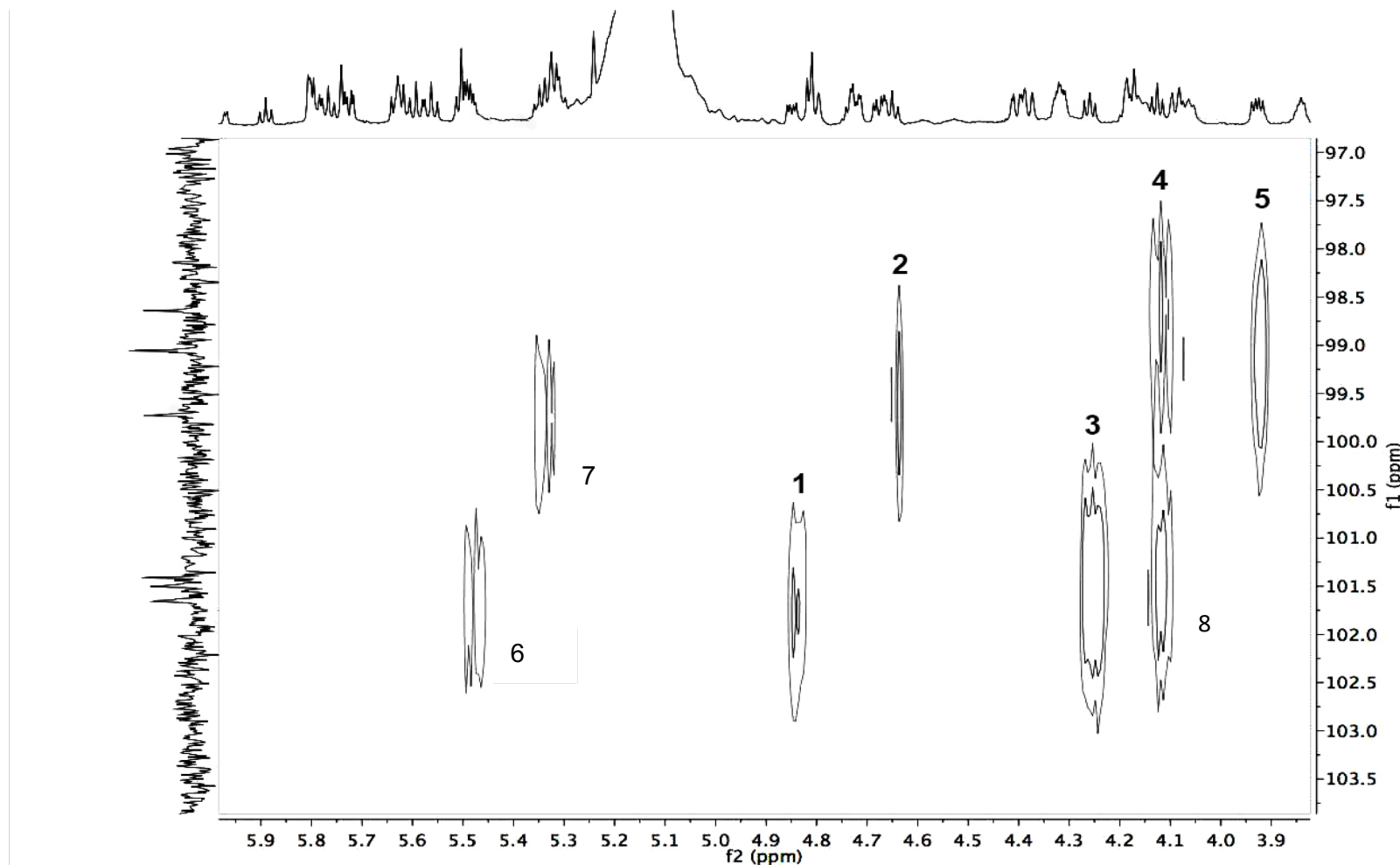
Figure S70. Expanded oligosaccharide core region of the ^{1}H-detected heteronuclear ($^{2,3}J_{CH}$) correlation (HMBC) spectrum for the peracetylated lactone derivative of operculinic acid H (**17**) with high-resolution 1D ^{1}H (800 MHz) and ^{13}C (200 MHz; anomeric region) projections in pyridine-d_5. Connectivity assignments for the glycosylation sequence ($^3J_{CH}$): **1**, H$_3$-Rha′/C$_1$- Glc‴; **2**, H$_3$-Glc′/C$_1$-Glc″; **3**, H$_2$-Glc/C$_1$-Glc′; **4**, H$_2$-Glc′/C$_1$-Rha′; **5**, H$_{6a}$-Glc/C$_1$-Rha; Additional cross-peaks ($^2J_{CH}$): **6**, C$_1$-Glc‴/H$_2$-Glc‴; **7**, C$_1$-Glc″/H$_2$-Glc″; **8**, H$_2$-Glc′/C$_1$-Glc′.
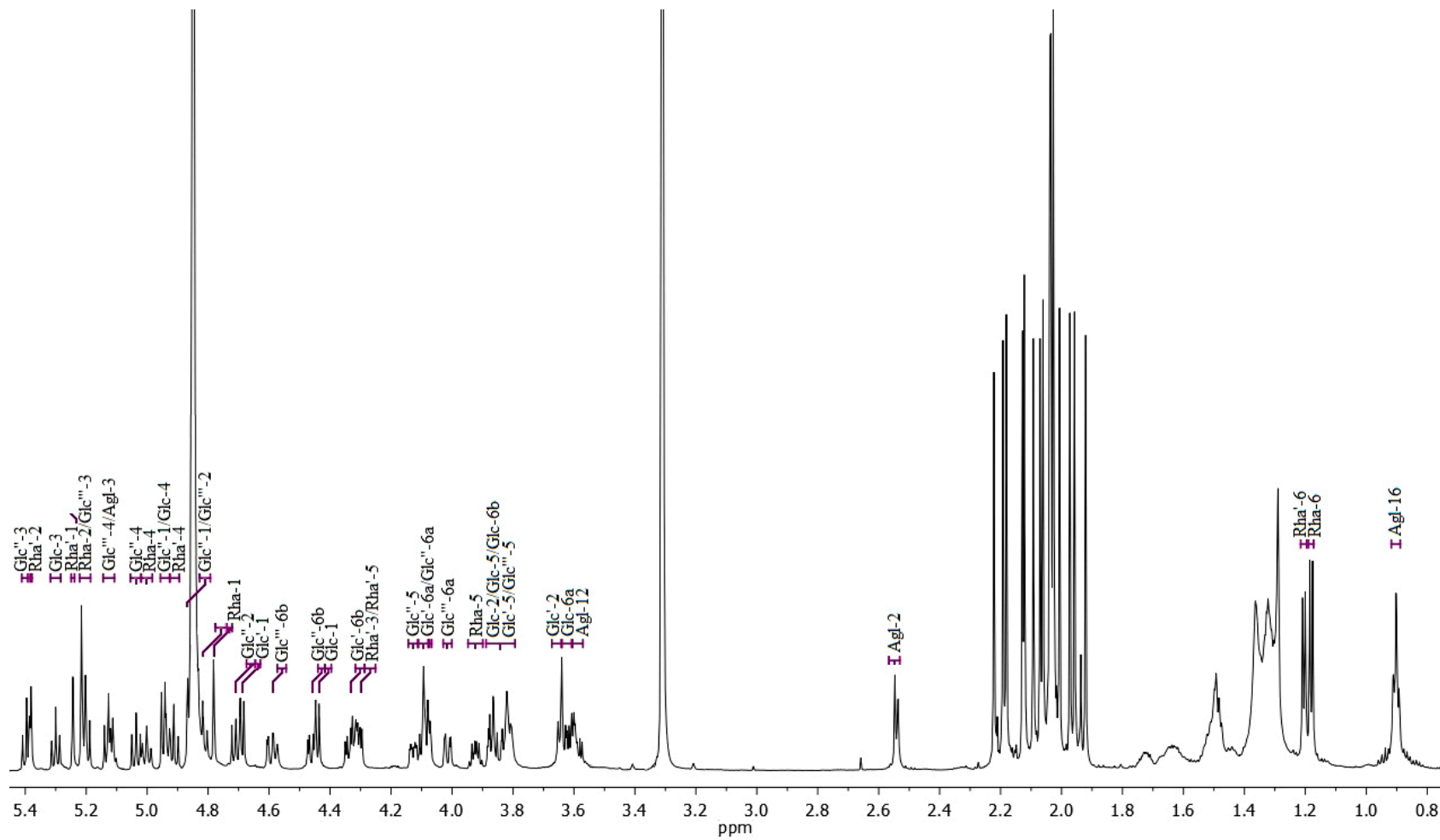
Figure S71. ¹H NMR spectra for the oligosaccharide core of the peracetylated lactone derivative of operculinic acid H (**17**, 700 MHz, below) in methanol-d_4.
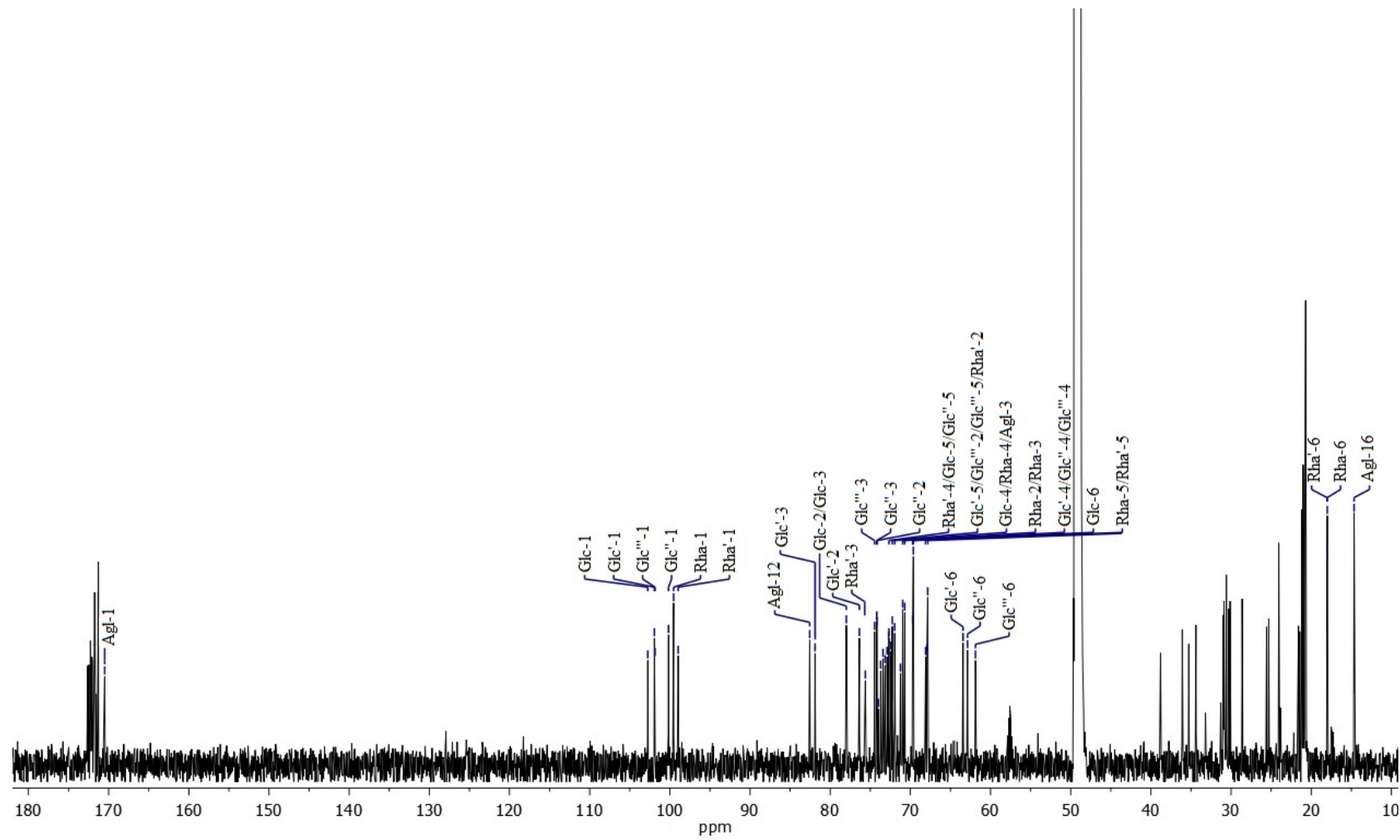
Figure S72. ^{13}C NMR spectra of the peracetylated lactone derivative of operculinic acid H (**17**, 175 MHz) in methanol-d_4.
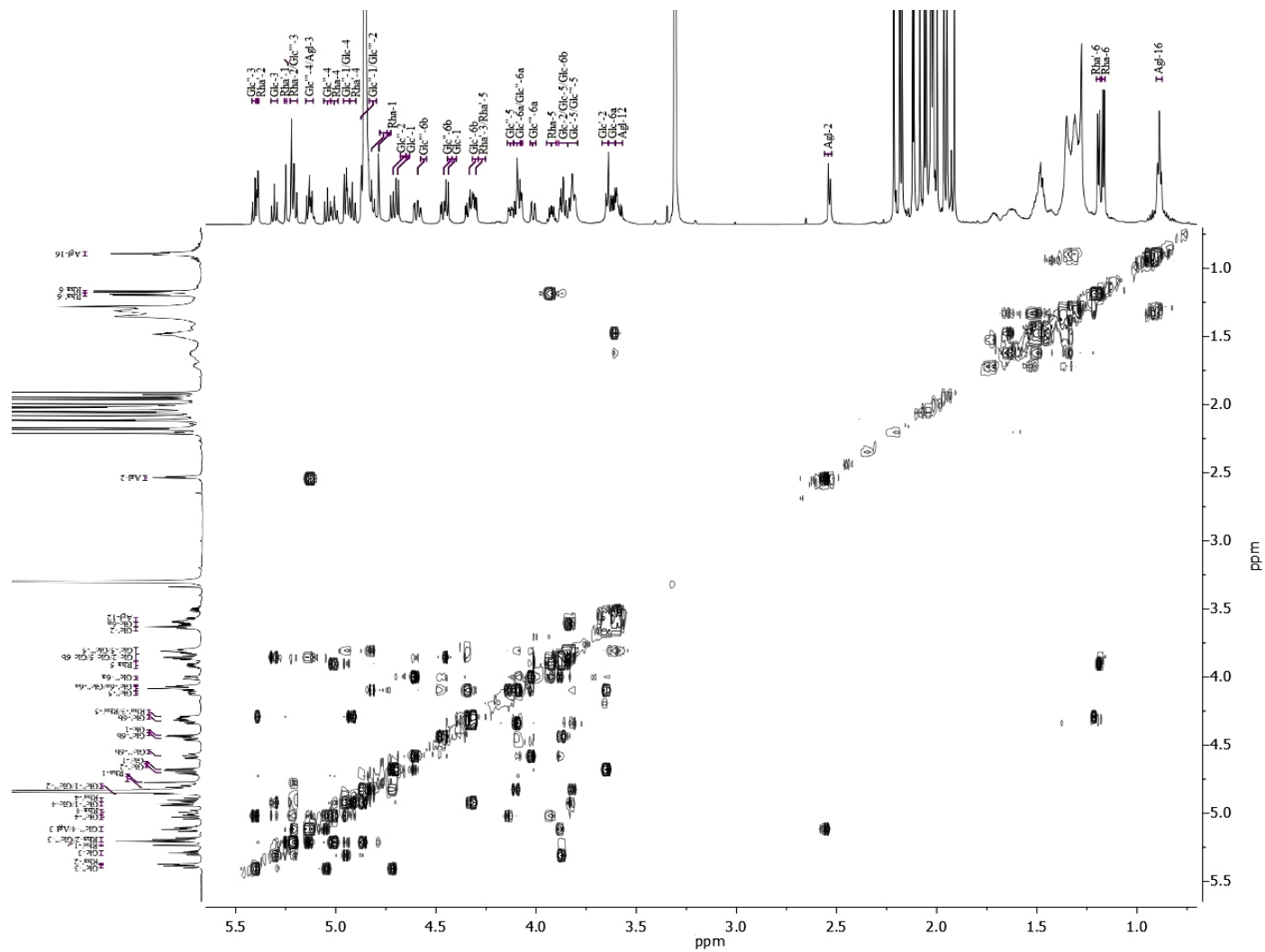
Figure S73. ^{1}H-Detected homonuclear $^3J_{HH}$ correlation (COSY) spectrum for the peracetylated lactone derivative of operculinic acid H (**17**) with high resolution 1D projections (700 MHz) in methanol-d_4.
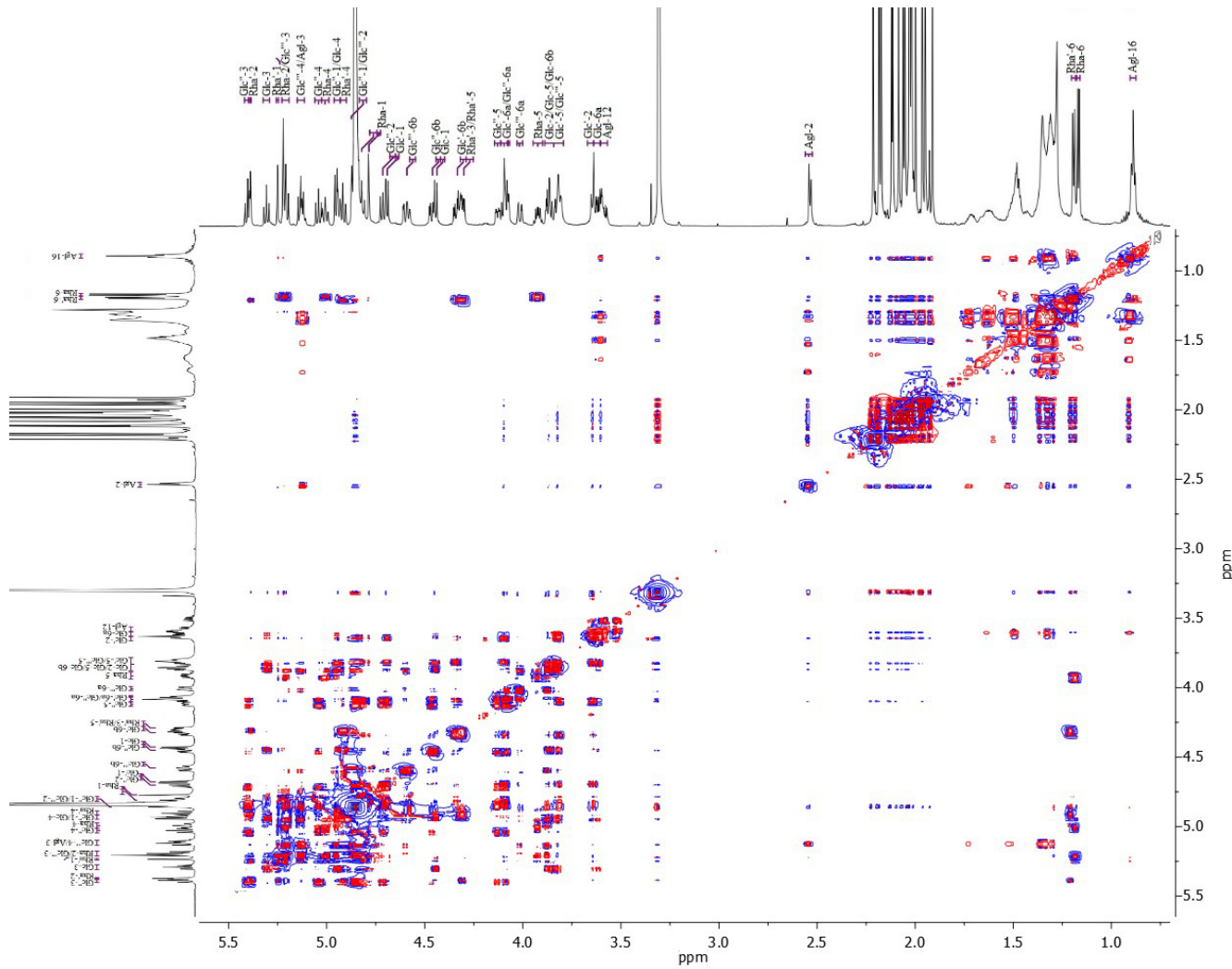
Figure S74. Expanded oligosaccharide core region of the ¹H-detected homonuclear total correlation (TOCSY) spectrum for the peracetylated lactone derivative of operculinic acid H (**17**) with high resolution 1D projections (700 MHz) in methanol-d_4

S81
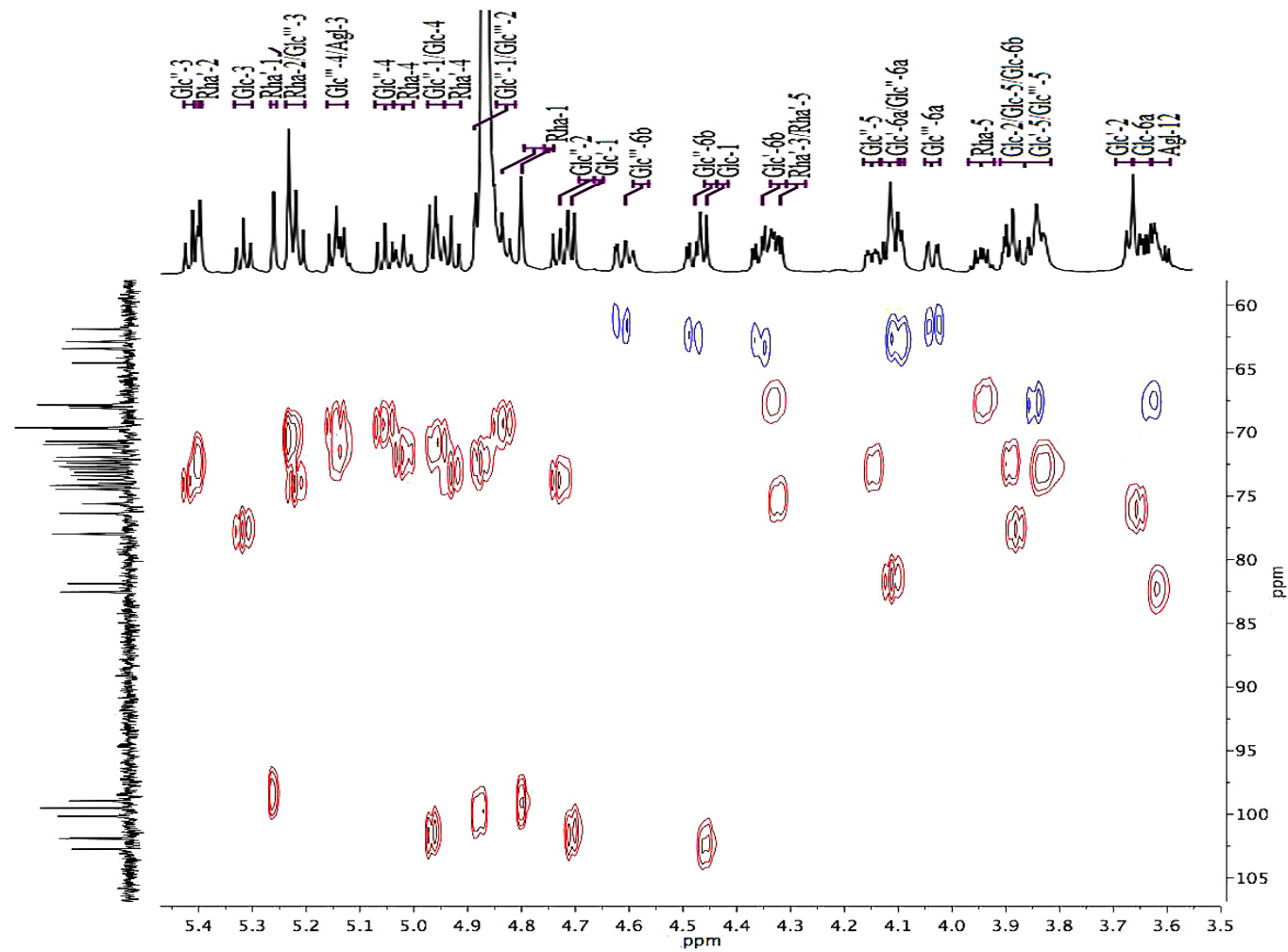
Figure S75. Expanded oligosaccharide core region of the ¹H-detected heteronuclear ($^1J_{CH}$) correlation (HSQC) spectrum for the peracetylated lactone derivative of operculinic acid H (**17**) with high-resolution 1D ¹H (700 MHz) and ¹³C (175 MHz) projections in methanol-d_4.
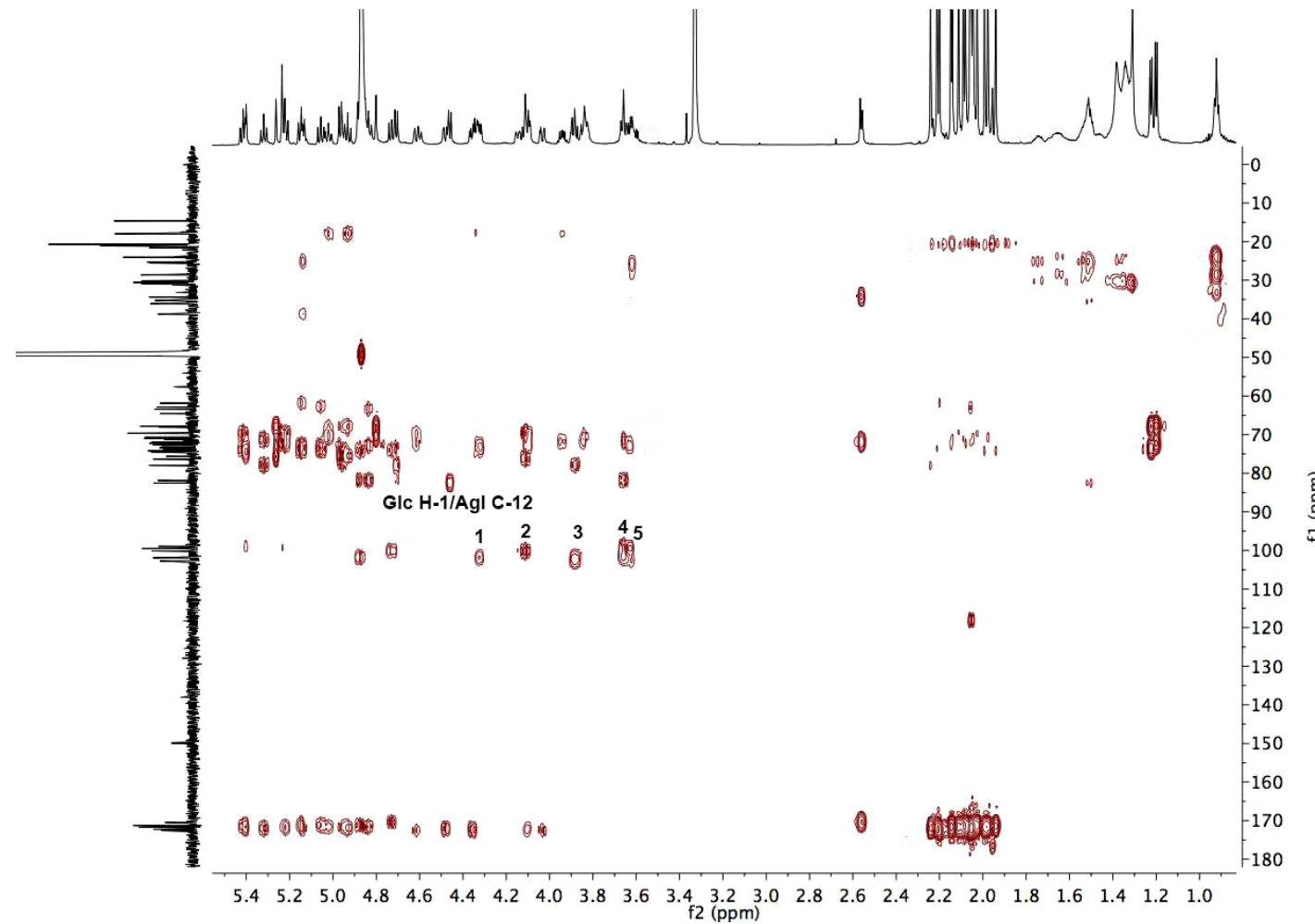
Figure S76. ^{1}H-detected heteronuclear ($^{2,3}J_{CH}$) correlation (HMBC) spectrum for the peracetylated lactone derivative of operculinic acid H (**17**) with high-resolution 1D ^{1}H (700 MHz) and ^{13}C (175 MHz) projections in pyridine-d_5. See Figure S52 for cross-peak assignments.
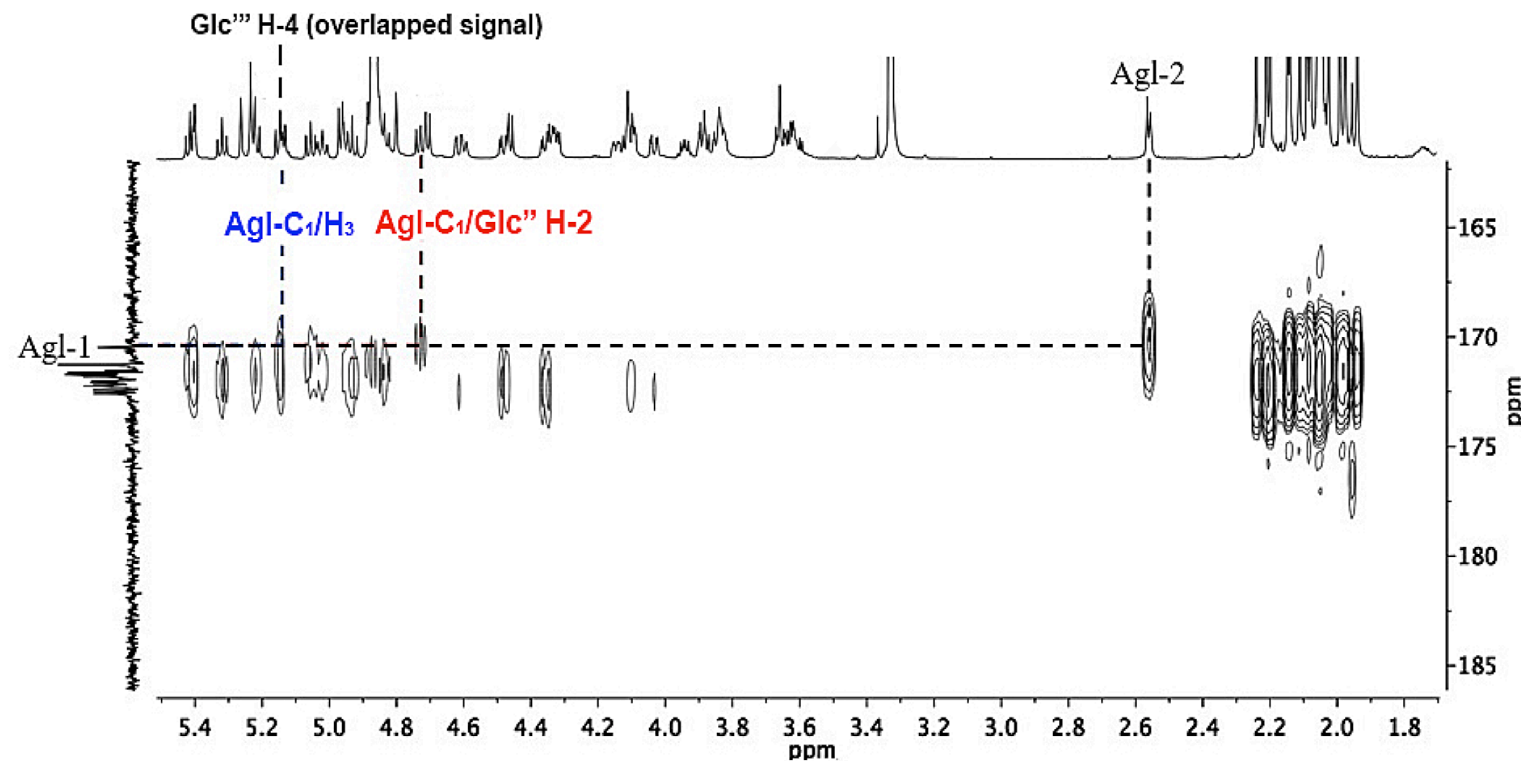
Figure S77. Expanded ^{1}H-detected heteronuclear ($^{2,3}J_{CH}$) correlation (HMBC) spectrum for the peracetylated lactone derivative of operculinic acid H (**17**) with high-resolution 1D ^{1}H (700 MHz) and ^{13}C (175 MHz; carbonyl signals) projections in methanol-d_4.

Formula: $[C_{86}H_{124}O_{48}Na]^+$
Exact mass: 1947.71542
Accurate mass: 1947.71870
Mass accuracy: +1.7 ppm
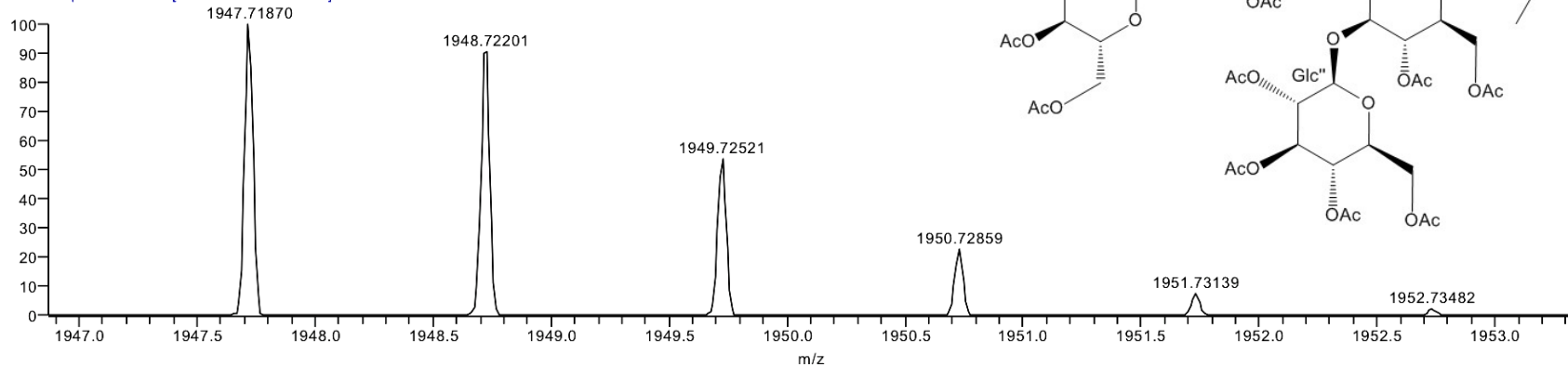
Figure S78. High-resolution positive ion mode ESI mass spectrum of peracetylated dehydrated operculinic acid H (**18**) showing isotopic distribution and relative abundances of the sodium adduct ion $[C_{86}H_{124}O_{48}Na]^+$.

Figure S79. EIMS of silylated 12-hydroxy-2-hexadecenoic acid methyl ester: m/z 299 ($[C_{13}H_{22}O_3TMS]^+$) and 159 ($[C_5H_{10}OTMS]^+$).
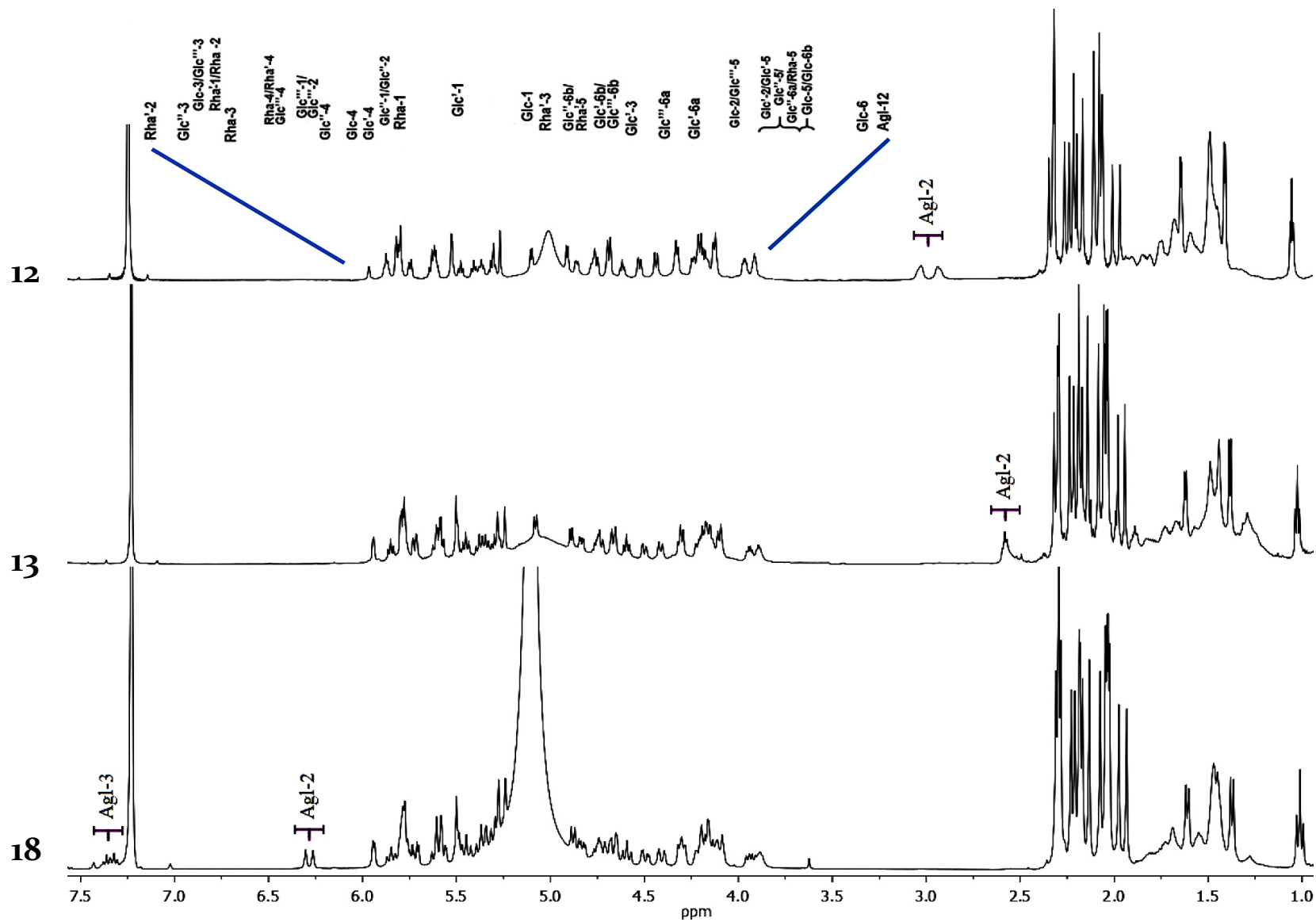
Figure S80. ¹H NMR spectra of peracetylated derivatives of operculinic acid H (**12**, above; 700 MHz), operculinic acid I (**13**, center; 600 MHz), and peracetylated dehydrated operculinic acid H (**18**, below; 400 MHz) in pyridine-d_5.
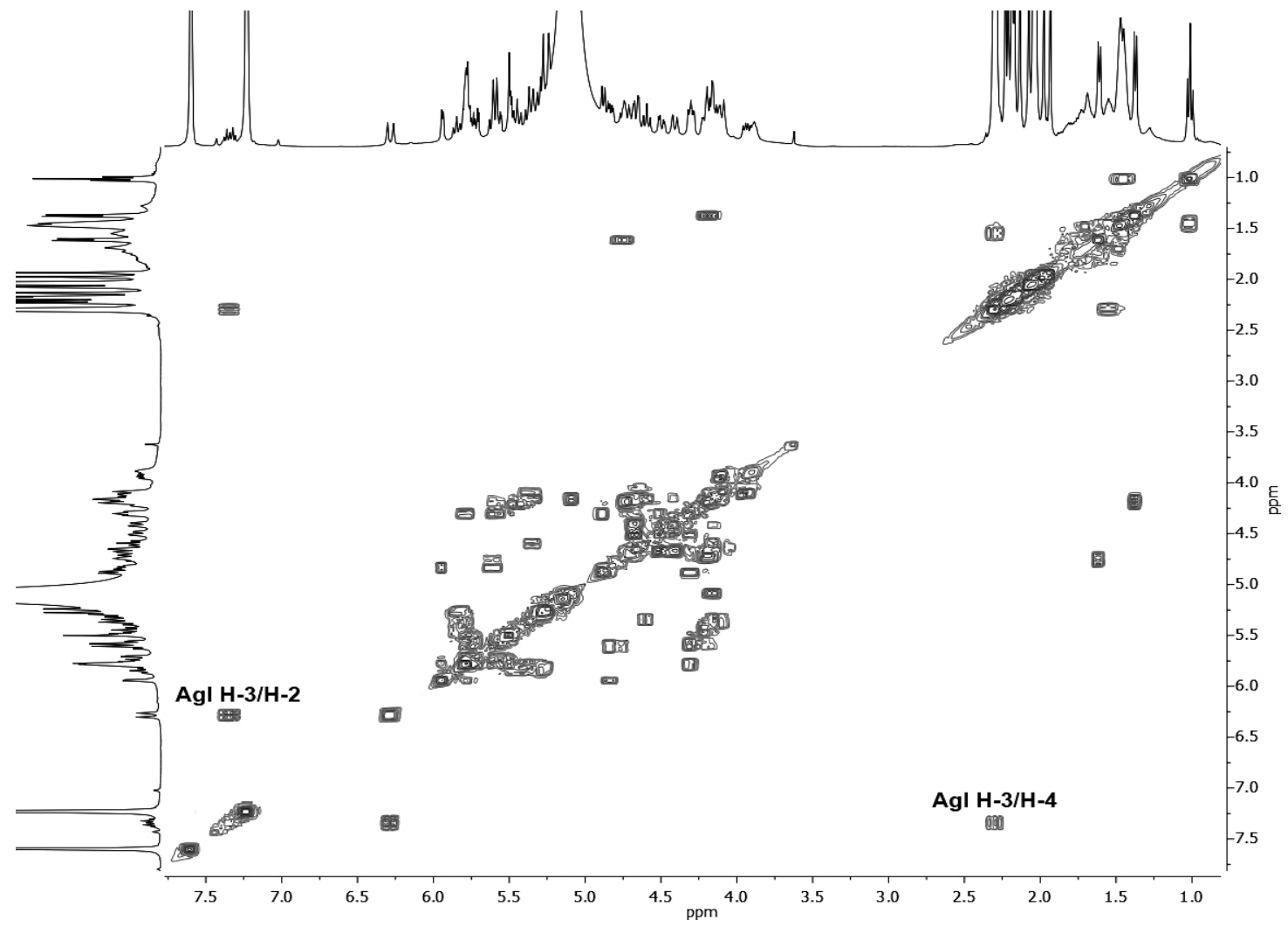
Figure S81. ¹H-Detected homonuclear total correlation (COSY) spectrum for the peracetylated dehydrated operculinic acid H (**18**) with high resolution 1D projections (400 MHz) in pyridine-d_5.
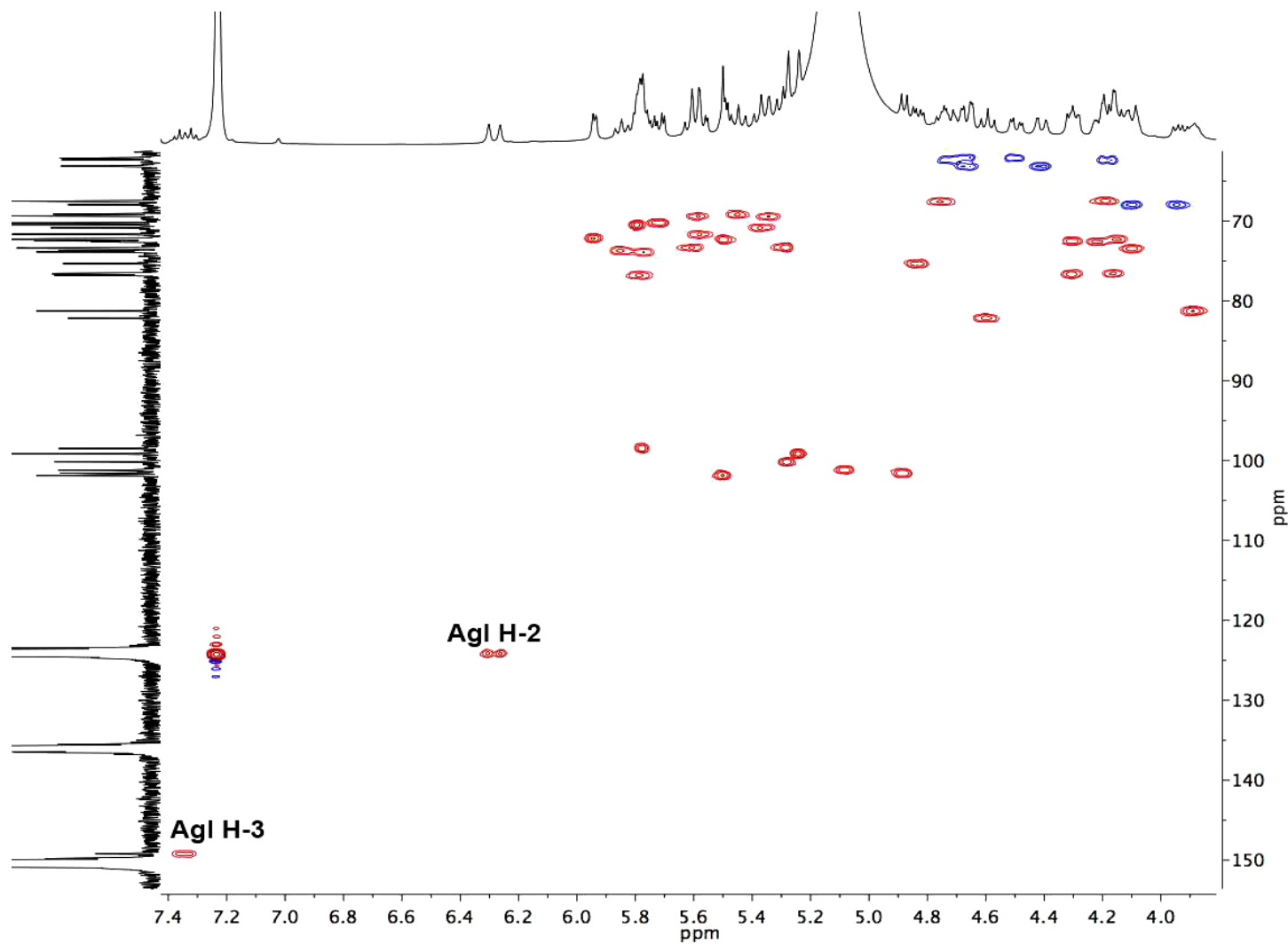
Figure S82. ^{1}H-Detected heteronuclear ($^1J_{CH}$) correlation (HSQC) spectrum for the peracetylated dehydrated operculinic acid H (**18**) with high resolution 1D ^{1}H projection (400 MHz) and ^{13}C (100 MHz) projections in pyridine-d_5. See Figure S18 for cross-peak assignments.

Formula: $[C_{77}H_{126}O_{38}Na]^+$
Exact mass: 1681.78193
**Accurate mass:** 1681.7805
Mass accuracy: −0.8 ppm
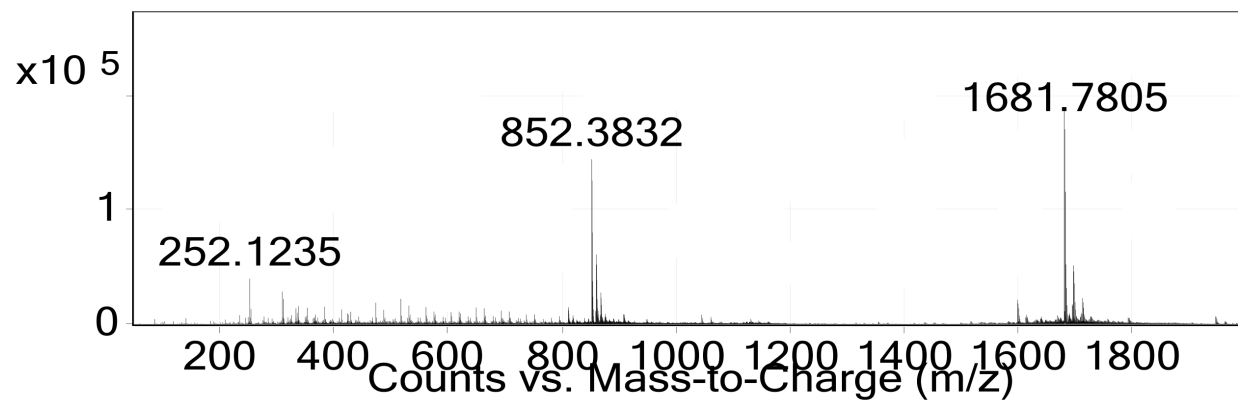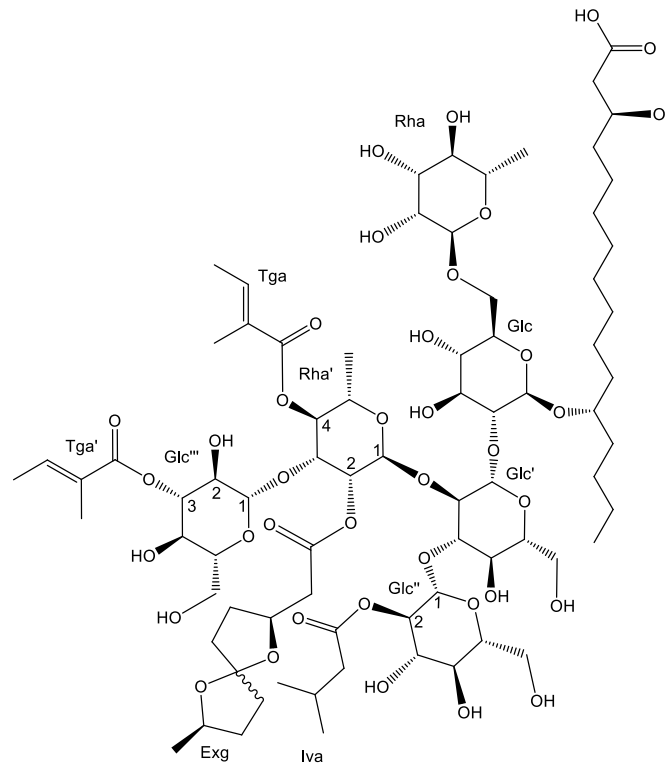
Figure S83. High-resolution positive ion mode ESI mass spectrum of macrocarpic acid A (**6**) showing relative abundance of the sodium adduct ion $[C_{77}H_{126}O_{38}Na]^+$ with exact mass at *m/z* 1681.78193.
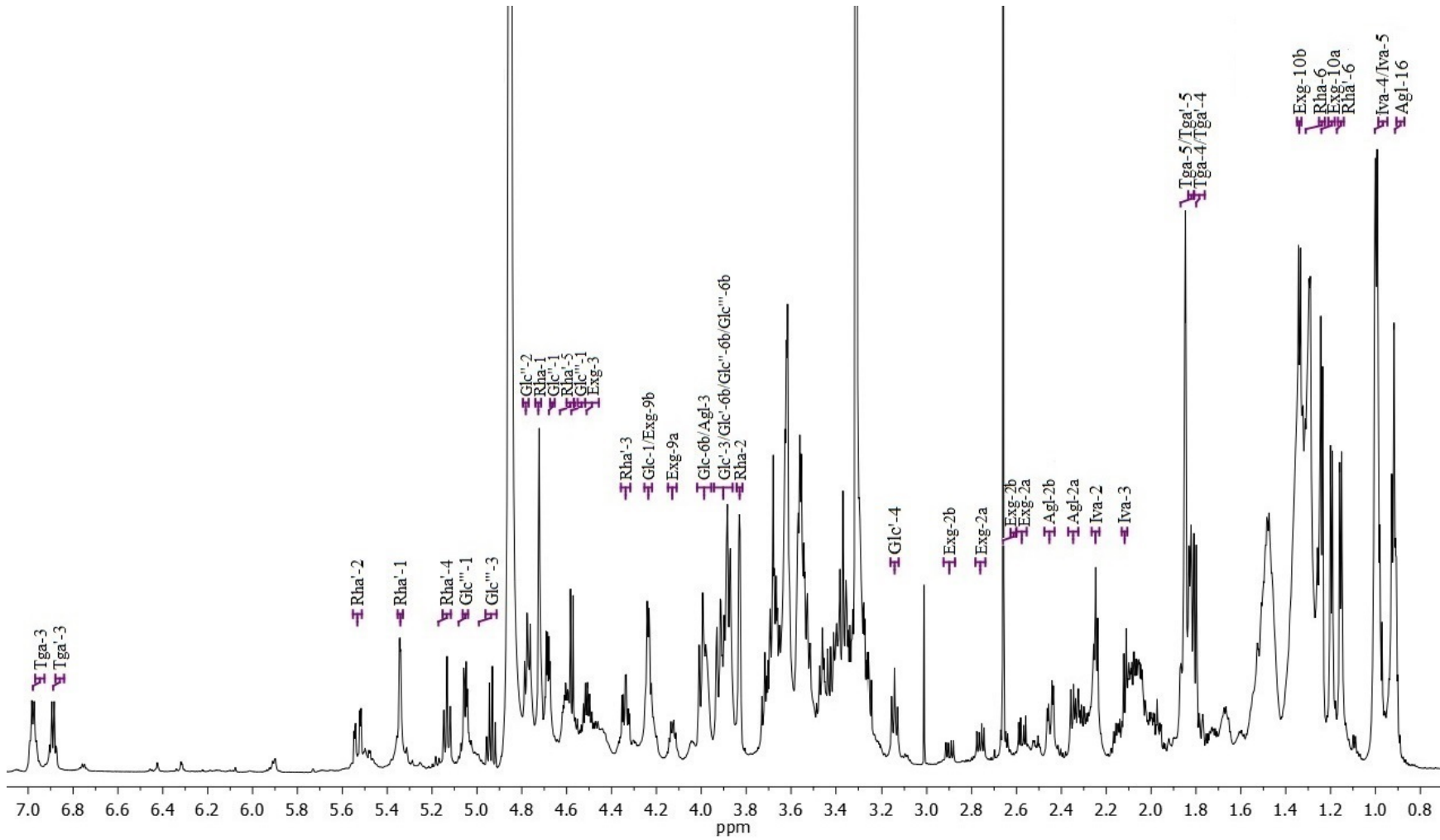
**Figure S84.** ¹H NMR spectrum (400 MHz) of macrocarpic acid A (**6**) in methanol-d_4
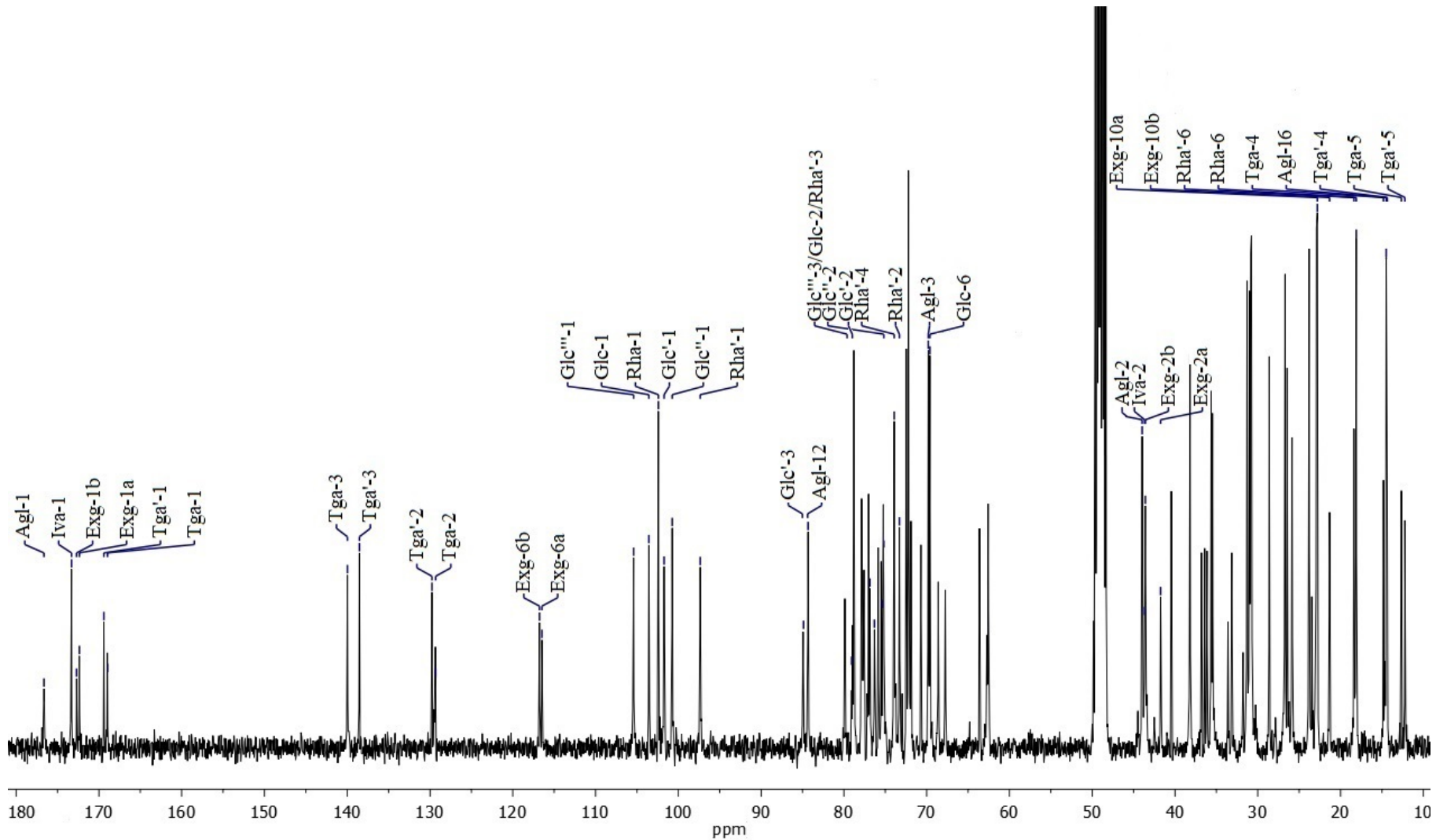
Figure S85. ^{13}C NMR spectrum (100 MHz) of macrocarpic acid A (**6**) in methanol-d_4.
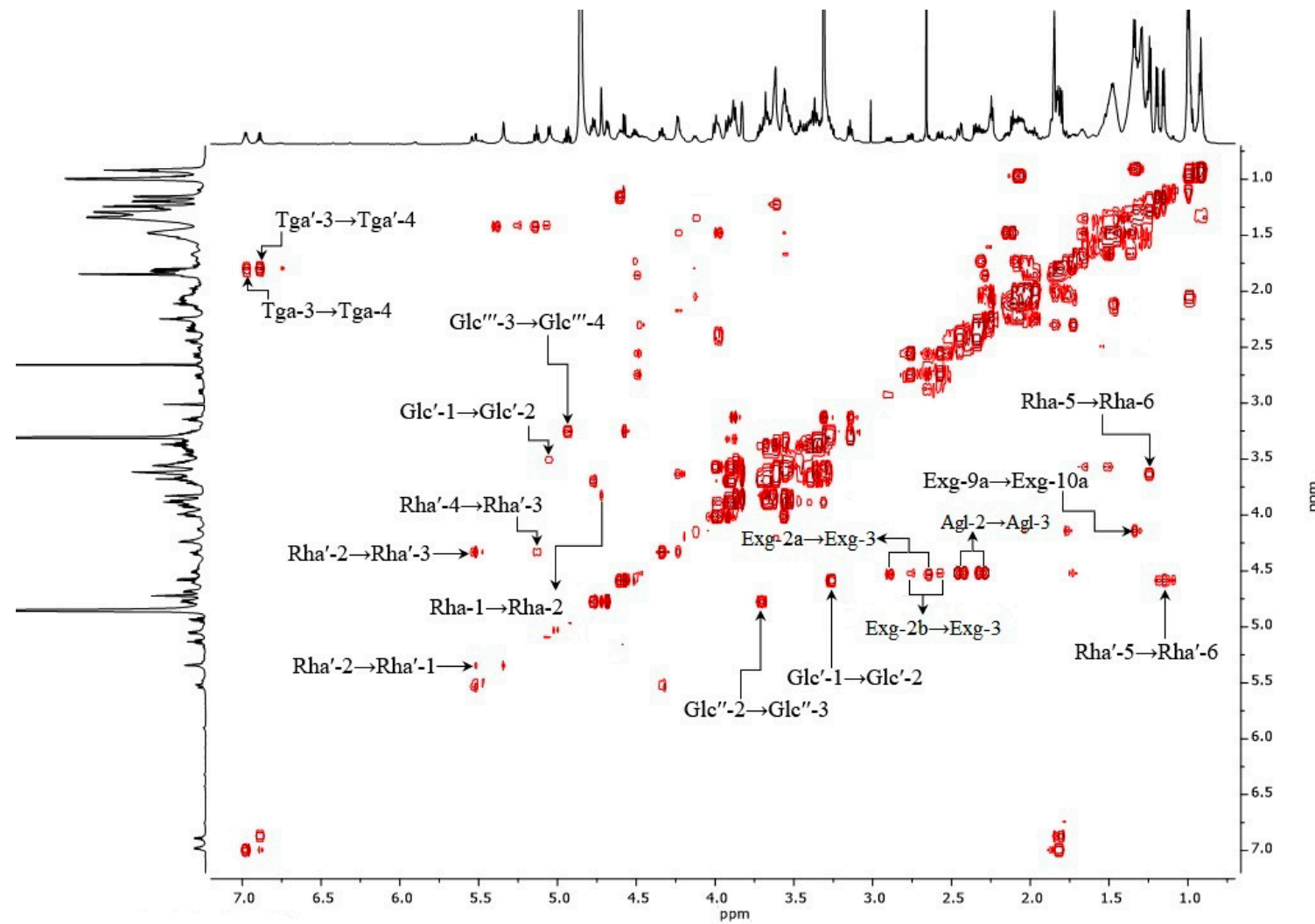
Figure S86. ¹H-Detected homonuclear total correlation (COSY) spectrum for macrocarpic acid A (**6**) with high resolution 1D projections (400 MHz) in methanol-d_4.
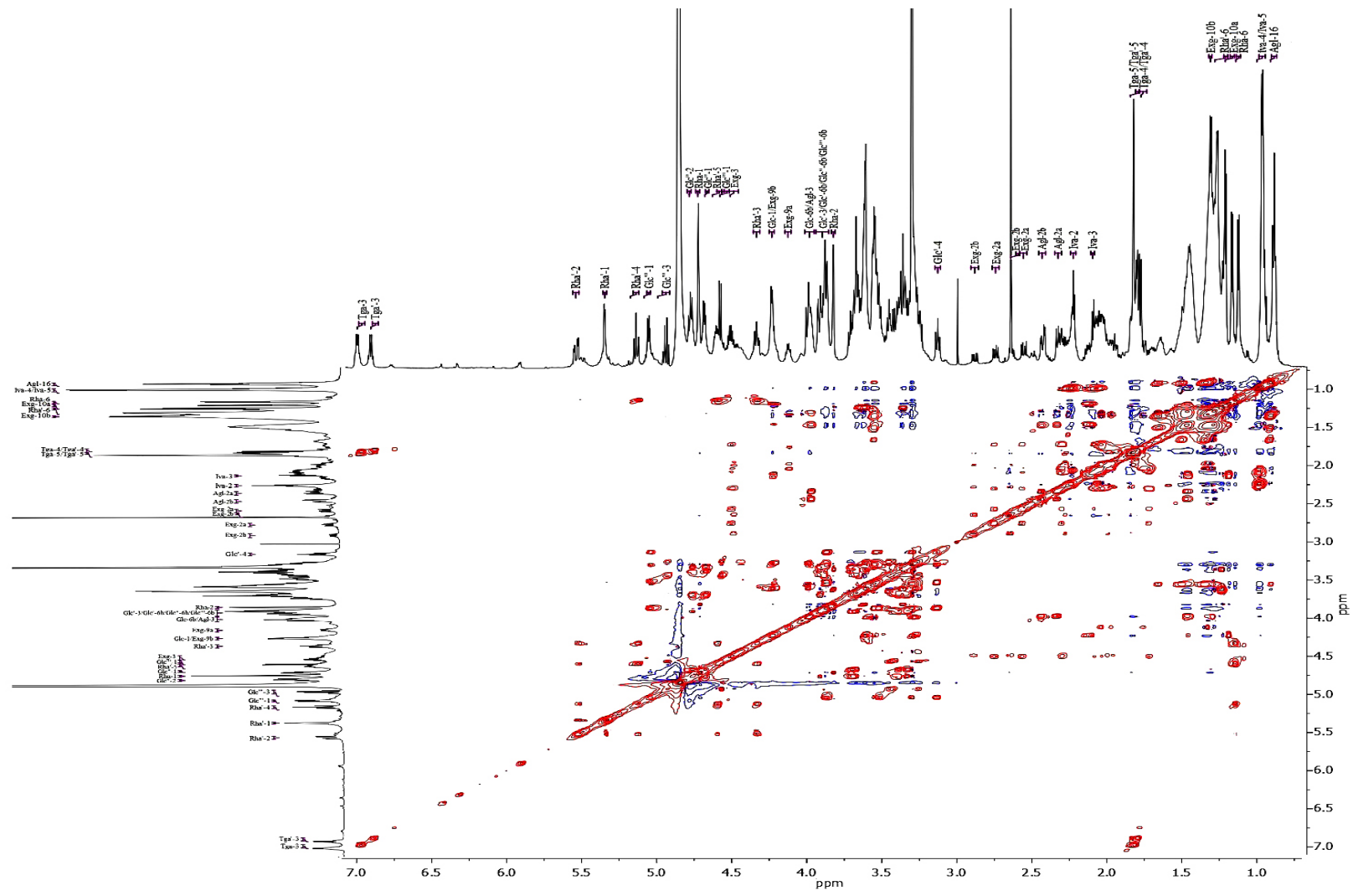
Figure S87. ¹H-Detected homonuclear total correlation (TOCSY) spectrum for macrocarpic acid A (**6**) with high resolution 1D projections (800 MHz) in methanol-d_4.

S94
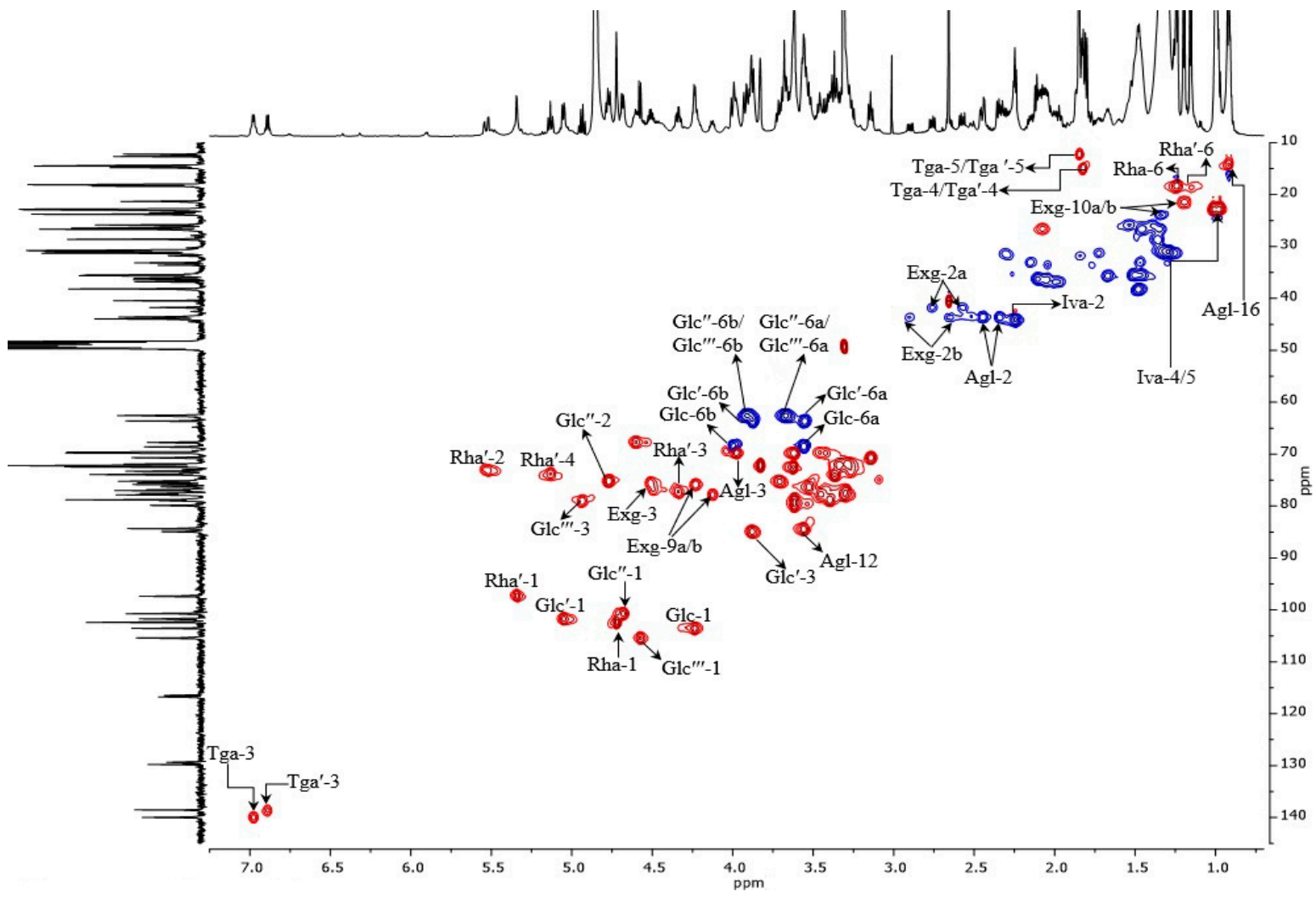
Figure S88. ¹H-Detected heteronuclear ($^1J_{CH}$) correlation (HSQC) spectrum for macrocarpic acid A (**6**) with high-resolution 1D ¹H (400 MHz) and ¹³C (100 MHz) projections in methanol-d_4.

Figure S89. ^{1}H-Detected heteronuclear ($^{2,3}J_{CH}$) correlation (HMBC) spectrum for macrocarpic acid A (**6**) with high-resolution 1D ^{1}H (400 MHz) and ^{13}C (100 MHz) projections in methanol-d_4. Connectivity assignments for acylation ($^3J_{CH}$): A, H_2-Rha′/C_1-Exg; B, H_4-Rha′/C_1-Tga; C, H_2-Glc″/C_1-Iva; D, H_3-Glc‴/C_1-Tga′; Connectivity assignments for glycosylation sequence ($^3J_{CH}$): **1**, H_1-Glc/C_{12}-Agl; **2**, C_1-Rha′/H_2-Glc′; **3**, C_1-Glc″/H_3-Glc′; **4**, C_1-Glc′/H_2-Glc; **5**, H_6-Glc/C_1-Rha; **6**, H_3-Rha′/C_1-Glc‴; Additional cross-peaks ($^{2,3}J_{CH}$): **7**, H_3-Tga/C_4-Tga; **8**, H_3-Tga′/C_4-Tga′; **9**, H_3-Tga/C_1-Tga; **10**, H_3-Tga′/C_1-Tga′; **11**, H_2-Rha′/C_1-Rha′; **12**, C_1-Glc″/H_2-Glc″; **13**, H_2-Rha/C_1-Rha; **14**, H_3-Exg/C_1-Exg; **15**, H_2-Exg/C_3-Exg; **16**, H_2-Exg/C_3-Exg; **17**, H_2-Exg/C_1-Exg; **18**, H_2-Exg/C_1-Exg; **19**, H_2-Agl/C_3-Agl; **20**, H_2-Agl/C_1-Agl; **21**, H_2-Iva/C_1-Iva; **22**, H_{10}-Exg/C_9-Exg.

S96

Formula: $[C_{77}H_{128}O_{38}Na]^+$
Exact mass: 1683.79758
Accurate mass: 1683.7988
Mass accuracy: +0.7 ppm
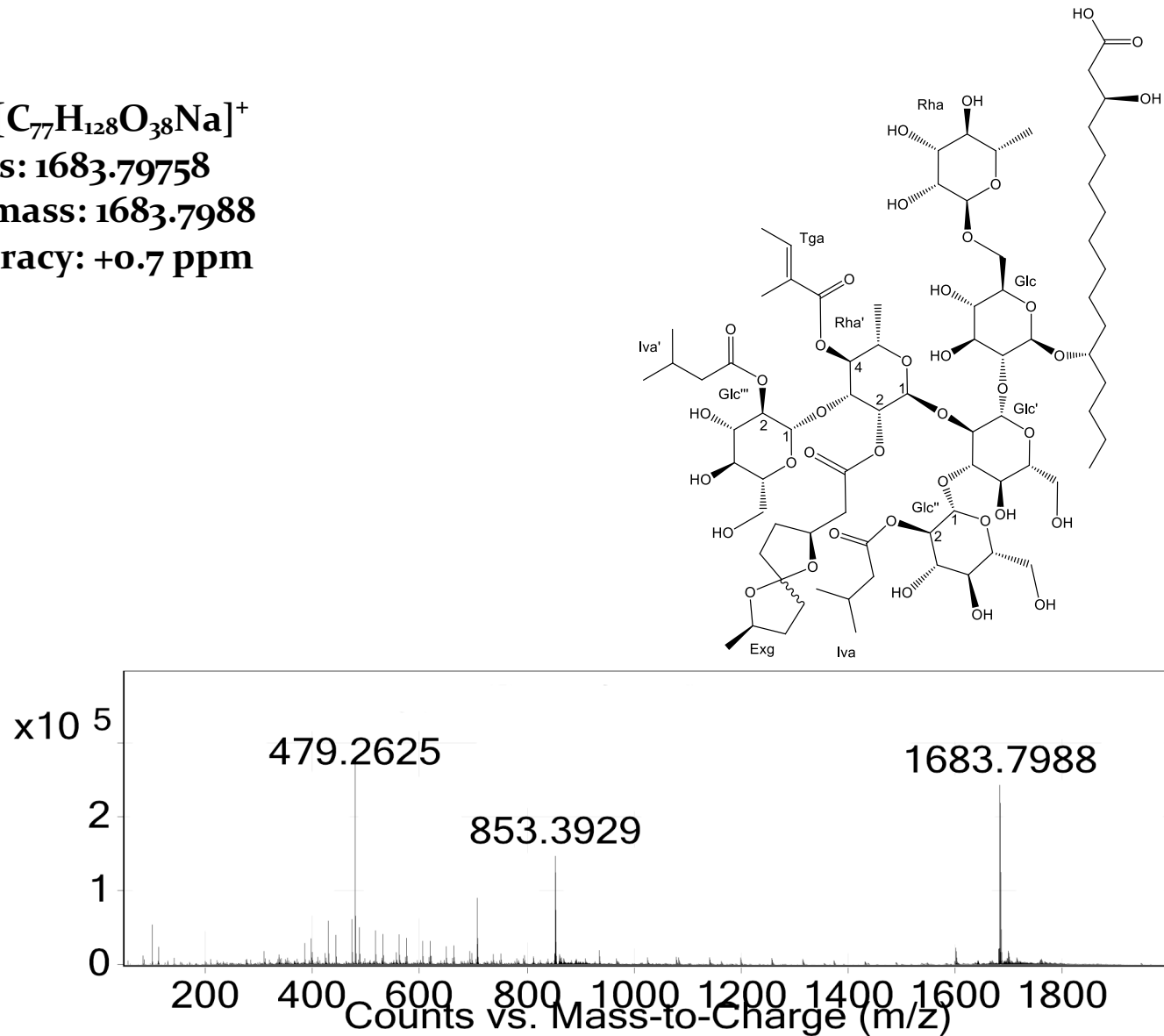
**Figure S90.** High-resolution positive ion mode ESI mass spectrum of macrocarpic acid B (**7**) showing relative abundance of the sodium adduct ion $[C_{77}H_{126}O_{38}Na]^+$ with exact mass at *m/z* 1683.79758.
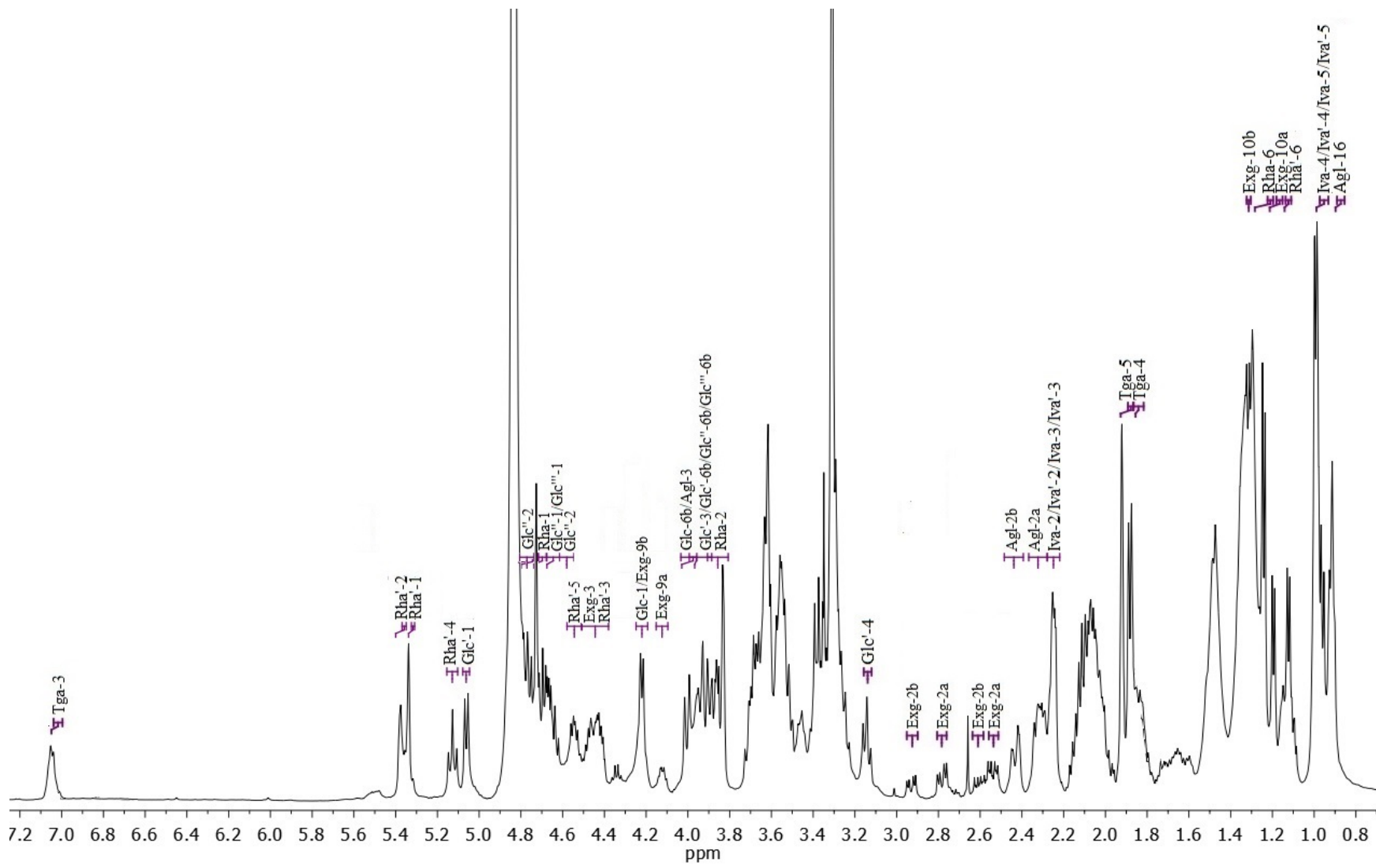
Figure S91. ^{1}H NMR spectrum (500 MHz) of macrocarpic acid B (**7**) in methanol-d_4.
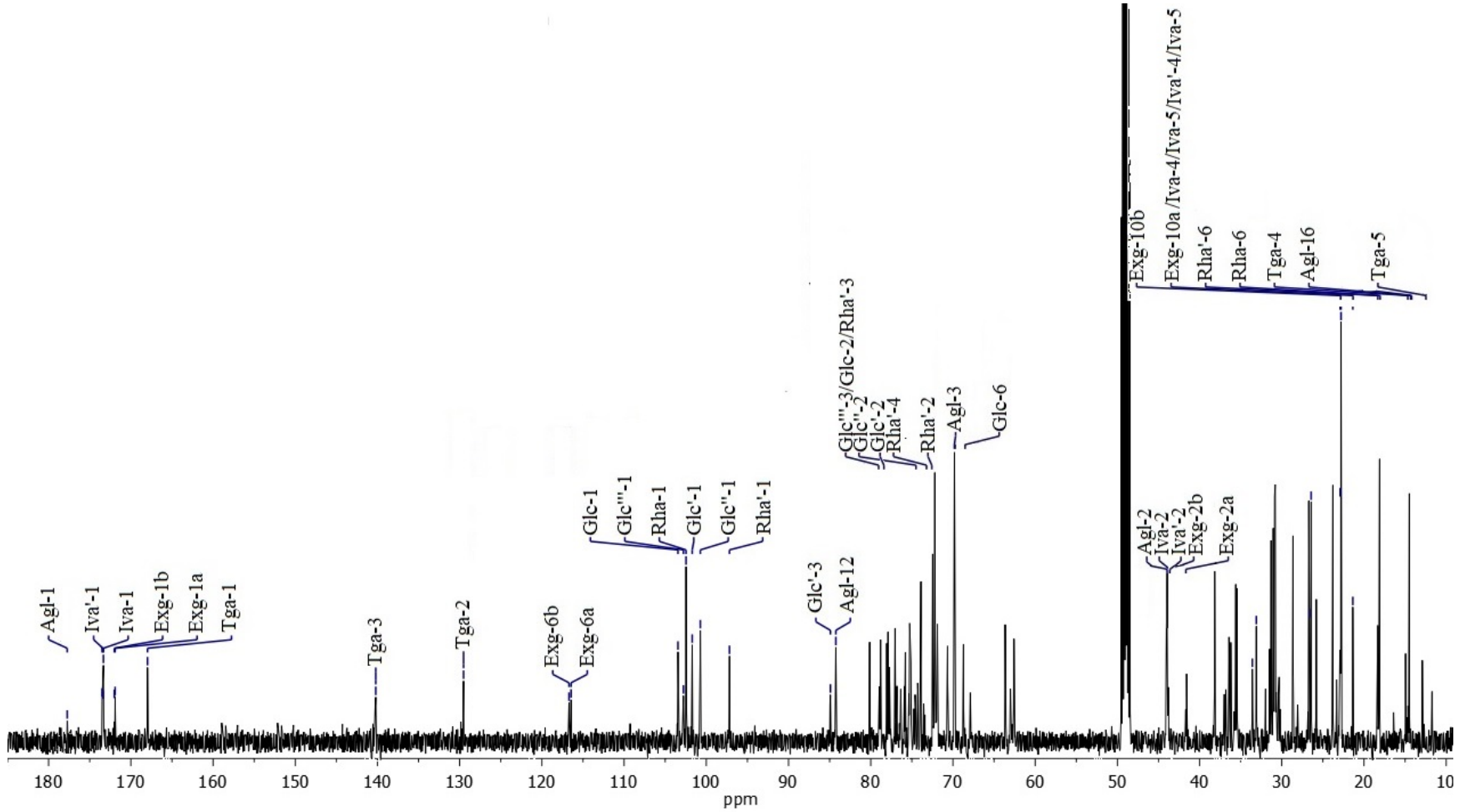
Figure S92. ^{13}C NMR spectrum (125 MHz) of macrocarpic acid B (**7**) in methanol-d_4.
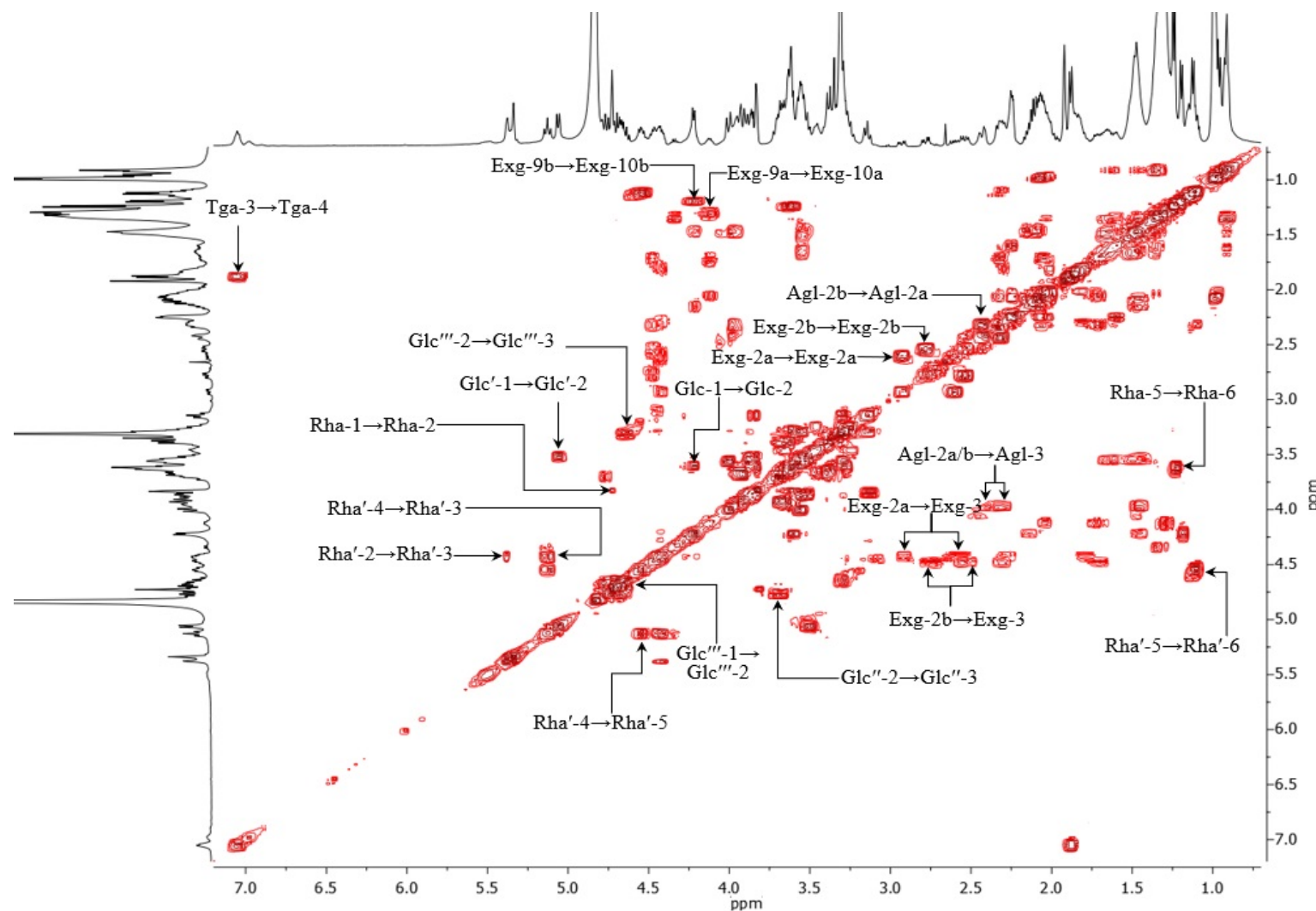
Figure S93. ¹H-Detected homonuclear total correlation (COSY) spectrum for macrocarpic acid B (**7**) with high resolution 1D projections (400 MHz) in methanol-d_4.
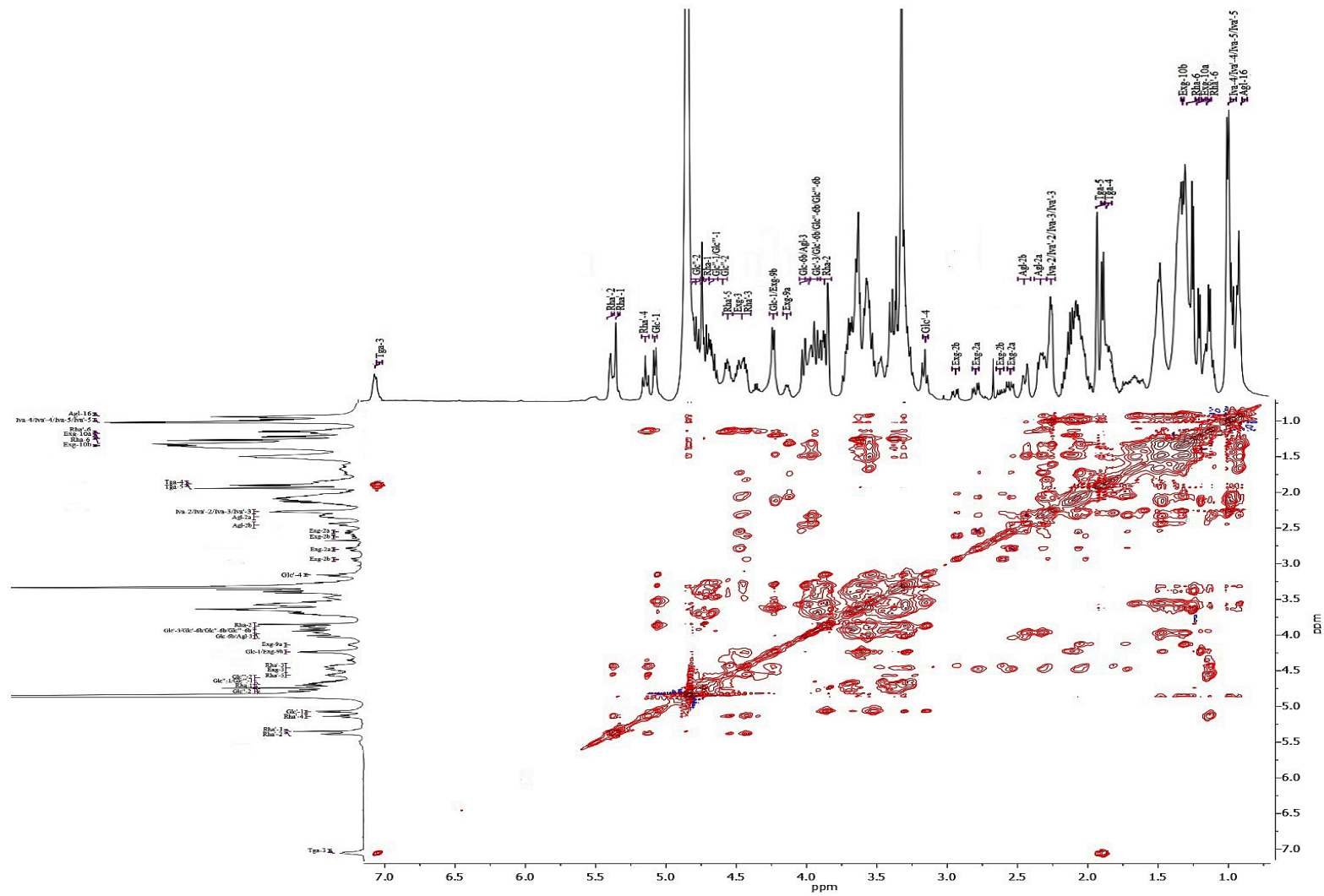
Figure S94. ¹H-Detected homonuclear total correlation (TOCSY) spectrum for macrocarpic acid B (**7**) with high resolution 1D projections (800 MHz) in methanol-d_4.

S101
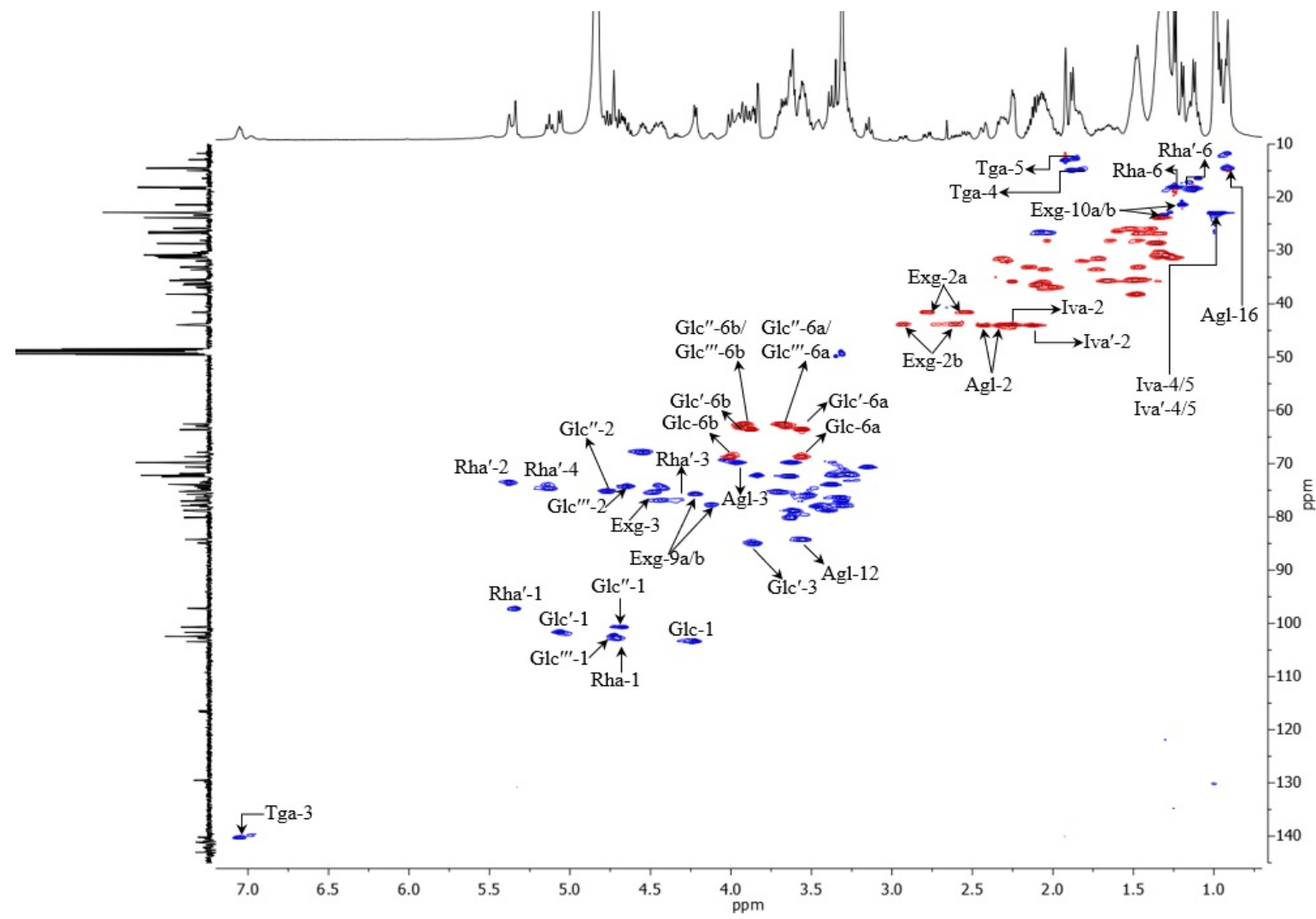
Figure S95. ^{1}H-Detected heteronuclear ($^1J_{CH}$) correlation (HSQC) spectrum for macrocarpic acid B (**7**) with high-resolution 1D ^{1}H (400 MHz) and ^{13}C (100 MHz) projections in methanol-d_4.

Figure Detected

S96. [1]H-heteronuclear ($^{2,3}J_{CH}$) correlation (HMBC) spectrum for macrocarpic acid B (**7**) with high-resolution 1D [1]H (400 MHz) and [13]C (100 MHz) projections in methanol-d_4. Connectivity assignments for acylation ($^3J_{CH}$): **A**, H_4-Rha′/C_1-Tga; **B**, H_2-Glc″/C_1-Iva; **C**, H_2-Glc‴/C_1-Iva′; **D**, H_2-Rha′/C_1-Exg; Connectivity assignments for glycosylation sequence ($^3J_{CH}$): **1**, H_1-Glc/C_{12}-Agl; **2**, C_1-Rha′/H_2-Glc′; **3**, C_1-Glc″/H_3-Glc′; **4**, C_1-Glc′/H_2-Glc; **5**, H_6-Glc/C_1-Rha; **6**, H_3-Rha′/C_1-Glc‴; Additional cross-peaks ($^{2,3}J_{CH}$): **7**, H_1-Glc′/C_2-Glc′; **8**, H_2-Glc″/C_1-Glc″; **9**, H_2-Glc‴/C_1-Glc‴; **10**, H_2-Iva/C_1-Iva; **11**, H_2-Iva′/C_1-Iva′; **12**, H_3-Tga/C_4-Tga; **13**, H_3-Tga/C_1-Tga; **14**, H_3-Exg/C_1-Exg; **15**, H_2-Exg/C_3-Exg; **16**, H_2-Exg/C_3-Exg; **17**, H_2-Exg/C_1-Exg; **18**, H_2-Exg/C_1-Exg; **19**, H_2-Agl/C_3-Agl; **20**, H_2-Agl/C_1-Agl; **21**, H_{10}-Exg/C_9-Exg.

S103

Formula: $[C_{77}H_{128}O_{38}Na]^+$
Exact mass: 1683.79758
Accurate mass: 1683.7984
Mass accuracy: +0.5 ppm
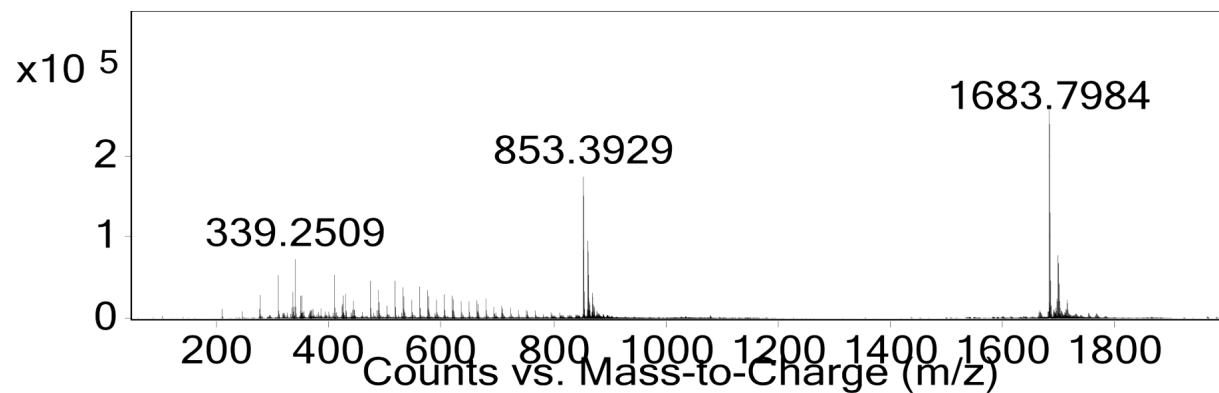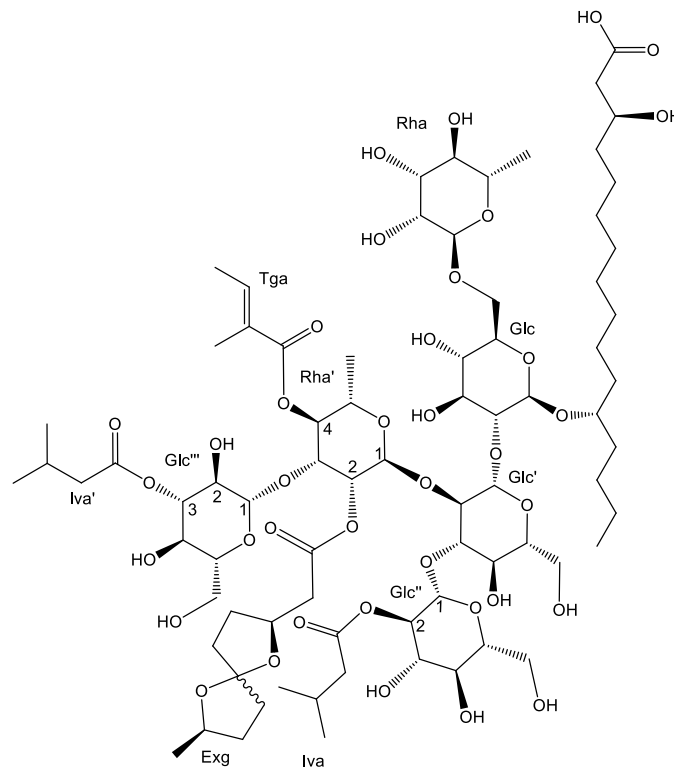
Figure S97. High-resolution positive ion mode ESI mass spectrum of macrocarpic acid C (**8**) showing relative abundance of the sodium adduct ion $[C_{77}H_{126}O_{38}Na]^+$ with exact mass at *m/z* 1683.79758.
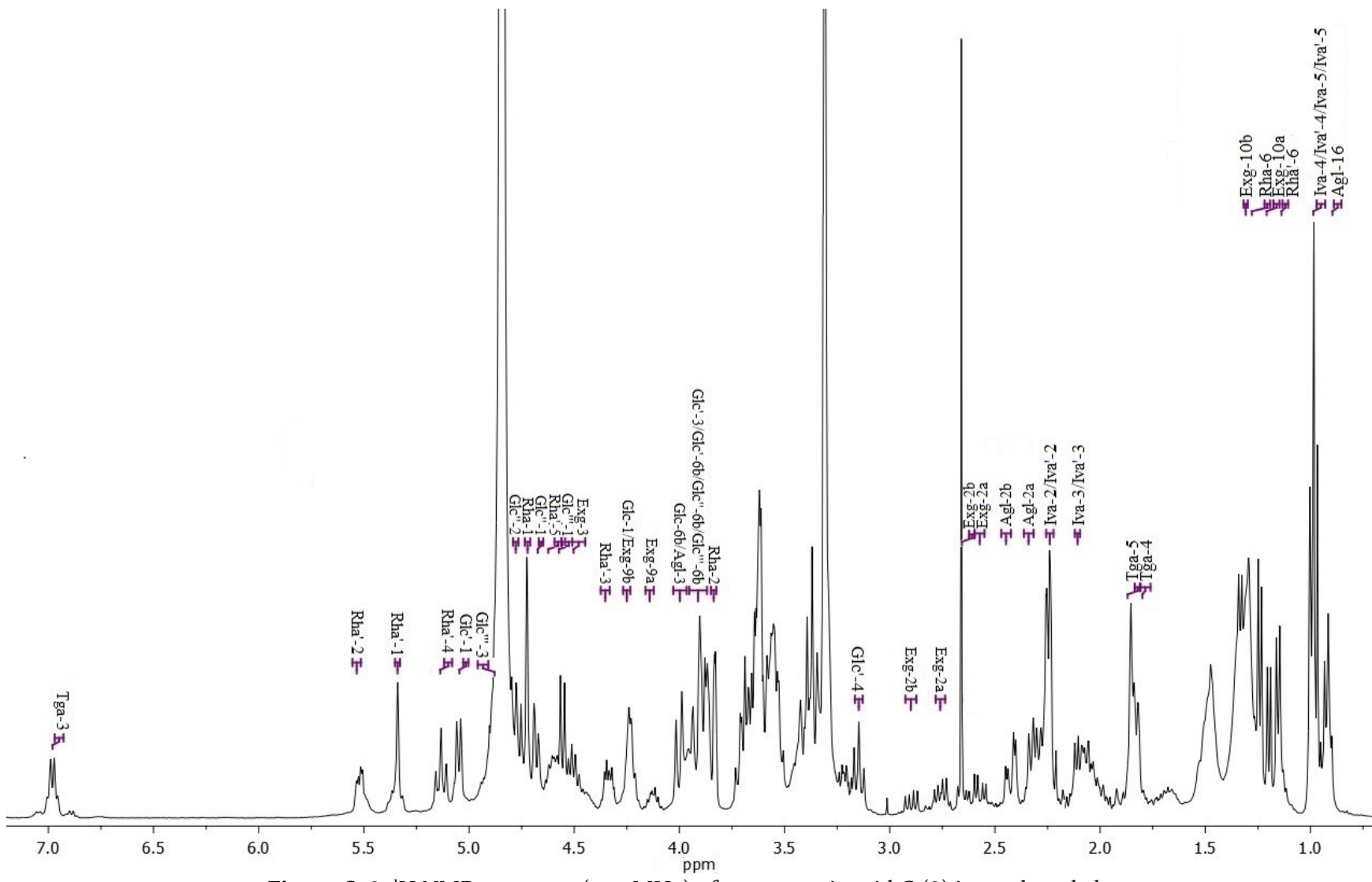
**Figure S98.** ¹H NMR spectrum (400 MHz) of macrocarpic acid C (**8**) in methanol-d_4.
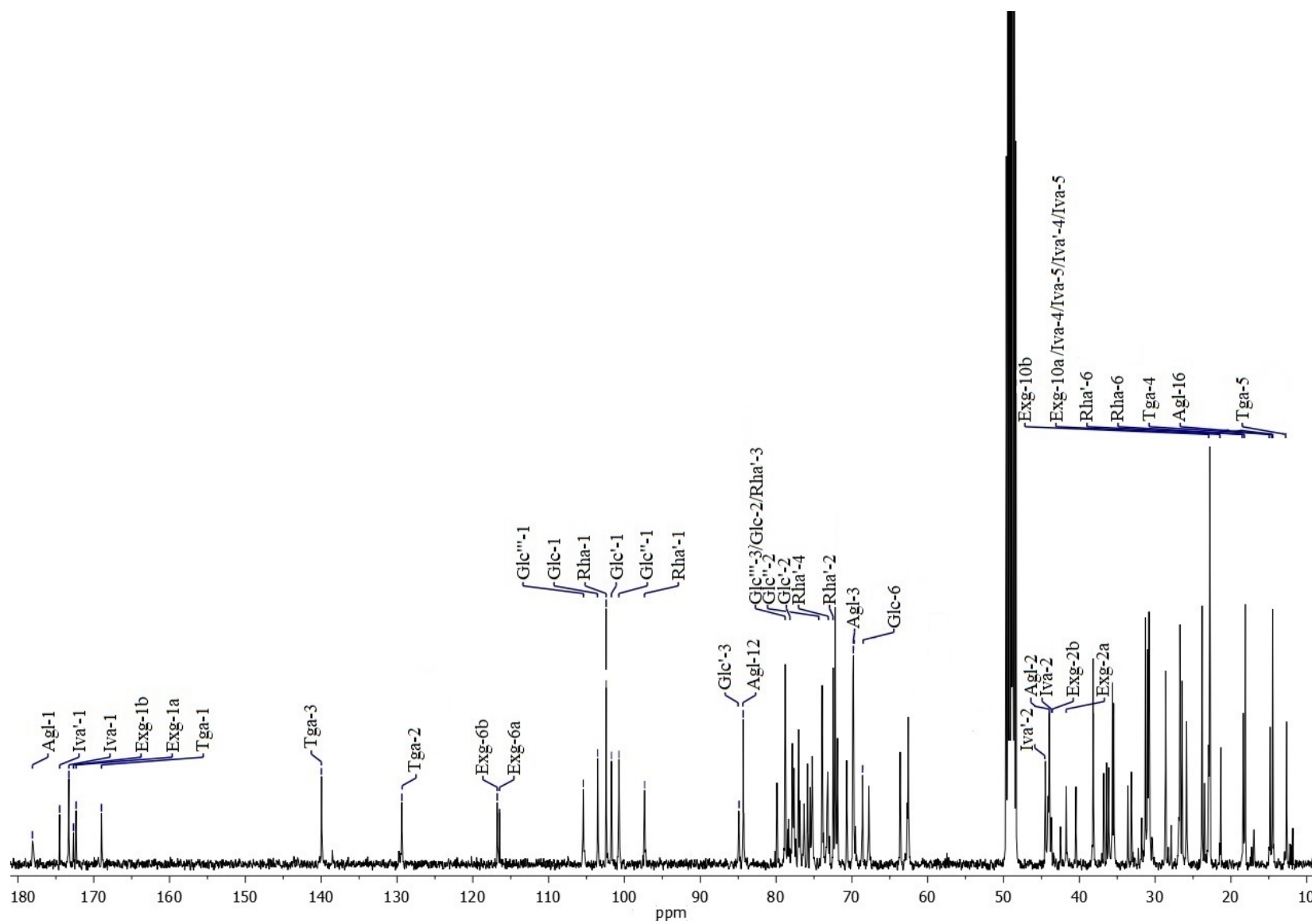
Figure S99. ^{13}C NMR spectrum (100 MHz) of macrocarpic acid C (**8**) in methanol-d_4.
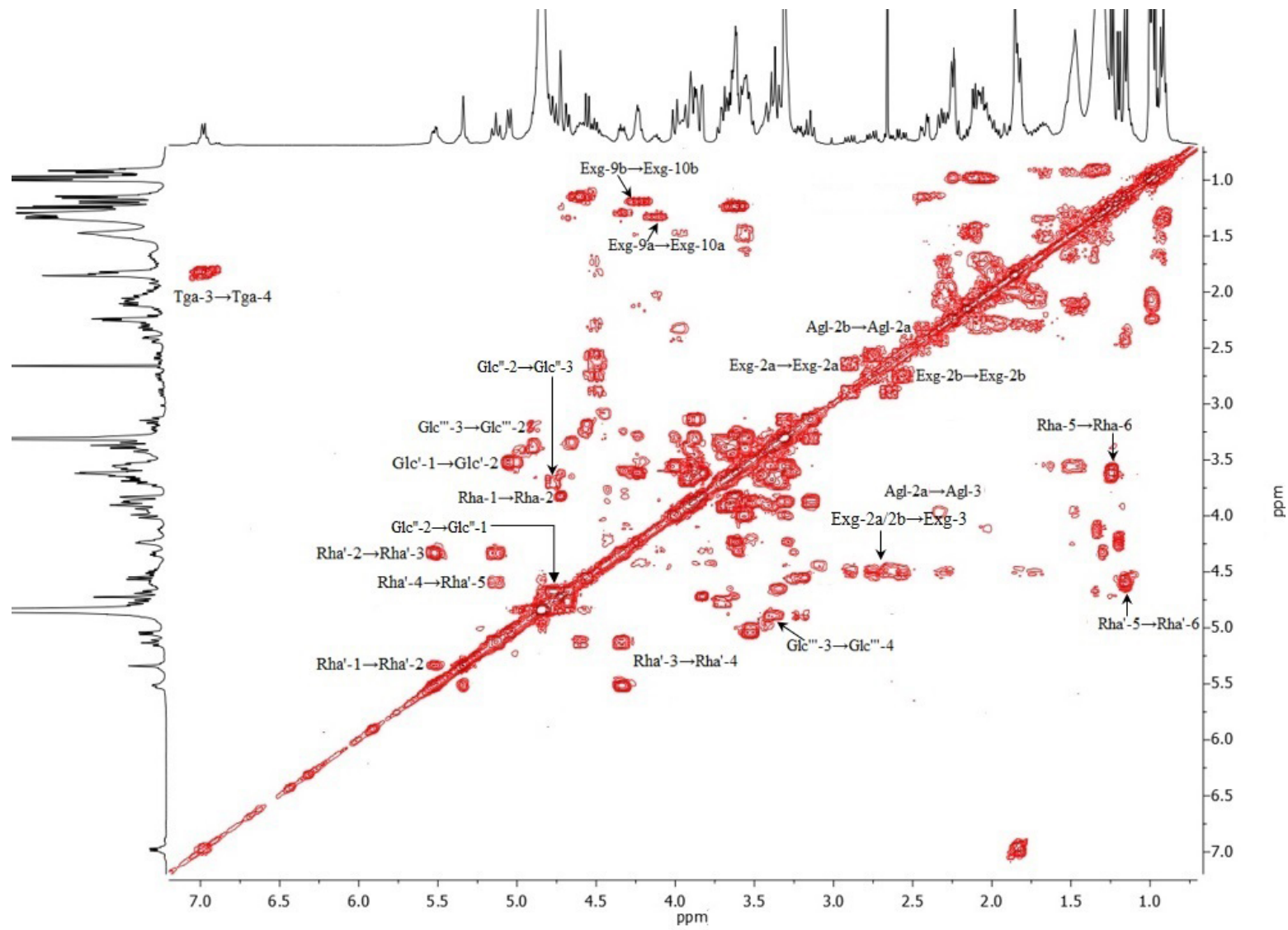
Figure S100. ¹H-Detected homonuclear total correlation (COSY) spectrum for macrocarpic acid C (**8**) with high resolution 1D projections (400 MHz) in methanol-d_4.
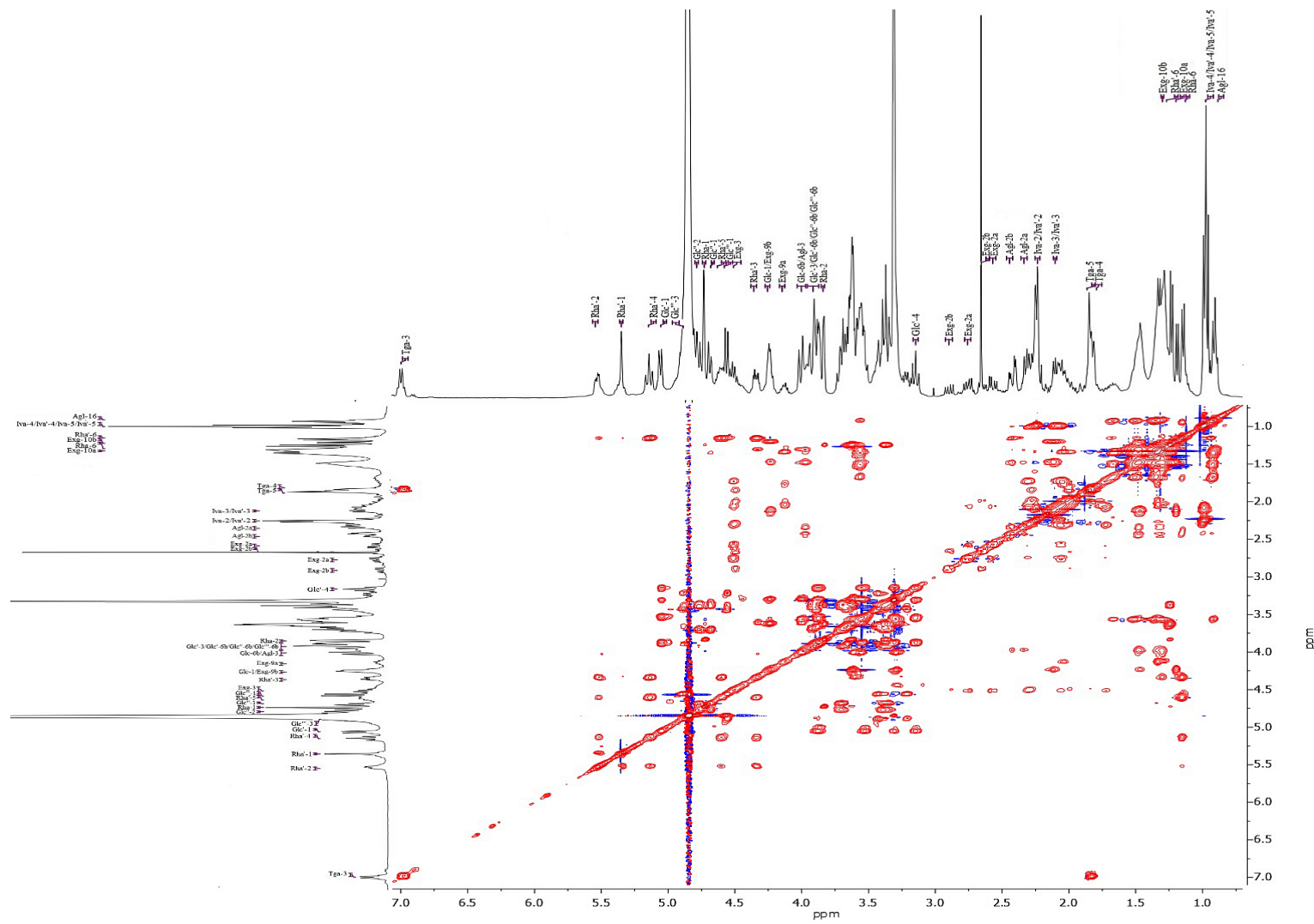
Figure S101. ^{1}H-Detected homonuclear total correlation (TOCSY) spectrum for macrocarpic acid C (**8**) with high resolution 1D projections (800 MHz) in methanol-d_4.
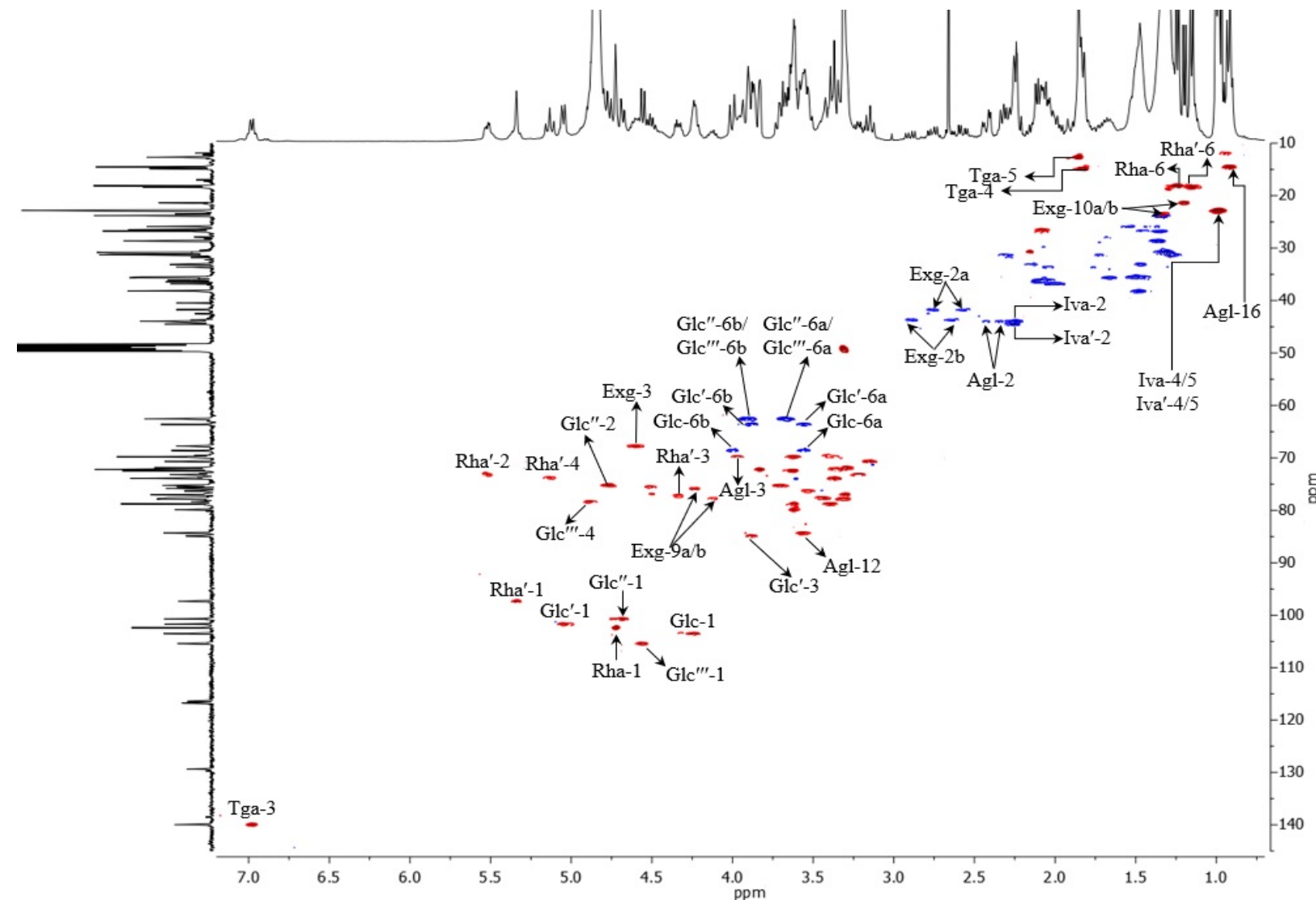
Figure S102. ^{1}H-Detected heteronuclear ($^1J_{CH}$) correlation (HSQC) spectrum for macrocarpic acid C (**8**) with high-resolution 1D ^{1}H (400 MHz) and ^{13}C (100 MHz) projections in methanol-d_4.
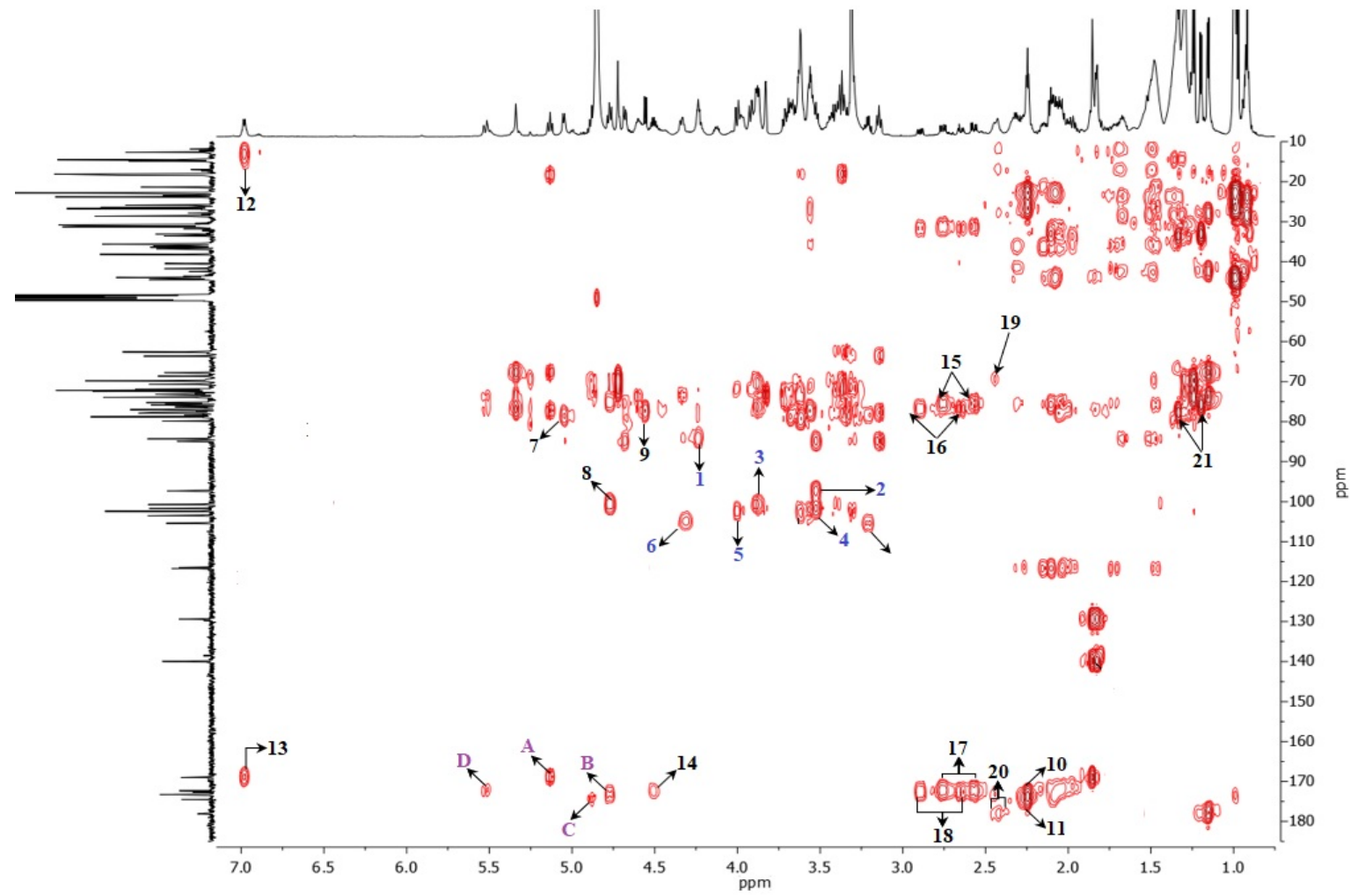
Figure S103. ^{1}H-Detected heteronuclear ($^{2,3}J_{CH}$) correlation (HMBC) spectrum for macrocarpic acid C (**8**) with high-resolution 1D ^{1}H (400 MHz) and ^{13}C (100 MHz) projections in methanol-d_4. Connectivity assignments for acylation ($^3J_{CH}$): A, H$_4$-Rha′/C$_1$-Tga; B, H$_2$-Glc″/C$_1$-Iva; C, H$_2$-Glc‴/C$_1$-Iva′; D, H$_2$-Rha′/C$_1$-Exg; Connectivity assignments for glycosylation sequence ($^3J_{CH}$): **1**, H$_1$-Glc/C$_{12}$-Agl; **2**, C$_1$-Rha′/H$_2$-Glc′; **3**, C$_1$-Glc″/H$_3$-Glc′; **4**, C$_1$-Glc′/H$_2$-Glc; **5**, H$_6$-Glc/C$_1$-Rha; **6**, H$_3$-Rha′/C$_1$-Glc‴; Additional cross-peaks ($^{2,3}J_{CH}$): **7**, H$_1$-Glc′/C$_2$-Glc′; **8**, H$_2$-Glc″/C$_1$-Glc″; **9**, H$_2$-Glc‴/C$_1$-Glc‴; **10**, H$_2$-Iva/C$_1$-Iva; **11**, H$_2$-Iva′/C$_1$-Iva′; **12**, H$_3$-Tga/C$_4$-Tga; **13**, H$_3$-Tga/C$_1$-Tga; **14**, H$_3$-Exg/C$_1$-Exg; **15**, H$_2$-Exg/C$_3$-Exg; **16**, H$_2$-Exg/C$_3$-Exg; **17**, H$_2$-Exg/C$_1$-Exg; **18**, H$_2$-Exg/C$_1$-Exg; **19**, H$_2$-Agl/C$_3$-Agl; **20**, H$_2$-Agl/C$_1$-Agl; **21**, H$_{10}$-Exg/C$_9$-Exg.

Figure S104. ¹H NMR spectrum (400 MHz) of macrocarpic acid C (**8**) in pyridine-d_5. For assignments, see reference 10: Ono, et al. (2017) *Chem. Pharm. Bull. 65*, 107–111.
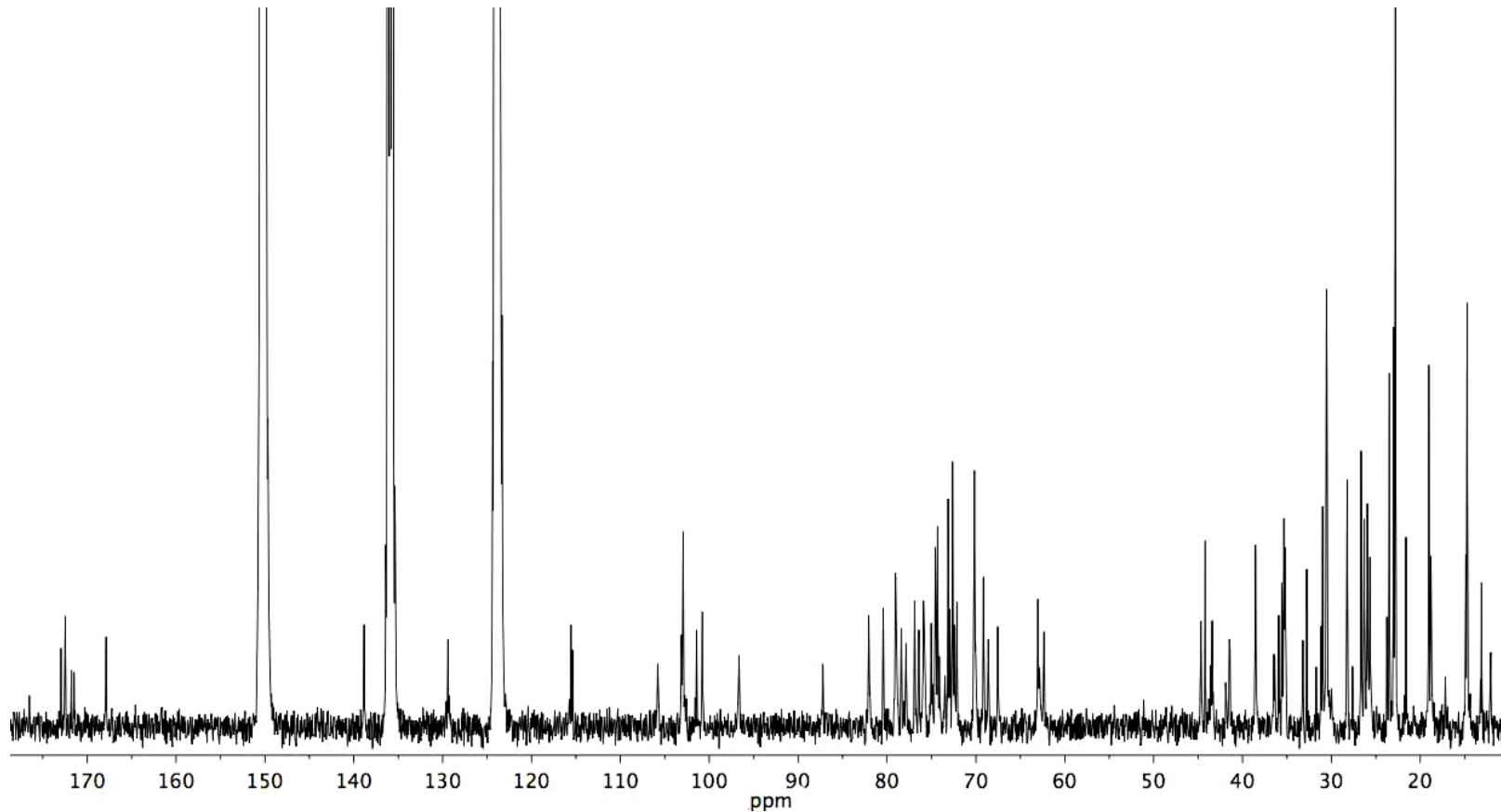
Figure S105. ^{13}C NMR spectrum (100 MHz) of macrocarpic acid C (**8**) in pyridine-d_5. For assignments, see reference 10. For assignments, see reference 10: Ono, et al. (2017) *Chem. Pharm. Bull. 65*, 107–111.